HOKKAIDO UNIVERSITY

Title	Prediction-based maintenance of existing structures considering multi-influential factors
Author(s)	苗, 鵬勇
Degree Grantor	北海道大学
Degree Name	博士(工学)
Dissertation Number	甲第14679号
Issue Date	2021-09-24
DOI	https://doi.org/10.14943/doctoral.k14679
Doc URL	https://hdl.handle.net/2115/86927
Type	doctoral thesis
File Information	Miao_Pengyong.pdf

Prediction-based maintenance of existing structures considering multi-influential factors

（複数の劣化要因を考慮した予測モデルに基づく既存構造物の維持管理）

By

Pengyong MIAO

A dissertation submitted to

Hokkaido University in partial fulfillment of the requirement for the

Doctoral Degree of Engineering

Doctoral Thesis No:
Division of Engineering and Policy for Sustainable Environment
Graduate School of Engineering, Hokkaido University
September 2021

Acknowledgements

This graduate thesis is completed at Hokkaido University under the generous help of my supervisor, Prof. Hiroshi YOKOTA.

Three years ago, I was fortunate and glad to be a member of Lifetime Engineering Laboratory, Hokkaido University. In the past three years, YOKOTA Sensei's kindness, erudition, and patience deeply inspired me. He contributed many valuable comments to my research. In addition, his guidance and spirits makes me treat this work objectively and comprehensively.

Honest appreciation must be extended to all the members of Lifetime Engineering Laboratory. I want to express my sincere appreciation for the friendly and supportive atmosphere that certainly helped me to carry out this research in a pleasant working environment.

My heartfelt thanks to Prof. Shunji KANIE for his help in applying for graduation.

Sincere appreciation goes to the CSC (China Scholarship Council) for offering scholarship to support my study at Hokkaido University.

I very much appreciate the supports from Prof. Bin SHI (Nanjing University, China) and Prof. Baojun WANG (Nanjing University, China) in preparing the documents for applying to study overseas. At the same while, Mr. Xing WANG and Ms. Min ZHANG should be thanked for their generosity to be my guarantors.

Appreciation should be given to my friend Shengchi MA. Without his help, I would not have the chance to study overseas, and have such a pleasant life experiences. I also thank Yafen ZHANG for helping me get acquainted with life in Sapporo.

No acknowledgment would ever adequately to express my obligation to my family, who has always wished to see me flying high up at the skies of success. The present work would not have been completed without their support and encouragement.

Last but not important, I would like to express my gratitude to my girlfriend, Ms. Yujuan WANG. Although we spent less time together and more time apart, she always gave encouragement to me silently. Hope we could meet soon and set up a happy family.

Words are not enough to express my gratitude to all those kind persons.

Pengyong MIAO

September, 2021

Abstract

Existing structures must be sufficiently managed to balance social, economic, and environmental requirements, and the maintenance of such structures has become a major social concern. Among all the maintenance approaches, prediction-based maintenance is an increasingly popular method to keep the structure sound. Progress has been made in adopting preventive measures, but performing prediction-based maintenance remains challenging because of the following four points: (1) prediction-based maintenance depends heavily on the accurate prediction of deterioration. For existing structures, deterioration is affected by various factors such as chloride, material, and traffic load. However, the relationships between factors and deterioration are neither explicitly determined, nor the relative effect of each factor on deterioration is well understood; (2) cracks are particularly important for the safety of structures. Although crack images were collected from onsite inspection, quantifying the cracks requires considerable time and effort; (3) in previous inspection, a large amount of inspection information including cracks was collected, but intuitive management of the information is not easy; and (4) a general civil structure is a complicated system, i.e., its deterioration situation, the propagation of cracks, and other damages should be comprehensively considered when performing the prediction-based maintenance.

Four types of bridges (PC, RC, steel-concrete composite and steel bridges) were considered in this study among civil structures. Onsite inspection databases for these existing bridges collected by engineers during regular inspections include abundant information on structural conditions, thus providing the possibility of using the database for formulating prediction models. The inspection database in this study includes twelve potentially influencing factors and three deterioration grades, grade 1 being the sound situation and grade 3 indicates the requirement of early intervention. In addition, crack images regarding concrete components and experimental samples were collected from onsite inspection and indoor experiment, respectively. These images can be used to build models to quantify cracks effectively.

Firstly, this study explored the feasibility of using the neural network to establish deterioration prediction models. Appropriate neural network architectures can be trained using the inspection database to predict deterioration situations. If the network parameters are appropriately designed, the network would show satisfactory forecasting performance. One of the best-known neural networks is the Multilayer Perceptron (MLP), consisting of an input layer, one or several hidden layers, and an output layer. The Recurrent Neural Network (RNN) is another type of neural network specialized in learning time-related patterns from time-series data. Among the RNNs, Long Short-Term Memory (LSTM) is most widely used, and therefore, was applied in this study.

Testing the MLP and LSTM models on an inspection database of 3,368 bridges indicated that the LSTM model achieved the accuracy of exceeding 80 %, i.e., outperformed the MLP model of 65 %. For four types of bridges, the LSTM showed the equivalent performance. In addition, the prediction ability of the LSTM for bridges in coastal regions was slightly superior to those outside of coastal regions. The LSTM showed no significant differences in accuracy between different deck areas.

Secondly, the Shapely value method and the Sobol indices method were applied to the LSTM to determine the contribution of each factor on deterioration by calculating the relative importance of each factor. The analysis preliminarily determined the five most important factors affecting the deterioration. They were

years in service, traffic volume, deck area, chloride, and lowest temperature. In addition, the analysis revealed that the structure type was another significant reason to induce deterioration differences. The results also demonstrated significant differences in bridge deterioration between coastal and non-coastal regions, which were caused by airborne salt.

Thirdly, a commonly used probabilistic method-Markov Chain (MC), was proposed using the aforementioned inspection database. Then, the MC model was compared with LSTM in terms of bridge degradation progress. Specifically, the MC and the LSTM models were compared from four aspects: the mean deterioration progress, the deterioration progress of different types of bridges, the deterioration progress of a specific bridge, and the influence of each factor on deterioration progress.

The results indicated no significant differences between these two models, except that the LSTM usually predicts deterioration occurring two years earlier than the MC. Both the MC and LSTM models predicted that the PC and steel bridges deteriorated slower than RC and composite bridges. The factors affecting the deterioration progress were the same as those found by the Shapely value and the Sobol indices methods.

Fourthly, the onsite and indoor collected images were employed to a Convolutional Neural Network (CNN) and a developed application for crack detection and quantification. Specifically, four commonly used CNNs (GoogLeNet, AlexNet, ResnNet-18, and VGG-16) were tested, and GoogLeNet was determined for this study. Then, the transfer learning and fully training of GoogLeNet were further tested on the testing dataset and a public dataset.

The results showed that the transfer learning GoogLeNet has relatively balanced performances on these two datasets, with an accuracy of 96.69 % and 88.39 %, respectively. A new sliding window technique (neighborhood scanning) was proposed and almost equivalent to the previous dual scanning method. A method for calculating crack widths was presented. The average relative error of this method was 14.58 % (0.05 mm), i.e., much smaller than the previous method having 36.37 % (0.14 mm) error.

An application was then developed to integrate the proposed methods and other techniques (such as edge detectors, boundary tracking, and threshold segmentation) to segment, quantify, and analyze cracks. Verifications on 23 untrained raw images (eleven with 10240×2048 pixels, twelve with 2592×4608 pixels) showed that: (1) the developed crack identification model and a previous pixel-level segmentation model required an average of 9.48 s and 10.35 s; and (2) these two models showed an 80.40 % and a 78.64 % average Intersection over Union (IoU). Therefore, the proposed crack identification model is a cost-effective solution for detecting and analyzing cracks on concrete surfaces.

Lastly, Building Information Modeling (BIM) was studied for five bridges as examples to integrate the deterioration prediction models and the crack identification model to form a collaborated BIM platform. In this platform, the crack identification model extracted the crack pixels and located them to the corresponding components; the deterioration prediction model determined the deterioration situations and reasons. This platform can intuitively visualize each component's crack damage, can determine the remaining life of each bridge, and can analyze external factors affecting the deterioration. In conclusion, this platform can be taken as a supplementary tool to help the engineer comprehensively evaluate the bridges' situations, determine the timing of interventions, and formulate corresponding intervention strategies.

List of publications

1. Journals

(1) Pengyong Miao, Hiroshi Yokota and Yafen Zhang. Extracting procedures of key data from a structural maintenance database. Engineering and Infrastructure Engineering, 2020, 1-11, doi: 10.1080/15732479.2020.1838561.

(2) Pengyong Miao, Hiroshi Yokota and Yafen Zhang. Deterioration prediction of existing concrete bridges using a LSTM recurrent neural network. Engineering and Infrastructure Engineering. (2021): 1-15. https://doi.org/10.1080/15732479.2021.1951778

(3) Pengyong Miao, Hiroshi Yokota and Yafen Zhang. Prediction-based maintenance of existing bridges using neural network and sensitivity analysis. Advances in civil engineering, 2021. https://doi.org/10.1155/2021/4598337.

(4) Miao, Pengyong, and Teeranai Srimahachota. "Cost-effective system for detection and quantification of concrete surface cracks by combination of convolutional neural network and image processing techniques." Construction and Building Materials 293 (2021): 123549. https://doi.org/10.1016/j.conbuildmat.2021.123549.

(5) Pengyong Miao and Hiroshi Yokota. Comparison of Markov chain and recurrent neural network in predicting bridge deterioration under various influencing factors. Engineering and Infrastructure Engineering (To be submitted soon).

(6) Pengyong Miao. Integrated bridge maintenance supporting platform: prototype model-based database, crack-pixel extraction, and deterioration prediction. Engineering and Infrastructure Engineering (To be submitted soon).

2. Conferences

(1) Pengyong Miao, Hiroshi Yokota and Yafen Zhang. Development of an artificial neural network for the deterioration prediction of existing concrete bridges. 9th Asia-Pacific Young Researchers and Graduates Symposium Performance Evolution and Control for Engineering Structures. 19-20 December 2019, Shanghai, China.

(2) Pengyong Miao, Hiroshi Yokota and Yafen Zhang. Prediction-based maintenance of concrete structures by using an artificial neural network. The 3rd ACF Symposium 2019-Assessment and Intervention of Existing Structures,10-11 September 2019, Sapporo, Japan.

(3) Zhang Y, Yokota H, Miao P and Zhu Y. Application of knowledge management and BIM technology for maintenance management of concrete structures, 16th East Asia-Pacific Conference on Structural Engineering and Construction (EASEC16), 3-6 December 2019, Brisbane, Australia.

(4) Zhang Y, Yokota H and Miao P. A visual integration information platform for maintenance management of concrete structures based on information technology. IABSE Congress – Resilient Technologies for Sustainable Infrastructure, February 3-5, 2021, Christchurch, New Zealand. (Proceedings: pp.849-857)

(5) Pengyong Miao, Hiroshi Yokota and Yafen Zhang. A framework for addressing the uncertainty of factors influencing the overall deterioration of existing concrete structures. 10th International Conference on Bridge Maintenance, Safety and Management (IABMAS 2020), 11 -18 April, 2021, Sapporo, Japan.

Dedication

To
Prof. Hiroshi YOKOTA, My family, My girlfriend
&
All the teachers and friends who have helped me

Contents

List of Figures

List of Tables

Chapter 1

Introduction

1.1 Overview

The outline of Chapter 1 is shown in Figure 1.1. This study's background was first reported. Later, literature reviews were extended from the three points: deterioration prediction of bridges, endeavors in crack identification from images, and application of Building Information Modeling (BIM) in practical engineering. The issues that arose would be further explained. Finally, the research objectives were outlined. The structure of this thesis was illustrated at the end of this chapter.
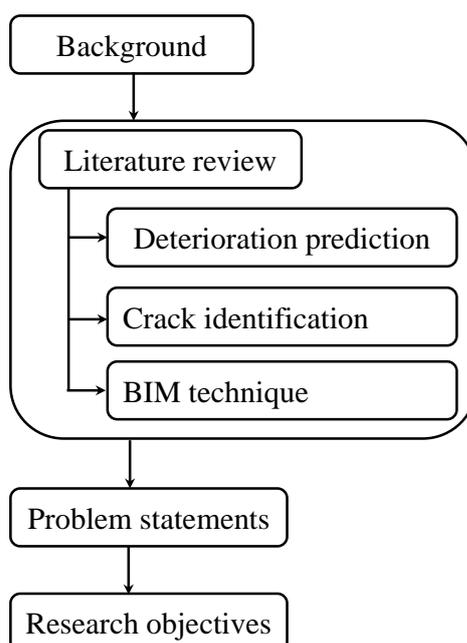
Figure 1.1 Outline of Chapter 1

1.2 Background

Bridges must be prudently managed to balance social, economic, and environmental requirements, and the maintenance of such infrastructures has become a major social concern [1]. Despite the several limitations of visual inspection, it is a frequently utilized approach in practice for the asset management of buildings and bridges [2]. Accordingly, inspection databases are collected by engineers for existing bridges during routine inspections.

Prediction-based maintenance is becoming more common for structural soundness maintenance [3]. Although progress has been made in taking preventive measures, performing prediction-based maintenance remains difficult, because a targeted prediction-based maintenance strategy relies heavily on a reasonable assessment of a structure's past and present conditions, as well as accurate deterioration prediction. In other words, prediction-based maintenance strategies need sufficient data on structural conditions and a suitable analytical approach. Inspection databases constitute abundant information on structural conditions, allowing the database to be used to develop predictive maintenance programs. Potential applications of such databases include evaluating structural conditions, predicting deterioration,

and developing maintenance strategies [4]. The potential analysis methods for the inspection database are elaborated in Section 1.3.1.

The investigation of concrete flaws, including cracks, is a frequent and required work in determining the state of concrete structures during an inspection. Researchers are now attempting to automate the inspection process using digital image analysis due to improvements in computer technology [2]. Cracks are very essential for the safety of concrete structures, and were therefore underlined in this study. Poor repairs, contractions due to fast temperature reductions, oscillations between contractions and expansions due to temperature changes, and additional loads are all causes of cracks in concrete buildings. Cracks, for whatever reason, can have an impact on the appearance of concrete structures and, more significantly, can signal serious structural distress or damage [5]. Even though extensive studied have been conducted in the literatures (Section 1.3.2), crack detection and quantification remains a challenging issue, because of: (1) some studies only established crack classifier to detect cracks; (2) pixel-level semantic segmentation method based on deep learning training requires a database of annotated pixels, generation of which is time and labor costly. Therefore, a crack identification model must be developed to analyze cracks efficiently and reliably from experimental images or field tests.

Since existing bridges have been or will be in service for a long time, a wealth of damage data on their components has been or will be accumulated. However, intuitively managing this information is not easy [6-7]. In other words, managers cannot comprehend the deterioration of a component unless they look for a large amount of documentation regarding that component. To address this issue, damage information such as cracks must be linked to the corresponding component. Furthermore, the damage information should be displayed intuitively on the components. The Building Information Modeling (BIM) of existing bridges is an optimal solution to these issues because it can include not only geometry information but also non-geometry information.

The existing bridge is a complicated system, i.e., its deterioration situation, the propagation of cracks, and other damages must all be taken into account when performing the prediction-based maintenance. To support decision-making, the deterioration prediction models, crack identification models, and the 3-D prototype model of existing bridges should be integrated together to constitute a collaborated BIM platform. The crack identification model in this platform extracts and locates the crack pixels to the corresponding components; the deterioration situations and reasons are determined by the deterioration prediction model. This platform is anticipated to easily show the crack damage of each component, determine the remaining life, and estimate the impacts of external variables influencing the deterioration.

1.3 Literature review

1.3.1 Deterioration prediction

Since the conditions of an existing bridge are typically dynamically changing, the conditions at a time affect its conditions at the subsequent time [8]. In addition, deterioration of existing bridges is associated with many factors, such as chloride and snowfall. Therefore, the cumulative effects of these factors on deterioration must be evaluated. Furthermore, the time-span of the data for these factors depends on the years in-service of the respective bridge. Some values of many time-dependent factors are irregularly observed. In summary, it is essential to properly analyze the inspection database when using the database for predictive maintenance. The method used to analyze the database should be able to: handle problems with many factors, consider the cumulative effects of time-dependent factors, and deal with nonlinear

relationships between factors and deterioration. Conforming to the aforementioned requirements, possible methods are detailed below.

Deterministic and probabilistic models are two kinds of approaches commonly used in predicting deterioration [9]. The former method deals with certain and known variables. Hyman et al. [10] established a piecewise linear regression model to relate deterioration to the age of bridge. Busa et al. [11] used linear regression to conclude that bridge deterioration is significantly affected by age and daily traffic. Abu-Tair [12] discussed the application of the factor method in predicting deterioration and noted that this method is highly subjective. Pan et al. [13] presented a matrix-driven fuzzy linear regression model to predict bridge conditions. Taking a similar method, Kim et al. [14] applied a sigmoid function to nondestructive evaluation data to evaluate the deterioration of a bridge deck. Jeong et al. [15] developed a non-linear regression model for determining the expected service life of a bridge. Although the performance of bridges in their service life can be described by the formulas of deterministic models, these models ignore the uncertainty of deterioration [16].

In addition, some studies have focused on probabilistic models, among which the most used model is the Markov chain (MC) model. Agrawal et al. [16] compared the Markov Chain with the Weibull distribution and concluded the later method would be better. Li et al. [17] and Wellalage et al. [18] used the Markov Chain–based deterioration models to predict bridge conditions. Zambon et al. [19] compared different Markov Chain based stochastic prediction models. He et al. [20] analyzed bridge deterioration by considering multi-factors and divided factors into hazards increased factors and protective factor.

Except for deterministic and probabilistic models, the neural network has been applied to practical maintenance engineering [21-22]. In the application of the neural network to establish a deterioration prediction model, Sobanjo [23] used the inspection records for 50 bridge superstructures to predict bridge deterioration that inputs only the age of the bridge and outputs the deterioration condition of the bridge superstructure. Huang [24] identified eleven significant factors and developed an artificial neural network model to predict the deterioration of bridge decks. Using the same operation, Al-Hussein [9] designed a neural network to estimate the deterioration considering the structure type, component types, exposure environments, and defects. Lim and Chi [25] developed a neural network to predict the number of damage occurrences on bridge decks and their severity, considering identification, structural, inspection, and environmental factors.

Appropriate neural network architectures can be trained using the inspection database to predict future deterioration situations. If the network parameters are appropriately designed, the network can result in satisfactory forecasting performance. One of the best-known neural models is the Multilayer Perceptron (MLP) consisting of an input layer, one or several hidden layers, and an output layer. On the other hand, the Recurrent Neural Network (RNN) is a type of artificial neural network specialized in learning time-related patterns from time-series data. Among the RNNs, Long Short-Term Memory (LSTM) is most widely used, and therefore, was applied in this study. Many studies have applied this method to practical engineering. Jeong et al. [26] used the method to monitor bridge vibrations caused by loads. Wang et al. [27] applied the method to predict the quality problems of structural components in construction projects. Razavi et al. [28] used the model to predict the load deflection of carbon fiber reinforced polymer strengthened reinforced concrete (RC) slab.

According to the aforementioned information, Markov Chain and neural network (including MLP and RNN) are two typical methods used to perform deterioration prediction. These methods are therefore

considered to analyze a censored database of bridges. The MLP and RNN were first compared to determine the optimal neural network model. Then, the optimal neural network is compared with the typical traditional method MC.

However, one problem occurs when applying the neural network to analyze an inspection database toward predicting deterioration of existing bridges to optimize further maintenance strategies. Zhang et al. [29] and Caruana et al. [30] noted that the neural network can give rise to a black box problem. Although the neural network model can predict deterioration under given influencing factors, the prediction model provides only one predicted value without any explanation. This makes it difficult for engineers to trust the prediction, to understand what factors affect the prediction, and to determine targeted intervention. To solve the difficulties, the Shapley value method and the Sobol indices method are applied to the optimal neural network model to determine the contribution of each factor on deterioration by calculating the relative importance of each factor.

1.3.2 Crack identification

Crack detection and quantification are two major challenges for efficiently assessing the severity of cracks [31]. Literature reviews regarding those two aspects will be described below.

Four ways are available to detect cracks from images: manual detection, image processing techniques, feature-based machine learning, and deep learning-based algorithms. Manual detection is usually time consuming and prone to inaccuracy due to inspector fatigue or human error, and is beyond the scope of this study. Study progress on the image processing techniques, feature-based machine learning, and deep learning-based algorithms are detailed below.

Many image processing techniques have been proposed and applied. These techniques include: thresholding [32-33]; original or modified edge detection [34-36]; and filter based methods [37-41]. Thresholding is performed to partition an image into multiple parts or regions based on the characteristics of the pixels in the image. Edge detectors and filter based methods detect crack edges by applying various filters to a grayscale image to emphasize discontinuities. However, image processing techniques cannot cope with the random shape and irregular size of cracks [5]. In addition, the results of these techniques are noticeably influenced by the illumination and distortion of images [42]. Although one de-noising technique has been proposed [43] and applied to a study [44], the usage of this technique is limited as images taken from the real-world vary extensively.

Another approach of crack detection is to use machine learning algorithms [45-50]. These algorithms are performed by evaluating whether the signals collected from non-destructive testing indicate defects. In addition, some researchers combined machine learning algorithms with image processing techniques [51-53]. Specifically, image processing techniques are first used to extract features, and then machine learning algorithms to classify these features. Although machine learning algorithms are introduced in their methods, the results of these methods are inevitably affected by the performance of image processing techniques, as image processing is usually the first step in extracting features from images.

In addition, a recent promising development is the introduction and widespread use of deep learning [54]. As a kind of deep learning, Convolutional Neural Network (CNN) has been emphasized in image recognition, as it does not rely on the expert set threshold, can effectively capture the grid topology of

images, has high accuracy, can distinguish a large number of categories, and is robust to image variations [44, 55-56]. Many studies have been conducted to demonstrate the feasibility of CNN and achieved considerable results. Depending on the level of detail required for prediction, the application of CNN in crack detection can be separated into three categories: image classification, object detection, and semantic segmentation [46]. Image classification uses the sub-image database cropped out from raw images to train a classifier for predicting whether a sub-image is cracked or complete. Target detection classifies targets and mark the range and location of each type of target (e.g., crack). Semantic segmentation is to perform pixel level prediction by classifying each pixel as a crack or an intact pixel.

In terms of image classification: Zhang et al. [57] conducted CNN training on pavement images taken by smartphone, and concluded a remarkable improvement in accuracy relative to machine learning classifiers trained on manual features. Cha et al. [42] trained a CNN classifier to classify images as crack or intact regions with help of a slide window. The accuracy of this classifier on cracks exceeds 98%, i.e., significantly better than the edge detection methods. Eisenbach et al. [58] trained a CNN to detect asphalt crack, and its performance is better than the two baseline models. Gopalakrishnan et al. [59] implemented transfer learning to train a classifier on a combination of asphalt and concrete pavement cracking images, and concluded that pre-trained VGG-16 CNN yielded the optimal performance. Zhang et al. [60] used transfer learning to propose a unified detection model for crack and sealed crack, and presented better performance than the three used benchmarks. Li and Zhao [61] established a CNN model with an accuracy of 99.06%, which is applicable for complicated images, such as thin cracks, rough surface, and shadows.

In terms of object detection: Cha et al. [62] used 2366 sub-images cropped from 297 annotated raw images to train a region-based CNN architecture for detecting five types of damage including concrete cracks. Its average accuracy is 88%. Liu et al. [63] proposed an automatic robot inspection system that using a CNN established by transfer learning as detection for three defects including concrete cracks.

In terms of semantic segmentation: Zhang et al. [64] studied the pixel-level pavement crack detection using the three-dimensional (3D) data (including depth information) from a 3D laser system. The method yields about 90% accuracy, without the capability of detecting hairline cracks. Dorafshan et al. [65] compared the performances of CNN with traditional crack detection methods and concluded that CNN shows significant promise for image-based damage detection in concrete. Fan et al. [66] used a CNN to learn the crack pixels in pavement images. Specifically, the model runs with a fixed-size 27×27 window at every pixel, and then provides a 5×5 pixel as a pixel-level output at the center of that patch. The essential of this approach is same as the image classification CNN. Similarly, Li et al. [67] proposed a pixel-level detection approach by using an 18×18 window centered at that pixel. Alipour et al. [66] reported a pixel-level detector by converting the fully connected layer of the image classification CNN architecture into convolutional filters. Then, features extracted from different order convolutional filters are up-sampled to generate a heat map for providing pixel-level prediction. Input of the model is a pixel annotated dataset. The model over 92% of crack pixels and 99.9% of intact pixels in the validation set. Using a similar method, Ni et al. [68] proposed a framework to combine the features extracted from different order convolutional filters to achieve pixel-level classification. Kang et al. [69] proposed a hybrid method to achieve crack segmentation. Specifically, a faster region proposal convolutional neural network (Faster R-CNN) is applied to detect the crack regions. Then, modified tubularity flow field (TuFF) and modified distance transform method (DTM) are used to segment the crack pixels and quantify crack thickness and length, respectively.

In addition to crack detection, crack quantification is also important for assessing the status of in-service infrastructure and determining corresponding maintenance measures. Further, many researches attempted to correlate detailed crack patterns to the quantitative damage states of concrete beams and panels at different loading stages [70-72].

According to the aforementioned information, the semantic segmentation can not only achieve crack detection but also crack segmentation, making it the optimal approach for detecting cracks. However, semantic segmentation algorithms of Fan et al. [65] and Li et al. [67] are not essentially different from image classification. Although Alipour et al. [56] and Ni et al. [68] achieved real pixel-level detection, crack detection and quantification remains a challenging issue because deep learning training using a database of annotated pixels is time and labor costly.

1.3.3 Building Information Modeling (BIM) platform

Over the past few decades, the building sector has been increasing interest in the use of Building Information Modeling (BIM) due to the many benefits and resource savings in the design, planning, and construction of new buildings [73-77]. In the preliminary stage, the use of BIM is mainly focused on pre-planning, design, construction, and integrated project delivery of buildings and infrastructure. However, in recent years, the research focus has shifted from the early life cycle (LC) phase to maintenance, renovation, demolition, and end-of-life considerations [78, 75, 79-83], especially for complex structures. Potential benefits of using BIM in facility management seem to be significant [79, 84, 85], e.g. management of the valuable documentation [75], maintenance of warranty and service information [79, 84, 86], quality control [87, 88], assessment and monitoring [75, 79, 84], energy and space management [79, 89], emergency management [84] or retrofit planning [90, 84].

Although BIM is suitable for larger and more complex buildings and has been applied to many new buildings [91], there are other challenges to implementing BIM in existing bridges. This challenge occurs mainly because incomplete, obsolete or fragmented building information dominates many existing bridges [79, 92]. Missing or obsolete building information might result in ineffective project management, uncertain process results, and time loss or cost increases in maintenance, retrofit or remediation processes.

As existing buildings often lack as-built documentation due to omitted updating, limitations of using BIM in existing bridges and research challenges are expected. One possible approach is to use information gathered by designers and on-site inspections to build a BIM model that is close to the actual situation.

1.4 Problem statements

(1) Bridge censored databases can be used to analyze and assess structural deterioration conditions, but doing so is difficult because of: (i) many factors affect deterioration; (ii) the time span of the data for these factors depends on the bridge age; and (iii) the values of some factors are not observed on a regular basis.

(2) Bridge deterioration is caused by a variety of factors. However, the connection between factors and deterioration is not clearly defined, nor is the relative influence of each factor on deterioration well recognized.

(3) Crack detection and quantification remains a challenging issue because deep learning training using a database of annotated pixels is time consuming and labor intensive.

(4) In the past, a great deal of damage information on existing bridge components was gathered. However,

intuitive information management is difficult since bridge managers are unable to connect damage information to the corresponding components.

(5) The existing bridge is a sophisticated system that is impacted by materials, surrounding environments, and other factors, i.e., its deteriorating status, crack propagation, and other damages should all be taken into account while doing prediction-based maintenance.

1.5 Research objectives

This work offered in-depth studies on the establishment of the deterioration prediction models utilizing the inspection database. Additionally, sensitivity analysis was performed on the established deterioration model to clarify the causes of deterioration. Furthermore, a crack identification model was established to detect, segment, and quantify cracks from images. Finally, all the developed models were integrated with a developed 3-D prototype model to generate a collaborative Building Information Modeling (BIM) platform. Specifically, the three main objectives for this research were detailed below:

(1) Establishment of the deterioration prediction models considering various influencing factors

Engineers evaluated the deterioration situations of existing bridges as deterioration grades during the inspection. Over time, an inspection database was collected. In addition, the meteorological information and the information regarding traffic vehicles of each bridge can be obtained from the Japan Meteorological Agency (JMA) and the Ministry of Land, Infrastructure, Transport and Tourism (MLIT), respectively. Finally, time series data regarding twelve factors were collected.

The inspection database including twelve potential factors and three deterioration grades were introduced to the Multilayer Perceptron (MLP), Recurrent Neural Network (RNN), and the Markov chain (MC) to establish deterioration prediction models. The MLP and the RNN belong to neural network. They were first compared to select the optimal model for deterioration prediction. RNN was finally confirmed has better performance than MLP. Then, the sensitivity analysis method such as the Shapley value method and the Sobol indices method were applied to the RNN to evaluate the causes for deterioration. In addition, the RNN was further compared with a traditional method MC by the deterioration progresses.

The inspection database, which included twelve possible variables and three degradation grades, was fed into the Multilayer Perceptron (MLP), Recurrent Neural Network (RNN), and Markov chain (MC) models. The MLP and the RNN belong to neural network. They were initially compared in order to choose the optimal model for degradation prediction. RNN has now been proven to outperform MLP in terms of performance. The RNN was then subjected to sensitivity analysis methods such as the Shapley value method and the Sobol indices approach to determine the causes of deterioration. Furthermore, the RNN was compared to a classic technique MC in the predicted deterioration progresses.

(2) Establishment of the crack identification model

Many images with cracks were collected from onsite inspection and indoor experiment. These images were cropped into crack or intact sub-images to generate an image dataset. This dataset can be applied to establish a crack detection classifier using the Convolutional Neural Network (CNN). This classifier is able to detect the image as crack or intact for the new collected image. To support the detection of cracks, a novel sliding window approach (neighborhood scanning) was developed. Additionally, a method for calculating crack widths was presented. Then, an application was developed to integrate the proposed techniques to segment and quantify the crack pixels from the sub-images (detected with crack by the CNN

classifier).

(3) The collaborated BIM platform.

Plenty of inspection information for existing bridges was collected in the past. To intuitively manage the inspection information, the 3-D prototype model of the existing bridges can be built using the onsite collected information and documentation-based information. Then, the 3-D model can be integrated with the models established in previous two objectives to construct a collaborative BIM platform. The crack identification model in this platform can extract the crack pixels and locate these pixels to the corresponding components; the deterioration situations and reasons can be identified by the deterioration prediction model. Five bridges were selected to conduct case studies. The crack pixels generated by the crack identification model were located on the surface of relevant components for the five bridges. Furthermore, the deterioration prediction models were utilized to comprehend future deterioration scenarios and determine the causes of deterioration. Finally, prediction-based maintenance/intervention timing and strategies for these five bridges were proposed.

1.6 Thesis structure

This dissertation is split into seven chapters. The first chapter is an introduction, followed by Chapter 2 on the applied techniques. The considerations for developing the deterioration models and the crack identification model were discussed in Chapters 3 and 4, respectively. In Chapter 5, five bridges were explored as examples to create 3-D models. The models from Chapters 3 and 4 were then intergraded to the 3-D models to build a collaborative BIM platform. This study's practical accomplishments and limitations were explored in Chapter 6. Chapter 7 summarized the findings of this study. Figure 1.2 depicts the framework of this dissertation. Details of each chapter were described below:

Chapter 1 provided the background for this study, including the importance of prediction-based maintenance, the management of existing bridges, and the processing of the inspection information (such as the inspection database and the collected image). Then, literature reviews are broadened from the three points: (1) bridge deterioration prediction; (2) endeavors in crack identification; and (3) building information modeling (BIM). Problem statements and the research objectives are described at the end of this chapter.

Chapter 2 listed the approaches used in this study. Specifically, the Multilayer Perceptron (MLP), the Recurrent Neural Network (RNN), and the Markov chain (MC) are used to analyze the inspection database. To identify the causes of deterioration, the Shapley value technique and Sobol indices are used. The Convolutional Neural Network (CNN) is used to create a classifier to determine if an image is cracked or intact. The cracks are then segmented, extracted, and analyzed using a created application. All of the models are integrated with 3-D models to generate a collaborative BIM platform.

Chapter 3 explained the considerations for establishing the deterioration model. Specifically, an inspection database including twelve potential factors and three deterioration grades is input into the Multilayer Perceptron (MLP) model, Recurrent Neural Network (RNN) model, and the Markov Chain (MC) model to build deterioration prediction models. The sensitivity analysis method is applied to evaluate the causes of deterioration. When establishing the prediction model, the cracking is not considered as a factor, because on the one hand, cracking is a typical kind of deterioration, on the other hand, crack identification model is anticipated to be established to facilitate the processing of onsite collected images.

Chapter 4 included information on the creation and validation of a crack identification model. To determine if an image is cracked or intact, a Convolutional Neural Network (CNN) classifier is initially built. Then, an application is created to segment, extract, and analyze the crack pixels.
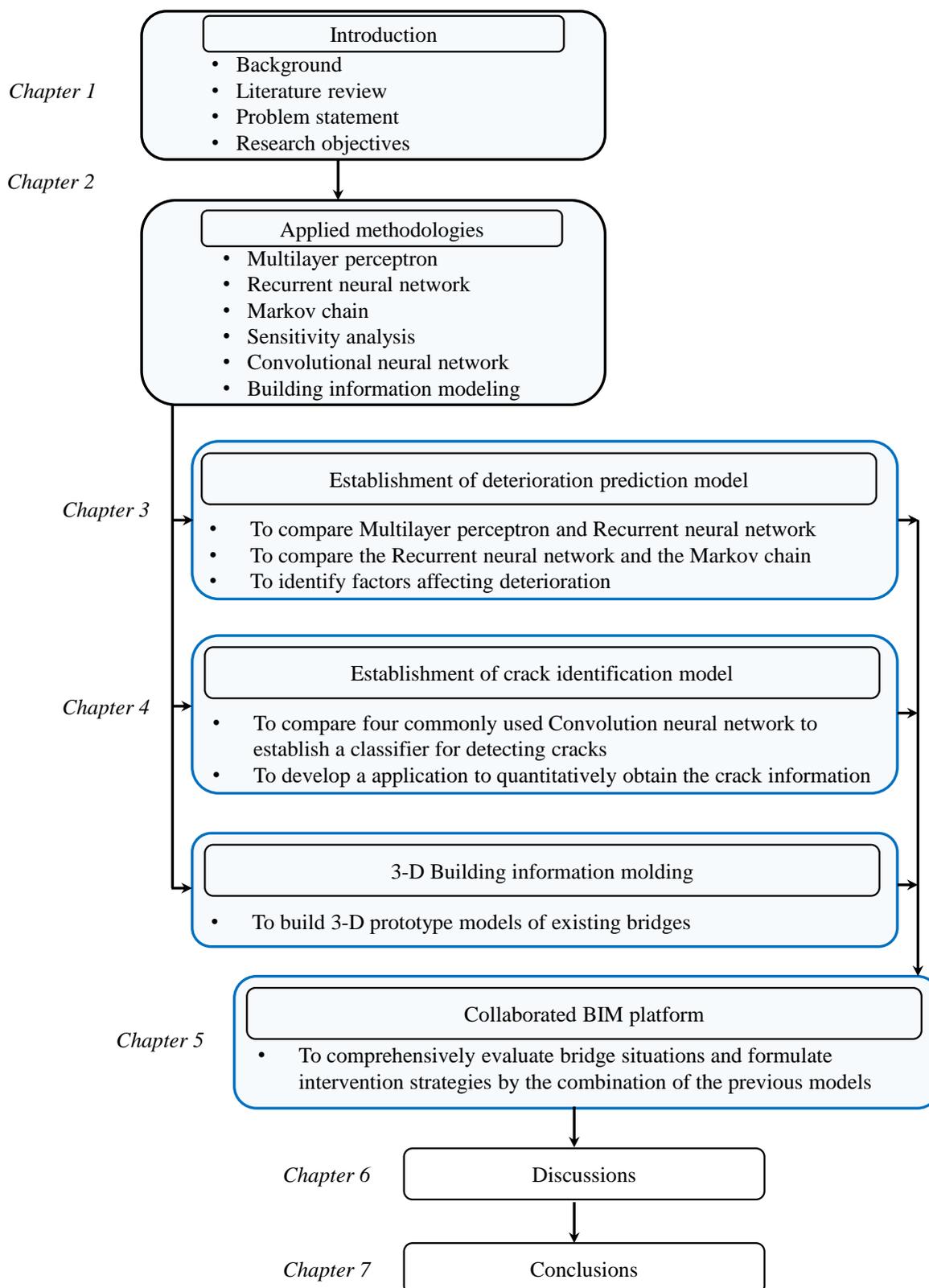
Figure 1.2 Thesis structure

Chapter 5 established and verified a collaborated Building Information Modeling (BIM) platform combined with case studies. Information collected from onsite inspection and documentation is used to build the 3-D prototype models. Then, the 3-D models are integrated with deterioration prediction model and the crack identification model to generate a collaborative BIM platform.

Chapter 6 discussed the achievements and limitations of this study in practical.

Chapter 7 summarized the findings of this study. In addition, the potential research topics are recommended as the future work.

References

[1] Zhang, L., Yang, F., Daniel Zhang, Y., & Zhu, Y. J. (2016). Road crack detection using deep convolutional neural network. Proceedings - International Conference on Image Processing, ICIP, 2016-Augus, 3708–3712. https://doi.org/10.1109/ICIP.2016.7533052

[2] Adhikari, R. S., Moselhi, O., & Bagchi, A. (2014). Image-based retrieval of concrete crack properties for bridge inspection. Automation in Construction, 39(February 2018), 180–194. https://doi.org/10.1016/j.autcon.2013.06.011

[3] Stenström, C., Norrbin, P., Parida, A., & Kumar, U. (2016). Preventive and corrective maintenance– cost comparison and cost–benefit analysis. Structure and Infrastructure Engineering, 12(5), 603-617. doi:10.1080/15732479.2015.1032983

[4] Chandra, R., & Zhang, M. (2012). Cooperative coevolution of Elman Recurrent Neural Networks for chaotic time series prediction. In Neurocomputing (Vol. 86, pp. 116–123). doi: 10.1016/j.neucom.2012.01.014

[5] Wang, P., & Huang, H. (2010). Comparison analysis on present image-based crack detection methods in concrete structures. Proceedings - 2010 3rd International Congress on Image and Signal Processing, CISP 2010, 5, 2530–2533. https://doi.org/10.1109/CISP.2010.5647496

[6] Hada, Y., Nakao, M., Yamada, M., Kobayashi, H., Sawasaki, N., Yoko Ji, K., Kanai, S., Tanaka, F., Date, H., Pathak, S., Yamashita, A., Yamada, M., & Sugawara, T. (2017). Development of a bridge inspection support system using two-wheeled multicopter and 3D modeling technology. Journal of Disaster Research, 12(3), 593–606. https://doi.org/10.20965/jdr.2017.p0593

[7] Tanaka, F., Tsuchida, M., Onosato, M., Date, H., Kanai, S., Hada, Y., Nakao, M., Kobayashi, H., Hasegawa, E., Sugawara, T., & Oyama, T. (2018). Bridge Information Modeling based on IFC for supporting maintenance management of existing bridges. https://icccbe2018.exordo.com/files/papers/149/final_draft/Final_ICCCBE2018_tanaka.pdf

[8] Jeong, S., Ferguson, M., Hou, R., Lynch, J. P., Sohn, H., & Law, K. H. (2019). Sensor data reconstruction using bidirectional Recurrent Neural Network with application to bridge monitoring. Advanced Engineering Informatics, 42(August), 100991. doi: 10.1016/j.aei.2019.100991.

[9] Al-Hussein, Estimating Bridge Deterioration Age Using Artificial Neural Networks (Doctoral dissertation, The British University in Dubai), (2017). https://bspace.buid.ac.ae/handle/1234/1128

[10] W. Hyman, D. Hughes, T. Dobson, The least cost mix of bridge replacement and repair work on Wisconsin's state highways over time—A computer simulation, Technical Rep., WisDOT, Madison,

Wis. (Apr 1983).

[11] G. Busa, M. Ben-Akiva, O. Buyukozturk, Modeling concrete deck deterioration, Department of Civil Engineering, Massachusetts Institute of Technology, Cambridge, Massachusetts. (1985)

[12] Abu-Tair, C. McParland, J. Lyness, A. Nadjai, Predictive models of deterioration rates of concrete bridges using the factor method based on historic inspection data, 9th International Conference on Durability of Building Materials and Components (DBMC). Australia. Brisbane. (March 2002).

[13] N.F. Pan, T.C. Lin, N.H. Pan, Estimating bridge performance based on a matrix-driven fuzzy linear regression model, Automation in construction. 18(5) (2009), 578-586. doi: 10.1016/j.autcon.2008.12.005

[14] J. Kim, N. Gucunski, K. Dinh, Deterioration and Predictive Condition Modeling of Concrete Bridge Decks Based on Data from Periodic NDE Surveys, Journal of Infrastructure Systems. 25(2) (2019), 04019010. doi: 10.1061/(ASCE)IS.1943-555X.0000483

[15] Y. Jeong, W. Kim, I. Lee, J. Lee, Bridge service life estimation considering inspection reliability, KSCE Journal of Civil Engineering. 21(5) (2017), 1882-1893. doi: 10.1007/s12205-016-1042-z

[16] A.K. Agrawal, A. Kawaguchi, Z. Chen, Deterioration rates of typical bridge elements in New York, Journal of Bridge Engineering. 15(4) (2010), 419-429. doi: 10.1061/(ASCE)BE.1943-5592.0000123

[17] L. Li, L. Sun, G. Ning, Deterioration prediction of urban bridges on network level using Markov-Chain model, Mathematical Problems in Engineering. (2014). doi: 10.1155/2014/728107

[18] N.K.W. Wellalage, T. Zhang, R. Dwight, Calibrating Markov Chain–based deterioration models for predicting future conditions of railway bridge elements, Journal of Bridge Engineering. 20(2) (2015) 04014060. doi: 10.1061/(ASCE)BE.1943-5592.0000640

[19] Ivan Zambon, Anja Vidovic, Alfred Strauss, Jose Matos & Joao Amado (2017) Comparison of stochastic prediction models based on visual inspections of bridge decks, Journal of Civil Engineering and Management, 23:5, 553-561, DOI: 10.3846/13923730.2017.1323795

[20] He, X., Wang, W., Hu, W., & Zhang, H. (2020, March). Bridge Deterioration Analysis Based on Censored Data: A Case Study in Yunnan Province. In IOP Conference Series: Materials Science and Engineering (Vol. 787, No. 1, p. 012035). IOP Publishing. https://iopscience.iop.org/article/10.1088/1757-899X/787/1/012035/meta

[21] R.S. Adhikari, O. Moselhi, A. Bagchi, Image-based retrieval of concrete crack properties for bridge inspection, Automation in construction. 39 (2014) 180-194. doi: 10.1016/j.autcon.2013.06.011

[22] O.A. Hodhod, H.I. Ahmed, Developing an artificial neural network model to evaluate chloride diffusivity in high performance concrete, HBRC Journal. 9(1) (2013) 15-21. doi: 10.1016/j.hbrcj.2013.04.001.

[23] J. O. Sobanjo, A neural network approach to modeling bridge deterioration, Computing in Civil Engineering, ASCE. (June.1997) 623-626.

[24] Y.H. Huang, Artificial neural network model of bridge deterioration, Journal of Performance of Constructed Facilities. 24(6) (2010) 597-602. doi: 10.1061/(ASCE)CF.1943-5509.0000124

[25] S. Lim, S. Chi, Bridge Damage Prediction Using Deep Neural Network, Computing in Civil Engineering 2019: Smart Cities, Sustainability, and Resilience. Reston, VA: American Society of Civil Engineers. (2019) 219-225. doi: 10.1061/9780784482445.028

[26] Jeong, S., Ferguson, M., Hou, R., Lynch, J. P., Sohn, H., & Law, K. H. (2019). Sensor data reconstruction using bidirectional Recurrent Neural Network with application to bridge monitoring.

Advanced Engineering Informatics, 42(August), 100991. doi: 10.1016/j.aei.2019.100991.

[27] Wang, D., Fan, J., Fu, H., & Zhang, B. (2018). Research on optimization of big data construction engineering quality management based on RnN-LSTM. Complexity, 2018. https://doi.org/10.1155/2018/9691868

[28] Razavi, S. V., Jumaat, M. Z., El-Shafie, A. H., & Ronagh, H. R. (2015). Load-deflection analysis prediction of CFRP strengthened RC slab using RNN. Advances in Concrete Construction, 3(2), 91–102. doi:10.12989/acc.2015.3.2.091

[29] Z. Zhang, M.W. Beck, D.A. Winkler, B. Huang, W. Sibanda, H. Goyal, Opening the black box of neural networks: methods for interpreting neural network models in clinical applications, Annals of translational medicine. 6(11) (2018). doi: 10.21037/atm.2018.05.32

[30] R. Caruana, Y. Lou, J. Gehrke, P. Koch, M. Sturm, N. Elhadad, Intelligible models for healthcare: Predicting pneumonia risk and hospital 30-day readmission, Proceedings of the 21st ACM SIGKDD International Conference on Knowledge Discovery and Data Mining. (2015) 1721-1730. ACM. doi: 10.1145/2783258.2788613

[31] Adhikari, R. S., Moselhi, O., & Bagchi, A. (2012). Image-based retrieval of concrete crack properties. 39(June), 180–194. https://doi.org/10.1016/j.autcon.2013.06.011

[32] Oliveira, H., and P. L. Correia. 2009. "Automatic road crack segmenta- tion using entropy and image dynamic thresholding." In Proc., 17th European Signal Processing Conf. New York: IEEE.

[33] Zou, Q., Y. Cao, Q. Li, Q. Mao, and S. Wang. 2012. "CrackTree: Automatic crack detection from pavement images." Pattern Recog. Lett. 33 (3): 227–238. https://doi.org/10.1016/j.patrec.2011.11.004.

[34] Abdel-Qader, I., O. Abudayyeh, and M. E. Kelly. 2003. "Analysis of edge-detection techniques for crack detection in bridges." J. Com- put. Civ. Eng. 17 (4): 255–263. https://doi.org/10.1061/(ASCE)0887 -3801(2003)17:4(255).

[35] Alaknanda, Anand, R. S. & Kumar, P. (2009), Flaw detection in radiographic weldment images using morphological watershed segmentation technique, NDT & E International, 42(1), 2–8.

[36] Nishikawa, T., Yoshida, J., Sugiyama, T. & Fujino, Y. (2012), Concrete crack detection by multiple sequential image fil- tering, Computer-Aided Civil and Infrastructure Engineering, 27(1), 29–47.

[37] Frangi, A. F., Niessen, W. J., Hoogeveen, R. M., Van Walsum, T. & Viergever, M. A. (1999), Model-based quantitation of 3-D magnetic resonance angiographic images, IEEE Trans- actions on Medical Imaging, 18(10), 946–56.

[38] Wang, K., Q. Li, and W. Gong. 2007. "Wavelet-based pavement dis- tress image edge detection with à trous algorithm." Transp. Res. Rec. 2007 (1): 73–81. https://doi.org/10.3141/2024-09.

[39] Ying, L., and E. Salari. 2010. "Beamlet transform-based technique for pavement crack detection and classification." Comput.-Aided Civ. Infrastruct. Eng. 25 (8): 572–580. https://doi.org/10.1111/j.1467-8667 .2010.00674.x.

[40] Zalama, E., J. G´omez-García-Bermejo, R. Medina, and J. Llamas. 2014. "Road crack detection using visual features extracted by Gabor filters." Comput.-Aided Civ. Infrastruct. Eng. 29 (5): 342–358. https://doi.org /10.1111/mice.12042.

[41] Yeum, C. M., and S. J. Dyke. 2015. "Vision-based automated crack detection for bridge inspection." Comput.-Aided Civ. Infrastruct. Eng. 30 (10): 759–770. https://doi.org/10.1111/mice.12141.

[42] Cha, Y. J., Choi, W., & Büyüköztürk, O. (2017). Deep Learning-Based Crack Damage Detection Using Convolutional Neural Networks. Computer-Aided Civil and Infrastructure Engineering, 32(5), 361–378. https://doi.org/10.1111/mice.12263

[43] Rudin, L. I., Osher, S. & Fatemi, E. (1992), Nonlinear total variation based noise removal algorithms, PhysicaD:Non- linear Phenomena, 60(1–4), 259–68.

[44] Cha, Y.-J., You, K. &Choi, W. (2016), Vision-based detection of loosened bolts using the Hough transform and support vector machines, Automation in Construction, 71(2), 181– 88. https://doi.org/10.1016/j.autcon.2016.06.008

[45] LeCun, Y., Bottou, L., Bengio, Y. & Haffner, P. (1998), Gradient-based learning applied to document recognition, in Proceedings ofthe IEEE, 2278–324.

[46] Liu, S. W., Huang, J. H., Sung, J. C. & Lee, C. C. (2002), De- tection of cracks using neural networks and computational mechanics, Computer Methods in Applied Mechanics and Engineering, 191(25–26), 2831–45.

[47] Jiang, X. & Adeli, H. (2007), Pseudospectra, MUSIC, and dynamic wavelet neural network for damage detection of highrise buildings, International Journal for Numerical Methods in Engineering, 71(5), 606–29.

[48] Butcher, J., Day, C., Austin, J., Haycock, P., Verstraeten, D. & Schrauwen, B. (2014), Defect detection in reinforced con- crete using random neural architectures, Computer-Aided Civil and Infrastructure Engineering, 29(3), 191–207.

[49] Prasanna, P., K. J. Dana, N. Gucunski, B. B. Basily, H. M. La, R. S. Lim, and H. Parvardeh. 2016. "Automated crack detection on concrete bridges." IEEE Trans. Autom. Sci. Eng. 13 (2): 591–599. https://doi.org /10.1109/TASE.2014.2354314.

[50] Shi, Y., L. Cui, Z. Qi, F. Meng, and Z. Chen. 2016. "Automatic road crack detection using random structured forests." IEEE Trans. Intell. Transp. Syst. 17 (12): 3434–3445. https://doi.org/10.1109/TITS.2016.2552248.

[51] Lattanzi, D., and G. R. Miller. 2012. "Robust automated concrete damage detection algorithms for field applications." J. Comput. Civ. Eng. 28 (2): 253–262. https://doi.org/10.1061/(ASCE)CP.1943-5487.0000257.

[52] Oliveira, H., and P. L. Correia. 2013. "Automatic road crack detection and characterization." IEEE Trans. Intell. Transp. Syst. 14 (1): 155–168. https://doi.org/10.1109/TITS.2012.2208630.

[53] Wu, L., Mokhtari, S., Nazef, A., Nam, B. & Yun, H.-B. (2014), Improvement of crack-detection accuracy using a novel crack defragmentation technique in image-based road as- sessment, Journal ofComputing in Civil Engineering, 30(1), 04014118-1 to 04014118-19.

[54] Ahmadlou, M. & Adeli, H. (2010), Enhanced probabilistic neural network with local decision circles: a robust classifier, Integrated Computer-Aided Engineering, 17(3), 197– 210.

[55] Krizhevsky, A., Sutskever, I. & Hinton, G. E. (2012), Imagenet classification with deep convolutional neural net- works, Advances in Neural Information Processing Systems, 1097–105.

[56] Alipour, M., Harris, D. K., & Miller, G. R. (2019). Robust Pixel-Level Crack Detection Using Deep Fully Convolutional Neural Networks. Journal of Computing in Civil Engineering, 33(6), 1–14. https://doi.org/10.1061/(ASCE)CP.1943-5487.0000854

[57] Zhang, L., Yang, F., Daniel Zhang, Y., & Zhu, Y. J. (2016). Road crack detection using deep convolutional neural network. Proceedings - International Conference on Image Processing, ICIP, 2016-Augus, 3708–3712. https://doi.org/10.1109/ICIP.2016.7533052

[58] Eisenbach, M., R. Stricker, D. Seichter, K. Amende, K. Debes, M. Sesselmann, D. Ebersbach, U. Stoeckert, and H.-M. Gross. 2017. "How to get pavement distress detection ready for deep learning? A systematic approach." In Proc., Int. Joint Conf. on, Neural Networks (IJCNN). New York: IEEE.

[59] Gopalakrishnan, K., S. K. Khaitan, A. Choudhary, and A. Agrawal. 2017. "Deep convolutional neural networks with transfer learning for computer vision-based data-driven pavement distress detection." Constr. Build. Mater. 157 (Dec): 322–330. https://doi.org/10.1016/j .conbuildmat.2017.09.110.

[60] Zhang, K., H. Cheng, and B. Zhang. 2018. "Unified approach to pavement crack and sealed crack detection using preclassification based on transfer learning." J. Comput. Civ. Eng. 32 (2): 04018001. https://doi.org/10 .1061/(ASCE)CP.1943-5487.0000736.

[61] Li, S., & Zhao, X. (2019). Image-Based Concrete Crack Detection Using Convolutional Neural Network and Exhaustive Search Technique. Advances in Civil Engineering, 2019(Ml). https://doi.org/10.1155/2019/6520620

[62] Cha, Y. J., W. Choi, G. Suh, S. Mahmoudkhani, and O. Büyüköztürk. 2017b. "Autonomous structural visual inspection using region-based deep learning for detecting multiple damage types." Comput.-Aided Civ. Infrastruct. Eng. 33 (9): 731–747.

[63] Liu, L., R.-J. Yan, V. Maruvanchery, E. Kayacan, I.-M. Chen, and L. K. Tiong. 2017. "Transfer learning on convolutional activation feature as applied to a building quality assessment robot." Int. J. Adv. Rob. Syst. 14 (3): 1729881417712620. https://doi.org/10.1177/17298814177 12620.

[64] Zhang, A., Wang, K. C., Li, B., Yang, E., Dai, X., Peng, Y., ... & Chen, C. (2017). Automated pixel-level pavement crack detection on 3D asphalt surfaces using a deep-learning network. Computer-Aided Civil and Infrastructure Engineering, 32(10), 805-819.   https://doi.org/10.1111/mice .12297.

[65] Dorafshan, S., Thomas, R. J., & Maguire, M. (2018). Comparison of deep convolutional neural networks and edge detectors for image-based crack detection in concrete. Construction and Building Materials, 186, 1031–1045. https://doi.org/10.1016/j.conbuildmat.2018.08.011

[66] Fan, Z., Y. Wu, J. Lu, and W. Li. 2018. "Automatic pavement crack detec- tion based on structured prediction with the convolutional neural network." Preprint, submitted February 1, 2018. http://arXiv.org/1802 .02208.

[67] Li, Y., H. Li, and H. Wang. 2018. "Pixel-wise crack detection using deep local pattern predictor for robot application." Sensors 18 (9): 3042. https://doi.org/10.3390/s18093042.

[68] Ni, F. T., Zhang, J., & Chen, Z. Q. (2019). Pixel-level crack delineation in images with convolutional

feature fusion. Structural Control and Health Monitoring, 26(1), 1–18. https://doi.org/10.1002/stc.2286

[69] Kang, D., Benipal, S. S., Gopal, D. L., & Cha, Y. J. (2020). Hybrid pixel-level concrete crack segmentation and quantification across complex backgrounds using deep learning. Automation in Construction, 118, 103291. https://doi.org/10.1016/j.autcon.2020.103291

[70] Davoudi, R., G. R. Miller, and J. N. Kutz. 2017. "Computer vision based inspection approach to predict damage state and load level for RC members." In Proc., 11th Int. Workshop on Structural Health Monitoring. Stanford, CA: Stanford Univ.

[71] Davoudi, R., G. R. Miller, and J. N. Kutz. 2018a. "Data-driven vision-based inspection for reinforced concrete beams and slabs: Quantitative damage and load estimation." Autom. Constr. 96 (Dec): 292–309. https://doi.org/10.1016/j.autcon.2018.09.024.

[72] Davoudi, R., G. R. Miller, P. Calvi, and J. N. Kutz. 2019. "Computer vision based inspection approach to predict damage state and load level for RC members." Comput. Civ. Eng. https://doi.org/10.12783/shm 2017/14225.

[73] M. Nepal, S. Staub-French, J. Zhang, M. Lawrence, R. Pottinger, Deriving construc- tion features from an IFC model, Proceedings of the CSCE 2008 Annual Conference, Quebec, Canada, 2008.

[74] F. Leite, A. Akcamete, B. Akinci, G. Atasoy, S. Kiziltas, Analysis ofmodeling effort and impact of different levels of detail in building information models, Autom. Constr. 20 (2011) 601–609.

[75] Teicholz Eastman, Liston Sacks, BIM Handbook — a guide to Building Information Modeling for owners, managers, designers, engineers and contractors, Aufl,2, Wiley, Hoboken, 2011.

[76] M. Gray, J. Gray, M. Teo, S. Chi, F. Cheung, Building Information Modeling, An Inter- national Survey, Brisbane, Australia, 2013.

[77] D. Bryde, M. Broquetas, J.M. Volm, The project benefits of Building Information Modeling (BIM), Int. J. Proj. Manag. 31 (2013) 971–980.

[78] A. Akbarnezhad, K. Ong, L. Chandra, Z. Lin, Economic and environmental assessment of deconstruction strategies using Building Information Modeling, Proceedings of Construction Research Congress 2012: Construction Challenges in a Flat World, West Lafayette, USA, 2012, pp. S. 1730–S. 1739.

[79] B. Becerik-Gerber, F. Jazizadeh, N. Li, G. Calis, Application areas and data requirements for BIM-enabled facilities management, J. Constr. Eng. Manag. 138 (2012) 431–442.

[80] C. Nicolle, C. Cruz, Semantic Building InformationModel andmultimedia for facility management, Web Information Systems and Technologies, Lecture Notes in Budiness Information Processing2011. S. 14–S. 29.

[81] L. Sabol, Building InformationModeling&FacilityManagement, Design+Construction Strategies, Washington, 2008.

[82] J. Lucas, T. Bulbul, W. Thabet, An object-oriented model to support healthcare facility information management, Autom. Constr. 31 (2013) 281–291.

[83] B. Becerik-Gerber, S. Rice, The perceived value of Building Information Modeling in the U.S. building industry, ITcon 15 (2010) 185–201.

[84] Y. Arayici, Towards building information modelling for existing structures, Struct. Surv. 26 (2008) 210–222.

[85] A. Akcamete, B. Akinci, J.H. Garrett Jr., Potential utilization of building models for planning maintenance activities, Proceedings of the International Conference on Computing in Civl and Building Engineering (ICCCBE), Nottingham, Britain, 2010.

[86] V. Singh, N. Gu, X. Wang, A theoretical framework of a BIM-based multi- disciplinary collaboration platform, Autom. Constr. 20 (2011) 134–144.

[87] F. Boukamp, B. Akinci, Automated processing of construction specifications to support inspection and quality control, Autom. Constr. 17 (2007) 90–106.

[88] B. Akinci, F. Boukamp, C. Gordon, D. Huber, C. Lyons, K. Park, A formalism for utili- zation of sensor systems and integrated project models for active construction quality control, Autom. Constr. 15 (2006) 124–138

[89] Y.S. Cho, S. Alaskar, T. Bode, BIM-integrated sustainable material and renewable energy simulation, Proceedings ofCRC2010, Banff, Canada, 2010, pp. S. 288–S. 297.

[90] T. Mill, A. Alt, R. Liias, Combined 3D building surveying techniques — terrestrial laser scanning (TLS) and total station surveying for BIM data management purposes, J. Civ. Eng. Manag. (2013)(iFirst 1-10, Published online: 24 Oct 2013)

[91] Volk, R., Stengel, J., & Schultmann, F. (2014). Building Information Modeling (BIM) for existing buildings - Literature review and future needs. Automation in Construction, 38, 109–127. https://doi.org/10.1016/j.autcon.2013.10.023

[92] I. Gursel, S. Sariyildiz, Ö. Akin, R. Stouffs, Modeling and visualization of lifecycle building performance assessment, Adv. Eng. Inform. 23 (2009) 369–417

Chapter 2

Applied methodologies

2.1 Overview

Figure 2.1 depicts this chapter's outline. The techniques employed in this study are depicted by the red-dashed boxes. Specifically, the inspection database, which included twelve influencing elements and three deterioration grades, was put into the Multilayer Perceptron (MLP), Recurrent Neural Network (RNN), and Markov Chain (MC) to develop deterioration prediction models. Then, sensitivity analysis methods, such as the Shapley value method and the Sobol indices method, were applied to make clear the reasons for deterioration.

As another main work, the images collected from experiment and onsite inspection were introduced into a Convolutional Neural Network (CNN) to establish a classifier to determine whether an image was cracked or intact. Following that, the cracked pictures were forced through the created application to segment, extract the crack pixels, and analyze the cracks.

Some model assessment indexes were presented in Section 2.8 in order to get the deterioration prediction models and the crack identification model.
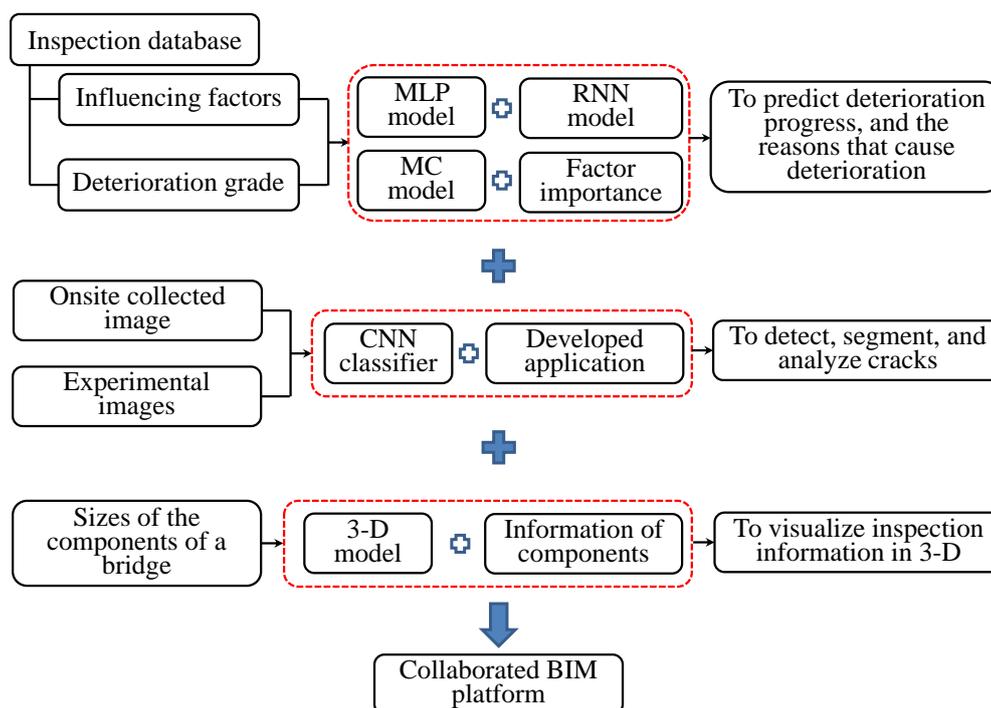
Figure 2.1 Outline of Chapter 2

To manage the inspection information in 3-D and visualize the damage of each component of a bridge, the 3-D prototype model of the existing bridge was built.

Then, the deterioration prediction model, the crack identification model and the 3-D model were combined to build a collaborative Building Information Modeling (BIM) platform. This platform can be used as a

supplementary tool to assist the managers in evaluating the conditions of existing bridges and developing appropriate intervention plans. These topics will be discussed in further depth below.

2.2 Mathematical representation

The inspection database was first converted into vectors in chronological order to represent data of potential factors as computable sequences. Supposing M factors are considered, the vector of those factors for a bridge can be expressed as:

$$x = [f_1 \, f_2 \, f_3 \, \cdots f_M]'$$
(1)

In practical calculation, bias f_0 (similar to the intercept of a linear equation), is needed to improve the accuracy of the model. Therefore, Equation (1) can be expanded as:

$$x = [f_0 \, f_1 \, f_2 \, f_3 \, \cdots f_M]'$$
(2)

Equation (2) indicates the values of these factors at a time t, specifically shown as:

$$x_t = [f_{t,0}, f_{t,1}, f_{t,2}, \dots, f_{t,M}]'$$
(3)

Suppose T observations were collected for each factor of a bridge, the factors and deterioration situation are represented as $B_d = (X; y)$. X is the input that consists of M factors, and y is the output indicating the deterioration grades. The input is arranged as:

$$X = [x_1, x_t, \dots, x_T] = \begin{bmatrix} f_{1,0} & f_{2,0} & f_{t,0} & \cdots & f_{T,0} \\ f_{1,1} & f_{2,1} & f_{t,1} & \cdots & f_{T,1} \\ \vdots & \vdots & \vdots & \ddots & \vdots \\ f_{1,M} & f_{2,M} & f_{t,M} & \cdots & f_{T,M} \end{bmatrix}$$
(4)

$f_{t,m}$ is the observed/measured value at time t for the m-th factor.

The matrix X only represents the time series for one bridge. Assuming K bridges are included in the inspection database, a corresponding matrix $X_k (k = 1, 2, \dots, K)$ with the same dimension M but a different length T_k will be obtained for each bridge. Therefore, the database can be expressed as:

$$D = [X_k; \, y_k] \, (k = 1, 2, \dots, K)$$
(5)

Since different factors are measured on separate scales, their values must be modified to a common scale to increase the efficiency of the training process. Therefore, each factor's value is normalized within 0–1 using:

$$f_{t,m} = \frac{f_{t,m} - \min(|f_{t,m}|)}{\max(|f_{t,m}|) - \min(|f_{t,m}|)}$$
(6)

where $\min(|f_{t,m}|)$ and max $(|f_{t,m}|)$ are, respectively, the minimum and the maximum of the input data $f_{t,m}$ among K total target bridges.

2.3 Multilayer Perceptron (MLP) model

Appropriate neural network architectures can be trained on the inspection databases to predict the future values of the dependent variables [1]. The noteworthy characteristic of a neural network is its learning ability. During the establishment of a neural network model, the network processes the inputs and produces an output, compares the output to the ideal answer, and calculates the errors. Then the parameters of connections (W_1 and W_2 in Figure 2.2) are updated according to the errors. If the network paradigm and parameters are appropriately designed, satisfactory predictive performance can be produced. One of the

best-known neural networks is the Multilayer Perceptron (MLP). For existing bridges, a neural network can assist maintenance work by establishing the relationships between the potential factors and the deterioration grades to predict the future deterioration.
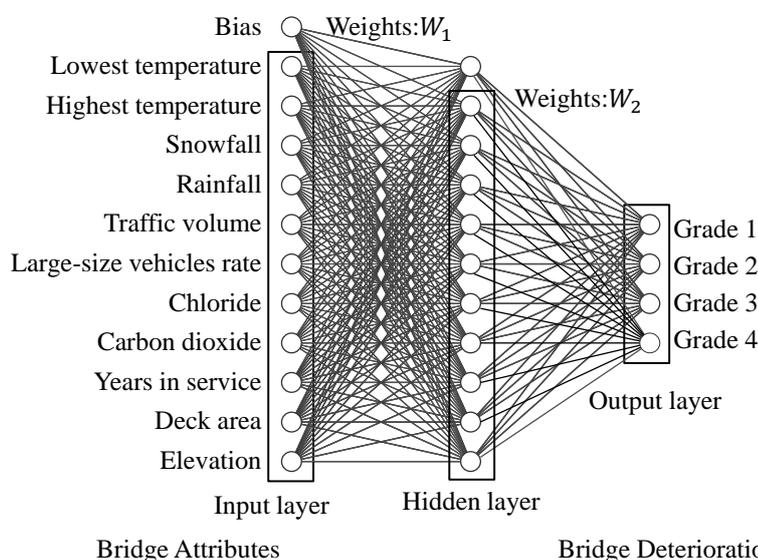
Figure 2.2 Configuration of a neural network used for prediction

Given the neural network's learning capacity, it may be used to establish the optimal connections between potential factors and deterioration grades. A neural network typically consists of an input layer, one or more hidden layers, and an output layer [2].

The input layer receives data and is made up of many neurons (Figure 2.2). The number of neurons is the same as the number of potential factors. As described in Section 2.2, if *M* factors are considered, the mean value of each factor among the *T* observations constitutes a vector that serves as the input of MLP.

It is simple to create a linear model between independent and dependent variables using linear regression/training the neural network. For the linear model, the hidden layer is unnecessary. However, nonlinear problems are usually encountered. Fortunately, a feed forward network with a linear input layer and at least one hidden layer with any activation function (such as the Softmax, Relu, and Tanh) can handle nonlinear issues if enough hidden neurons are provided. The feed forward network's derivatives can also well approximate the derivatives of any arbitrary function [2]. The activation function defines the output given an input. Guliyev and Ismailov [3] gave rich examples of the activation function used in a neural network.

The rules for setting the specific number of hidden layers and their neurons remain unknown. Setting the hidden layer configuration, however, may follow the guidelines for almost all problems: (i) one hidden layer; and (ii) the number of neurons in that layer are between the sizes of the input and output [2].

As the starting weight values are set at random during training, the predicted grades are frequently discordant with the actual grades. Therefore, cross-entropy defined by Equation (7) was used to evaluate the error between the predicted grade $\hat{Y}$ and the actual grade Y. N_s is the number of samples, C is the number of classes, η_j denotes the weight for class j to deal with sample imbalance, and p_j represents the probability that a sample belongs to class j. If a sample belongs to class j, $y_j = 1$, otherwise $y_j = 0$.

$$Cross\ entropy = -\sum_{i=1}^{N_s}\sum_{j=1}^{C}\eta_j\,y_j\,log(p_j) \tag{7}$$

Afterwards, the derivatives of the cross-entropy value are allocated to the parameter matrices of W_2 and W_1 to update their values by Equations (8) and (9), respectively.

$$W_2 = W_2 - \alpha_2\frac{\partial Cross\_entropy}{\partial W_2} \tag{8}$$

$$W_1 = W_1 - \alpha_1\frac{\partial Cross\_entropy}{\partial W_1} \tag{9}$$

where α_1 and α_2 are the learning rate coefficients. To obtain the optimal results, the above procedures will be iterated to minimize the cross-entropy value.

In our situation, we may use an MLP model to connect possible factors and deterioration grades. By incorporating fresh inspection data and updating the prediction model on a regular basis, the model will be constantly improved. As a result, two parameter matrices W_2 and W_1 will be calculated, representing the whole connection between the input and the output. The model does not offer precise deterioration forecasts, but it may be used as a supplement to design bridge maintenance strategies. However, the correlations are difficult to grasp since these two matrices represent the complex nonlinear computation. Thus, the neural network is reduced to the status of a black box. The sensitivity approaches will be applied to offer insights to understand the prediction model in Section 2.5.

2.4 Recurrent Neural Network (RNN) model

As previously stated, the MLP can build relationships between the deterioration grades and the influencing factors. However, The time-dependence of some factors' time series cannot be addressed adequately. Recurrent Neural Network (RNN) is another type of neural network specialized in learning time-related patterns from time-series data. Therefore, the RNN is introduced to perform feasiablity research.
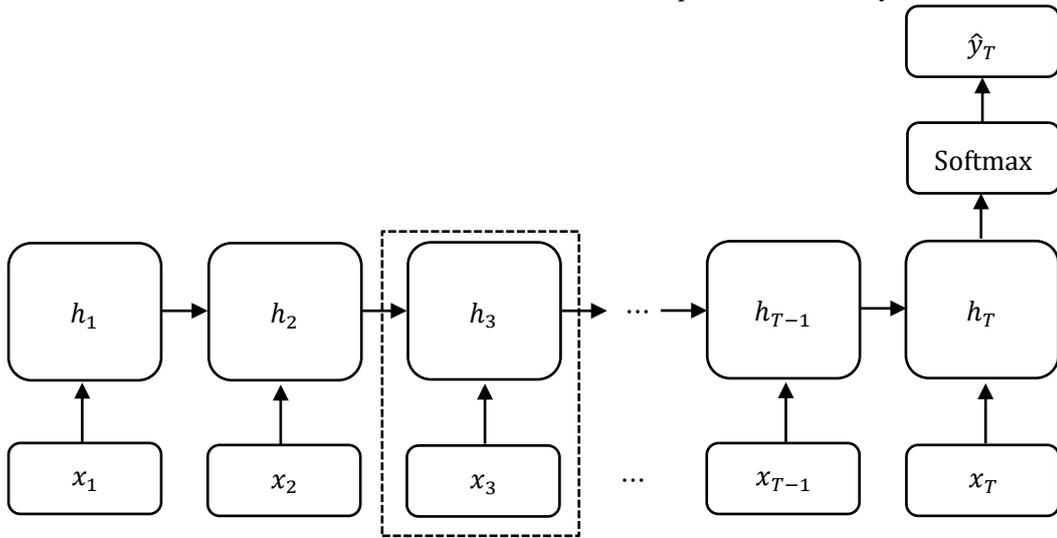
Figure 2.3 A schematic RNN model for deterioration prediction

Among all RNNs, Long Short-Term Memory (LSTM) [4] and Gated Recurrent Units (GRUs) [5] are most commonly used. GRU is structurally similar to, but less complicated than, LSTM. The model used for

deterioration prediction in this study is an LSTM-based RNN, as illustrated in Figure 2.3. The LSTM accepts an input vector x_t at time step t and stores the state of the input in the hidden layer h_t. To classify input data, it is necessary to have a layer for predicting grades, which is usually located at the end of the LSTM architecture. The most prominent method to date is using the softmax activation function. After the entire inspection time series is input into the LSTM, the softmax activation function is applied to the final hidden layer h_T and produces a value $\hat{y}_T$. $\hat{y}_T$ is the estimated deterioration grade for a bridge. In other words, an LSTM-based RNN provides a neural network with a memory function, enabling the neural network to achieve good modeling ability on time series data [6].
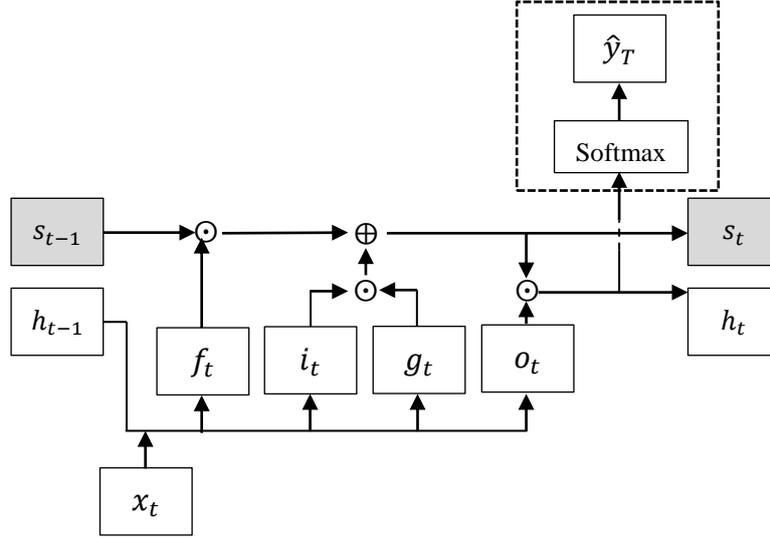
Figure 2.4 Configuration of the LSTM unit

The dashed box of Figure 2.3 refers to the LSTM unit used for processing current and prior information. The detailed components of the dashed box in Figure 2.3 are shown in Figure 2.4. The update and usage of cumulative information are controlled by three gates: the input gate i_t, the forget gate f_t, and the output gate o_t [6]. s_t, g_t and h_t are the state memory cell, input candidate memory cell and hidden layer, respectively [7]. The calculation of all gates is affected by both the current input x_t and the output of the previous LSTM cell h_{t-1}. The input gate is applied to process the impact of the current input on the status of the memory cell s_t. The forget gate is used to control the influence of cumulative information on the memory cell s_t. The output gate is applied to control the status value of the memory cell s_t. The mathematical formulation of Figure 2.4 and the update of the LSTM unit can be divided into the following steps [4]:

(1) Calculate the value of the current candidate memory cell g_t.

$$g_t = \tanh(W_{gx}x_t + W_{gh}h_{t-1} + b_g) \tag{10}$$

(2) Calculate the value of the input gate i_t.

$$i_t = \text{sigmoid}(W_{ix}x_t + W_{ih}h_{t-1} + b_i) \tag{11}$$

(3) Compute the value of the forget gate f_t.

$$f_t = \text{sigmoid}(W_{fx}x_t + W_{fh}h_{t-1} + b_f) \tag{12}$$

(4) Calculate the state value s_t of the current memory cell.

$$s_t = g_t \odot i_t + s_{t-1} \odot f_t \tag{13}$$

(5) Calculate the value of the output gate o_t.

$$o_t = \text{sigmoid}(W_{ox}x_t + W_{oh}h_{t-1} + b_o) \tag{14}$$

(6) Calculate the value of the current hidden layer h_t.

$$h_t = \tanh(s_t) \odot o_t \tag{15}$$

(7) The output of the last LSTM unit is shown by the dashed part of Fig.3 and is calculated by:

$$\hat{y}_T = \text{softmax}(h_T) \tag{16}$$

In these equations, the tanh, sigmoid, and softmax are three commonly used activation functions in the field of deep learning [4]. W and b are the parameters for calculating the three gates. In LSTM, the previous hidden layer h_{t-1} and the current input x_t do not directly affect the value of the current hidden layer h_t. Instead, they change the values for gates i_t, f_t, and o_t and the intermediate memory cell s_t. Then, the current hidden layer h_t is determined by s_t and o_t. In the calculation for s_t and h_t, $\odot$ denotes elementwise multiplication. All three gates have values between zero and one: zero means the information stored in the gate is ignored, and one means the information is accumulated and passed to the next calculation. The architecture of the three gates and separate memory cells enables the LSTM unit to save, read, reset, and update long-distance cumulative information. These characteristics of LSTM are especially useful because LSTM can process non-linear problems with many factors [8]. In addition, the cumulative effects caused by the time-dependent factors can be appropriately solved using the functions of the three gates.

As the initial values of W are randomly assigned during training, the predicted and actual classes do not usually coincide. To calculate the amount of deviations between the predicted and actual classes, the loss function is defined by Equation (17).

$$L(\hat{y}_T, y) = \frac{1}{T}\sum_{t=1}^{t=T} -(y_t \cdot \log(\hat{y}_t) + (1 - y_t) \cdot \log(1 - \hat{y}_t)) \tag{17}$$

The update of the weights is achieved using a Stochastic Gradient Descent (SGD) approach. In addition, a momentum algorithm was combined with the SGD to accelerate the convergence process of the training. The gradient $\nabla_W L$ of loss function is calculated with respect to W at time t. Then the velocity V_{t+1} in Equation (18) is updated ($\leftarrow$) by combination of the previous velocity V_t and the gradient $\nabla_W L$, where momentum μ and learning rate α are two parameters [9]. Finally, the W are updated using Equation (19).

$$V_{t+1} \leftarrow \mu V_t - \alpha \nabla_W L \tag{18}$$

$$W_{t+1} \leftarrow W_t + V_{t+1} \tag{19}$$

The optimal model is determined by iteratively updating the model's parameters until the minimum error is obtained.

2.5 Confirmation of factors affecting deterioration

Sensitivity analysis can be applied to overcome the uncertainty of factors on deterioration, because it can tell engineers what factors affect the deterioration and their relative importance. A prediction can be explained by assuming that each factor is a "player" in a game where the prediction is the "payout". Shapley values method tells how to fairly distribute the "payout" among the factors [10]. Next, the Shapley

value method was briefly introduced. The set of M potentially influencing factors is represented by $N = \{x_1, x_2, \dots x_M\}$, and any permutation S of N is a coalition. The characteristic function v maps all permutations to "payout", which in our case is the deterioration grade. The function v has the following definitions: if S is a permutation (coalition) of all factors; then $v(S)$ describes the total impact of all factors in coalition S [11]. The value of $v(S)$ is determined by inputting S in the prediction model.

The importance $\varphi_i(v)$ of factor x_i is determined as follows:

$$\varphi_i(v) = \sum_{S \subseteq N/\{i\}} \frac{(M - |S| - 1)! \, |S|!}{M!} (v(S \cup \{x_i\}) - v(S)) \tag{20}$$

where M is the total number of factors. The sum extends over all subsets S of N excluding factor x_i. The formula can be interpreted as follows: the contribution of factor x_i in S is $v(S \cup \{x_i\}) - v(S)$; the average of this contribution over the possible permutations is the final contribution of this factor. In our case, $\varphi(v)$ refers to the deterioration grade, and is indicated as:

$$\varphi(v) = \sum_{i}^{M} \varphi_i(v) \tag{21}$$

The Shapley value method can calculate the relative importance of each factor, regardless of the complexity of the prediction model. Therefore, it can explain any prediction model [11]. Specifically, the calculated importance is related to the magnitude of difference in prediction results when a factor is considered (such as bridge width) versus when it is not considered (such as when bridge width is unknown) [12]. In summary, the Shapley value method identifies all factors and evaluates their relative importance, enabling an engineer to identify factors that significantly influence the deterioration and to formulate a matching intervention strategy. This is an important step towards putting the neural network to practical maintenance because the sensitivity analysis converts abstract and inexplicable predictions into the relative importance of factors that are easy for engineers to understand and act on.

Except for the Shapley value method, Sobol indices [13] is another useful method to detect the sensitivity of predictions to inputs. In this study, these two methods will be compared by using an actual case in the Section 3.6. Conforming to the descriptions of these two methods, we present the specific steps to perform the sensitivity analysis of the predictions. Given values of factors, the predicted grades of a bridge can be obtained (Section 3.4), with some predictions being successful (i.e., the same grade as that evaluated by the engineer) and the rest being unsuccessful. All correctly predicted bridges are extracted to create a new database, because failed predictions may result in inaccurate importance estimations. The Shapley value and Sobol indices approaches are applied to the new database to determine the sensitivity of the prediction model to each factor.

2.6 Markov Chain (MC) model

The MLP and the RNN are two neural network techniques. Aside from the neural network, the Markov Chain (MC), an typically probabilistic approach, was utilized to predict the deterioration progresses of bridges. To establish a MC model, a hazard model with exponential distribution was first formulated. The MC was then used to infer transition probability. Finally, maximum likelihood estimation was performed to determine the optimal parameters based on the censored database. These three parts were detailed below.

2.6.1 Hazard model formulation

To estimate the deterioration conditions of a bridge, the censored data on this bridge is necessary. Figure 2.5 illustrates the deterioration progress of a bridge. In this section, the problem of bridge deterioration is mathematically formulated.
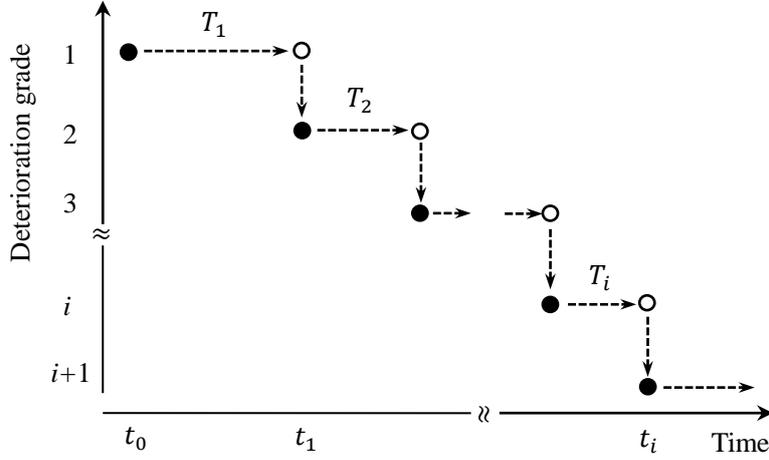
Figure 2.5 Time transition of soundness

As shown in Figure 2.5, sojourn time T_i $[0, \infty)$ of staying deterioration grade i is a random variable. Supposing the probability density function (PDF) of T_i is $f_i(T_i)$, the cumulative distribution function can be represented as $F_i(T_i) = P(T_i < t_i) = \int_0^{t_i} f_i(T_i)dT_i$. $F_i(T_i)$ represents the probability that the bridge survives less than t_i. The survival function defines the probability that sojourn time T_i will be t_i or more.

$$P(T_i \geq t_i) = \tilde{F}_i(T_i) = 1 - F_i(T_i) \tag{22}$$

The hazard function represents the risk of failure at time t_i. Specifically, it is the probability that a bridge will failure at time t_i, provided that this bridge has survived to time t_i. Therefore, the probability that T_i belong to interval $[t_i, t_i + \delta t_i]$ is:

$$P(t_i \leq T_i \leq t_i + \delta t_i | T_i \geq t_i) = \frac{P(t_i \leq T_i \leq t_i + \delta t_i)}{P(T_i \geq y_i)} \tag{23}$$

The derivative of Equation (23) to δt_i gives the definition of hazard function $h(t_i)$, as shown in Equation (24).

$$h(t_i) = \lim_{\delta t_i \to 0} \frac{P(t_i \leq T_i \leq t_i + \delta t_i | T_i \geq t_i)}{\delta t_i} \tag{24}$$

Furthermore, Equation (24) can be expressed as:

$$h(t_i) = \lim_{\delta t_i \to 0} \left\{ \frac{P(t_i \leq T_i \leq t_i + \delta t_i)}{P(T_i \geq t_i)} \times \frac{1}{\delta t_i} \right\}$$

$$= \lim_{\delta t_i \to 0} \left\{ \frac{F_i(t_i + \delta t_i) - F_i(t_i)}{P(T_i \geq t_i)} \times \frac{1}{\delta t_i} \right\}$$

$$= \lim_{\delta t_i \to 0} \left\{ \frac{F_i(t_i + \delta t_i) - F_i(t_i)}{\delta t_i} \times \frac{1}{P(T_i \geq t_i)} \right\}$$

$$= \lim_{\delta t_i \to 0} \left\{ \frac{F_i(t_i + \delta t_i) - F_i(t_i)}{\delta t_i} \times \frac{1}{\tilde{F}_i(t_i)} \right\}$$

$$= \frac{f_i(t_i)}{\tilde{F}_i(t_i)} = \frac{F_i{}'(t_i)}{1 - F_i(t_i)} \tag{25}$$

Based on Equation (25), the following relationship can be inferred.

$$\int \frac{F_i{}'(t_i)}{1 - F_i(t_i)} = -log(1 - F_i(t_i)) = -log(\tilde{F}_i(t_i)) \tag{26}$$

Therefore, the hazard function $h(t_i)$ is:

$$h(t_i) = -\frac{d}{dy_i} \{log(\tilde{F}_i(t_i))\} \tag{27}$$

Assuming the hazard function $h(t_i)$ is a variable determined by bridge's properties such as the material, traffic volume, and external environments. $h(t_i)$ can be denoted as:

$$h(t_i) = \lambda_i = x\beta_i{}' \ldots .. \tag{28}$$

where $x = (x_1, \ldots, x_m, \ldots, x_M)$ is a characteristic vector that represents the structural characteristics and usage environments of the bridge. x_m represents the observed value of the *m*-th characteristic variable. $\beta_i = (\beta_{i,1}, \ldots, \beta_{i,M})$ is a row vector of unknown parameters. The signal $'$ indicates the transpose operation.

Accordingly, the survival function can be represented as:

$$\tilde{F}_i(t_i) = \exp\left(-\int_0^{t_i} h(u)\, du\right) = e^{-t_i \lambda_i} \tag{29}$$

The probability density function $f_i(t_i)$ is an exponential distribution, as represented in Equation (30)

$$f_i(t_i) = \lambda_i e^{-\lambda_i t_i} \tag{30}$$

The expected survival time from the beginning of grade i to the next grade $i + 1$ is E_i.

$$E_i = \int_0^\infty \tilde{F}_i(t_i)dt_i = \int_0^\infty e^{-t_i \lambda_i}\, dt_i = -\frac{1}{\lambda_i} \tag{31}$$

2.6.2 Markov transition probability

This section will infer the transition probability from grade i to grade j, coming with a transition matrix finally. The probability that a bridge's is evaluated to be grade i at inspection time t_A and is evaluated to be grade j at the next inspection time $t_B = t_A + z$ is expressed as:

$$\pi_{ij} = P(G(t_B) = j | G(t_A) = i) \tag{32}$$

According to TSUDA et al [14], if the probability density function $f_i(t_i)$ is an exponential distribution, the transition probabilities can be summarized as:

$$\pi_{ii} = \exp(-z\lambda_i)$$

$$\pi_{ij} = \sum_{s=i}^{j} \left(\prod_{l=i}^{s-1} \frac{\lambda_l}{\lambda_{l,s}} \prod_{l=s}^{j-1} \frac{\lambda_l}{\lambda_{l+1,s}} \right) \exp(-\lambda_s z)$$

$$(i = 1,2,\dots,J-2; j = i+1, i+2, \dots, J-1)$$

$$\pi_{iJ} = 1 - \sum_{j=i}^{J-1} \pi_{ij} \tag{33}$$

where z is the inspection interval. $\lambda_{l,j} = \lambda_l - \lambda_j$. $\prod_{l=i}^{s-1} \frac{\lambda_l}{\lambda_{l,s}}$ is 1 when $s = i$. $\prod_{l=s}^{j-1} \frac{\lambda_l}{\lambda_{l+1,s}}$ is 1 when $s = j$. In reality, the probability of π_{ij} and π_{iJ} is quite low.

All transition probabilities conform to the following constraints.

$$\pi_{ij} \geq 0$$

$$\sum_{j=i}^{J} \pi_{ij} = 1$$

$$\pi_{ij} = 0 (i > j) \tag{34}$$

The state J represents the most serious deteriorated state. If bridges are not repaired, the Markov chain will converge to a stationary state, i.e. $\pi_{JJ} = 1$. Therefore, the Markov Chain transition matrix is:

$$\pi = \begin{pmatrix} \pi_{11} & \cdots & \pi_{1J} \\ \vdots & \ddots & \vdots \\ 0 & \cdots & \pi_{JJ} \end{pmatrix} \tag{35}$$

2.6.3 Estimating the hazard model

The hazard variable λ_i can be determined by vector x of potentially influencing factors and unknown parameters β_i using Equation (30). In addition, the transition probability is also affected by the inspection interval z. Therefore, the transition probability is a function regarding the inspection data (x, z) and unknown parameters β_i, as represented as $\pi_{ij}(\beta_i | x, z)$. Supposing the deterioration of each bridge is independent, the simultaneous deterioration of all inspected bridges can be represented as a log-likelihood function $\ln[\mathcal{L}(\beta)]$.

$$\ln[\mathcal{L}(\beta)] = \ln \left[\prod_{i=1}^{J-1} \prod_{j=i}^{J} \prod_{k=1}^{K} \left\{ \pi_{ij}(x^k, Z^k, \beta_i) \right\}^{\delta_{ij}^k} \right] = \sum_{i=1}^{J-1} \sum_{j=i}^{J} \sum_{k=1}^{K} \delta_{ij}^k \ln\left\{ \pi_{ij}(x^k, Z^k, \beta_i) \right\} \tag{36}$$

Censoring indicator δ_{ij}^k equals 1 when the deterioration grade of the k-th bridge at time $t_B{}^k$ is j and that at time $t_A{}^k$ is i, otherwise is 0.

The log-likelihood function is a function of unknown parameter β. Equation (37) is an nonlinear equations of $(J-1) \times M$ used to determine the optimal parameter for $\ln[\mathcal{L}(\beta)]$.

$$\frac{\vartheta \ln[\mathcal{L}(\beta)]}{\vartheta \beta_{i,m}} = 0 \ (i = 1,\dots,J-1; m = 1,\dots M) \tag{37}$$

The gradient decent method can be used to calculate the optimal values of parameter β to satisfy Equation (37).

2.7 Crack identification model

As explained in Section 1.6, cracking is not considered as a factor of the deterioration prediction model. Instead, an independent crack identification model including crack detection and quantification is anticipated to be established. Crack detection and quantification aims to detect crack locations and measure the extent of surface cracks from the collected digital images, as required for quickly diagnosing crack propagation [15]. The entire crack identification model includes three stages: pre-processing, crack detection, and post-processing. In the pre-processing phase, images that collected from onsite inspections and indoor experiments (Section 4.2.1) were provided to a computer. Then, the images were subjected to calibration and database generation. In the crack detection phase, the locations of the cracks were identified from the entire image. In the post-processing phase, the characteristics of the cracks, such as the width, length, and orientations were analyzed and visualized. Each of these phases is described more fully below. Figure 4.1 shows a flowchart of the crack identification model used in this study for detecting and quantifying crack conditions.

2.7.1 Pre-processing

A digital image is a 2D projection of 3D real-world objects. Images are not necessarily to be orthographic projections. Although a Convolutional Neural Network (CNN) classifier can identify cracks from raw images without calibration, the perspective error will affect the calculation of the detailed crack properties, such as the width. Therefore, the images need to be corrected and calibrated against such perspective errors to facilitate post-processing. In this study, the calibration was only performed to the indoor experimental images by a composition of rotations, translations, projective transformation, magnifications, and shears, according to [16]. Onsite inspection images were not calibrated because of the inability to confirm the exact perspective angle and the distance from the camera to the structures.

Figure 2.6 Example of calibration

An example of the calibration is shown in Figure 2.6. In addition, part of these raw images needed to be cropped into unified sub-images to generate image dataset for establishing a crack detection classifier (Section 4.2.1). In summary, image preprocessing includes calibrating the image and cropping the raw image into smaller sub-images. The sub-images were manually annotated as crack or intact to generate the

database for training and validation.

2.7.2 Crack detection

As mentioned in Section 1.3.1, a CNN can be used for crack detection in three ways: image classification, object localization, or pixel segmentation. Training a CNN classifier is the primary goal of the crack identification model to detect whether a sub-image is cracked or intact. Many CNNs are available to fulfill this purpose, such as AlexNet [17], GoogLeNet [18], Resnet18 [19], and VGG-16 [20]. In addition, it is feasible to establish a classifier on the training dataset by two modes: fully training and transfer learning [21]. The former trains the CNN fully from scratch on the training dataset. The latter modifies a few layers of the CNN configuration according to the dataset. In this study, transfer training was first performed to the CNN architectures of AlexNet, GoogLeNet, ResNet18, and VGG-16 to select a suitable CNN for our dataset. Then, the transfer learning and fully training of the selected CNN will be further tested on the testing dataset and a public dataset SDNET2018 to determine the optimal generic model. Detailed testing procedures and results can be found in Section 4.2.

(1) Overall configuration

In general, a CNN architecture includes an input layer, learning layers, and an output layer. The input layer reads the image and transfers it to the learning layers. The learning layers perform convolution operations by applying filters to extract image features. The output layer classifies the image according to the target categories, using the features extracted in the learning layers. The CNN can be trained by assigning target categories to images in a training dataset and modifying the filter values iteratively through back propagation until the desired accuracy is achieved.
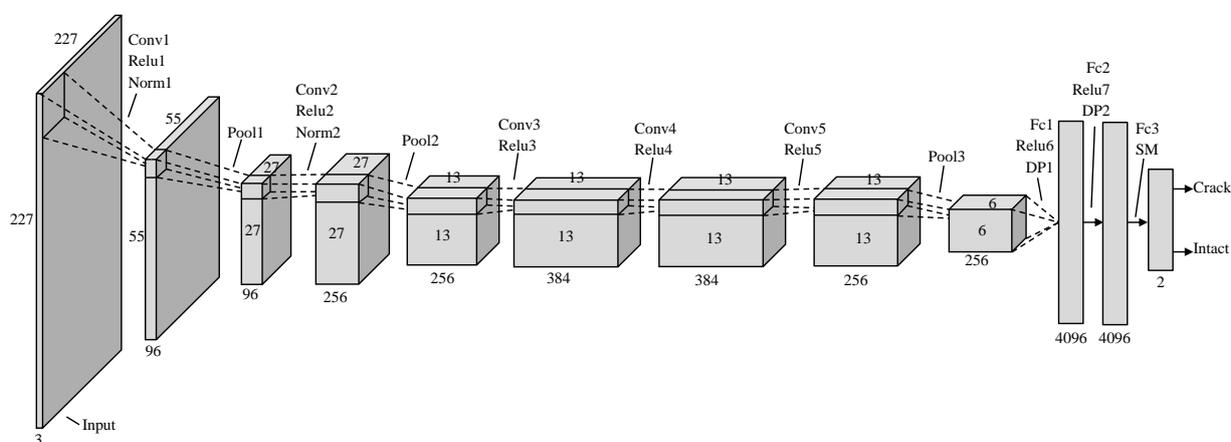
Figure 2.7 Illustration of the AlexNet's architecture. conv# = convolution; pool# = pooling; Relu #= activation function; Norm#= normalization; fc# =full connection; k# = kernel of each operation; DP#=Dropout; SM=softmax;

AlexNet was taken as an example to illustrate the modification of CNNs for this study. AlexNet is a remarkable CNN for image classification [22]. It is trained on the ImageNet database, and provides an output with 1000 classes. Since the number of image classes in this study is two (images with and without cracks), the output number of the classes was modified to two. The modified AlexNet is shown in Figure 2.7; each dimension in the input image indicates the height, width, and channel (red, green, and blue), respectively. Table 2.1 presents the detailed specifications of the modified AlexNet CNN. Notably, the

Relu activation function is applied after the convolution operation and fully connection operation. In addition, normalization and dropout are also implemented. The softmax layer predicts whether each input image does or does not contain a crack. Similarly, the last two layers of the GoogLeNet, ResNet18, and VGG-16 were modified to classify images as crack or intact.

Table 2.1 Detailed specifications of the AlexNet

Layer	Kernel size (Height×Width×Depth)	Number of Kernel	Stride	Pad	Output size (Height×Width×Depth)
Input	-		-	-	227×227×3
Conv1	11×11×3	96	4	0	55×55×96
Pool1	3×3		2	0	27×27×96
Conv2	5×5×48	96	1	2	27×27×256
Pool2	3×3		2	0	13×13×256
Conv3	3×3×256	384	1	1	13×13×384
Conv4	3×3×192	384	1	1	13×13×384
Conv5	3×3×192	256	1	1	13×13×256
Pool3	3×3		2	0	6×6×256
Fc1	6×6×256	4096	-	-	1×1×4096
Fc2	-		-	-	1×1×4096
Fc3	-		-	-	1×1×4096
SM	-		-	-	1×1×2

(2) Update of the connection weights

As the initial values of weights are randomly assigned during training, the predicted classes are usually inconsistent with the actual classes. The softmax loss function was therefore applied to assess the deviations between the predicted and actual classes, as defined by Equation (40).

$$L = \frac{1}{N}\left[\sum_{i=1}^{N}\sum_{j=1}^{k}\left(-log\frac{e^{W_j^T x^{(i)}}}{\sum_{m=1}^{k}e^{W_m^T x^{(i)}}}\right)\right] + \frac{p}{2}\sum_{j=1}^{k}W_j^2 \tag{38}$$

where N and k are the number of samples and that of classes, respectively. W are weights. $\sum_{m=1}^{k}e^{W_m^T x^{(i)}}$ is independent of $\sum_{j=1}^{k}(\cdot)$. The parameter p is a regularization to penalize large weights for preventing overfitting [17].

To minimize the deviation during training, the weights are updated to obtain true classes. The update of the weights is achieved using a Stochastic Gradient Descent (SGD) approach. In addition, a momentum algorithm is combined with the SGD to accelerate the convergence process of the training. As shown in Equation (41), the gradient $\nabla_W L$ of loss function is calculated with respect to W at time *t*. Then the velocity V_{t+1} in Equation (42) is updated ($\leftarrow$) by combination of the previous velocity V_t and the gradient $\nabla_W L$, where momentum μ and learning rate α are two parameters [9]. Finally, the W are updated using Equation (43).

$$\nabla_W L(W; x^{(i)}, y^{(i)}) = \frac{1}{N}\sum_{i=1}^{N}\left[x^{(i)}(-p(y^{(i)} = j^{(i)}|x^{(i)}; W))\right] + \lambda W_j \tag{39}$$

$$V_{t+1} \leftarrow \mu V_t - \alpha \nabla_W L(W; x^{(i)}, y^{(i)}) \tag{40}$$

$$W_{t+1} \leftarrow W_t + V_{t+1} \tag{41}$$

The CNN is tuned by repeating the described procedures until desired accuracy is achieved. During the training, the training dataset is usually separated into sub-training sets to speed up the training. These

sub-sets are called batch sizes. Each complete update out of a batch size is called an iteration, and each complete update out of the entire training dataset is called an epoch.

2.7.3 Post-processing

The crack identification model's second objective is to segment and quantity cracks after the established CNN classifier detect sub-images with cracks, because cracks information (such as width, length, and orientations) is important for assessing structural damage conditions. The post-processing procedures are shown in Figure 2.8. Firstly, the sub-images are converted to grayscale. Then, the contrast of the grayscale image is enhanced. Mask processing is used for reducing noise and smoothing image. Next, edge detectors, boundary tracking and threshold segmentation are performed to segment the image. More details regarding these techniques have been shown in Gonzales and Woods [23]. Finally, the crack properties such as crack thickness, length, and orientation can be obtained, as detailed in (1) and (2) of this section. Commercial software is available to achieve such functions, but the use of commercial software makes: (i) the combination of the CNN classifier and post-processing techniques difficult; (ii) the use of different software will increase the learning costs for human. In addition, it is time and labor consuming to process all of the sub-images, as every raw image is cropped to thousands of sub-images. To simplify the processing procedures, an application was developed to integrate these techniques. The details of this application are described in Section 4.3, along with validation with practical examples.

```
┌─────────────────────────┐
│   Sub-image with crack  │
└─────────────────────────┘
            │
            ▼
┌─────────────────────────┐
│    Convert to grayscale │
└─────────────────────────┘
            │
            ▼
┌─────────────────────────┐
│ Image contrast enhancement │
└─────────────────────────┘
            │
            ▼
┌─────────────────────────┐
│ Image filtering and smoothing │
└─────────────────────────┘
            │
            ▼
┌─────────────────────────┐
│    Image segmentation   │
└─────────────────────────┘
            │
            ▼
┌─────────────────────────┐
│ Image properties calculation │
└─────────────────────────┘
```
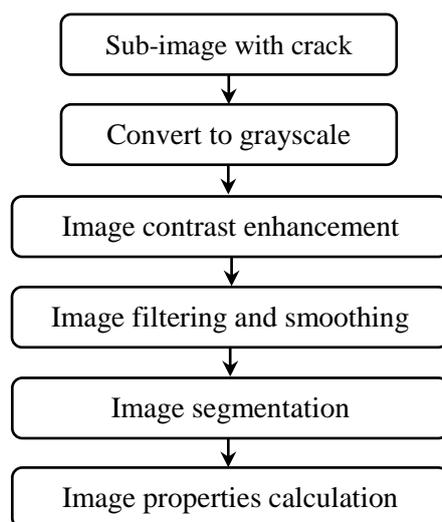
Figure 2.8 Flow chart for post-processing

(1) Crack quantification

Once the crack has been delineated, an automatic algorithm can be applied to measure the properties of the crack [16]. The calculable properties include crack width, crack length, crack orientations, and the others.

Crack width is the most important information for quantifying the cracking of a concrete component. In a previous study [24], the crack's mean width is calculated to represent its width. To obtain the crack width more precisely, a different method was proposed, as shown in Figure 2.9.

To utilize this method, a neighborhood value δ is pre-defined. S_1 and S_2 are the edges of a crack. The steps for calculating crack width at point P are summarized in Algorithm 1: (i) forming a dataset using the points between the neighborhood lines on edges S_1 and S_2; (ii) performing linear regression to the dataset for getting a fitting line l; (iii) acquiring line l' that perpendicular to l through point P; and (iv)

computing the distance from point P to point P'.
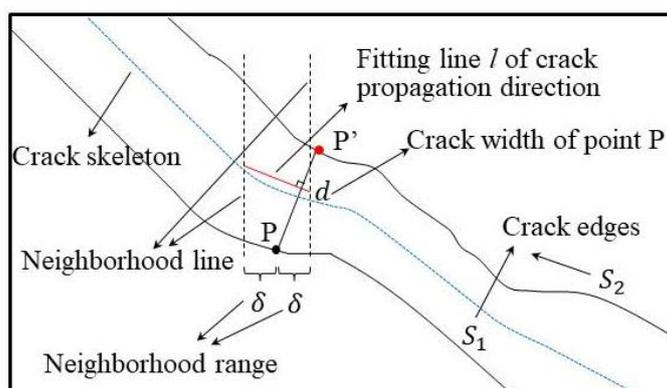
Figure 2.9 Depiction for calculating crack properties

Algorithm 1 Crack width calculation.

Input: *neighborhood* δ, $P(x_1, y_1)$, S_1, S_2
Output: *distance d*
for *i between* $x_1 - \delta$ *and* $x_1 + \delta$
        dataset $\leftarrow \{S_1(i); S_2(i)\}$
end for
l $\leftarrow$ *linear regression(dataset)*
l' $\leftarrow$ *line perpendicular to l through P*
P' $\leftarrow$ *intersection of l' and* S_2
d $\leftarrow$ *distance(P,P')*

In the calculation of the crack width, the points between the neighborhood lines on the edges S_1 and S_2 are applied to obtain a fitting line. If the entire points on the edges S_1 and S_2 are used, the orientation of the crack can be obtained. The ratio of the crack pixels in the raw image can be easily obtained, as all sub-images with cracks are segmented in the post-processing. The crack length can be obtained by calculating the length of the crack skeleton, as indicated in Figure 2.9. Details regarding crack skeleton can be found in Gonzales and Woods [23].

(2) Crack statistics and visualization

For each raw image, all cracks can be counted to obtain the statistical characteristics of the cracking. If raw images of the same structural component are collected in chronological order, the crack propagation can be inferred using a wind rose map. In addition, if cracks are detected on each surface of the structural component, crack characteristics can be visualized in 3D [16, 25-26]. These functions are elaborated in Section 4.3 with practical examples.

2.8 Model evaluation

Because the MLP, RNN and the CNN models belong to neural network, the performance of these three models will be evaluated using five metrics. The definitions in terms of these metrics are introduced in Figure 2.10 by seperating the bridges into two groups : bridges being grade 1 and bridges beling in grade 2 & 3. TP, TN, FP, and FN refer to true positives, true negatives, false positives, and false negatives, respectively. Recall or true positive rate (TPR) is the ratio of correct predictions to all grade 1 bridges.

Precision is the ratio of correct predictions to all predictions of grade 1. The F1 score is the harmonic mean of the recall and precision. The true negative rate (TNR) indicates the ratio of correct predictions on other grade bridges to the total number of other grade bridges. The definition of accuracy (ACC) is shown in Figure 2.10. A model is considered better performance with higher the values of these metrics. Details about these metrics can refer to Goodfellow et al [2].

$$Recall = \frac{TP}{TP + FN}$$

$$Precision = \frac{TP}{TP + FP}$$

$$ACC = \frac{TP + TN}{TP + FP + TN + FN}$$

$$F1 = \frac{2 * Recall * Precision}{(Recall + Precision)}$$

$$TNR = \frac{TN}{TN + FP}$$
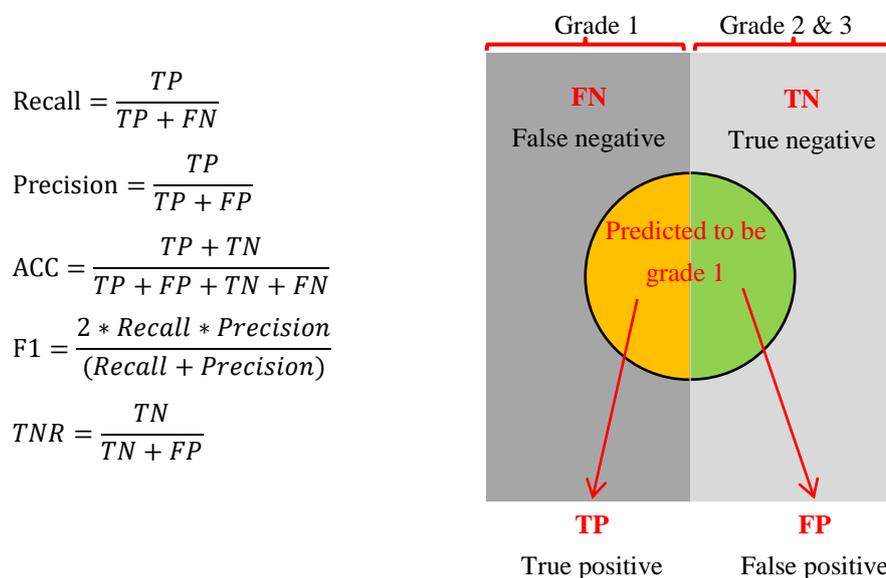
Figure 2.10 Performance evaluation metrics used in this study (Taking Grade 1 for example)

In addition, comparative researches will be conducted, as stated below.

The MLP and RNN model will be compared to select the optimal prediction model in terms of five metrics mentioned above. Since a perfect prediction model is usually infeasible, the predictions for some bridges will inevitably fail. Therefore, error analysis will be performed to the optimal model to determine the reasons of failure (Section 3.4.2).

Two sensitivity analysis methods, Shapley value method and Sobol indices, will be compared to provide insights into the optimal model between MLP and RNN. In addition, case studies will be performed to verify the proposed models and methods, as described in each section.

To establish a robust classifier for the cracks, four transfer learned CNN configurations (AlexNet, GoogLeNet, Resnet18, and VGG-16) are compared to select the optimal CNN. Then, the transfer learning and the fully training of the optimal CNN configuration will be tested on our testing dataset and a public dataset SDENT2018 [27]. In addition, the performance of the model for crack identification will be compared with a previous crack pixel level framework [20] on 23 raw images. Detail implementation can refer to Chapter 4.

The MC approach is a typical probabilistic model. To evaluate the performance of the RNN in predicting deterioration, the RNN and MC methods will be compared in terms of the mean deterioration progress, the deterioration progresses of different types of bridges, the deterioration progress of a specific bridge, and the influence of each factor on deterioration progresses.

2.9 Building Information Modeling (BIM)

Traditional building design was largely reliant upon two-dimensional technical drawings (plans, elevations, sections, etc). Building Information Modeling (BIM) extends the three primary spatial dimensions (width, height and depth), incorporating information about time (so-called 4-D BIM) [28], cost (5-D BIM) [29], asset management, sustainability, etc. BIM therefore covers more than just geometry.

As described in the introduction, BIM has been greatly used in the design, construction stages, but seldom in the maintenance stage. However, BIM can contain more information than just geometry; therefore, it is the optimal solution for managing inspection and intervening information.

Inspired by the concept of 4-D BIM and 5-D BIM, it is feasible to integrate the 3-D prototype model of the existing bridges with the inspection information, the deterioration prediction model, and the crack identification model to form a collaborative BIM platform. This platform can reduce mistakes and can enhanced the management efficiency of existing bridges.

References

[1] D. E. Rumelhart, G. E. Hinton, R. J. Williams, Learning representations by back-propagating errors. Nature, 323(6088) (1986) 533-536. doi: 10.1038/323533a0

[2] I. Goodfellow, Y. Bengio, A. Courville, Deep Learning, MIT Press. (2016). http://www.deeplearningbook.org, Access date: November, 2019.

[3] N.J. Guliyev, V.E. Ismailov, A single hidden layer feedforward network with only one neuron in the hidden layer can approximate any univariate function, Neural computation. 28(7) (2016) 1289-1304. doi: 10.1162/NECO_a_00849

[4] Hochreiter, S., & Urgen Schmidhuber, J. (1997). Long Shortterm Memory. Neural Computation, 9(8), 17351780.

[5] Cho, K., Van Merriënboer, B., Gulcehre, C., Bahdanau, D., Bougares, F., Schwenk, H., & Bengio, Y. (2014). Learning phrase representations using RNN encoder-decoder for statistical machine translation. arXiv preprint arXiv:1406.1078. https://arxiv.org/abs/1406.1078

[6] Wang, D., Fan, J., Fu, H., & Zhang, B. (2018). Research on optimization of big data construction engineering quality management based on RnN-LSTM. Complexity, 2018. https://doi.org/10.1155/2018/9691868

[7] Lipton, Z. C., Kale, D. C., Elkan, C., & Wetzel, R. (2016). Learning to diagnose with LSTM Recurrent Neural Networks. 4th International Conference on Learning Representations, ICLR 2016 - Conference Track Proceedings, 1–18.

[8] Choi, E., Schuetz, A., Stewart, W. F., & Sun, J. (2017). Using Recurrent Neural Network models for early detection of heart failure onset. Journal of the American Medical Informatics Association, 24(2), 361–370. doi:10.1093/jamia/ocw112

[9] Bengio, Y. (2012), Practical recommendations for gradient- based training of deep architectures, in G. Montavon, G. B. Orr, and K.-R.M˙uller (eds.), Neural Networks: Tricks ofthe Trade, 2nd edn., Springer, Berlin Heidelberg, pp. 437–78.

[10] A.B. Owen, C. Prieur, On Shapley value for measuring importance of dependent inputs, SIAM/ASA Journal on Uncertainty Quantification. 5(1) (2017) 986-1002. doi: 10.1137/16M1097717

[11] I.E. Kumar, S. Venkatasubramanian, C. Scheidegger, S. Friedler, Problems with Shapley-value-based explanations as feature importance measures, arXiv preprint arXiv:2002.11097, 2020, https://arxiv.org/pdf/2002.11097.pdf.

[12] S.M. Lundberg, B. Nair, M.S. Vavilala, M. Horibe, M.J. Eisses, T. Adams, S.I. Lee, Explainable machine-learning predictions for the prevention of hypoxaemia during surgery, Nature Biomedical Engineering. 2(10) (2018) 749. doi: 10.1038/s41551-018-0304-0

[13] I.M. Sobol, Global sensitivity indices for nonlinear mathematical models and their Monte Carlo estimates. MATH COMPUT SIMULAT,55(1–3)(2001)271-280, doi:10.1016/S0378-4754(00)00270-6

[14] Yoshitane TSUDA, Kiyoyuki KAITO, Kazuya AOKI, Kiyoshi KOBAYASHI. (2005). Estimating Markovian transition probabilities for bridge deterioration forecasting. Journal of JSCE, (801), 69-82. https://pdfs.semanticscholar.org/5f0f/f57f1d3e5ba87fb14ab5e9957e4818f84615.pdf.

[15] Ayaho, M., Masa-Aki, K., & Eugen, B. (2007). Automatic crack recognition system for concrete structures using image processing approach. Asian Journal of Information Technology, 5(5), 553–561. http://docsdrive.com/pdfs/medwelljournals/ajit/2007/553-561.pdf

[16] Adhikari, R. S., Moselhi, O., & Bagchi, A. (2014). Image-based retrieval of concrete crack properties for bridge inspection. Automation in Construction, 39(February 2018), 180–194. https://doi.org/10.1016/j.autcon.2013.06.011

[17] Cha, Y. J., Choi, W., & Büyüköztürk, O. (2017). Deep Learning-Based Crack Damage Detection Using Convolutional Neural Networks. Computer-Aided Civil and Infrastructure Engineering, 32(5), 361–378. https://doi.org/10.1111/mice.12263

[18] Ni, F. T., Zhang, J., & Chen, Z. Q. (2019). Pixel-level crack delineation in images with convolutional feature fusion. Structural Control and Health Monitoring, 26(1), 1–18. https://doi.org/10.1002/stc.2286

[19] X. Jia, X. Yang, X. Yu and H. Gao, "A Modified CenterNet for Crack Detection of Sanitary Ceramics," IECON 2020 The 46th Annual Conference of the IEEE Industrial Electronics Society, Singapore, Singapore, 2020, pp. 5311-5316, doi: 10.1109/IECON43393.2020.9254351

[20] Alipour, M., Harris, D. K., & Miller, G. R. (2019). Robust Pixel-Level Crack Detection Using Deep Fully Convolutional Neural Networks. Journal of Computing in Civil Engineering, 33(6), 1–14. https://doi.org/10.1061/(ASCE)CP.1943-5487.0000854

[21] Dorafshan, S., Thomas, R. J., & Maguire, M. (2018). Comparison of deep convolutional neural networks and edge detectors for image-based crack detection in concrete. Construction and Building Materials, 186, 1031–1045. https://doi.org/10.1016/j.conbuildmat.2018.08.011

[22] Li, S., & Zhao, X. (2019). Image-Based Concrete Crack Detection Using Convolutional Neural Network and Exhaustive Search Technique. Advances in Civil Engineering, 2019(Ml). https://doi.org/10.1155/2019/6520620

[23] Gonzales, R. C., & Woods, R. E. (2018). Digital image processing, 4th Edition.

[24] Albareda-Valls, A., Herrera, A. B., Mestre, J. L. Z., & Zaribaf, S. S. (2018). Image post-processing method for quantification of cracking in RC precast beams under bending. Buildings, 8(11). https://doi.org/10.3390/buildings8110158

[25] Torok, M. M., Golparvar-Fard, M., & Kochersberger, K. B. (2014). Image-based automated 3D crack detection for post-disaster building assessment. Journal of Computing in Civil Engineering, 28(5), 1–13. https://doi.org/10.1061/(ASCE)CP.1943-5487.0000334

[26] Bengio, Y., Goodfellow, I. J. & Courville, A. (2016), Deep Learning, An MIT Press book. Online version is available at: http://www.deeplearningbook.org, accessed July 2016.

[27] Dorafshan, S., Thomas, R. J., & Maguire, M. (2018). Comparison of deep convolutional neural networks and edge detectors for image-based crack detection in concrete. Construction and Building Materials, 186, 1031–1045. https://doi.org/10.1016/j.conbuildmat.2018.08.011

[28] 4D BIM or Simulation-Based Modeling". structuremag.org. Retrieved 9 January2021. https://web.archive.org/web/20120530011123/http://structuremag.org/article.aspx?articleID=1234

[29] ASHRAE Introduction to BIM, 4D and 5D. cadsoft-consult.com. Retrieved 29 May 2021. https://web.archive.org/web/20130403091827/http://www.cadsoft-consult.com/blogs/architecture/2009/09/ashrae-introduction-to-bim-4d-and-5d/

Chapter 3

Establishment of deterioration prediction models

3.1 Overview

The outline of this chapter is shown in Figure 3.1. At the beginning, the applied database was described from the influencing factors, inspection results, and the characteristics of these data. Secondly, three models were established to establish relationships between these affecting factors and the inspection results (deterioration grade). The Multilayer Perceptron (MLP) was used to establish simple relationship between influencing factors and deterioration grade. The Recurrent Neural Network (RNN) was applied to consider the time dependence of time related factors, and to improve the relationship between the influencing factors and deterioration grades. Since the functions of the three gates described in Section 2.4, the RNN is especially efficient to process the time series data. Different from MLP and RNN models, the Markov Chain (MC) is a typical probabilistic model usually applied to in predicting deterioration [1]. Later, deterioration progresses obtained by the MC model and the RNN model were compared with each other. Afterwards, two sensitivity analysis methods (Shapley value and Sobol indices methods) were applied to the optimal model between MLP and RNN to recognize the reasons for deterioration. In addition, the sensitivity analysis was conducted by modifying the value of each factor to observe the influence of each factor on the deterioration. Details on these procedures were explained blow.
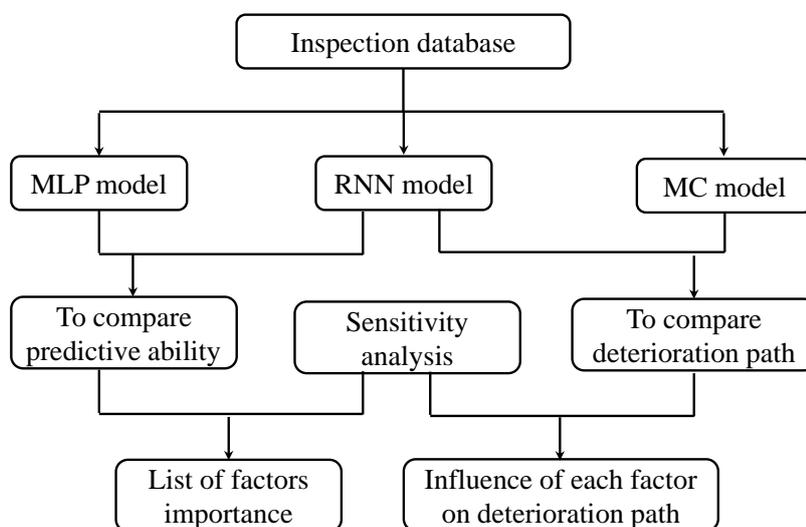
Figure 3.1 Outline of Chapter 3

3.2 Data description

A bridge inspection database of 3,386 bridges in Hokkaido, Japan was employed to verify the feasibility of MLP, RNN, and MC models. The locations of these bridges are shown in Figure 3.2. We eliminated incomplete and unreasonable data from the database and selected 3,368 out of 3,386 bridges. Specifically, the bridges with unknown age were discarded. In conjunction with the age constrain, the constraint of non-decreasing deterioration grade were introduced. For example, a bridge was assessed grade 2 in an inspection and assessed grade 1 in the next inspection, this kind of bridges was not considered.

Furthermore, only bridges with consecutive series data were considered, such as some bridges whose traffic volume was counted only once were unconsidered. Then, we divided the data of the selected bridges into two categories: potentially influencing factors and deterioration grades. Details on these two categories are described in the following subsections. Since the years in service of the bridge vary from a few years to a few decades, the annual average value of each factor is taken as the value of this factor at a certain moment in the time series. Accordingly, a time series is obtained for each factor of each bridge. The time span of the time series is the bridge age.
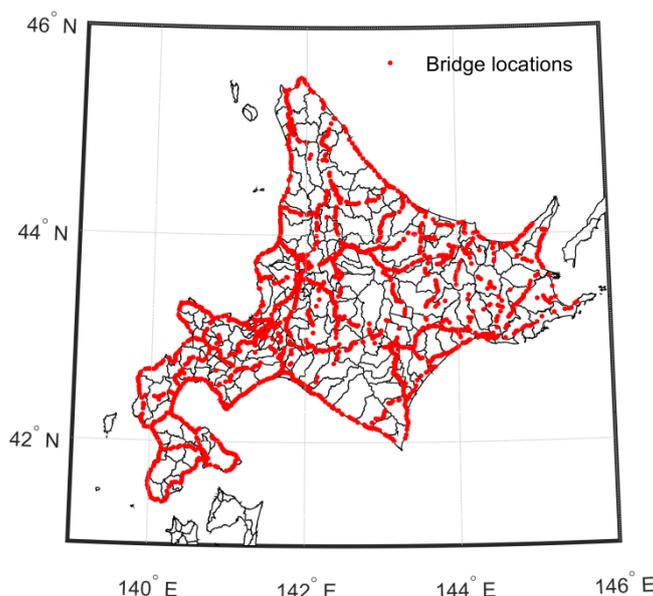
Figure 3.2 Locations of the bridges

3.1.1 Potentially influencing factors

Factors that may affect deterioration are regarded as inputs in the prediction model. The bridge features, such as the bridge length, bridge width, elevation, and years in service were extracted from the inspection database. In addition, factors of the temperature, rainfall, snowfall and carbon dioxide concentration were derived from Japan Meteorological Agency [2]. The traffic volumes were retrieved from MLIT [3-5]. Airborne salt and carbonation were calculated according to previous studies [6-9].

Table 3.1 Potentially influencing factors

	Attributes (units)
Bridge geometry factors	Length (m)
	width (m)
Environment factors	Elevation (m)
	Yearly highest and lowest temperatures (°C)
	Carbon dioxide concentration (ppm)
	Airborne salt concentration (mdd•NaCl),
	Yearly average snowfall (cm)
	Yearly average rainfall (cm)
Loading condition	Daily traffic volume (vehicles/day)[*]
	Rate of the large-size vehicles (%/day)
Bridge age	Years in service (years)

[*] Statistics on traffic volume include large and small vehicles [10].

In summary, the potentially influencing factors considered in this study included bridge geometry factors,

environmental factors, bridge age, and loading conditions, as summarized in Table 3.1. This study considered four types of bridges, including PC bridges, RC bridges, steel and concrete composite bridges, and steel bridges. But only the concrete components of the above four bridge types were considered when calculating the carbonation and the penetration of chloride ions. Discussions regarding the performance of the models on different types of bridges were described in the discussion of each model. Many other factors were not considered due to the inability to collect relevant data.

Factors such as the geometry and elevation of the bridge are constant. More details were described for the factors of the traffic volume, airborne salt, and carbon dioxide concentration.

(1) Traffic volume

According to the survey of the daily traffic volume [10], the proportion of large-sized vehicles (including buses, lorries, construction heavy equipment and other special equipment) R_V can be calculated by Equation (1). Since the inspection database includes the data of R_V, this equation can be used to calculate the number of the large-size vehicles.

$$R_V = \frac{Number\ of\ large\ size\ vehicles\ daily}{Daily\ traffic\ volume} \times 100\% \tag{1}$$

(2) Airborne salt

The bridges within 1 km of a coastline were considered influenced by the airborne salt. The airborne salt concentration can be calculated using Equation (2) [6]:

$$C_{ab} = C_1 \cdot x^{-b} \tag{2}$$

where C_{ab}: Airborne salt concentration (mdd · NaCl),

C_1: 1 km equivalent airborne salt concentration (mdd·NaCl),

x: Distance from a coastline (km), and

b: Degree of distance attenuation ($b = 0.6$).
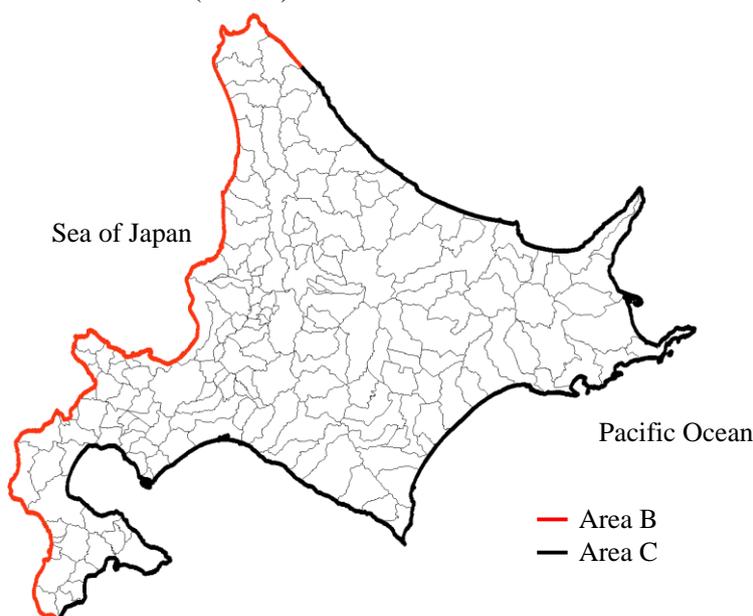
Figure 3.3 Salt damage area classification in Hokkaido

C_1 for areas B and C shown in Figure 3.3 are 1.174 and 0.072, respectively [6]. Then, Equation (3) [7] can be used to compute the concentration of chloride ions that adheres on the surface of the concrete. Only the situation of $C_{ab} \leq 30$ was considered because all C_{ab} data considered in this study conform to this constrain.

$$C_0 = -0.016 \times C_{ab}{}^2 + C_{ab} + 1.7 (C_{ab} \leq 30) \tag{3}$$

where C_0: Chloride ions concentration of concrete surface (kg/m^3), and

C_{ab}: Air-borne salt content at the bridge location (mdd $\cdot$ NaCl).

Figure 3.4 shows the relationship between the concentration of chloride ions on concrete surface and the distance from a coastline. For comparison, the chloride ions concentration on the concrete surface obtained according to the Standard Specifications for Concrete Structures [7] was also displayed. Figure 3.4 shows that the concentration of chloride ion in areas B and C decreases with the increase of distance from the coastline.
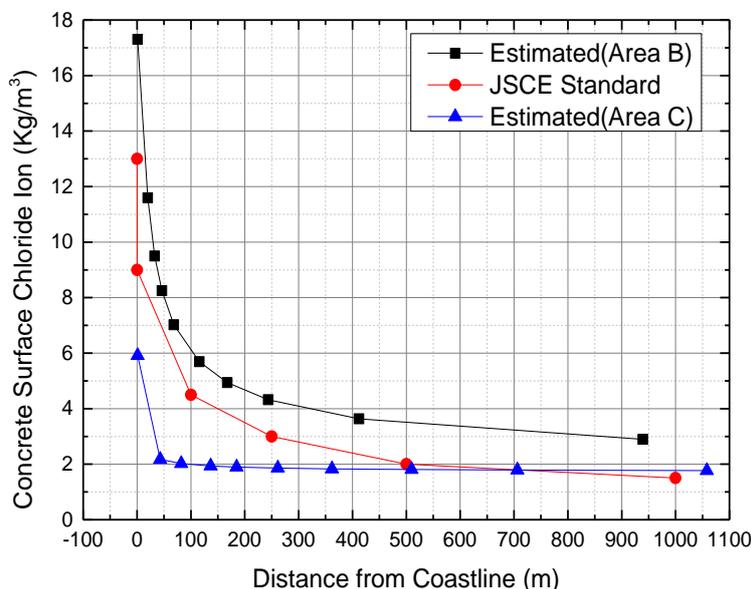
Figure 3.4 Comparison of estimated chloride ion concentration and the JSCE standard

The estimated chloride ions concentrations in area B are slightly larger than the JSCE standard and those in area C are lower than the standard. One possible reason is that the standard considers the results from all regions in Japan. The reason that the value in area B is greater than that of area C is that the wind is stronger on the side of the Sea of Japan and is relatively weak on the Pacific Ocean side [6]. Then, Fick's second law was applied to determine the penetration of chloride ions into concrete:

$$C(x,t) = C_0 \left(1 - \text{erf} \left(\frac{x}{2\sqrt{D_c \cdot t}} \right) \right) + C(x,0) \tag{4}$$

where $C(x,t)$ is the chloride ions concentration (kg/m^3) at a depth of x after t (year); C_0 is the chloride ions concentration on the concrete surface (kg/m^3) and can be obtained from Equation (3); $C(x,0)$ is the initial chloride ions content (kg/m^3), for which the value is usually 0.3 kg/m^3 [8]; and D_c is the diffusion coefficient (cm^2/year).

Deterioration is characterized by the corrosion of the rebar or crack propagation. The chloride ions

concentration at the surface of the rebar was calculated and used as a criterion to identify deterioration. According to previous experimental studies, the corrosion threshold concentration of chloride ions for ordinary steel in concrete in Japan is 1.2 to 2.5 kg/m^3 [11]. In addition, in previous surveys of existing bridges, almost no steel corrosion was observed when the chloride ions concentration was less than 1.2 kg/m^3 [8]. Therefore, 1.2 kg/m^3 was thought to be the chloride ions concentration for the onset of rebar corrosion.

Furthermore, Equation (5) was used to calculate the diffusion coefficient D_c (cm^2/year):

$$\log(D_c) = -3.9(W/C)^2 + 7.2(W/C) - 2.5 \tag{5}$$

where W/C is the water-to-cement ratio.

In this study, there are few structures with a clear water-to-cement ratio. However, Tamakoshi [12] suggested that if there are no specific data, materials information can be obtained according to Table 3.2. Therefore, the values of water-to-cement ratio and thickness of the concrete cover were extracted from Table 3.2.

Table 3.2 Suggested materials information for bridge components [12]

Built Year	Item	Salt damage countermeasure category	Structure type		Pier	Abutment
			RC	PC		
Before 1983	Protective Cover(cm)	-	3.5	2.5	7	7
	W/C (%)	-	55	35	60	60
After 1983	Protective Cover(cm)	0~100m*	7	7	7	7
		100~300m	7	5	7	7
		300~500m	5	3.5	7	7
		others	3.5	2.5	7	7
	W/C (%)	-	50	35	55	55

* 0~100m denote distance from a coastline.
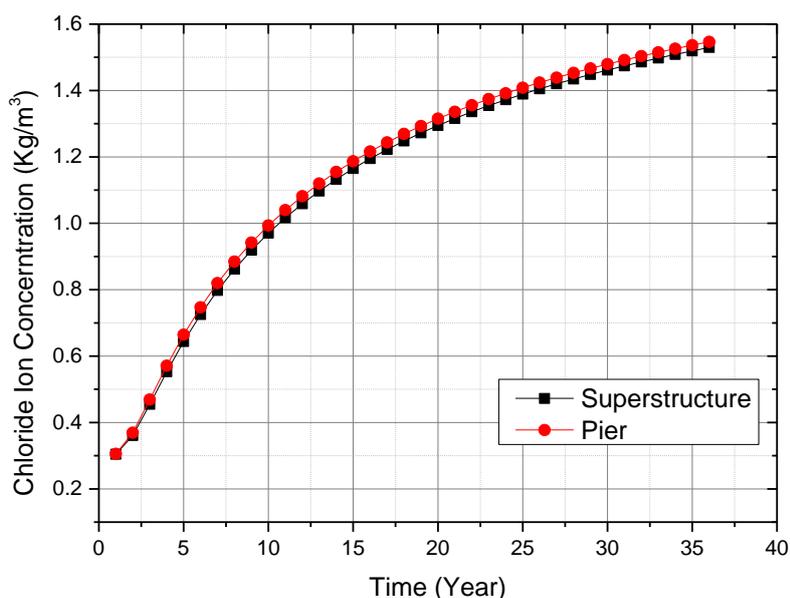
Figure 3.5 Chloride ions concentration for superstructure and pier

For each bridge, the chloride ions concentrations on the surface of all bridge components were calculated. According to the inspection guideline [13], the bridge is considered corroded once any component is corroded. Figure 3.5 was an example to show the chloride ions concentrations on the surface of the rebar for a bridge superstructure and pier. The results revealed that the corrosion of the pier occurs slightly earlier than that of the superstructure. Therefore, the corrosion time of the pier was considered to be the initial corrosion of the bridge.

(3) Carbonation

According to the investigation of Kishitani [14], the carbonation depth of concrete structures in the natural environment can be estimated by Equation (6):

$$d = A \cdot \sqrt{t} \tag{6}$$

where d is the carbonation depth(mm),

  A is the deterioration index for carbonation (mm$/\sqrt{\text{year}}$), and

  t is the years in service.

The deterioration index A is calculated by:

$$A = R(4.6\,W/C - 1.76)/\sqrt{7.2} \tag{7}$$

where R is related to the type of cement, aggregate, and admixture. In this study, R is 1 according to Kawakami [15] and NRA [9]. W/C can be obtained from Table 3.2.

Equation (6) was obtained assuming the CO_2 concentration was constant. However, the CO_2 concentration was observed to increase with time in the past decades, as shown in Figure 8. In addition, the measured carbonation depth for a concrete structure was very different from the value estimated by Equation (6) [9]. Therefore, the equation was modified as:

$$d = k(t) * A \cdot \sqrt{t} \tag{8}$$

where $k(t)$ is the correction factor. According to Uomoto [16], the carbonation depth is related to the square root of the CO_2 concentration, and the factor $k(t)$ is therefore defined by:

$$k(t) = \frac{\sqrt{C(t)}}{\sqrt{C_{t0}}} \tag{9}$$

where C_{t0} is the CO_2 concentration in the study of Kishitani [14], and the value of $C(t)$ can be obtained from the Japan Meteorological Agency [2]. Figure 3.6 shows the CO_2 concentration over time in Hokkaido.

Accordingly, the carbonation depth of a concrete structure that served for T years was modified as:

$$d = \int_0^T \frac{k(t) \cdot A}{2\sqrt{t}}\, dt \tag{10}$$

If $k(t)$ is a constant value, Equation (10) is simplified as Equation (8).
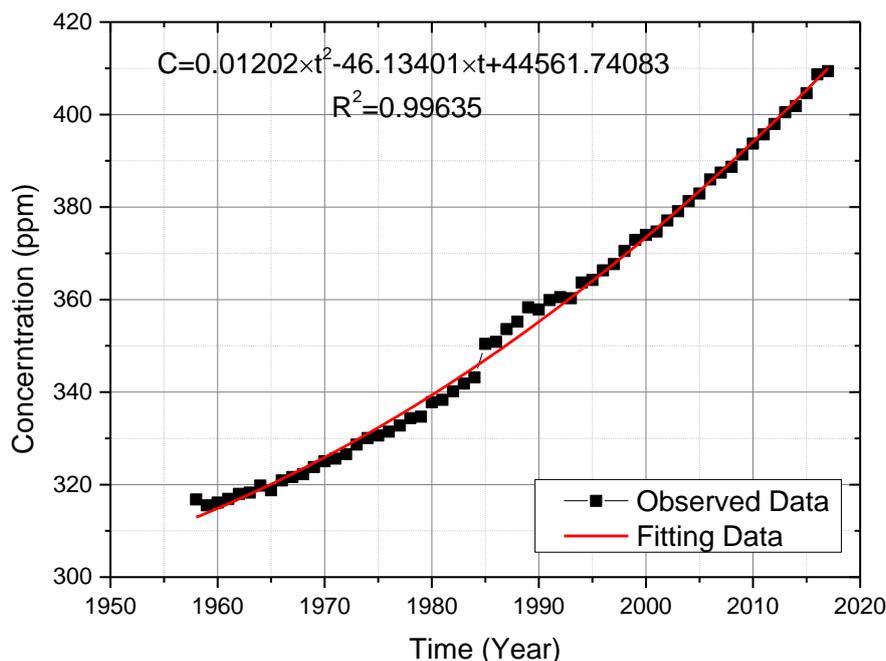
Figure 3.6 Carbon dioxide concentration versus time

3.1.2 Inspection results

The deterioration grades of bridges are used to understand the conditions of the bridges. Based on the inspection guidelines [13], bridges are required to be visually inspected every five years, the results of which are categorized as: (i) grade 1: healthy; (ii) grade 2: preventive maintenance required; (iii) grade 3: prompt action required; and (iv) grade 4: emergency action required. The grades and corresponding descriptions are given in Table 3.3. Since the grade 4 is considered critical condition, meaning that these bridges has to be subjected to a repair timely, this philosophy results in infrequent occurrence of grade 4. Therefore, the grade 3 is considered to be the upper threshold, because the grade 3 indicates the necessary of early actions. This urges us to build a predictive model to predict the situation before an emergency occurs.

Table 3.3 Deterioration grades and corresponding descriptions

Grade	Conditions	Descriptions
1	Healthy	A state that the function of the structure is not disturbed.
2	Preventive action required	Although the function of the structure is not hindered, it is desirable to take measures from the viewpoint of preventive maintenance.
3	Early action required	The function of the structure has interfered and measures should be taken as soon as possible.
4	Emergency action required	A condition in which the function of the structure has been or is likely to be impaired, and measures should be taken urgently.

3.1.3 Data characteristics analysis

Twelve factors that have the potential to influence deterioration are listed in Table 3.1. The deck area is the

value of bridge length multiplies bridge width. All factors were scaled to the range of 0-1 according to Equation (6) in Section 2.2 to accelerate the convergence of training. The results were listed in Table 3.4. The type of bridge was excluded when establishing the MLP, RNN, and MC models, as it is irrational to represent different bridge types with a number. Although it is feasible to create unique models for different types of bridges, this endeavor is hampered by a lack of data on different types of bridges. Discussions regarding the performance of the established models on different types of bridges were described in Section 3.3, Section 3.4 and Section 3.5, respectively.

Table 3.4 Data characteristics analysis

| | | After scaled | |
| | Original data | | Standard |
Factor	range	Mean	deviation
Deck area (m^2)	6~27,216	0.0253	0.05376
Elevation (m)	-0.3~1,106	0.0909	0.1347
Carbon dioxide (ppm)	348.86~409.87	0.3933	0.2413
Chloride (kg/m^3)	0~11.79	0.0490	0.1238
Rainfall (cm)	776~1,491	0.3617	0.2268
Snowfall (cm)	12.0~1,263.8	0.4493	0.2166
Highest temperature (°C)	16~26	0.7025	0.1737
Lowest temperature (°C)	-11~-3	0.5851	0.2361
Traffic volume (daily)	0~56,874	0.0946	0.1143
Large-size vehicles (daily)	0~13,906	0.3076	0.1786
Years in service (years)	1~84	0.3833	0.2008

In addition, we counted the distribution of each factor divided by the three deterioration grades. Specifically, the histogram of each factor was firstly obtained. Then, the Gamma, exponential, and the normal distributions were used to fit the histograms to select the optimal distribution. The results were shown in Figure 3.7. The detailed parameters for the fitted distributions were shown in Table 3.5. The results show that:

(1) For the elevation, there were no obvious differences in distribution between of the three deterioration grades.

(2) The deterioration grade was positive related to the deck area, because the mean deck area increaed from grade 1 to grade 3.

(3) Similarly, the mean years in service was positive related to the deterioration grade.

(4) The deterioration grade was negative related to avergae CO2 concentration. Because the serviced years of bridges being grade 1 is shorter, and the CO2 concentration is increasing.

(5) There is no necessary relations between the deterioration grades and the chloride ions, because the deteriration has many reasons and the content of chloride ions is decided by the bridges' location.

(6) The deterioration grade was positive related to number of average large-size vehicles.

(7) Similarly, the deterioration grade was positive related to the number of average traffic volume.

(8) The deterioration grade was not necessarily related to the average rainfall.

(9) The deterioration grade was negative to the average snowfall. However, the histogram of grade 3 does not fit well with any distribution; it can only concluded that deterioration grade was not

necessarily related to average snowfall.

(10) The deterioration grade has no absolute relationships with average highest temperature and average lowest temperature.
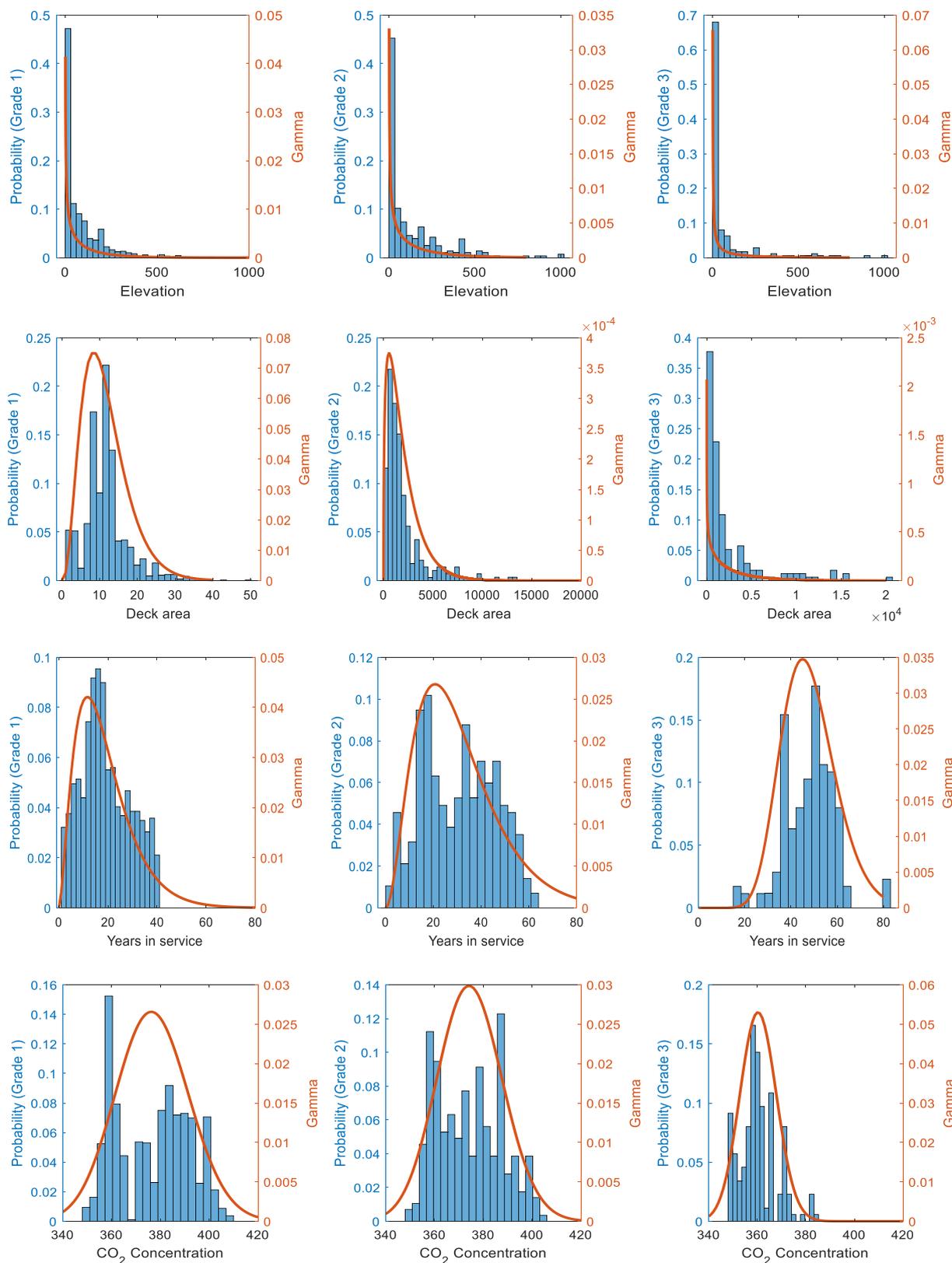

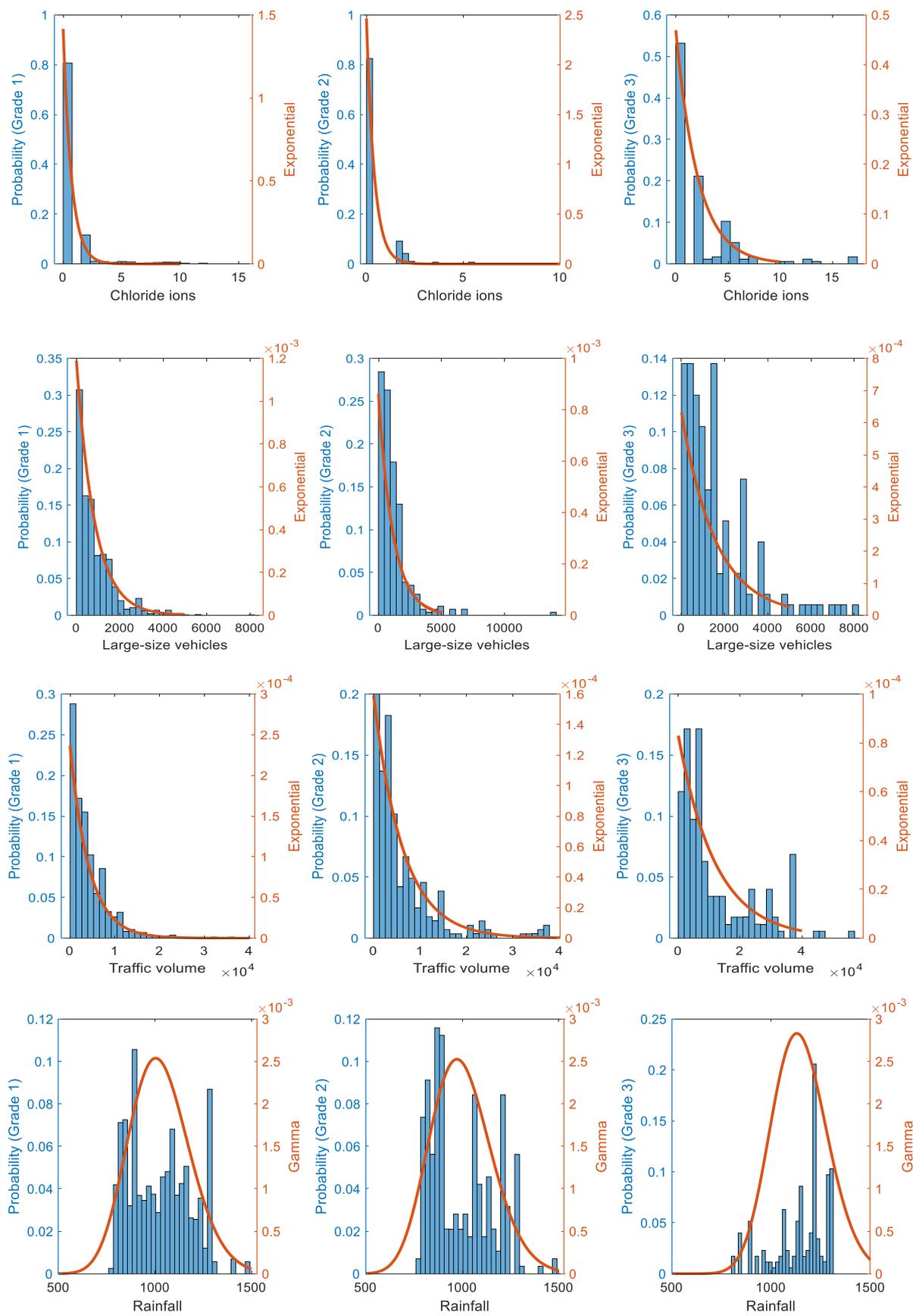Figure 3.7 Distribudion of each factor's values

Figure 3.7 Distribudion of each factor's values (Contiue)
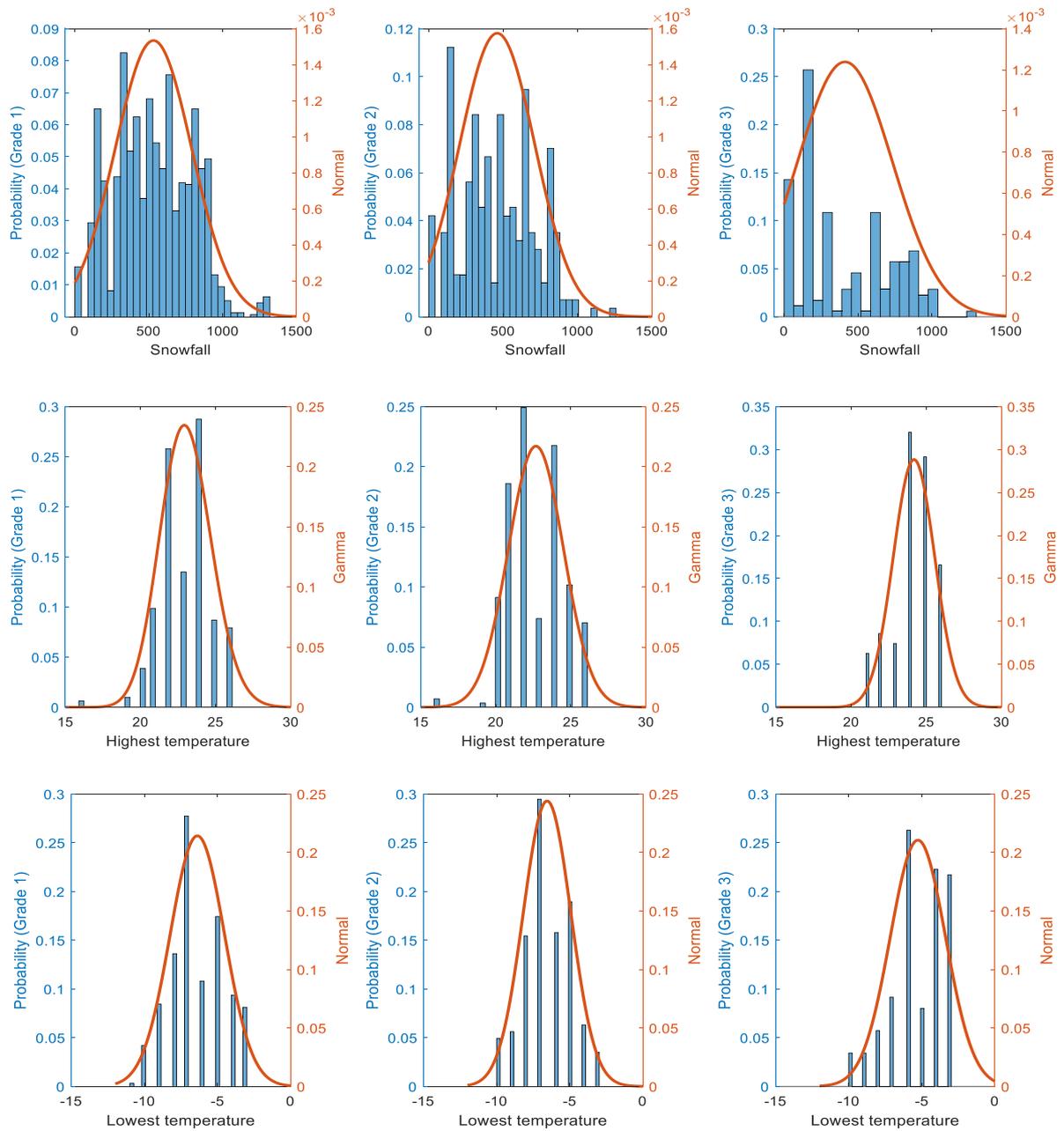
Figure 3.7 Distribudion of each factor's values (Contiue)

Table 3.5 The fitted distribution of the histogram

Factor	Grades	Distribution	Parameters [95% confidence intervals]		Mean
			Shape(Mu)	Scale(Sigma)	
Elevation	Grade 1	Gamma	0.509 [-Inf, Inf]	172.758 [-Inf, Inf]	87.935
	Grade 2	Gamma	0.520 [-Inf, Inf]	248.956 [-Inf, Inf]	129.573
	Grade 3	Gamma	0.219 [-Inf, Inf]	364.051 [-Inf, Inf]	79.717
Deck Area	Grade 1	Gamma	3.703 [3.466, 3.958]	3.129 [2.914, 3.360]	11.5890
	Grade 2	Gamma	1.401 [1.207, 1.626]	1400 [1171.57, 1672.97]	1961.5
	Grade 3	Gamma	0.736 [0.615,0.881]	3288.34 [2563.54,4218.06]	2420.6
Years in service	Grade 1	Gamma	2.665 [2.462, 2.885]	6.989 [6.405, 7.626]	18.628
	Grade 2	Gamma	3.092 [2.645, 3.614]	9.900 [8.356, 11.729]	30.611
	Grade 3	Gamma	16.535 [13.437, 20.347]	2.897 [2.347, 3.577]	47.909
CO_2	Grade 1	Gamma	629.057[586.966, 674.166]	0.599 [0.559, 0.642]	376.882
	Grade 2	Gamma	785.434 [666.529, 925.55]	0.4769 [0.405, 0.562]	374.576
	Grade 3	Gamma	2293.47[1859.95, 2828.02]	0.157 [0.127, 0.194]	360.430
Chloride ions	Grade 1	Exponential	841.018 [801.295,883.784]	-	0.707
	Grade 2	Exponential	1161.42 [1037.56, 1309]	-	0.406
	Grade 3	Exponential	1585.17[1374.23, 1848.97]	-	2.131
Large-size vehicles	Grade 1	Exponential	841.018[801.295, 883.784]	-	841.018
	Grade 2	Exponential	1161.42 [1037.56, 1309]	-	1161.4
	Grade 3	Exponential	1585.17 [1374.23,1848.97]	-	1585.2
Traffic Vehicles	Grade 1	Exponential	4230.44[4030.63, 4445.55]	-	4230.44
	Grade 2	Exponential	6296.62[5625.07, 7096.7]	-	6296.62
	Grade 3	Exponential	12051.7 [10448, 14057.4]	-	12051.7
Rainfall	Grade 1	Gamma	41.943[39.146, 44.939]	24.513 [22.869, 26.275]	1028.1
	Grade 2	Gamma	39.071 [33.178, 46.0111]	25.544 [21.669, 30.113]	998.046
	Grade 3	Gamma	65.405[53.069, 80.607]	17.542 [14.222, 21.637]	1147.3
Snowfall	Grade 1	Normal	531.934 [519.189, 544.68]	260.002[251.298,269.335]	531.934
	Grade 2	Normal	461.00 [431.469, 490.537]	253.305[234.076, 276.002]	461.003
	Grade 3	Normal	411.548[363.499,459.598]	322.054 [291.478,359.851]	411.548
Highest temperature	Grade 1	Gamma	182.682[170.466,195.773]	0.12614 [0.118, 0.136]	23.044
	Grade 2	Gamma	22.674 [22.460, 22.888]	1.837 [1.698, 2.002]	22.674
	Grade 3	Gamma	24.189[23.982, 24.395]	1.3829 [1.252, 1.545]	24.189
Lowest temperature	Grade 1	Normal	-6.380 [-6.472, -6.289]	1.862 [1.799, 1.9285]	-6.3804
	Grade 2	Normal	-6.547 [-6.738, -6.357]	1.634 [1.5103, 1.781]	-6.5474
	Grade 3	Normal	-5.268 [-5.551, -4.986]	1.894 [1.714, 2.117]	-5.2686

3.3 Establishment of a MLP model

3.3.1 Model establishment

Conforming to the descriptions in Section 2.3, the mean value of each factor among all its observations is taken as the input value of this factor. As a result, the input consist of eleven factors was obtained for each bridge. Using the database including eleven factors (Table 3.4) and the three deterioration grades in Table

3.3, the MLP neural network prediction model was constructed. The optimal configuration of the prediction model was determined by trial and error. The accuracy is used as an indicator with a higher identification competence. In the trial and error, various values were tested for each parameter [17], as listed in Table 3.6. Figure 3.8 depicts the nonlinear activation functions used in the trial and error. The Softmax was applied between the hidden layer and the output layer. Relu and Tanh were applied between the input and hidden layers.
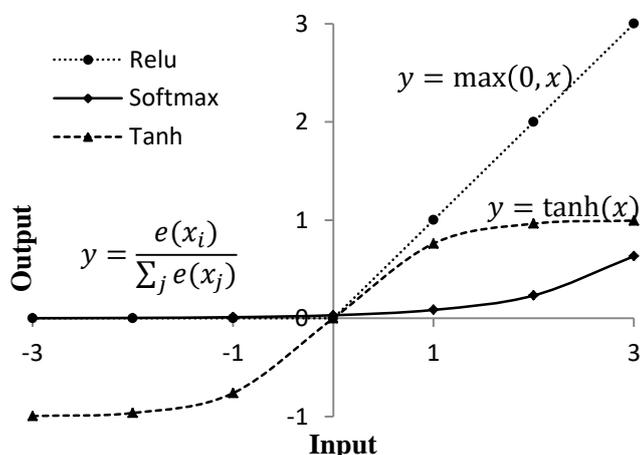
Figure 3.8 Activation functions

Table 3.6 Configuration test results

Parameters	Parameters	*p*-value	
		Training	Testing
Number of hidden layers	1, 2	5.489×10^{-1}	1.154×10^{-1}
Number of hidden neurons	5, 10	4.236×10^{-1}	8.454×10^{-1}
Learning rate	0.01, 0.001	3.222×10^{-4a}	3.860×10^{-2a}
Learning algorithm	SGD, RMSProp, Adagrad, Adadelta, Adam, Adamax, Nadam	5.513×10^{-14a}	8.490×10^{-15a}
Hidden activation function	Relu, tanh	4.904×10^{-1}	7.622×10^{-1}

[a] Significant at 95% level of confidence

Considering all combinations of the five parameters, 112 cases were tested (Appendix A). In each trial, stratified sampling was used to randomly divided dataset into the training, testing, and validation subsets, which accounted for 70%, 15%, and 15% of the maintenance database, respectively. Then each case was tested three times to obtain an average value to eliminate the differences in each test. Analysis of variance (ANOVA) is an tool used in statistics to observe whether the independent variables have a significant impact on the dependent variable. Therefore, ANOVA analysis was applied to the testing results to examine the significance of each parameter on training/testing accuracy. A *p*-value of 0.05 or less means that a factor is considered to have a significant influence on deterioration. The *p*-value summarized in Table 3.6 indicated that the learning rate and learning algorithm influence training/testing accuracy significantly. Looking through the testing results, the MLP produces higher accuracy when it has one hidden layer of ten neurons, has the activation function of Relu, and it is trained with adaptive moment estimation (Adam) algorithm with the learning rate of 0.01.

The expected MLP consisted of a 3,368×12 matrix as the inputs (including the bias), and a 3,368×1 matrix as the output. As the initial values of W_1 and W_2 (Figure 2.2) are randomly assigned during training, the predicted grades are usually inconsistent with the actual grades. The cross-entropy value expressed in

Equation (7) in Chapter 2 was used to calculate the error between the actual grades and the predicted grades.

The training calculation iterated 2000 times, and the error between the predicted and the actual grades was evaluated using the cross entropy. As shown in Figure 3.9, the accuracy converged to approximately 65%, and the error converged to approximately 0.2.

(a)   (b)

Figure 3.9 Loss and accuracy.

3.3.2 Model evaluation
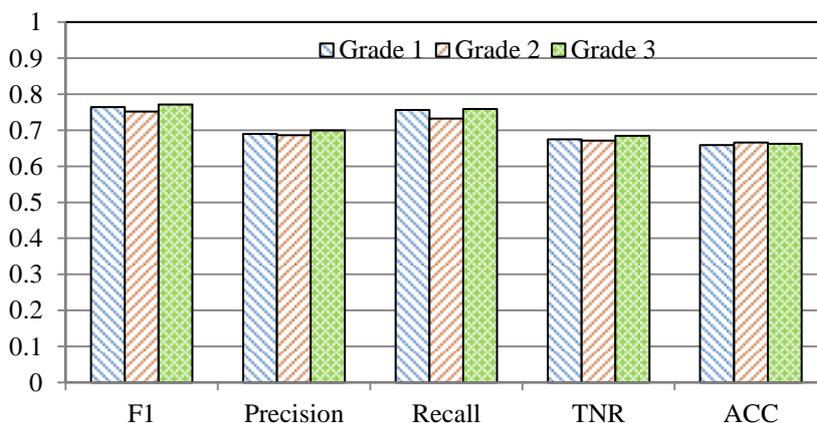
Figure 3.10 Performances of the MLP neural network for different grades

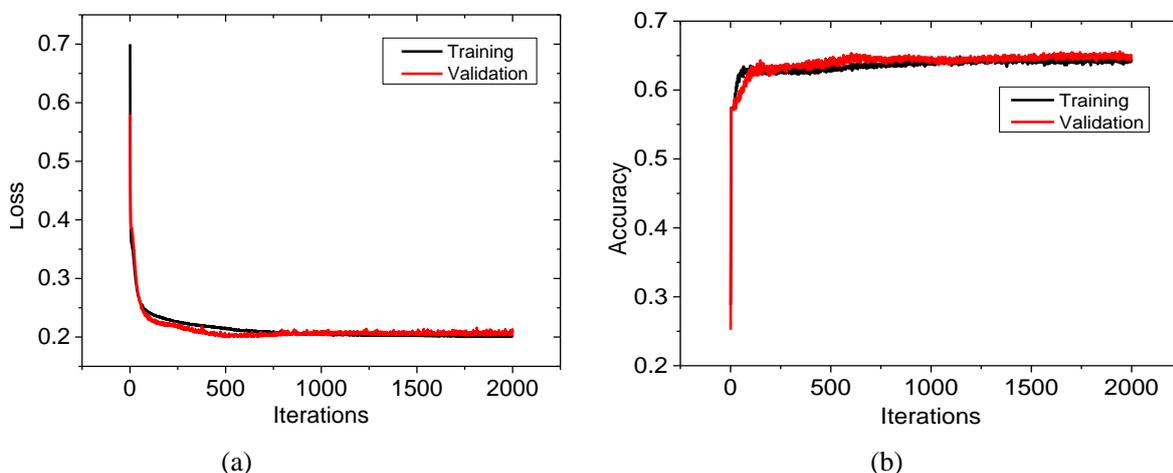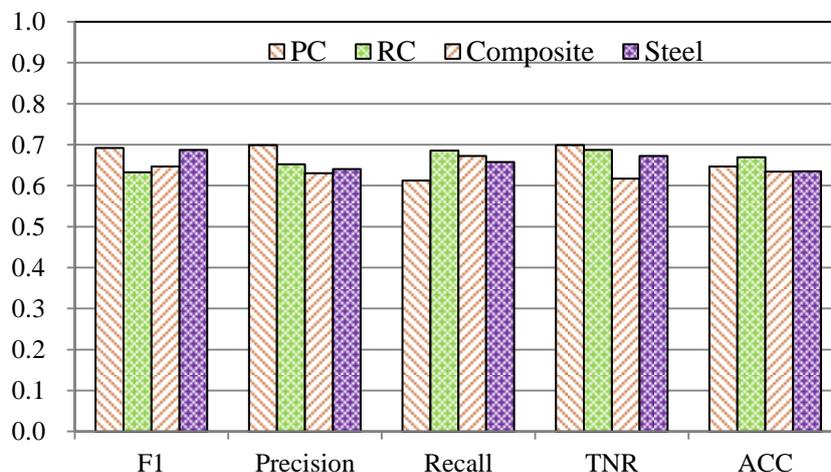Figure 3.11 Performances of the established neural network for different types of bridges.

Figure 3.10 shows these metrics' values of the MLP model for the three deterioration grades. The results indicated that the established MLP model has equivalent performance for the three deterioration grades. In addition, the model was applied to PC, RC, steel & concrete composite, and steel bridges to evaluate the performance of the model for corresponding types of bridges. Figure 3.11 shows that the model has equivalent performance regardless of the types of bridges. Although the established MLP model is not yet perfect, the model is unbiased for the different deterioration grades and different types of bridges.

3.4 Establishment of a RNN model

A further overview of the steps taken to establish a RNN model and to perform deterioration prediction is given in Figure 3.12. In the training phase, we first converted the influencing factors from the inspection database to vectors and normalized the vectors to the range of 0-1. The training and validation sets are then applied to train a deterioration prediction model using the LSTM-based RNN. The model is optimized by iteratively updating the weights between the potential influencing factors and the predicted results [18]. In the prediction phase, the testing data of a bridge are first converted into normalized vectors, and the vectors are then introduced into the trained model, which in turn will calculate the grade of deterioration. According to previous studies [18-19], the LSTM model was trained on 70% of the data and validated on 15% of the data, and the remaining 15% was used as the testing set. The training algorithm of the adaptive moment estimation (Adam) was adopted to speed up the training operations.
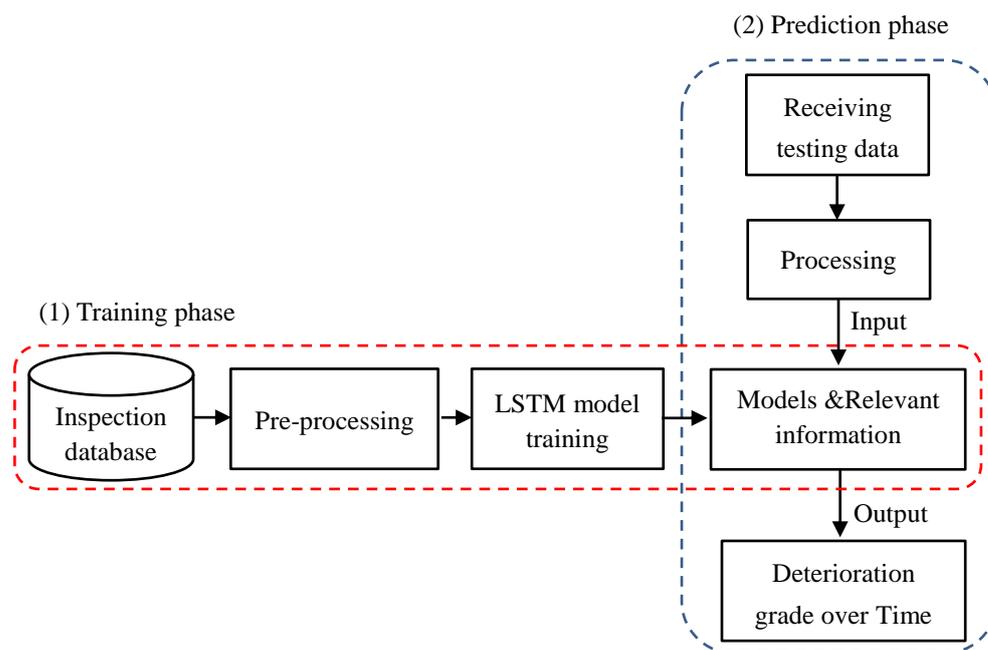
Figure 3.12 Procedures for establishing RNN model

Using the inspection database, we explored the ability of the LSTM-based RNN to model the relationships between potentially influencing factors and bridge deterioration. The optimal configuration of the LSTM model was determined by trial and error, as summarized in Table 3.7. The accuracy of the model was first tested using from 50 to 200 hidden units. The results showed that 150 hidden layers yield better results for this database. Different batch sizes were then tested with 150 hidden units as a second step to determine the LSTM configuration. The results indicated that the LSTM model performed better when the model had 150 hidden units and a batch size of 1024.

Table 3.7 Configuration test of LSTM model

LSTM type	Accuracy rate (%) (training/testing)	Average accuracy rate (%) (training/testing)
	Number of hidden units	
50	66.2/69.3 67.3/66.9 67.4/69.5	66.97/68.57
100	70.7/72.4 69.1/69 70.4/69.3	70.07/70.23
150	81.19/80.8 80.06/80.5 80.86/81.08	80.70/80.79
200	75.2/72.2 77.3/72.4 73.8/72.7	75.43/72.43
	Batch size	
256	55.2/54.7 55.18/54.69 55.23/53.2	55.2/54.19
512	68.1/64.4 67.8/66.6 70.1/67	68.67/66.0
1024	81.19/80.8 80.06/80.5 80.86/81.08	80.70/80.79

Figure 3.13 Accuracy and loss with respect to iteration.

The training calculation iterated 6000 times, and the error between the predicted value and the ground truth was evaluated by using the cross-entropy. As shown in Figure 3.13, the accuracy converged to approximately 80%, and the error converged to approximately 0.35. Future endeavors are necessary to improve the established model by actions described in Section 3.4.3.

As eleven factors are considered to affect the deterioration, the relationship between the affecting factors and the deterioration grades is a 12-D model. To intuitively reflect this relationship determined by the LSTM model, Figure 3.14 shows the mapping between the affecting factors and the deterioration grades. The results in Figure 3.14 and the performance of the model in Section 3.4.1 reveal that the complicated relationships are preliminarily established.
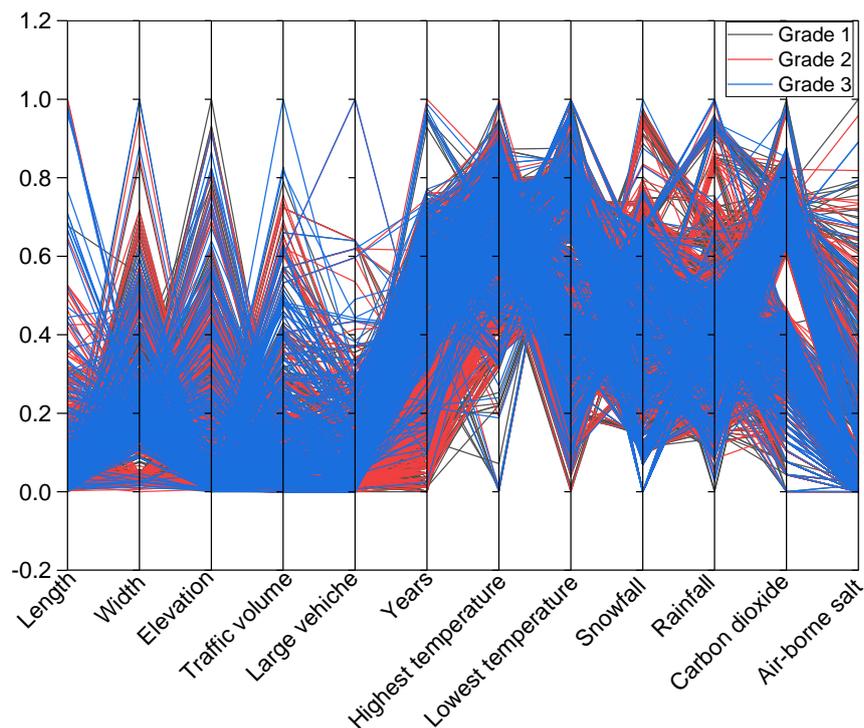
Figure 3.14 Mapping between affecting factors and deterioration grades

3.4.1 Performance of the model

The performance of the LSTM-based RNN was evaluated from two aspects: (1) the performance of the LSTM compared with the MLP model; and (2) the performance of the LSTM for different bridge types, different environments, and different deck area.

(1) The performance of the LSTM compared with the MLP model

The performance of the LSTM model was first compared with that of the MLP model. Figure 3.13 showed that the accuracy of the LSTM model exceeded 80%. As a comparison, an MLP model obtained an accuracy of 65% on the same database in Section 3.3. Obviously, the prediction accuracy of the LSTM-based RNN model exceeds that of the MLP model by approximately 17%.
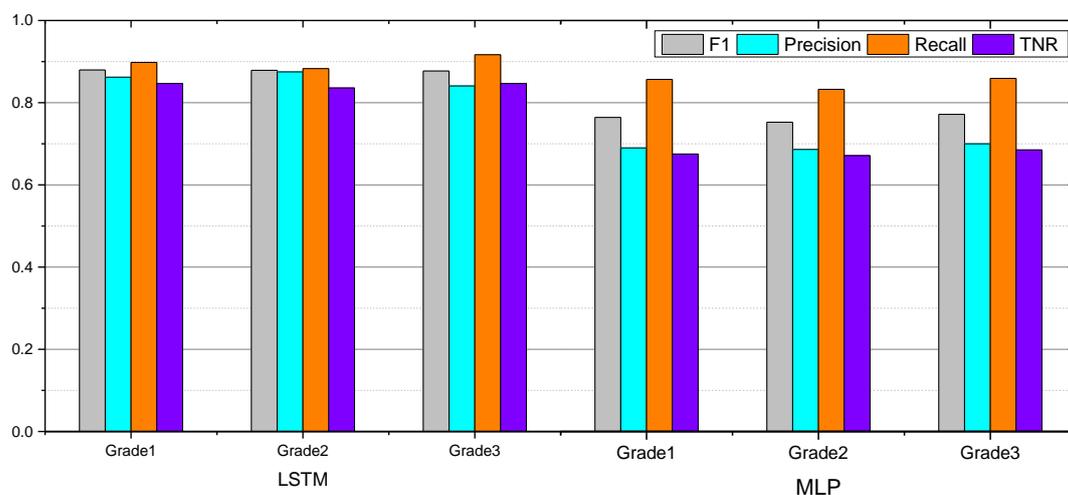
Figure 3.15 Comparison of the LSTM and MLP models

In addition, the recall, precision, TNR, and F1 score of the two models were calculated, as shown in Figure 3.15. These four indexes showed that the LSTM model obtained greater values regardless of the grades. Therefore, it can be concluded that the grades estimated by the LSTM model is more accurate than those estimated by the MLP model. Through comparative research of the LSTM and MLP models, the results show that the LTSM model yields considerable improvement and has a relative superiority compared to the MLP model. However, it should be remembered that the LSTM architecture is much more complicated. In other words, although an LSTM-based RNN prediction model is more robust, the complex architecture and calculations make it difficult for engineers to establish such a model easily.

(2) The performance of the LSTM for different bridge types, environments, and deck area

Furthermore, the model was applied to PC, RC, steel & concrete composite and steel bridges to evaluate the performance of the model for corresponding types of bridges. Figure 3.16 showed that the model has the equivalent performance regardless of the types of bridges.
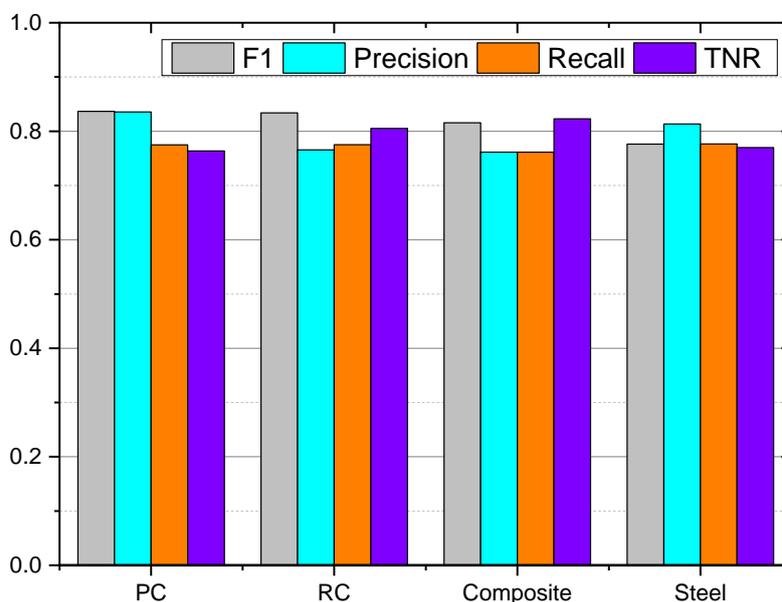
Figure 3.16 Performance of the LSTM for the PC, RC, steel & concrete composite, and steel bridges
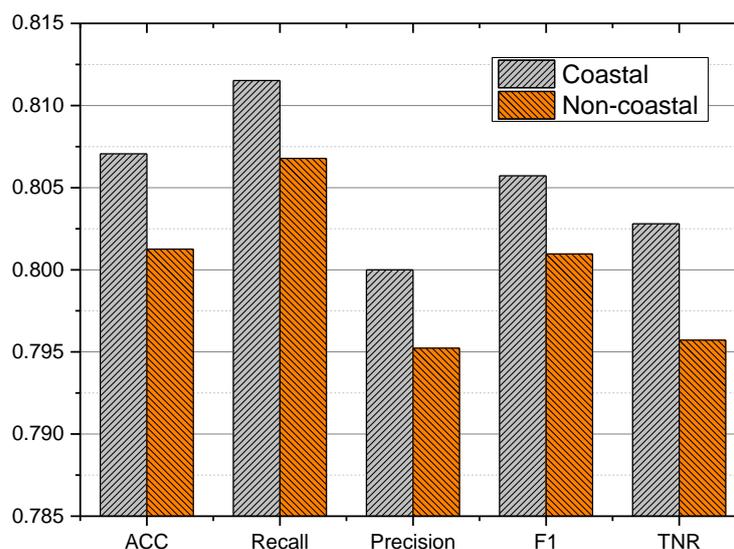
Figure 3.17 Performance of the LSTM for bridges in costal and non-coastal regions

Similarly, the performances of the LSTM model for bridges in coastal and non-coastal regions were evaluated, as displayed in Figure 3.17. The results showed that prediction ability of the model for coastal bridges were slightly outperforms that for the non-coastal bridges. One possible reason is that de-icing salt was not considered for non-coastal bridges because relevant data cannot be collected.

The accuracies of the model versus the deck area were also assessed, as shown in Figure 3.18. The evaluation implies that there is no significant difference in accuracy between different deck areas. The reason is that the established model is unbiased for the different deck areas, although the LSTM model is not yet perfect.
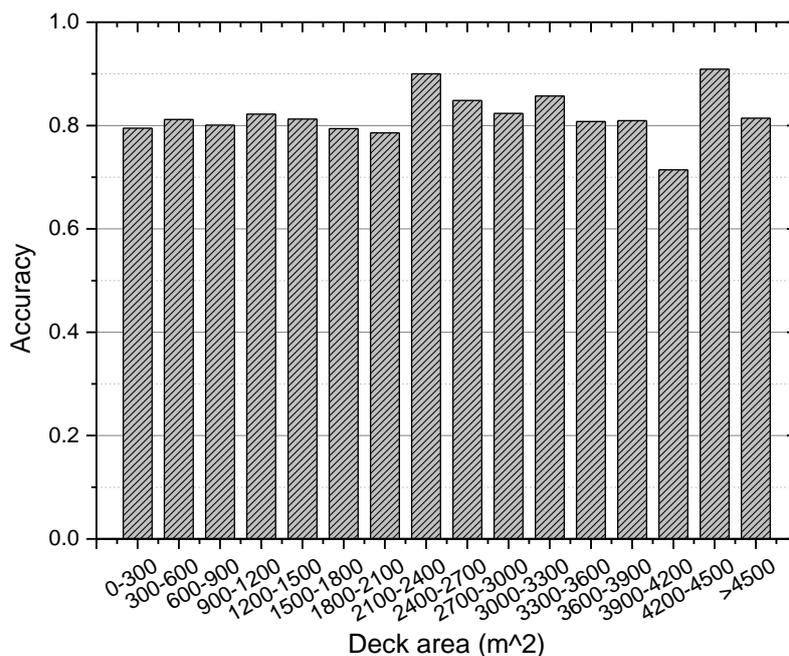
Figure 3.18 Accuracy of the LSTM versus the deck area

3.4.2 Error analysis

(1) Distribution of incorrect predictions

The percentages of incorrect predictions made by the LSTM model in various situations were calculated, as summarized in Table 3.8. For example, the situation where an actual grade 1 bridge is predicted to be grade 2 accounts for 17.3% of all incorrect predictions. As Table 3.8 shows, predicting actual grade 2 brides to be grade 1 and predicting actual grade 1 bridges to be grade 2 accounts for more than half of all incorrect predictions. The confusion between actual grade 2 and predicted grade 3 is another major source of incorrect predictions. The percentages of incorrect predictions in other conditions do not show obvious differences.

For the dark marked area in Table 3.8, the predicted grades are usually larger than the actual grades, which mean that the predictions are aggressive. Under aggressive conditions, timely maintenance can be conducted to ensure the soundness of the bridge, but this will increase costs. For the non-dark marked areas, the predicted grades are smaller than the actual grades, which mean that the predictions are conservative. If suggestions under conservative conditions are followed, the timely maintenance of the bridge may be ignored. Aggressive and conservative situations accounted for 45.7% and 55.3% of all incorrect predictions, respectively. It is believed that using more abundant information (such as quantitative deterioration grades) will assist in overcoming this challenge and yield fewer incorrect

predictions.

Table 3.8 Percentages of incorrect predictions.

Actual grade \ Predicted grade	1	2	3
1	-	17.3%	10.4%
2	34.4%	-	17.0%
3	10.7%	10.2%	-
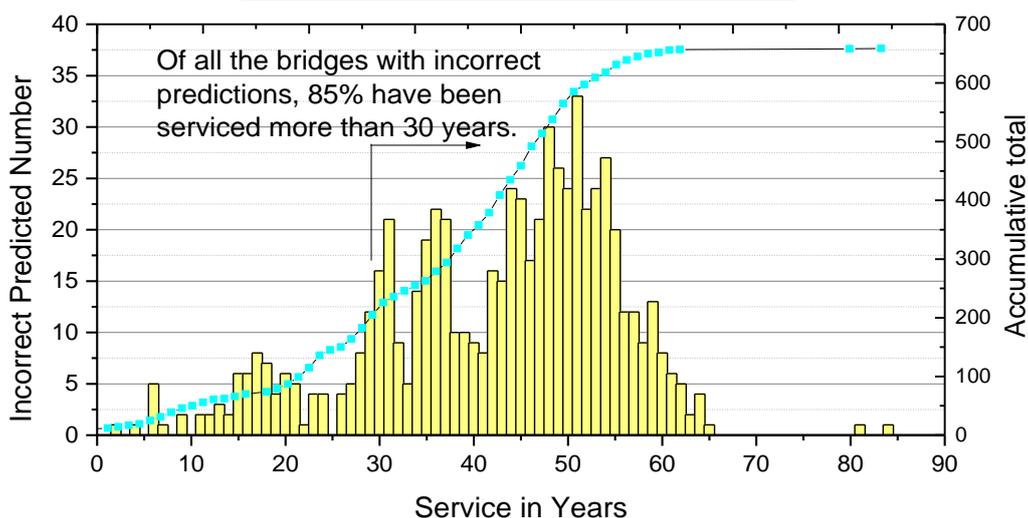
Figure 3.19 Numbers of incorrect predictions versus years in service

(2) Related factors

In addition, we also assessed which factors result in incorrect predictions for these bridges. Among all considered factors in this study, other factors do not necessarily have relationships with the incorrect predictions except for the factor of years in service. The numbers of incorrect predictions versus the years of in service are shown in Figure 3.19. If incorrect predictions are divided into two parts by 30 years in service, the calculations show that almost 85% of all incorrect predictions are bridges that have been in service for more than 30 years.
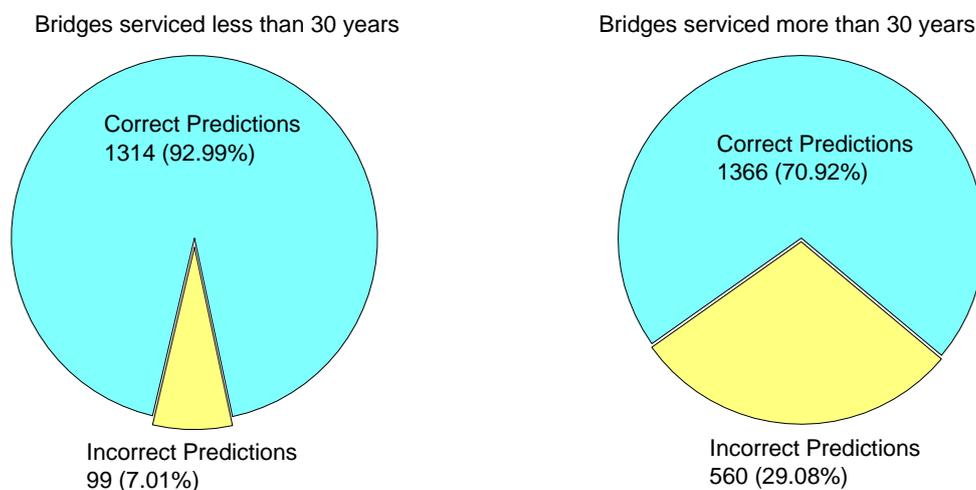
Figure 3.20 Percentage of incorrectly predictions (Dividing by 30 years)

Furthermore, the inspection database was divided into two groups. One group is aged from 0 to 30 years, and the other is aged 31 and above. Then, the percentages of incorrect predictions in the corresponding groups were calculated, as shown in Figure 3.20. Among the first group, incorrect predictions account for 7.01%, while that rate is up to 29.08% for the second group. Interventions are thought of as the main reasons that lead to the differences between the two groups. This occurs because interventions were mainly implemented for bridges that have been in service more than 30 years, but relatively few interventions are implemented for bridges that have been in service less than 30 years. In addition, the observations of some factors 30 years ago were the estimated values. The observed values in the last three decades were more convincing given that the improvement of observation methods and techniques. Therefore, caution should be exercised when making predictions for bridges that have been in service for more than 30 years.
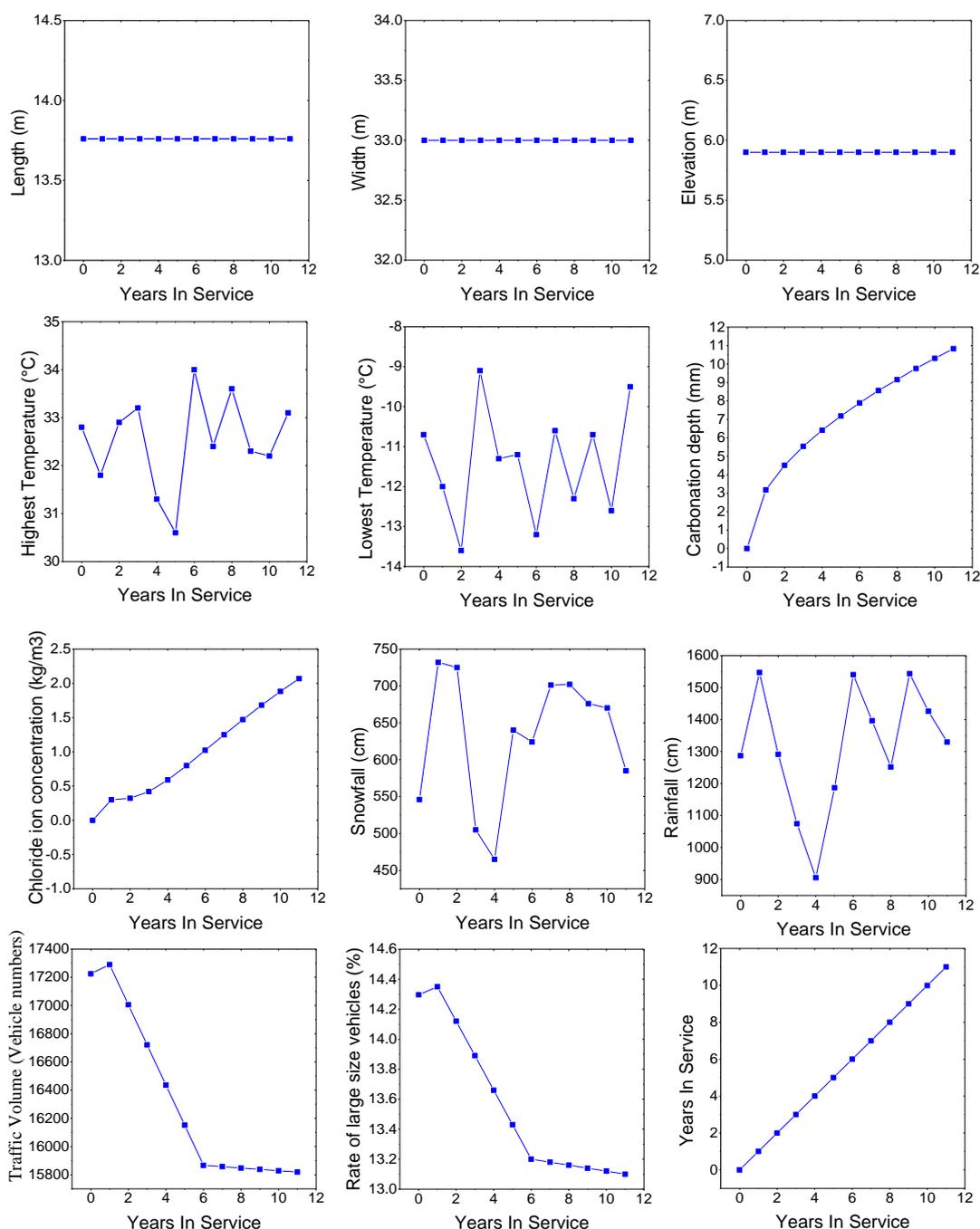
Figure 3.21 Time series diagram of all factors
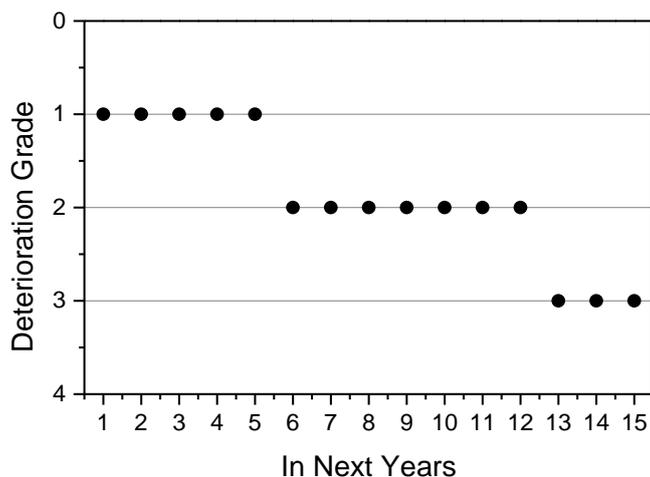
Figure 3.22 Prediction of deterioration grade in the next fifteen years.

3.4.3 Discussions

(1) Usefulness

The results indicated that the prediction model could guide the quality inspection of existing structures. Specifically, provided the time series of all factors for a bridge, future deterioration can be estimated. Figure 3.21 shows the time series diagram of all factors for an RC bridge. The latest inspected deterioration grade is 1.

Using the prediction model, the deterioration conditions of the bridge in the next fifteen years were predicted, as shown in Figure 3.22. It can be inferred from the predicted results that the condition of the bridge in the next five years will not deteriorate significantly. Therefore, the inspection of the bridge can be postponed. Of course, if the bridge deteriorates significantly in the next five years, the bridge can be inspected in advance, and corresponding intervention measures can be taken. The prediction model makes it possible for the decision-makers to formulate a flexible inspection schedule according to the deterioration situation.

In addition, the initial achievements in this study provided a case to explore the deterioration prediction for other infrastructures. Then, we can integrate all these deterioration prediction models into the infrastructure management system (IMS) to enable managers or local authorities to manage and formulate intervention strategies for infrastructure. Furthermore, the limitations revealed in this study (Section 3.4.3 (2)) will prompt the collection of more detailed data during the inspection process in the future.

(2) Insufficiency

Our proposed model focused on the goal of making accurate and robust predictions relying on time series data of many potential factors. Therefore, the outcome of the model is closely related to the data quality of each factor. If the information of some factors is missed/incomplete, or the inherent collation between factors and deterioration is not clear, our model may achieve limited improvements or even fail. This means that it is necessary to check the quality of the data for each factor. In addition, although our proposed model considered twelve potentially influencing factors, it does not mean these factors necessarily influence deterioration, or other factors that are not considered in this model may also impact deterioration. One good thing is that we can include more influencing factors or remove some factors by

57

updating the rows of the input matrix and by modifying the configuration (size of input x_t) of the LSTM model (Section 2.4).

Although the performance of the LSTM model is improved relative to an MLP model, the architecture of the LSTM-RNN model is much more complicated than that of the MLP. In addition, more data are needed to train an LSTM-RNN model. Therefore, it is not easy to establish a model such as that in this study considering the availability of the database, especially in practical engineering. In the calculation of chloride ions penetrating into concrete, the diffusion coefficient D_c is considered a constant. This assumption is inconsistent with the actual situation, which makes the LSTM model deviate from reality to a certain extent. In addition, error analysis found that the model is prone to be confused between grades 1 and 2 bridges, because the misclassification between these two grades accounts for half of the failed predictions. It should be cautious when applying the model for predicting conditions of bridges that are more than 30 years old. Incorrect prediction increases greatly when applying the model for predicting conditions of bridges that are more than 30 years old.

The proposed model is evaluated by using a database formed using past inspection data. However, a good prediction model should be generalizable. This means that the LSTM-based RNN in the study should fit future observations well but cannot be verified now. The requirements will motivate us to improve data collection strategies to acquire more valuable data. In addition, other time series approaches such as Bayesian approach will be verified and compared with the model in this study.

3.5 Establishment of a Markov Chain model

As described in Section 2.6, Markov Chain (MC) is a probabilistic method. In this section, an MC model was built using the inspection database mentioned in Section 3.2. Later, the MC model was compared with the LSTM model in the deterioration progresses. These contents were detailed below.

3.5.1 Markov Chain model

The hazard variable can be obtained according to Equation (11). Therefore, 20 unknown parameters regarding the deterioration grades are need to be estimated. According to Equation (38) in Chapter 2, the maximum log-likelihood is considered the optimal parameters combinations of the hazard model. Table 3.9 shows the estimated values for these parameters. Interval 1-2 means deterioration from grade 1 to grade 2, and 2-3 means deterioration from grade 2 to grade 3.

$$\lambda_i^{\,k} = x_1^k \beta_{i,1} + x_2^k \beta_{i,2} + \cdots + x_{11}^k \beta_{i,11} \quad (\text{i}=1,2,3; \text{k}=1,2,\dots,K) \tag{11}$$

Table 3.9 Hazard model based on Markov chain exponential distribution

		Deterioration intervals	
		1-2	2-3
Number of Samples		2273	1331
Deck area	$\beta_{i,1}$	0.1034	0.1623
Elevation	$\beta_{i,2}$	0.4890	0.2658
Carbon dioxide	$\beta_{i,3}$	0.4063	0.1052
Chloride	$\beta_{i,4}$	0.3380	0.2881
Rainfall	$\beta_{i,5}$	0.1307	0.0468
Snowfall	$\beta_{i,6}$	0.0474	0.1467
Highest temperature	$\beta_{i,7}$	0.2436	0.0591
Lowest temperature	$\beta_{i,8}$	0.5923	0.0451
Traffic volume	$\beta_{i,9}$	0.5783	0.0350
Large-size vehicles	$\beta_{i,10}$	0.5803	0.0396

Afterwards, the Markov transition probability matrix can be obtained using the estimated values based on Equation (33) in Chapter 2, as shown in Equation (12). As described, the probability of a direct deterioration from grade 1 to grade 3 is low.

$$\pi = \begin{pmatrix} \pi_{11} & \cdots & \pi_{13} \\ \vdots & \ddots & \vdots \\ 0 & \cdots & \pi_{33} \end{pmatrix} = \begin{pmatrix} 0.8055 & 0.1738 & 0.0207 \\ 0 & 0.6704 & 0.3296 \\ 0 & 0 & 1 \end{pmatrix} \tag{12}$$

In addition, the expected survival time were calculated according to Equation (31) in Section 2.6. As a result, the average survival time being in grade 1 and grade 2 are 24.2555 and 10.5121 years, respectively. In other words, the bridge cost an average time of 24.2555 years to deteriorate from grade 1 to grade 2, and cost an average time of 34.7626 years to deteriorate from grade 1 to grade 3.

3.5.2 Comparisons on deterioration progresses using the RNN and MC

Comparisons of the RNN and MC will be elaborated from: (1) the mean deterioration progresses; (2) the deterioration progresses of different type of bridge; (3) the deterioration progress of a specific bridge; and (4) the influence of each factor on deterioration progresses.

(1) Mean deterioration progresses

A deterioration progress represents the deterioration process in which the years required to transfer from one grade to the next grade are exhibited. Figure 3.23 shows the average deterioration progresses obtained using the MC and RNN models. The MC model predicts bridge will deteriorate to grade 2 and grade 3 in 24.26 and 34.77 years, respectively. The results of the RNN show that the bridge will deteriorate to grade 2 and grade 3 at 22.50 and 32.52 years, respectively. The results indicate that no significant differences can be found from the deterioration progresses by these two models, except that the deterioration obtained by the RNN model is slightly earlier than that by the MC model. Therefore, it can be concluded that the deterioration tendency by those two approaches are approximately the same.
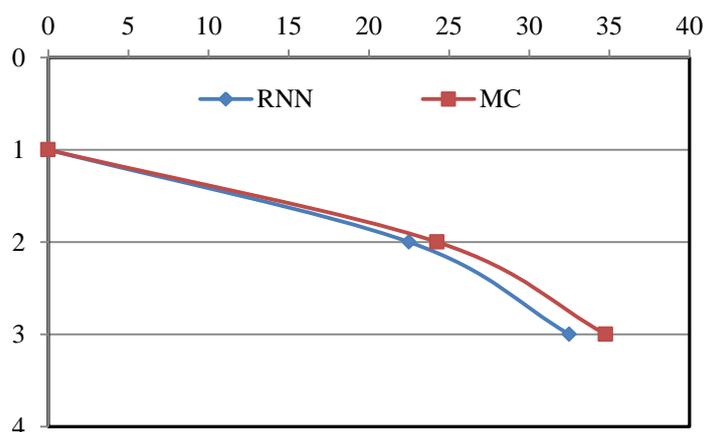
Figure 3.23 Mean deterioration progresses obtained using RNN and MC.

(2) Deterioration progresses of different types of bridges

To assess the influence of bridge type on the deterioration, the deterioration progresses of the four types of bridges were plotted, as shown in Figure 8. The mean deterioration progresses in Figure 3.24 (a) and (b) correspond to that in Figure 3.23. The results of these two approaches all indicate that: (i) the deterioration

of PC and the steel bridges are approximately the same; (ii) the RC and steel & concrete composite bridges deteriorate earlier than the rest two types of bridges; and (iii) the RC shows a worse durability compared to the remaining three types of bridges.

(a)

(b)
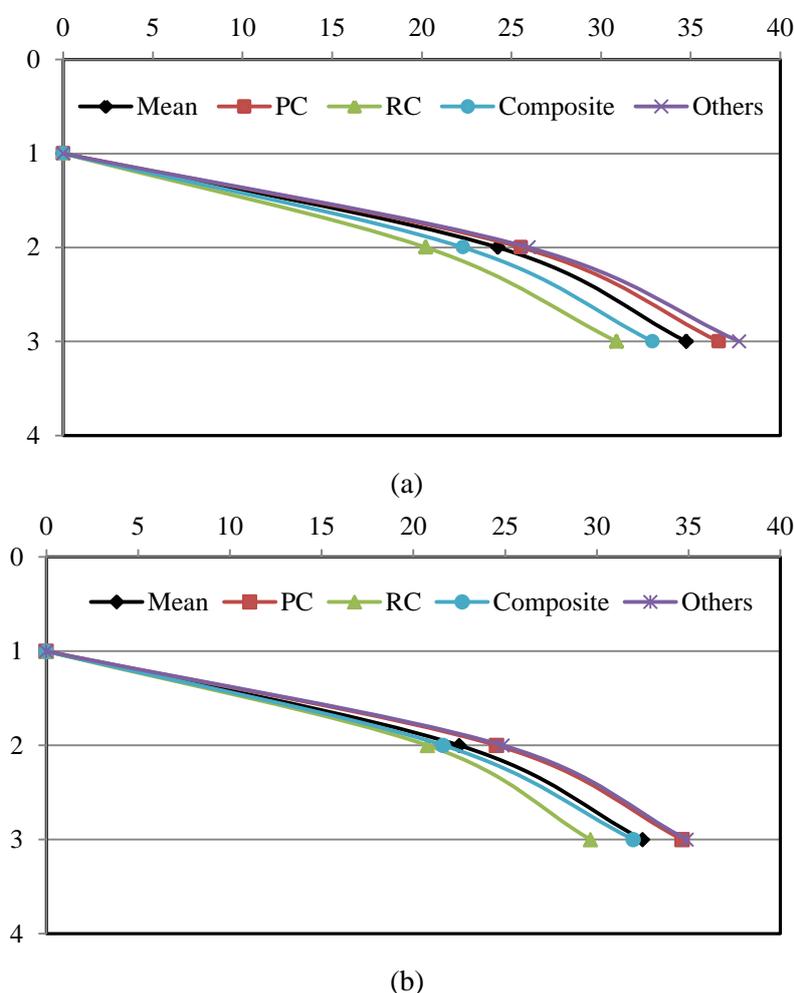
Figure 3.24 Deterioration progresses for different types of bridges: (a) using MC; (b) using RNN

Quantitatively, the MC model estimates that the PC bridge will deteriorate to grade 2 and 3 in 25.75 and 36. 81 years, this is not significantly deviated from the 24.55 and 34.81 years estimated by the RNN model. In terms of RC bridge, similarly tendency can be found, with 20.89 and 30.83 years by the MC model and with 20.17 and 29.50 by the RNN model. The steel & concrete composite bridge will deteriorates into the next two grades in 22.87 and 32.39 years by the MC model, and in 21.62 and 31.23 years by the RNN model. For steel bridges, the MC model obtained the deterioration moments of 25.43 and 37.86 years, and the RNN model achieved deterioration moments of 24.64 and 34.68 years. In summary, the estimated service time of the two methods for each type of bridge differs by no more than 5 years. In addition, the RNN model usually obtained a shorter lifetime than the MC model. Since MC and RNN models adopt all types of bridges, the deterioration progress of each type of bridge is averaged. As a result, the deterioration progress of each type of bridge obtained by these two approaches is almost the same. In addition, the type of bridge is a cause of the deterioration differences.

(3) Deterioration progress of a specific bridge

Further, bridges A and B with properties summarized in table 3.10 were selected. Then, the MC and RNN

were used to predict and compare their deterioration progresses for these two the two newly inspected grade 1 bridges. Because the bridges are inspected every five years, two approaches were used to predict deterioration conditions every five years, as shown in Figure 3.25.

Table 3.10 Information of bridges A and B

	Bridge A	Bridge B
Deck area (m^2)	332.5	137.94
Elevation (m)	3	2.9
Years in service (years)	12	50
Carbon dioxide (ppm)	393.32	356.38
Chloride (kg/m^3)	2.2	2
Rainfall (cm)	954	1060
Snowfall (cm)	345.77	635.60
Highest temperature (°C)	19	24
Lowest temperature (°C)	-3	-3
Traffic volume (Daily)	1057	13233
Large-size vehicles (Daily)	162	2686

Figure 3.24 shows that the deterioration progresses of bridge A and B obtained by MC and RNN, respectively. Bridge A just been in service for 12 years; therefore, the bridge will deteriorate gradually. Since bridge B has been in service for 50 years, both approaches conclude that bridge B will deteriorate to grade 3 rapidly. Similar with the findings in (1) and (2) of this section, the time from one grade to the next grade obtained by the RNN is earlier than that by the MC model. However, the results indicate that the overall tendencies by these two methods are approximately the same.
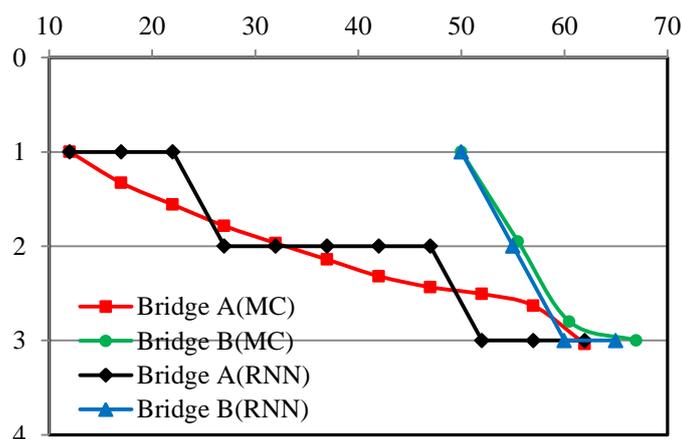
Figure 3.25 Deterioration progresses of bridges A and B using MC and RNN
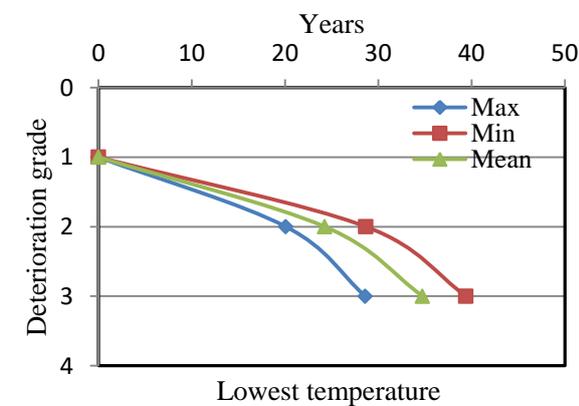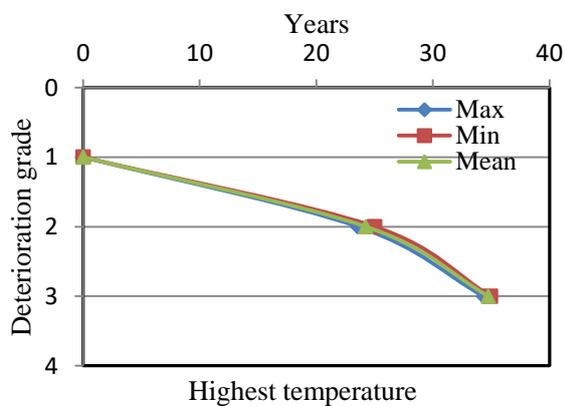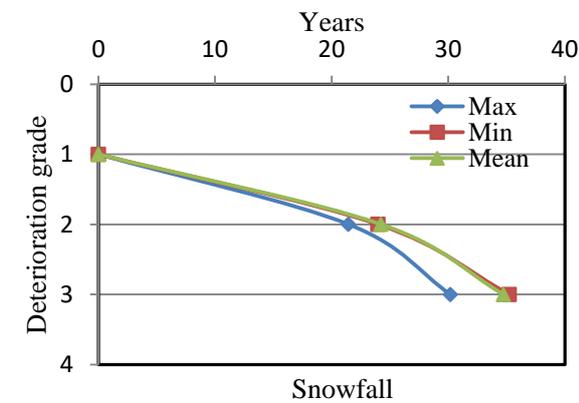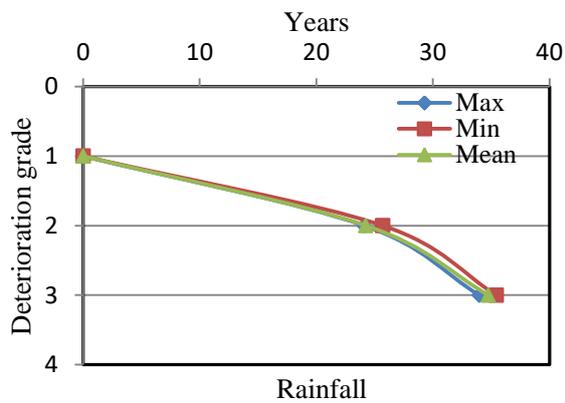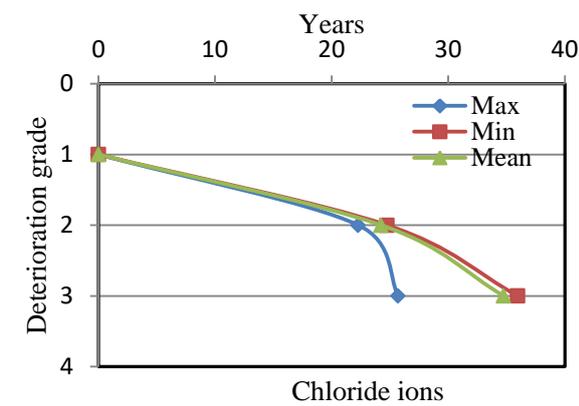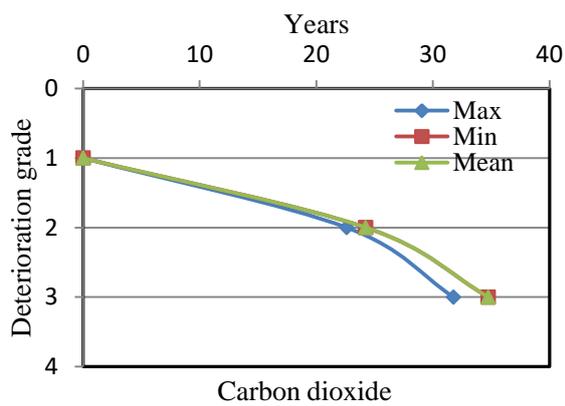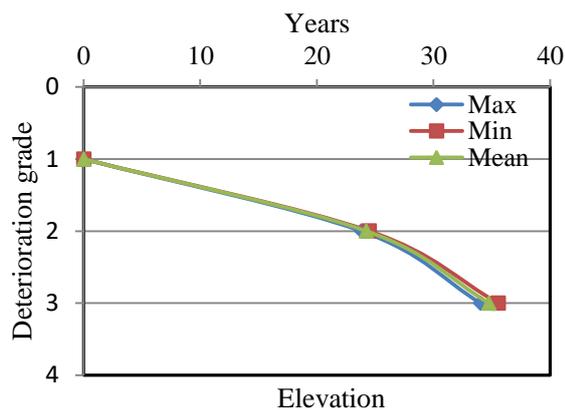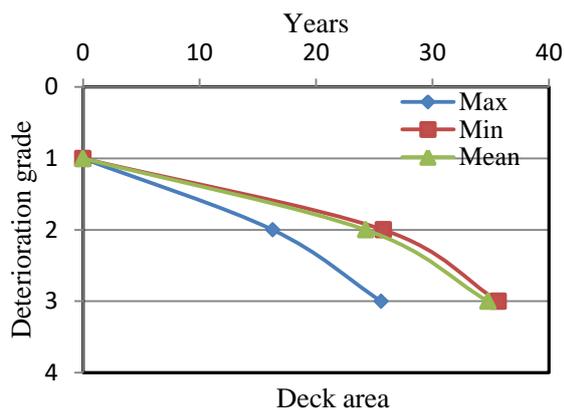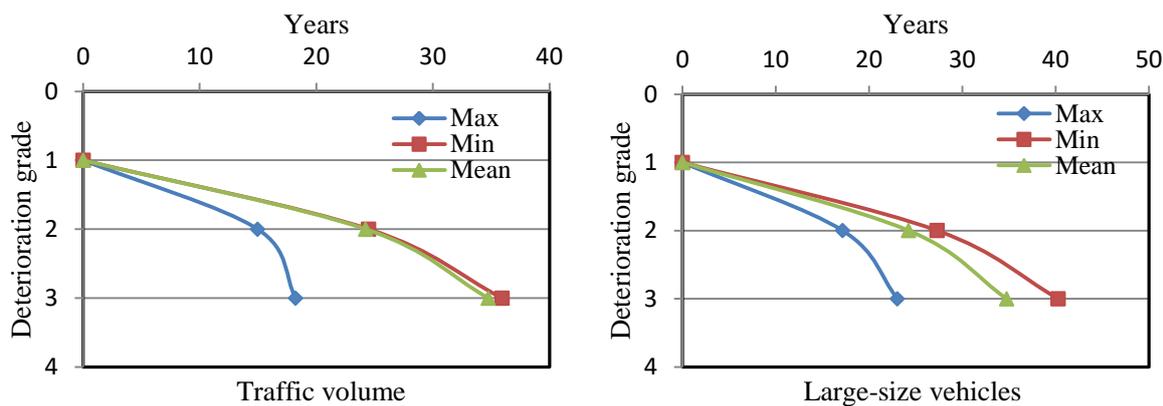
Figure 3.26 Deterioration progresses with the influence of each factor individually.
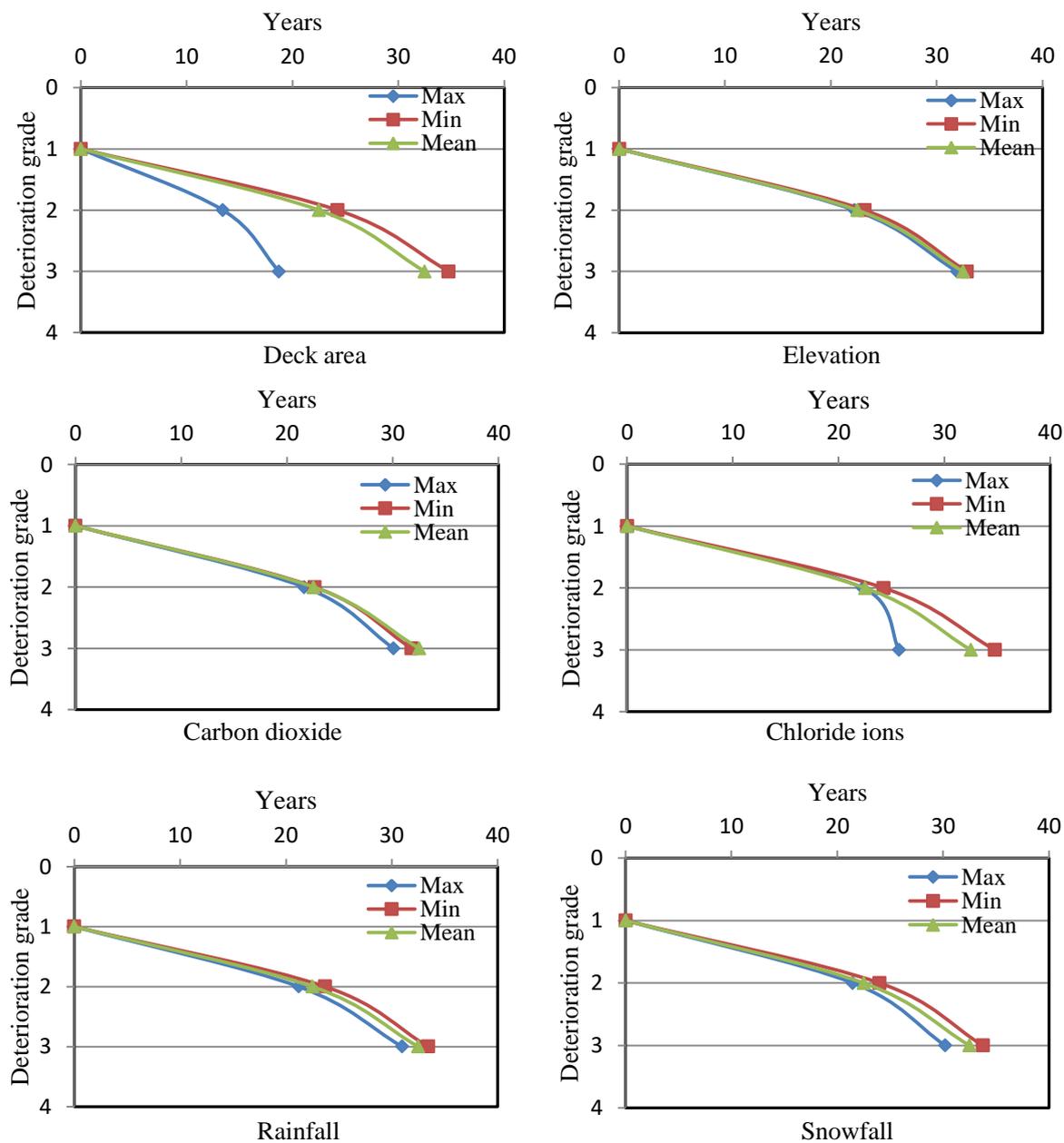
Figure 3.27 Deterioration progresses with the influence of each factor individually (using RNN)
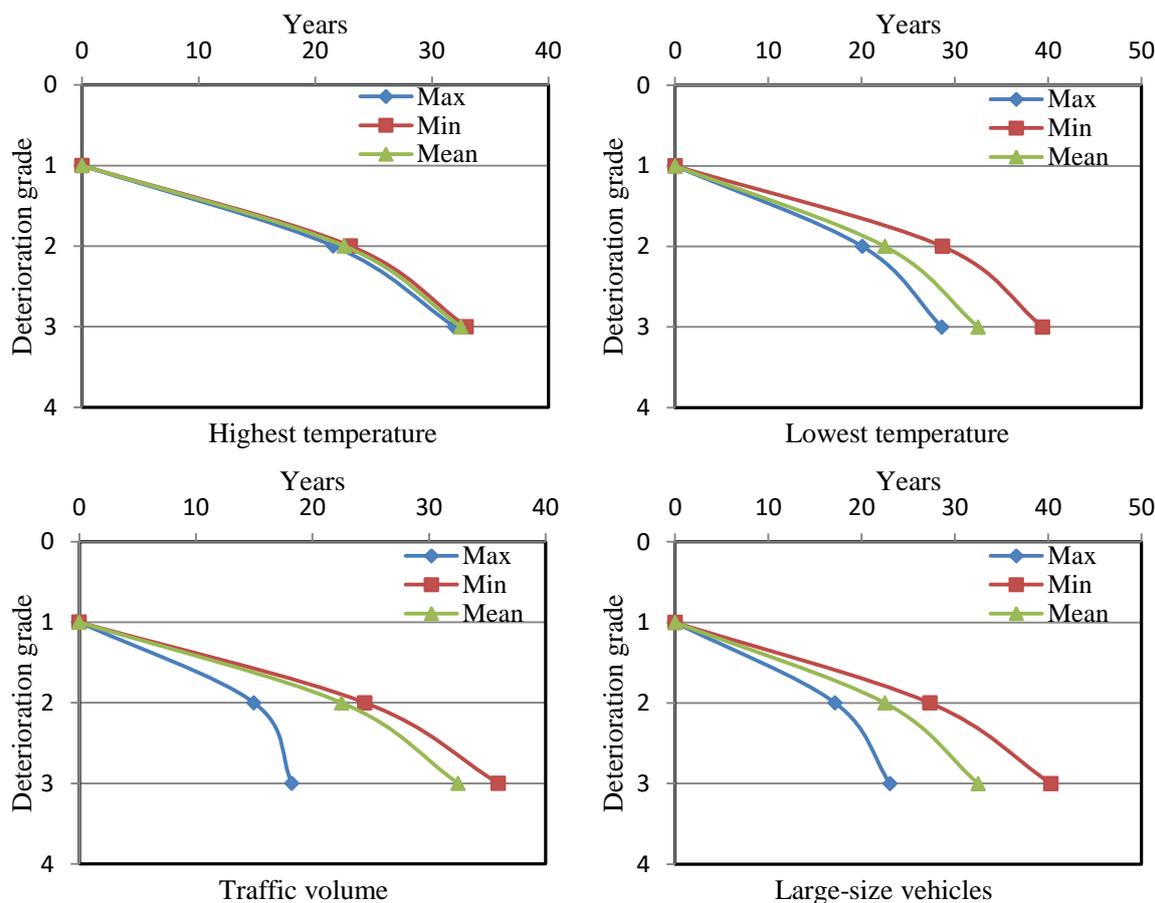
Figure 3.26 Deterioration progresses with the influence of each factor individually (using RNN)

(Continue)

(4) Influence of each factor on deterioration progresses

The influence of each factor on the deterioration progress was analyzed by changing the value of each factor. Figures 3.26 and 3.27 are the results using the MC and RNN model, respectively. The mean deterioration progress is the same as Figure 3.23, the minimum deterioration progress is obtained by setting the value of the corresponding individual factor to 0, and the maximum deterioration progress is obtained by setting the value of the corresponding individual factor to 1.0.

Figure 3.26 shows that: (i) a bigger deck area deteriorates earlier. This finding is the same as another study [20]; (ii) the elevation, rainfall, highest temperature has no significant influence on the deterioration progresses, because there are no remarkable differences between the mean, maximum, and minimum deterioration progresses; (iii) the deterioration progresses of carbon dioxide, chloride ions and the snowfall have no significant differences between the deterioration progresses from grade 1 to grade 2. However, the maximum deterioration progresses of these factors are deviated from grade 2 to grade 3 because the cumulated effect of the corresponding factors; (iv) heavy traffic volume will make the bridge deteriorates earlier. One another finding is that the mean and the minimum deterioration progress are almost same because the influence of normal traffic volume is tiny; and (v) the deterioration progresses of other factors, including lowest temperature and large-size vehicles, reveal that these factors have an impact from the beginning.

Similar findings can be determined when using the RNN model. One difference is that the mean and the minimum deterioration progresses of factors, such as deck area, chloride ions, snowfall, and traffic volume are quite different. Another difference is that the influence of rainfall obtained by the RNN model is more significant than that obtained by the MC model.

3.5.3 Discussions

Although the effectiveness of the MC model and RNN model proposed in this study were verified through a censored database, it is necessary to perform more application research and updating our models in the future. The concerns of this study were summarized as follows:

In actual inspection work, the soundness is usually evaluated by visual inspection, and it is inevitable that the soundness includes a subjective error. Therefore, it is necessary to develop an estimation method that can take this kind of subjective error into consideration. In addition, the routine maintenance makes the estimated model produce values later than the reality. Since the amount of data on each type of bridge is insufficient, data on all types of bridges are used to build two models, enabling the estimated deterioration progress for each bridge type to be averaged. Therefore, these two models may have certain errors for each type of bridge. It is necessary to compare and evaluate these two models with the models established for each type of bridge. This insufficient can be solved by collecting mode high quality data. Although our proposed model considered twelve potentially influencing factors, it does not mean these factors necessarily influence deterioration, or other factors that are not considered in this model may also impact deterioration.

Although the assumption of the time range in which a bridge stays in a certain grade is more like an engineering way of thinking than the concept of transition probability, these estimates are still subjective and their influence on the prediction results is crucial. Another drawback of Markov process models is that they do not take into account the length of the structural element already being in current condition state, and presume it just entered this state. The transition probabilities have nothing to do with time, which is unrealistic, especially when determining the transition probabilities of old bridges, because these probabilities change over time. Therefore, stationary transition probabilities in the transition matrix are difficult to be obtained and to assess non-subjectively.

In Markov chain, the time is not continuous, but discrete and finite. Instead, the RNN model can process continuous time serial data and provide continuous predictions. Since variations in inspection periods are frequent, continuous-time models have a significant advantage compared to discrete-time models. In addition, Markov exponential process does not include the age of the bridge, just the probability of staying in a certain state for a certain sojourn time. Markovian chain assumes duration independence for simplicity, i.e. the future facility condition depends only on the current facility condition and not on the facility condition history, which is unrealistic. Conversely, the RNN model can consider the cumulative effect along the whole time serial data through the three gates described in Section 2.4. In other words, the RNN can consider the age of bridges and the historical information. However, the established RNN model is far from perfect, and need more improvements.

This study assumes that periodic inspection data can be obtained at multiple time points. In reality, it is often the case that only once inspection is available. Even in such cases, the time when the civil engineering facilities are put into use and the time of the first inspection can be used as two time points for obtaining deterioration grade information. Then, The MC and RNN model can be estimated. To improve

the work of this study, future works will emphasis on collecting more quality data and modifying our models.

3.6 Estimation of factor importance

Using the LSTM prediction model, successful predictions were made for 2,695 out of the 3,368 bridges. Therefore, a new database of 2,695 bridges was set up. The Shapley value and Sobol indices methods were then applied to perform the sensitivity analysis of each factor from the new database. The calculated sensitivities were normalized to show their relative importance, as indicated in Figure 3.28. The five most important factors determined by the Sobol indices and Shapley value method are the same, although their values are different. Deck area (bridge length ×bridge width) and years in service were determined to be the most important factors affecting the deterioration. In addition, traffic volume, lowest temperature and chloride ions are the three external factors affecting deterioration, which is consistent with known findings. Therefore, the Shapley value method was considered a suitable solution to determine the contribution of factors on deterioration. Furthermore, the Shapley value method was applied to analyze the new database from other perspectives.
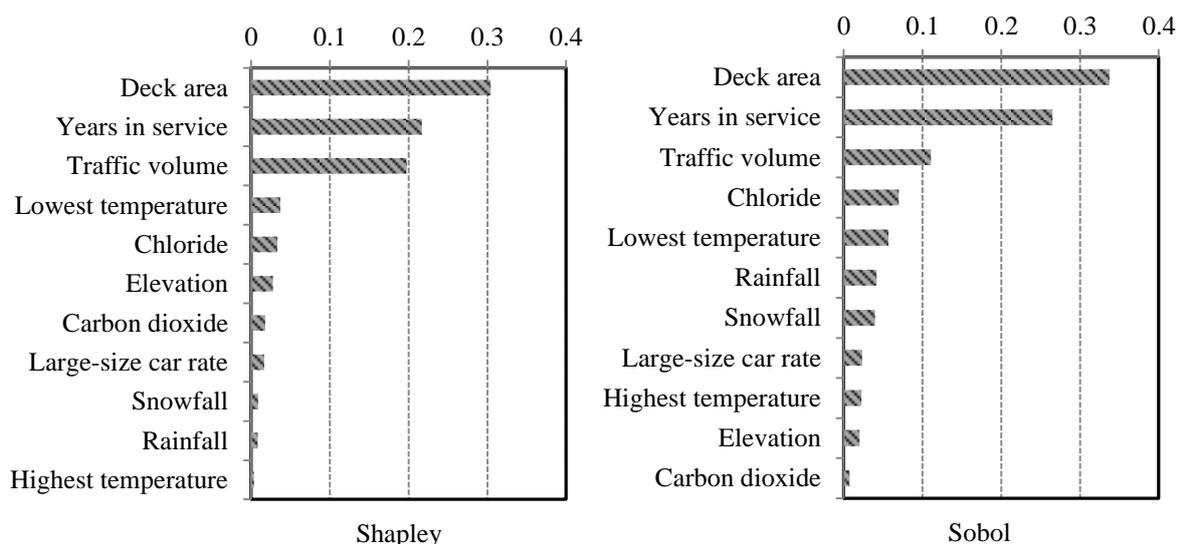
Figure 3.28 Sensitivity analysis by Sobol and Shapley value methods.

3.6.1 Distribution of each potentially influencing factor

According to the Shapley value method, the estimated importance of all factors was calculated for each bridge, as shown in Figure 3.29 separated by each factor. The estimated importance indicates the relative importance of each factor for a bridge. For the estimated importance, the positive value represents that the factor will accelerate the deterioration, and the negative value means that the factor will slow down the deterioration. Therefore, factors, such as years in service, carbon dioxide concentration, and the chloride ion show accelerated effects on deterioration. Other factors such as elevation, deck area, and bridge width, rate of the large-size vehicles, rainfall, and highest temperature do not show consistent effects. Another finding is that the number of the large size vehicles will affect the deterioration, even though rate of the large-size vehicles is not necessarily related to deterioration. Since the total traffic volume is found with obvious effect, the number of the large size vehicles will not be considered independently. In summary, six

factors with acceleration are discussed hereafter, as other factors do not show the consistent relationships with deterioration. In addition, Figure 3.28 reveals that the estimated importance of lowest temperature negatively related to the measured value. The estimated importance of other five accelerated factors, such as years in service, traffic volume, are positive correlated with the measured values.
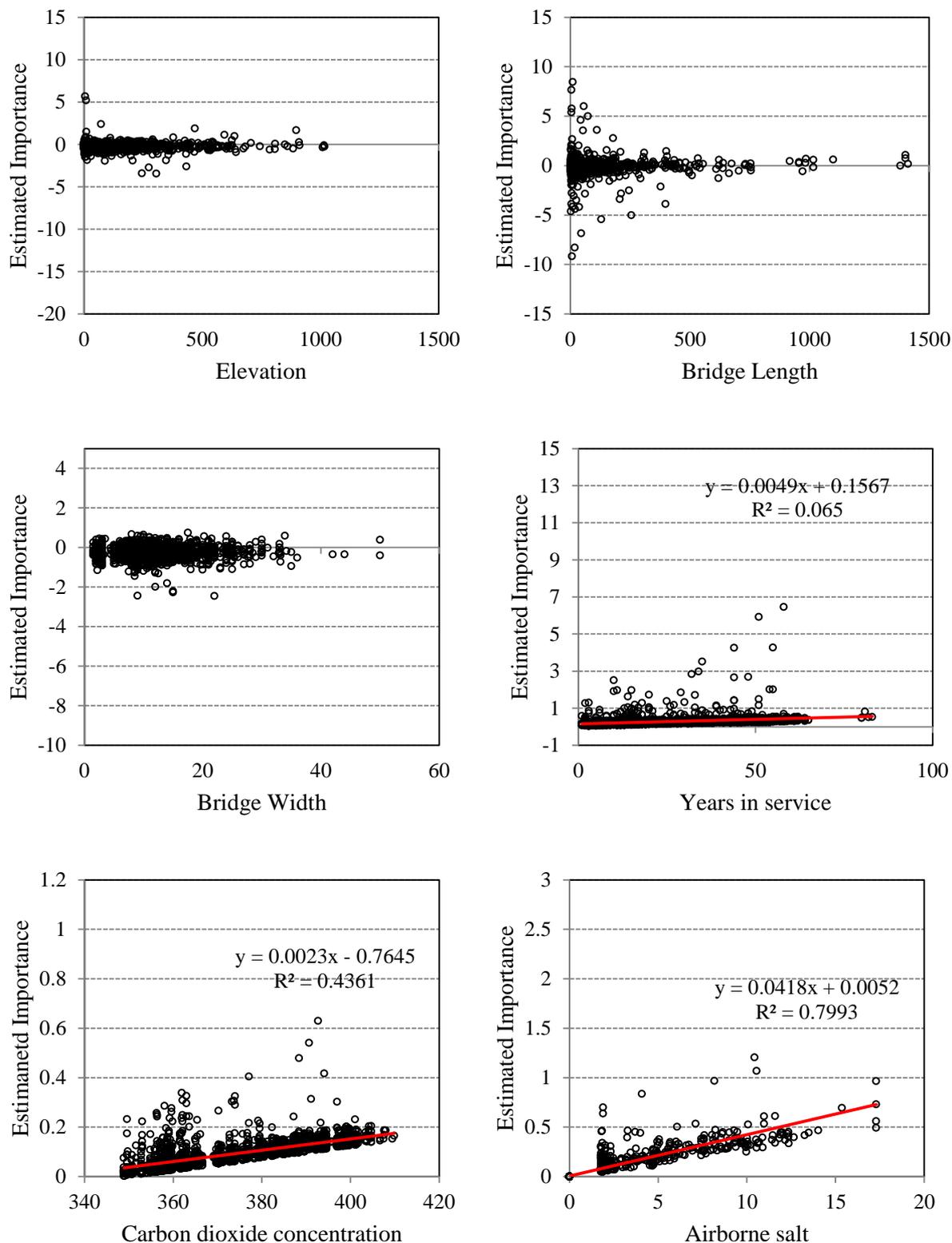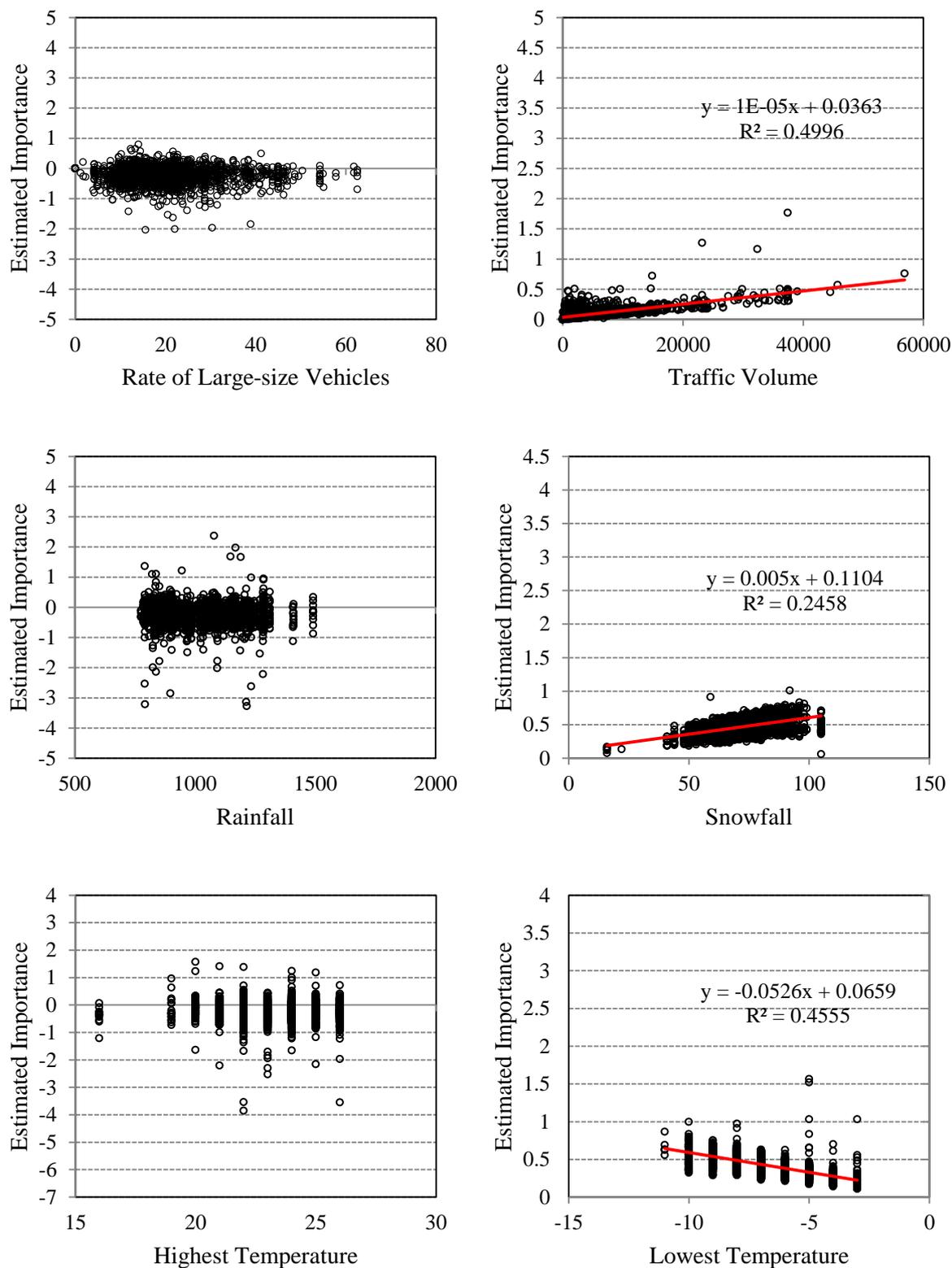
Figure 3.29. Estimated importance of each factor for all bridges (Continue)

3.6.2 Estimated importance for target bridges

Figure 3.30 shows the estimated importance of each factor for bridges A and B (Section 3.5.2). The results show that the years in service, chloride ions, and traffic volume are the three most significant factors for

these bridges. The other three factors have relatively fewer influences.

However, the estimated importance for the two bridges shows significant differences. For bridge A, the most significant factor is the traffic volume, the other factors are relatively lower. This is because bridge A has been in service for only 12 years, the natural degradation of the material is not obvious, and the impact of carbonation and chloride ion is still tiny. Considering bridge A will remain in grade 1 for the next 20 years (Section 3.5.2), no special maintenance is necessary for bridge A in ten years. As bridge B has been in service for 50 years and has recently accommodated many large-size vehicles, the lowest temperature, traffic volume, chloride ion have all had important impacts except for years in service. In addition, the deterioration of bridge B will be worse from grade 1 to 3 soon, according to the deterioration curve in Figure 3.24. Therefore, the bridge B should be fully maintained in five years. The results indicate that even though the deterioration of bridges A and B are both evaluated being grade 1, the calculated relative importance of all factors is different. Obviously, the estimated relative importance can reflect the bridges properties and the reasons for deterioration. Additionally, corresponding maintenance strategies can be set up.
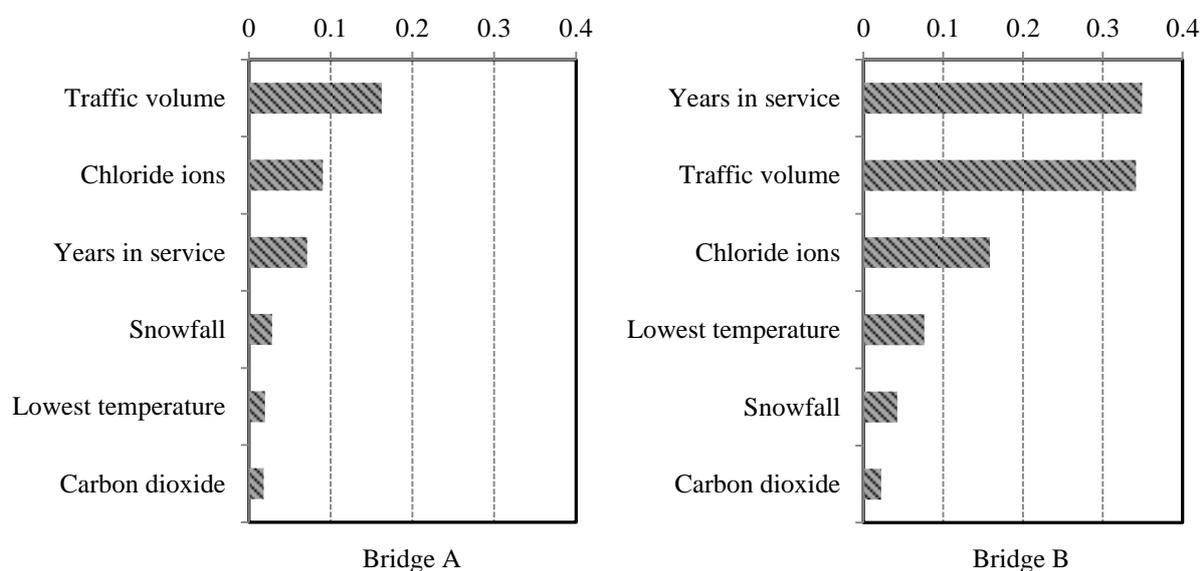
Figure 3.29 Estimated importance value for bridges A and B.

3.6.3 Estimated importance of each grade

To compare the difference between the grades, the average importance of each factor for its respective grade was computed, as shown in Figure 3.31. Unlike the explanations shown in Figure 3.30, which are specific to individual bridges, Figure 3.31 shows the mean estimated importance for bridges with the same deterioration grade.

Of all the factors, years in service and traffic volume are the two most significant factors for all grades. Other factors have relatively fewer impacts. As bridges in grade 1 are generally relatively short in service, environmental factors such as the lowest temperature and the chloride have not had significant impacts. Therefore, the years in service and the traffic volume are the most significant factors. As time goes by, the importance gap between the years in service and the traffic volume traffic has narrowed, as shown in grade 2. It is indicated that the relative importance of the traffic volume has increased, and its impact on deterioration has also increased. Further, the importance of the years in service and the traffic volume is

almost the same in grade 3. In addition, the influences of the lowest temperature and the chloride are increased. Owing to the bridges in grade 3 have been in service for an average of more than 46 years, a relatively smaller importance of a factor does not mean the factor is unimportant, as the cumulative effects of these factors were not considered. Therefore, various factors should be comprehensively considered to provide recommendations for future maintenance. In addition, intervention was performed for some bridges from construction to the latest inspection, which is difficult to be considered in our model.
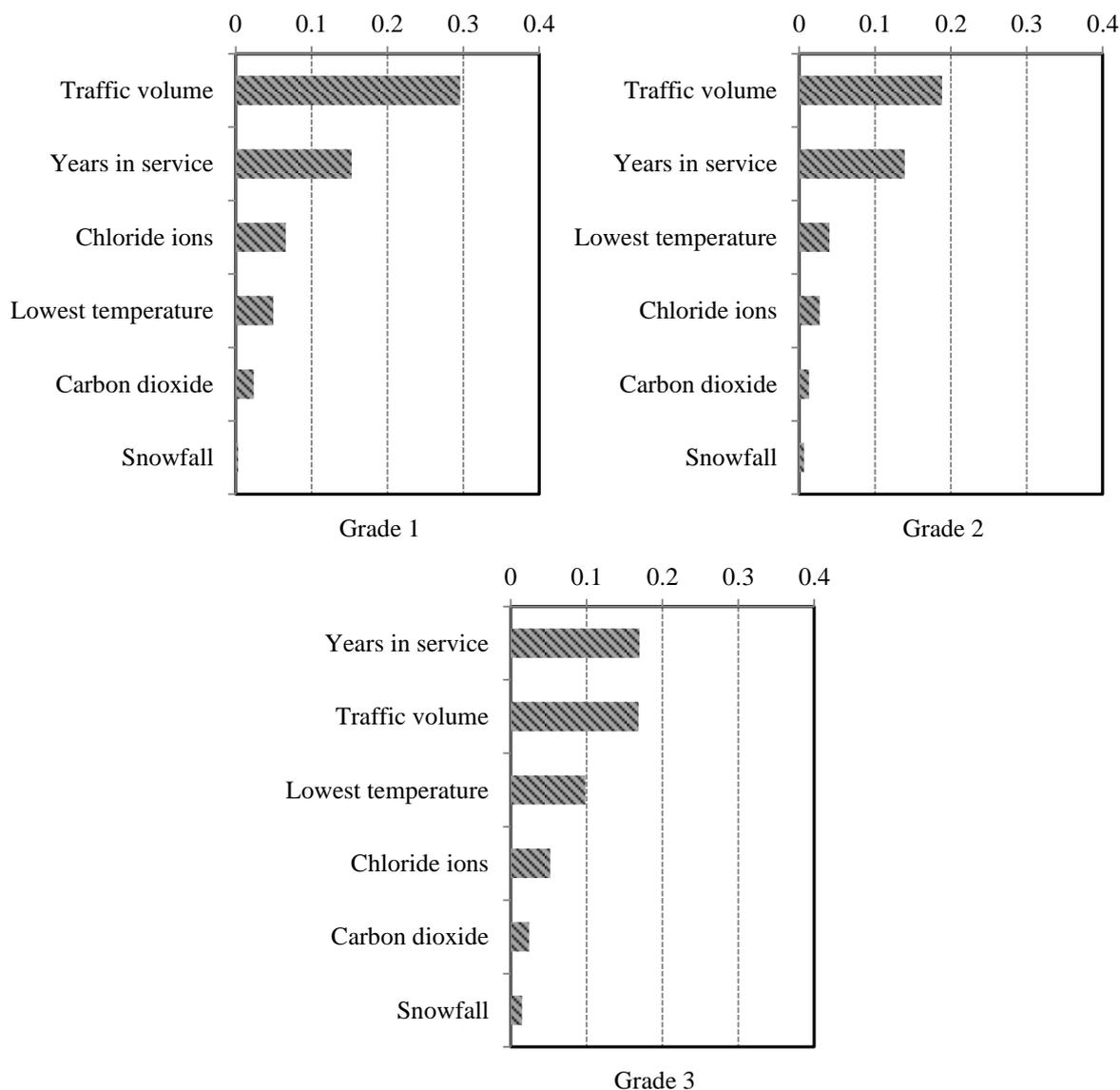
Figure 3.30 Average importance of each factor, broken down by grade (Grades 1, 2 and 3).

3.6.4 Estimated importance of different structure type

The deterioration differs for different types of bridges. To observe whether the estimated importance can reflect the differences caused by different types of bridges, the average estimated importance of all factors, broken down by structure types is shown in Figure 3.32.

Similar to the findings in previous sections, the years in service and the traffic volume are the two most significant factors for all the bridge types. The distribution of these factors differs in different bridge types.

For the PC bridges, other factors are less important relative to the years in service, as PC bridges are generally able to withstand harsher conditions and have better durability. Compared with the PC bridge, the importance of the RC bridge is more uniformly distributed. Because RC bridges are more susceptible to loads (traffic volume) and environmental factors (lowest temperature and chloride ion). The steel & concrete composite bridge is almost in the middle of the PC and RC bridges. For steel bridges, the importance of traffic volume is increased because the average daily traffic volume of this type of bridge in the applied database is usually more than 10,000 (vehicles/day) and usually accommodates many large vehicles (3,337 vehicles/day).
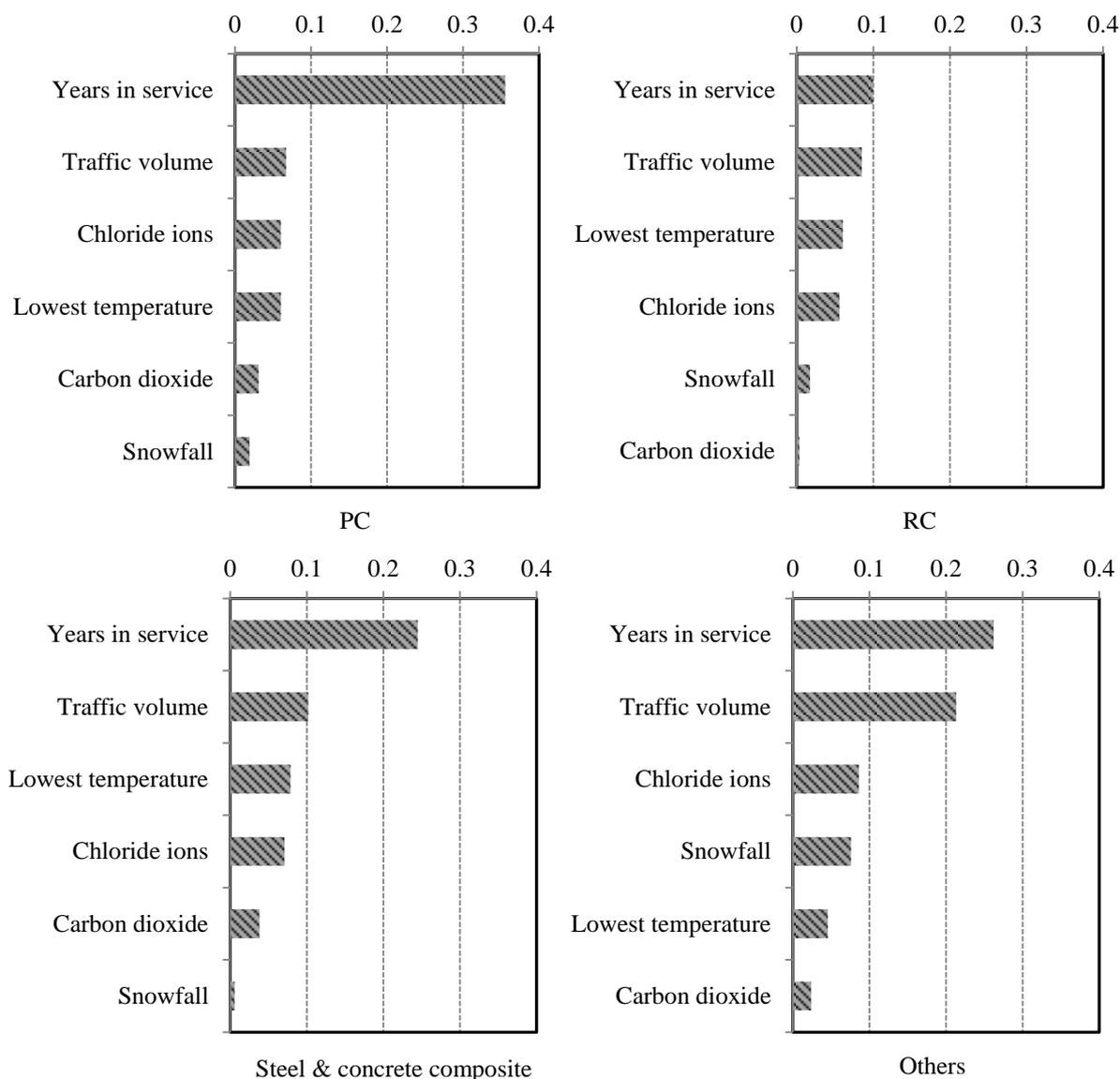
Figure 3.31 Average importance of each factor, broken down by the bridge type

As a result, the bridge type is determined another reason to affect the deterioration. As for other researcher's finding [21], material and surrounding environment should be the most significant factors. Since the database regarding the bridge materials is unavailable, the differences induced by the material will not be considered in this study. In terms of the environment, bridges will be divided into two groups depending on they are located in coastal or outside of coastal regions, which will be discussed later.

3.6.5 Estimated importance of different environments

Since concrete bridges (components) in coastal areas are exposed to extremely severe environments for materials [22], bridges are divided in terms of their location, such as in coastal and non-coastal areas, and average importance for these two environments is calculated, as shown in Figure 3.33. For the bridge in non-coastal areas, the distribution of these factors is the same as the previous sections except for the value of chloride ion been zero, as de-icing salt is not considered. Compared with non-coastal conditions, the impact of chloride ions is greatly increased. In addition, the order of importance of the traffic volume and lowest temperature are the same.

As results, the influence of air-borne salt is the main reason for the differences of the two environments. In addition, the results indicate that the bridges in coastal areas are more strongly affected by air-borne salt, and the estimated importance of the sensitivity analysis methods conform to reality. In general, there is a reasonable agreement between the estimated factors with accelerated effects and factors already known to affect the deterioration, which means that the sensitivity analysis can identify factors influencing deterioration and can calculate their relative importance.
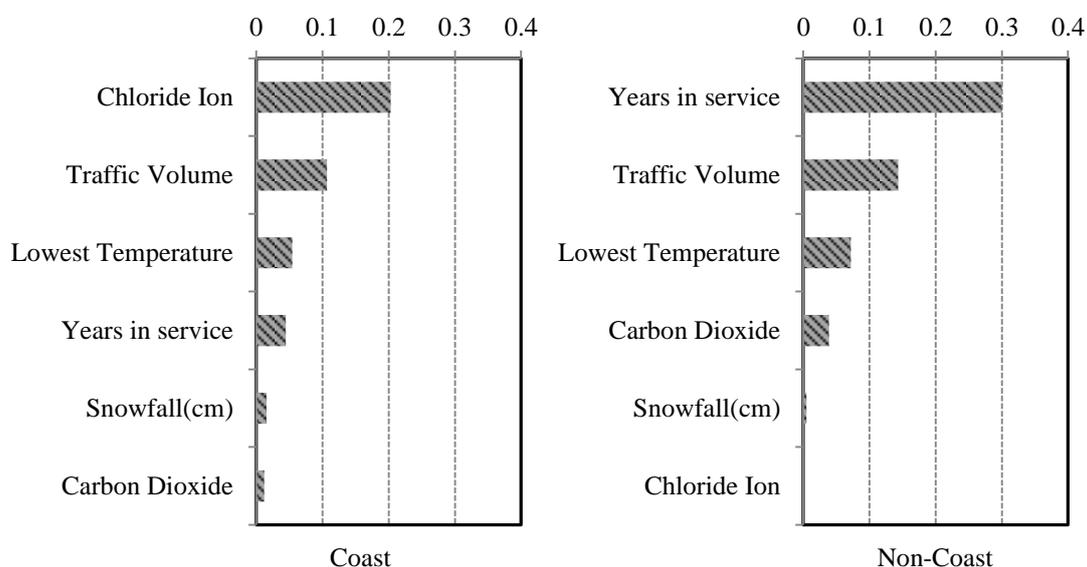
Figure 3.32 Average importance of each factor, broken down by coastal/none coastal area.

Appendix A

No.	ANN type					Average training loss	Average training accuracy	Average validation loss	Average validation accuracy
	Number of hidden layers	Number of hidden neurons	Lr	Algorithm	AcFun				
1	1	5	0.01	SGD	relu	0.8288	0.6063	0.8870	0.5669
2	1	5	0.01	SGD	tanh	0.8208	0.6073	0.8645	0.5751
3	1	5	0.01	RMSProp	relu	0.8194	0.6055	0.8756	0.5658
4	1	5	0.01	RMSProp	tanh	0.7586	0.6335	0.8483	0.5972
5	1	5	0.01	Adagrad	relu	0.8301	0.5985	0.8855	0.5693
6	1	5	0.01	Adagrad	tanh	0.8223	0.6105	0.8815	0.5658
7	1	5	0.01	Adadelta	relu	0.9482	0.5571	0.9850	0.5363
8	1	5	0.01	Adadelta	tanh	0.9241	0.5607	0.9710	0.5336
9	1	5	0.01	Adam	relu	0.7826	0.6164	0.8462	0.6050
10	1	5	0.01	Adam	tanh	0.7608	0.6379	0.8592	0.5968
11	1	5	0.01	Adamax	relu	0.7836	0.6252	0.8245	0.6244
12	1	5	0.01	Adamax	tanh	0.7731	0.6262	0.8513	0.5949
13	1	5	0.01	Nadam	relu	0.7733	0.6193	0.8382	0.6119
14	1	5	0.01	Nadam	tanh	0.7637	0.6367	0.8397	0.6088
15	1	5	0.001	SGD	relu	0.8333	0.5953	0.8743	0.5767
16	1	5	0.001	SGD	tanh	0.8307	0.5960	0.8883	0.5708
17	1	5	0.001	RMSProp	relu	0.8029	0.6136	0.8521	0.5910
18	1	5	0.001	RMSProp	tanh	0.7784	0.6205	0.8565	0.5937
19	1	5	0.001	Adagrad	relu	0.8632	0.5911	0.9037	0.5588
20	1	5	0.001	Adagrad	tanh	0.8446	0.5976	0.8975	0.5642
21	1	5	0.001	Adadelta	relu	0.9663	0.5594	1.0021	0.5359
22	1	5	0.001	Adadelta	tanh	0.9503	0.5589	0.9999	0.5289
23	1	5	0.001	Adam	relu	0.8259	0.6041	0.8741	0.5743
24	1	5	0.001	Adam	tanh	0.7756	0.6224	0.8623	0.5894
25	1	5	0.001	Adamax	relu	0.7993	0.6164	0.8529	0.5918
26	1	5	0.001	Adamax	tanh	0.7905	0.6203	0.8563	0.5902
27	1	5	0.001	Nadam	relu	0.8104	0.6136	0.8600	0.5856
28	1	5	0.001	Nadam	tanh	0.7852	0.6143	0.8515	0.6026
29	1	10	0.01	SGD	relu	0.8284	0.6045	0.8751	0.5716
30	1	10	0.01	SGD	tanh	0.8258	0.6076	0.8835	0.5661
31	1	10	0.01	RMSProp	relu	0.7748	0.6271	0.8633	0.5820
32	1	10	0.01	RMSProp	tanh	0.7661	0.6410	0.8382	0.5991
33	1	10	0.01	Adagrad	relu	0.8516	0.5975	0.8993	0.5530
34	1	10	0.01	Adagrad	tanh	0.8377	0.5983	0.8830	0.5623
35	1	10	0.01	Adadelta	relu	0.9534	0.5626	0.9920	0.5410
36	1	10	0.01	Adadelta	tanh	0.9408	0.5642	0.9955	0.5289
37	1	10	0.01	Adam	relu	0.7780	0.6262	0.8458	0.5968
38	1	10	0.01	Adam	tanh	0.7618	0.6360	0.8414	0.6054
39	1	10	0.01	Adamax	relu	0.7782	0.6294	0.8421	0.6046
40	1	10	0.01	Adamax	tanh	0.7812	0.6214	0.8573	0.5953
41	1	10	0.01	Nadam	relu	0.7707	0.6261	0.8411	0.5999
42	1	10	0.01	Nadam	tanh	0.7527	0.6467	0.8479	0.6022
43	1	10	0.001	SGD	relu	0.9139	0.5624	0.9597	0.5386
44	1	10	0.001	SGD	tanh	0.9046	0.5644	0.9513	0.5402
45	1	10	0.001	RMSProp	relu	0.7943	0.6184	0.8455	0.5976

No.	ANN type					Average training loss	Average training accuracy	Average validation loss	Average validation accuracy
	Number of hidden layers	Number of hidden neurons	Lr	Algorithm	AcFun				
46	1	10	0.001	RMSProp	tanh	0.7972	0.6153	0.8778	0.5692
47	1	10	0.001	Adagrad	relu	0.9413	0.5647	0.9936	0.5320
48	1	10	0.001	Adagrad	tanh	0.9377	0.5592	0.9788	0.5359
49	1	10	0.001	Adadelta	relu	0.9690	0.5597	0.9943	0.5367
50	1	10	0.001	Adadelta	tanh	0.9780	0.5607	1.0038	0.5382
51	1	10	0.001	Adam	relu	0.7739	0.6284	0.8222	0.6077
52	1	10	0.001	Adam	tanh	0.7819	0.6205	0.8504	0.5948
53	1	10	0.001	Adamax	relu	0.8018	0.6081	0.8507	0.5953
54	1	10	0.001	Adamax	tanh	0.8009	0.6135	0.8489	0.5952
55	1	10	0.001	Nadam	relu	0.8129	0.6105	0.8669	0.5755
56	1	10	0.001	Nadam	tanh	0.7877	0.6163	0.8690	0.5891
57	2	5	0.01	SGD	relu	0.8379	0.5946	0.8846	0.5627
58	2	5	0.01	SGD	tanh	0.8291	0.6018	0.8814	0.5658
59	2	5	0.01	RMSProp	relu	0.7862	0.6216	0.8925	0.5875
60	2	5	0.01	RMSProp	tanh	0.7737	0.6276	0.8649	0.5964
61	2	5	0.01	Adagrad	relu	0.8459	0.5940	0.8836	0.5716
62	2	5	0.01	Adagrad	tanh	0.8390	0.5895	0.8905	0.5685
63	2	5	0.01	Adadelta	relu	0.9678	0.5562	1.0007	0.5343
64	2	5	0.01	Adadelta	tanh	0.9566	0.5561	0.9878	0.5359
65	2	5	0.01	Adam	relu	0.7929	0.6115	0.8557	0.5902
66	2	5	0.01	Adam	tanh	0.7588	0.6301	0.8639	0.5956
67	2	5	0.01	Adamax	relu	0.8241	0.6043	0.8821	0.5701
68	2	5	0.01	Adamax	tanh	0.7891	0.6145	0.8571	0.5957
69	2	5	0.01	Nadam	relu	0.7877	0.6050	0.8395	0.6120
70	2	5	0.01	Nadam	tanh	0.7681	0.6244	0.8660	0.5879
71	2	5	0.001	SGD	relu	0.9496	0.5622	0.9933	0.5371
72	2	5	0.001	SGD	tanh	0.9399	0.5621	0.9813	0.5371
73	2	5	0.001	RMSProp	relu	0.8268	0.6101	0.8883	0.5778
74	2	5	0.001	RMSProp	tanh	0.8014	0.6093	0.8596	0.5953
75	2	5	0.001	Adagrad	relu	0.9574	0.5632	0.9952	0.5363
76	2	5	0.001	Adagrad	tanh	0.9591	0.5612	0.9997	0.5335
77	2	5	0.001	Adadelta	relu	1.0376	0.5592	1.0472	0.5153
78	2	5	0.001	Adadelta	tanh	1.0048	0.5637	1.0321	0.5320
79	2	5	0.001	Adam	relu	0.8149	0.5978	0.8589	0.5743
80	2	5	0.001	Adam	tanh	0.8024	0.6095	0.8497	0.6026
81	2	5	0.001	Adamax	relu	0.8255	0.6060	0.8767	0.5743
82	2	5	0.001	Adamax	tanh	0.8217	0.6073	0.8813	0.5689
83	2	5	0.001	Nadam	relu	0.8063	0.6036	0.8589	0.5887
84	2	5	0.001	Nadam	tanh	0.7973	0.6130	0.8665	0.5852
85	2	10	0.01	SGD	relu	0.8167	0.6068	0.8800	0.5770
86	2	10	0.01	SGD	tanh	0.8205	0.6075	0.8752	0.5673
87	2	10	0.01	RMSProp	relu	0.7522	0.6427	0.8756	0.5941
88	2	10	0.01	RMSProp	tanh	0.7334	0.6612	0.8897	0.5906
89	2	10	0.01	Adagrad	relu	0.8402	0.5938	0.8898	0.5708
90	2	10	0.01	Adagrad	tanh	0.8226	0.6048	0.8680	0.5770
91	2	10	0.01	Adadelta	relu	0.9373	0.5587	0.9804	0.5339
92	2	10	0.01	Adadelta	tanh	0.9340	0.5586	0.9747	0.5332

No.	ANN type					Average training loss	Average training accuracy	Average validation loss	Average validation accuracy
	Number of hidden layers	Number of hidden neurons	Lr	Algorithm	AcFun				
93	2	10	0.01	Adam	relu	0.7580	0.6301	0.8598	0.5890
94	2	10	0.01	Adam	tanh	0.7265	0.6612	0.9027	0.5918
95	2	10	0.01	Adamax	relu	0.8024	0.6121	0.8759	0.5697
96	2	10	0.01	Adamax	tanh	0.7094	0.6675	0.9310	0.5712
97	2	10	0.01	Nadam	relu	0.7449	0.6470	0.8868	0.5801
98	2	10	0.01	Nadam	tanh	0.6999	0.6720	0.9382	0.5693
99	2	10	0.001	SGD	relu	0.9172	0.5616	0.9579	0.5316
100	2	10	0.001	SGD	tanh	0.9306	0.5607	0.9703	0.5417
101	2	10	0.001	RMSProp	relu	0.7927	0.6180	0.8684	0.5875
102	2	10	0.001	RMSProp	tanh	0.7996	0.6118	0.8673	0.5871
103	2	10	0.001	Adagrad	relu	0.9396	0.5597	0.9764	0.5409
104	2	10	0.001	Adagrad	tanh	0.9303	0.5652	0.9719	0.5390
105	2	10	0.001	Adadelta	relu	1.0238	0.5609	1.0294	0.5402
106	2	10	0.001	Adadelta	tanh	0.9915	0.5519	1.0128	0.5270
107	2	10	0.001	Adam	relu	0.8108	0.6056	0.8618	0.5852
108	2	10	0.001	Adam	tanh	0.8000	0.6116	0.8584	0.5922
109	2	10	0.001	Adamax	relu	0.7866	0.6184	0.8457	0.6065
110	2	10	0.001	Adamax	tanh	0.7854	0.6148	0.8584	0.5871
111	2	10	0.001	Nadam	relu	0.8147	0.6048	0.8826	0.5704
112	2	10	0.001	Nadam	tanh	0.7909	0.6163	0.8573	0.5964

References

[1] Al-Hussein, Estimating Bridge Deterioration Age Using Artificial Neural Networks (Doctoral dissertation, The British University in Dubai), (2017). https://bspace.buid.ac.ae/handle/1234/1128

[2] JMA. (2019, October). Annual changes of carbon dioxide concentration by locations. Retrieved from https://ds.data.jma.go.jp/ghg/kanshi/co2timeser/co2timeser.html.

[3] MLIT. (2005). 2005 National road and street traffic situation survey (general traffic volume survey). Retrieved from http://www.mlit.go.jp/road/census/h17/

[4] MLIT. (2010). 2010 National road and street traffic situation survey (general traffic volume survey). Retrieved from http://www.mlit.go.jp/road/census/h22-1/

[5] MLIT. (2015a). 2015 National road and street traffic situation survey (general traffic volume survey). Retrieved from http://www.mlit.go.jp/road/census/h27/index.html

[6] Kobayashi, R. (2010). Field survey on salt infiltration of existing bridges along the coast of Oshima Peninsula, Hokkaido. Concrete engineering proceedings. 48(7): 52-55. doi:10.3151/coj.48.7_52

[7] JSCE. 2012. Standard Specifications for Concrete Structures (Design). Japan Society of Civil Engineers, JSCE Guidelines for Concrete.

[8] Tamakoshi, T., Kubota,K., Hoshino,M., & Yokoi, Y. 2012. Examination about countermeasure of salt damage to concrete bridge based on result of close visual inspection. MLIT. ISSN 1346－7328.No.711: 15-21.

[9] NRA. 2016, March. Investigation and research on long-term soundness evaluation of concrete structures. Retrieved from https://www.nsr.go.jp/data/000186088.pdf.

[10] MLIT. (2015b) Guidelines for general traffic survey. www.mlit.go.jp/road/census/h22-1/data/kasyorep.pdf, Access date: October, 2019.

[11] Daisoku, N., Katawaki, K., Miyagawa, T., Kashino, N., Kobayashi, A. (1986). Durability series of concrete structures. Salt Damage (I). Gihodo Publishing.

[12] Tamakoshi, T., Okubo, M., & Watanabe, Y. 2009. Research on highway bridges management-Bridge Manage System. MLIT, ISSN 1346-7328.No.523:25-27.

[13] MLIT. (2014). Guidelines for Regular Inspection of Road Bridges. Retrieved from https://www.mlit.go.jp/road/sisaku/yobohozen/tenken/yobo4_1.pdf.

[14] Kishitani,K., Kobayashi, K., Kashino,K. Uno,Y. 1991. Relationship between rebar corrosion and carbonation in concrete containing chloride. Concrete engineering proceedings. 2(1), 77-84. doi:10.3151/crt1990.2.1_77.

[15] Kawakami, H., Waki, K.,Tada, M.1995. Evaluation of durability of old building concrete-analysis of investigation results. Fukui University,Faculty of Engineering Research Report, 43(1):51-58.

[16] Uomoto, K., & Takada, Y.1992. Factors affecting the neutralization rate of concrete. JSCE Proceedings, 1992(451):119-128. doi:10.2208/jscej.1992.451_119

[17] I. Goodfellow, Y. Bengio, A. Courville, Deep Learning, MIT Press. (2016). http://www.deeplearningbook.org, Access date: November, 2019.

[18] Wang, D., Fan, J., Fu, H., & Zhang, B. (2018). Research on optimization of big data construction engineering quality management based on RnN-LSTM. Complexity, 2018. https://doi.org/10.1155/2018/9691868

[19] Lipton, Z. C., Kale, D. C., Elkan, C., & Wetzel, R. (2016). Learning to diagnose with LSTM Recurrent Neural Networks. 4th International Conference on Learning Representations, ICLR 2016 - Conference Track Proceedings, 1–18.

[20] Yoshitane TSUDA, Kiyoyuki KAITO, Kazuya AOKI, Kiyoshi KOBAYASHI. (2005). Estimating Markovian transition probabilities for bridge deterioration forecasting. Journal of JSCE, (801), 69-82. https://pdfs.semanticscholar.org/5f0f/f57f1d3e5ba87fb14ab5e9957e4818f84615.pdf.

[21] Y.H. Huang, Artificial neural network model of bridge deterioration, Journal of Performance of Constructed Facilities. 24(6) (2010) 597-602. doi: 10.1061/(ASCE)CF.1943-5509.0000124

[22] H. Yokota, Practical application of life-cycle management system for shore protection facilities, Structure and Infrastructure Engineering.13 (1) (2017) 34-43, doi: 10.1080/15732479.2016.1198391

Chapter 4

Establishment of crack identification model

4.1. Overview

Conforming to the procedures described in Section 2.7, this chapter provided details on the establishment and verification of a crack identification model. Figure 4.1 shows the flowchart applied to establish the crack identification model used for detecting and quantifying crack conditions. The entire procedures include three stages: pre-processing, crack detection, and post-processing. Pre-processing is used to calibrate the raw images, as described in Section 2.7.1. In this chapter, we detailed the considerations to build a robust crack classifier (Crack detection) and to develop an application to segment and analyze cracks (Post-processing).
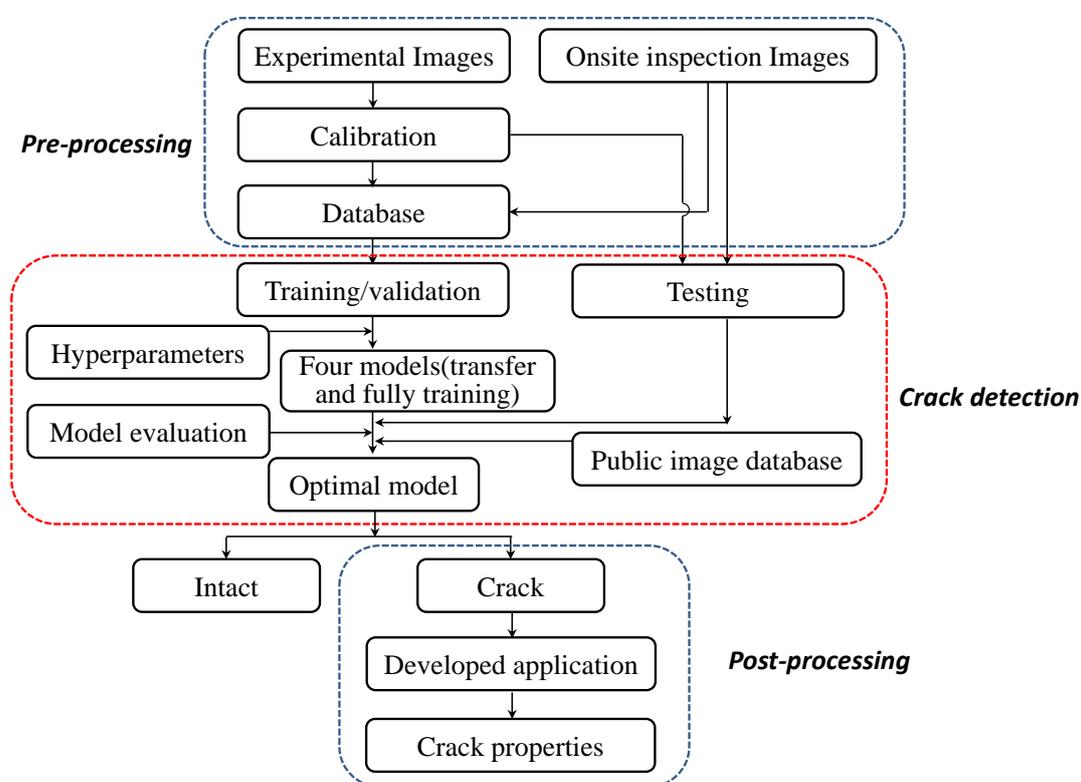
Figure 4.1 Flowchart for establishing the crack identification model

4.2. Building a robust crack classifier

This section introduced the considerations when generating the database and setting the basic hyperparameters, and the procedures of acquiring a robust a CNN. The optimal hyperparameters were confirmed by trial and error, according to Bengio et al. [1]. All of the study was performed on a personal computer with two GPUs (CPU: Intel© Core© i5-8300H CPU@2.30GHz, RAM: 32GB and GUP NVIDIA GeForce GTX 1050).

4.2.1 Database generation

In this study, a total of 150 raw images from indoor experiments and onsite bridge inspections were used, as summarized in Table 4.1. The experimental images were captured with a distance of 1.0 m during the beam bending test. Before the test, these beams have been exposed in the field for one or two years. The pictures collected during the bridge inspection were shot without knowing the distance from the camera to the object. The combination of images from experiments and inspections was intended to make the classifier general and practically applicable. The experimental raw images were calibrated. Then 58 experimental and 69 onsite inspection images were randomly selected from the corresponding groups. The remaining 11 and 12 images in corresponding groups were used for testing, respectively. The 127 raw images were cropped into sub-images with 256×256 pixel resolution to build the database for training and validation. Totally, the database includes 30,480 sub-images, with the ratio of crack and intact images at 1:1; and includes a broad range of images variances for establishing a robust classifier, as shown in Figures 4.2 (a) and 6(b). In addition, sub-images with cracks on the edge of images and with other kinds of damages are disregarded, based on the study of Cha et al. [2], as shown in Figure 4.2 (c).

Table 4.1 Specification of raw images and generation of database

Source	Raw Images				Database	
	No	Size	Training/Validation	Testing	Pixel	Training/Validation
Experiment	69	10240×2048	58	11	256×256	30,480
Field	81	2592×4608	69	12		

(a)　　　　　　　　　　　　　　　　(b)

(c)
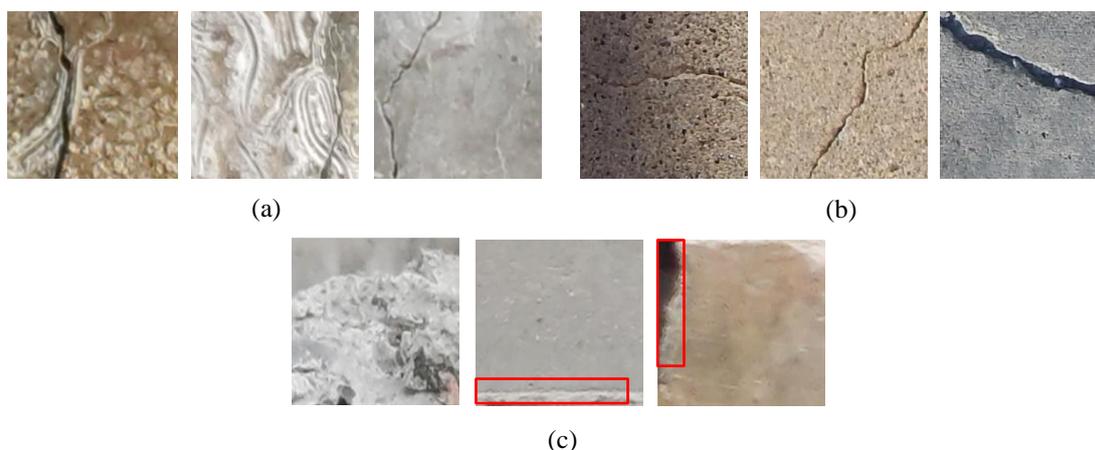
Figure 4.2 Typical cropped images: (a) images with crack from experiment; (b) images with crack from onsite inspection; and (c) disregarded images

4.2.2 Optimal model

(1) Performance evaluation

To obtain a CNN model with excellent robustness, four commonly used CNNs from other studies were tested: AlexNet [2], GoogLeNet [3], Resnet18 [4], and VGG-16 [5]; the results were summarized in Table 4.2. The performances of these CNNs were evaluated using five metrics, as depicted in Section 2.8. For a crack classifier, Recall or true positive rate (TPR) is the ratio of correct predictions to total crack sub-images. Similarly, the true negative rate (TNR) indicates the ratio of correct non-crack predictions to the total number of non-crack sub-images. Precision is the ratio of correct crack predictions to all crack predictions. Accuracy (ACC) is the ratio of correct crack or intact predictions to the total number of

sub-images. The F1 score is the harmonic mean of the recall and precision. In addition, time cost is used as an index to evaluate these four CNNs.

(2) Hyperparameters

All of the CNNs were trained using an SGD algorithm with a mini-batch size of 256 out of 30,480 images. The last layers of all of the CNNs were modified to two outputs, as the output of our dataset was "crack" or "intact". A logarithmically decreasing learning rate was applied in the training, according to Cha and Choi [2]. The dropout rate at the dropout layer was 0.5. The other hyperparameters remained at default values.

(3) Comparisons

The database was divided into 70% for training and 30% for validation. The four commonly used CNNs were trained for 80 epochs on the training set until the loss function reached a plateau, which showed the convergence of the weights. Table 4.2 presents the detailed performance of the four transfer learning CNNs on the training and validation sets. Figure 4.3 shows that the accuracies of the models increase from the AlexNet to the best performing VGG-16. However, VGG-16 spends 346 minutes per epoch in the training of the model. In addition, there is no significant difference in performance between GoogLeNet and RestNet18 on the applied database. The GoogLeNet was therefore chosen to analyze the rest of this study.

Table 4.2 Performances of the four pre-trained CNN configurations

	Re	TNR	Pre	ACC	F1	Time per epoch (min)
AlexNet	0.9377	0.9831	0.9819	0.9606	0.9593	24.84
Googlenet	0.9604	0.9736	0.9737	0.9669	0.9670	38.82
Resnet18	0.9661	0.9678	0.9678	0.9689	0.9670	45.33
VGG-16	0.9724	0.9680	0.9683	0.9740	0.9704	346.6
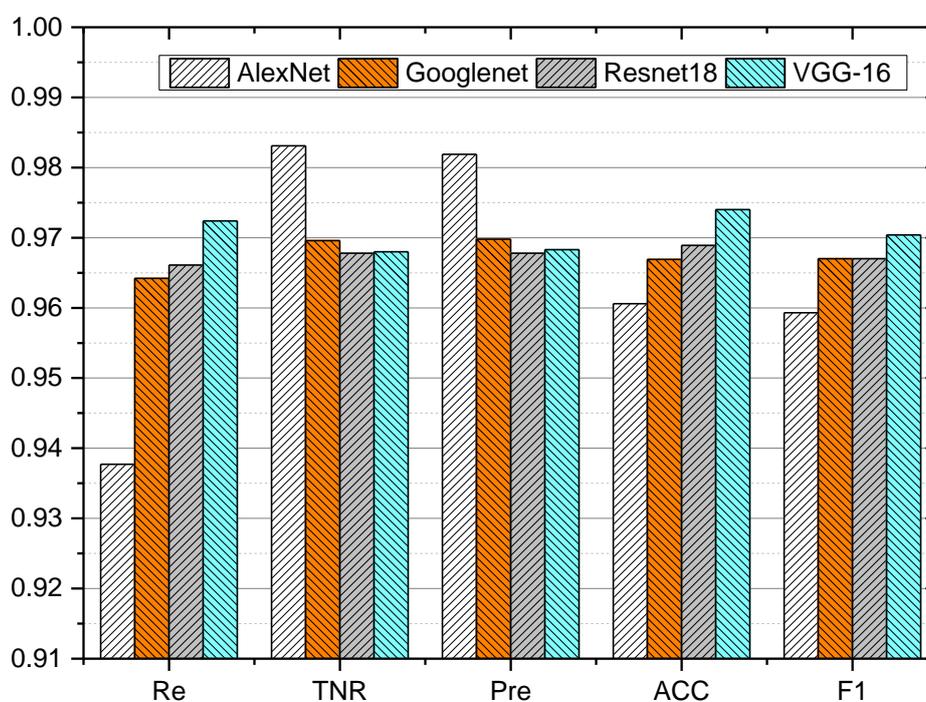
Figure 4.3 Performances of different CNNs

Furthermore, the performances of the fully training and transfer learning using the GoogLeNet were tested, as summarized in Table 4.3. Figure 4.4 clearly indicates that fully training outperforms transfer learning. Table 4.4 shows the testing results of the transfer learning model and the fully training model on a public database SDNET2018 [6]. On this public database, the performance of the transfer learning model is superior to that of the fully training model (Figure 4.5), which is contrary to the test results on the testing dataset of this study. In addition, the test results of fully training on SDNET2018 are greatly compromised compared with that on the testing dataset of this study. One possible reason is that the transfer learning can avoid overfitting to some extent. Therefore, the transfer training GoogLeNet was considered the optimal model to implement further analysis.

Table 4.3 Performances of the transfer and fully training of GoogLeNet.

	Re	TNR	Pre	ACC	F1
Transfer	0.9603	0.9735	0.9737	0.9669	0.9670
Fully	0.9720	0.9758	0.9761	0.9709	0.9740
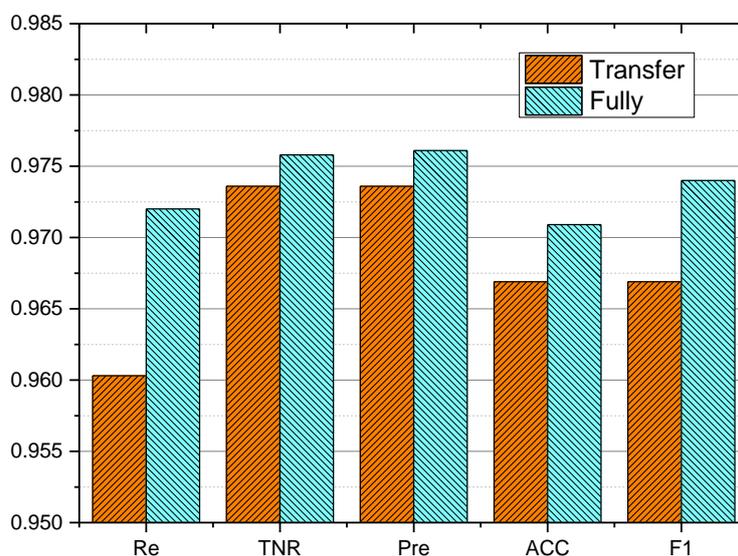
Figure 4.4 Metrics of the GoogLeNet in transfer and full learning

Table 4.4 Performances of the transfer and fully training on SDNET2018

	Re	TNR	Pre	ACC	F1
Transfer(SDNET2018)	0.8905	0.8772	0.8798	0.8839	0.8851
Fully(SDNET2018)	0.8100	0.8004	0.8048	0.8133	0.8074
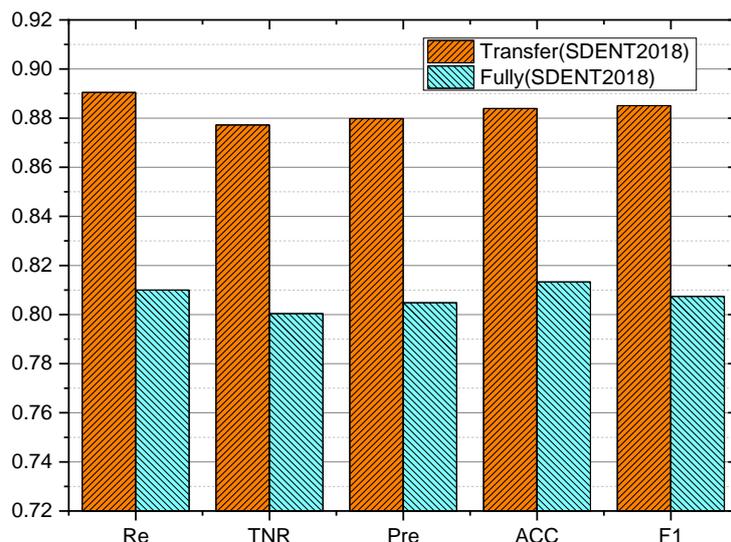
Figure 4.5 Performances of the transfer and fully learned GoogLeNet on SDNT2018

Figure 4.6 shows the loss and accuracy during training and validation. Each epoch of training and validation took approximately 39 minutes. The accuracy converged to 95%, and the error converged to 0.1. The trained GoogLeNet was further tested below.
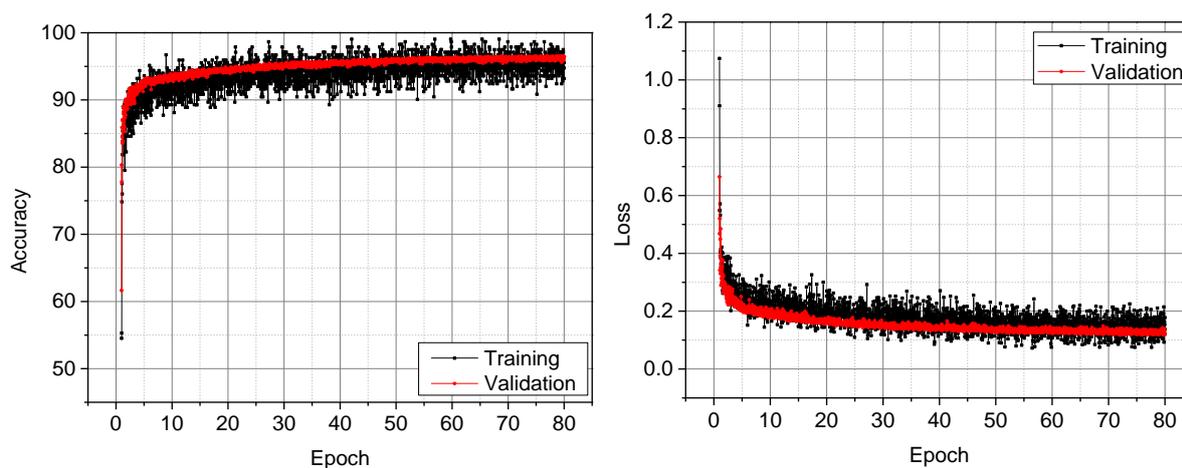
Figure 4.6 Loss and accuracy during training and validation

4.2.3 Comparisons of scanning approaches

Extensive tests were conducted to validate the optimal CNN from the previous section. Owing to the random distribution of the cracks, it was difficult to locate cracks depending only on lump-sum scan in a large image. Therefore, other algorithms were required to locate the crack positions. In addition, a sub-image with cracks on the edge of it can cause misclassification. To correctly identify the cracks, a 256 × 256 pixel window was designed for scanning the image twice [2], as shown in Figure 4.7(a). This method is hereafter referred to as "dual scanning". Except for the dual scanning method, a new scanning method called "neighborhood scanning" was proposed, as depicted in Figure 4.7(b). The first scanning of this novel scanning method is the same as the previous method. The only difference is that the second scanning of the proposed method is not performed on the entire image, but rather only on the neighborhood of the cracks identified in the first scanning. To avoid repeat scanning in the second

operation of the proposed method, the same region is scanned only once.

(a)   (b)
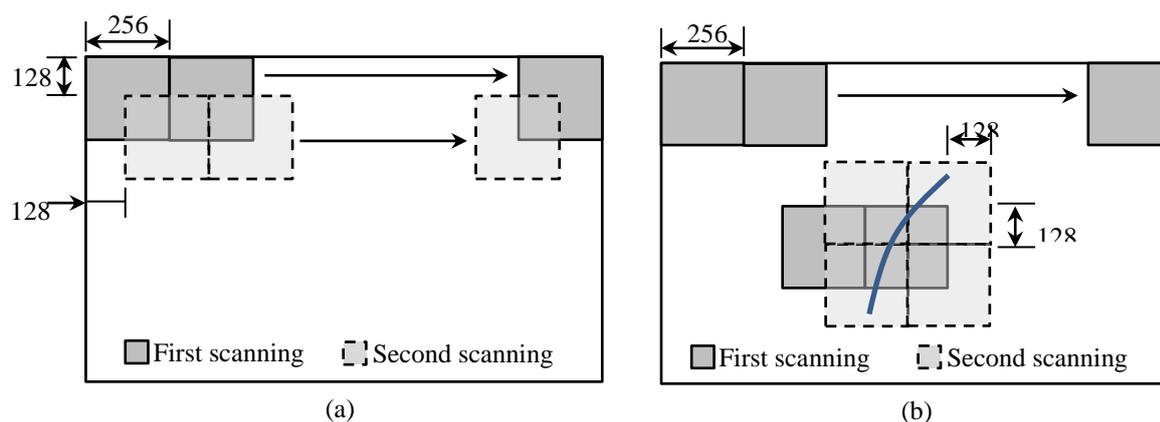
Figure 4.7 Crack detection: (a) Dual scanning; and (b) Neighborhood scanning

To compare the proposed and previous scanning methods, 23 of the raw images that were not used to build the training and validation sets were scanned according to the abovementioned procedures. Using the evaluation metrics in Section 2.8, the performances of the two scanning methods are summarized in Table 4.5. Neighborhood scanning shows a performance equivalent to that of the previous dual scanning method in terms of the five metrics, as shown in Figure 4.8. In addition, the achieved accuracy of the two methods are quite remarkable with around 95.5 %, i.e., nearly identical to the accuracy (96.69%) of the validation in the previous section. Encouragingly, the performance of the trained CNN is still impressive, even though field and experimental images are used for testing. The average recorded testing time required for each image using the neighbourhood and dual scanning methods are 6.48 s and 7.11 s, respectively.

Table 4.5 Comparisons of the dual scanning and the neighborhood scanning

	Rec	TNR	Pre	ACC	F1	Average time(s)
Neig	0.9533	0.9526	0.9651	0.9555	0.9592	6.48
Dual	0.9517	0.9587	0.9672	0.9551	0.9594	7.11
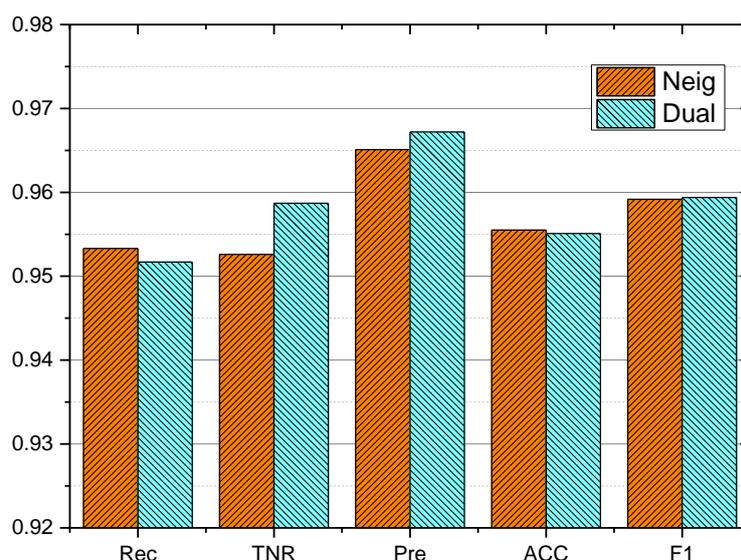
Figure 4.8 Test results using dual scanning and neighborhood scanning
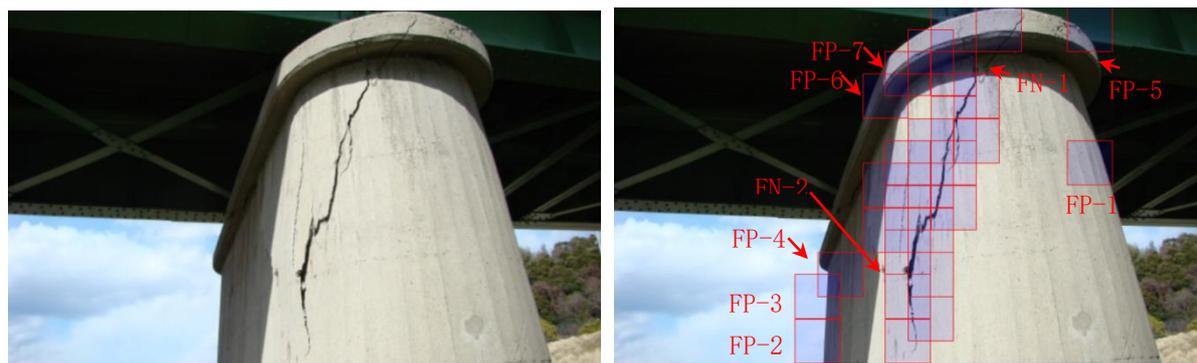
(a) Original

(b) Dual (Number of crack position =28)
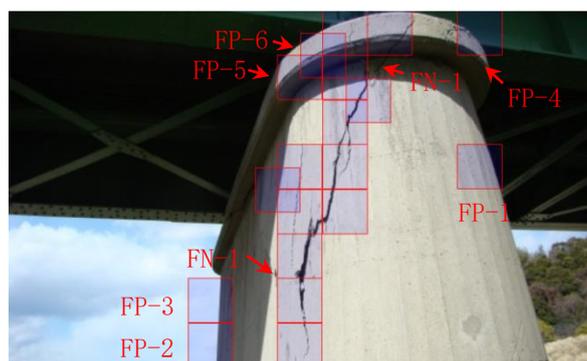
(c) Neighborhood (Number of crack position =19)

Figure 4.9 Crack detection on field image 1
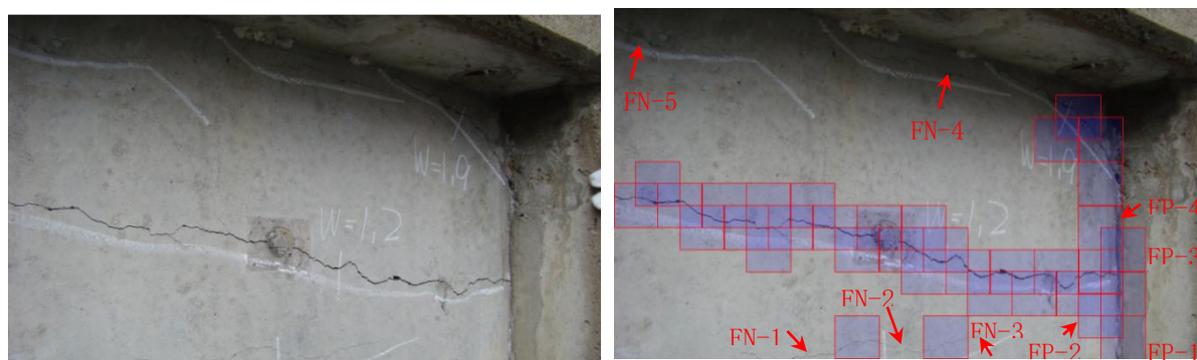
(a) Original

(b) Dual (Number of crack position =34)
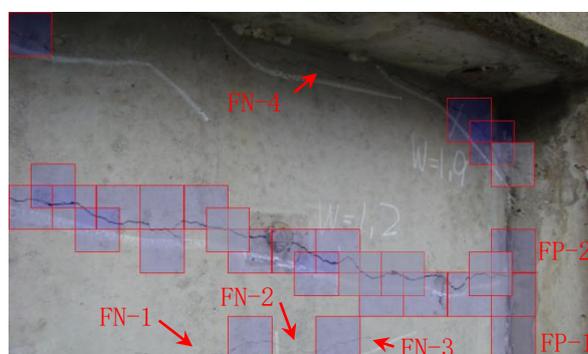
(c) Neighborhood (Number of crack position =28)

Figure 4.10 Crack detection on field image 2

Because the raw images used in this study were collected from bridge inspections and beam bending tests,

the inspection and experimental images were separately applied to verify the classifier. Figures 4.9 and 4.10 show the testing results of two onsite images. These images can provide a clear understanding of how the classifier functions. For inspection images, all evident cracks can be identified by these two scanning methods. In addition, the unions of the detected crack regions using these two methods are almost the same. However, the numbers of crack regions detected by the neighbourhood are less than that by the dual scanning method. This occurs because the dual scanning method detected more sub-images with cracks on the edges of them. The false positive and false negative regions (positions) were marked in Figures 4.9 (b) and (c) and Figures 4.10 (b) and (c). Most false positives are distributed at: (i) the interface between the pier and background, as shown in FP-1~FP-4 in Figure 4.9 (b) and FP-1~FP-3 in Figure 4.9 (c); (ii) the edges of the pier, as shown in FP-5~FP-7 in Figure 4.9 (b) and FP-4~FP-6 in Figure 4.9 (c); and (iii) the corners, as shown in FP-1~FP-4 in Figure 4.10 (b) and FP-1~FP-3 in Figure 4.10 (c). Most false negatives are caused by insufficient illumination (FN-1 in Figures 4.9 (b) and (c), FN-4~FN-5 in Figures 4.10 (b) and (c)), and tiny cracks (FN-2 in Figures 4.9 (b) and (c), FN-1~FN-3 in Figures 4.10 (b) and (c)). These occur because our database included insufficient samples regarding these situations.

(a) Original

(b) Dual (Number of crack regions =139)

(c) Neighborhood (Number of crack regions =122)

Figure 4.11 Crack detection on an experimental image
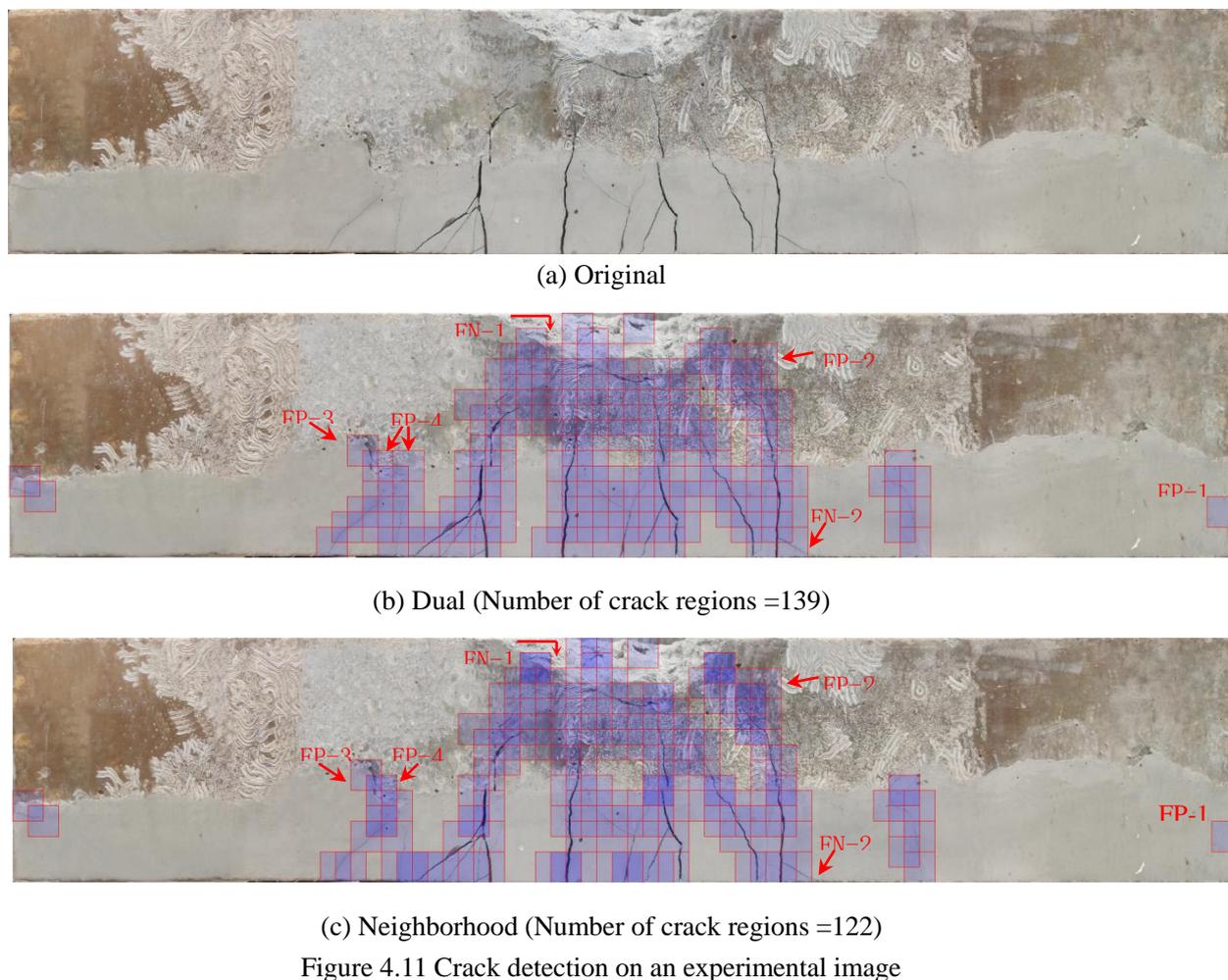
Figure 4.11 shows testing results for an experimental image using the two scanning methods. Figures 4.11 (b) and (c) show that both scanning methods can detect thick cracks, even though the numbers of detected regions in those two methods are different. The dual scanning and neighbourhood scanning methods detected 139 and 122 regions, respectively. In Figures 4.11 (b) and (c), all false negatives are found to be caused by the tiny cracks, because illumination conditions in the laboratory are more ideal than the onsite

conditions. Some false positive regions are located at the interface between the fresh and elder cement, as shown at FP-3 and FP-4 in Figures 4.11 (b) and (c). The rest false positive regions are distributed where thin and long voids exist (FP-1 in Figures 4.11 (b) and (c)), and where shellfish growth linearly (FP-2 in Figures 4.11 (b) and (c)).

The testing results indicate that the built classifier can correctly detect most cracks or intact regions, by combining with the dual or neighborhood scanning methods. However, the classifier will cause misdetections in the previously mentioned situations. In addition, there are no significant differences between the dual and neighborhood scanning methods in terms of the evaluation metrics. The former method can detect more edge cracks. The latter method usually takes less time to scan the same raw image. Considering the unions of the regions detected by these two methods are almost the same, the performance of the neighborhood scanning method is acceptable for the post-processing described below.

4.3 Development of the post-processing application

The trained CNN can be used to classify a new image combined with the neighborhood scanning method, but the specification of the crack pixel cannot be determined. In addition, the misidentified regions must be addressed in post-processing. As a result, an application was developed to fulfil these purposes. Image processing techniques described in Section 2.7 are included in the application. Therefore, different processing techniques can be used depend on images to obtain the optimal segmentation effect. In addition, the crack property acquisition methods including the algorithm described in Section 2.7.3 were integrated in the developed application. The introductions and verifications of this application were described below.

(a)   (b)
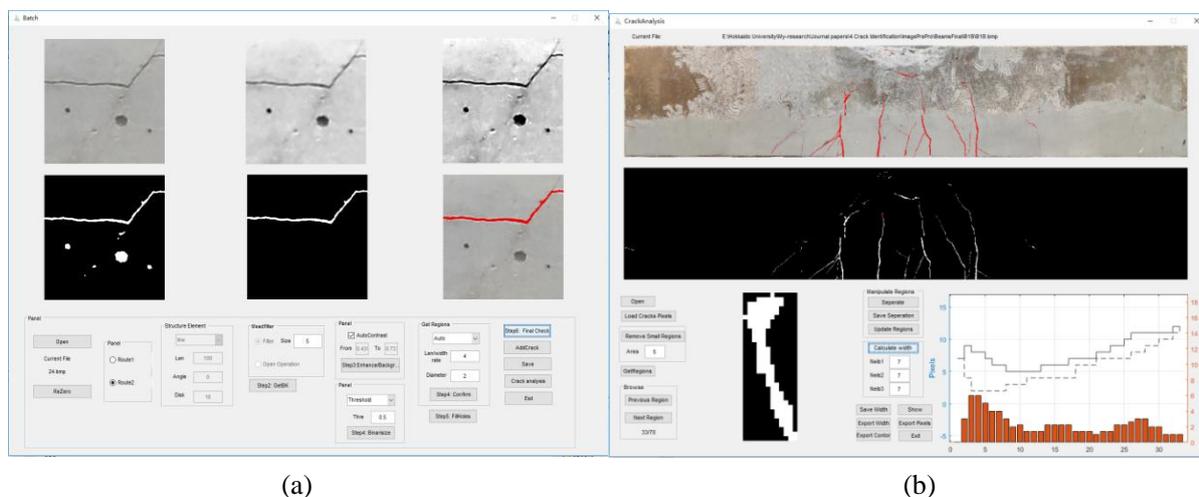
Figure 4.12 The developed application for post-processing: (a) processing for every regions; (b) crack analysis for each raw image

4.3.1 Application development

Figure 4.12 shows screenshots of the developed application for post-processing. The developed application mainly includes two modules: module 1 for processing the detected crack regions, and module 2 for providing the crack analysis of the raw image. Specifically, the first model is mainly used for rapidly processing of crack regions detected by the optimal classifier in Section 4.2, so as to obtain crack pixels. Once all of the crack pixels are obtained, they are stitched together and transferred to the second module for calculating other properties of the crack, such as the crack width, length, and orientation. These two modules are shown in Figures 4.12 (a) and (b), respectively. The application can be run automatically or

manually. The former analyzes images according to the default settings and the latter according to the settings of the operator. Verification of the developed application was conducted based on practical examples, as described below.

4.3.2 Practical comparisons

On the raw images in the testing set (Section 4.2.1), the practical performances of the developed crack identification model were compared with that of a previous pixel-level crack segmentation framework [5], using Intersection over Union (IoU) and time cost as evaluation indexes. The equation of IoU is:

$$IoU = \frac{target \cap prediction}{target \cup prediction} \tag{5}$$

Table 4.6 Comparison of the developed model and the previous framework

Image	IoU		Time cost	
	This	Previous	This	Previous
im1	0.7535	0.6958	7.0209	7.6364
im2	0.7005	0.6523	7.0114	7.6142
im3	0.8184	0.8301	7.0030	7.6435
im4	0.8350	0.8385	7.0373	7.6772
im5	0.7583	0.5540	7.0436	7.6369
im6	0.8427	0.8456	7.0591	7.6207
im7	0.8266	0.8192	7.0398	7.6466
im8	0.8389	0.8270	6.9890	7.6141
im9	0.7544	0.7573	6.9825	7.6854
im10	0.8301	0.8211	7.0557	7.6059
im11	0.8030	0.8015	7.0241	7.5988
im12	0.8265	0.8165	7.0181	7.6024
im13	0.8206	0.8292	12.2009	13.2951
im14	0.7585	0.7603	12.1531	13.3312
im15	0.8441	0.8127	12.1458	13.3013
im16	0.8069	0.8184	12.1485	13.3193
im17	0.8424	0.8159	12.1506	13.3248
im18	0.8228	0.8123	12.1455	13.2847
im19	0.7888	0.7652	12.1369	13.3349
im20	0.7933	0.7993	12.1436	13.3010
im21	0.8359	0.8042	12.2002	13.3236
im22	0.7840	0.7956	12.1751	13.3112
im23	0.8076	0.8165	12.1552	13.3408

The results show that the developed crack identification model and the previous framework exhibited an 80.40% and a 78.64% average IoU, respectively. The developed model took an average of 9.48s, and the previous framework took an average of 10.35s. Specifically, the performances of the developed model and the previous framework vary with image conditions. Experimental images take more time than onsite images because of the larger size of the images. For the same raw image, the developed model usually takes less time than the previous framework. IoU shows that the developed model is comparable to the previous framework for the experimental images. The reason is that the images taken in the laboratory have less interference; enabling both methods achieve good results. These two methods also show approximately the same IoU values for the onsite images except for im1, im2, and im5.

On these three images, the IoU of the development model is 0.05 greater than that of the previous

framework. Therefore, these three images with complex backgrounds were detailed in Figure 4.13. Although the previous framework shows good performance on trained images with monotonous backgrounds and good illumination, its performance is inferior to our developed model when the method is tested on untrained complex backgrounds (Figure 4.13).

Ground truth	This study	Segmentaion
	IoU=0.7535	IoU=0.6958
	IoU=0.7005	IoU=0.6523
	IoU=0.7583	IoU=0.5540

Figure 4.13 Comparative studies using our model and a picel-level segmentation framework.

These 23 examples show that the performance of the developed model is not inferior to the previous framework. In addition, the developed model usually cost less time than the previous framework. Therefore, the developed model is a cost-effective solution that can detect and quantify cracks from images collected from onsite inspections or from experiments.

4.3.3 Crack analysis

Detailed information such as crack patterns, width and length are also crucial for understanding the damage in structures, because this information can be used to track the damage status of different components in civil structures. Therefore, the crack analysis focuses on the accurate acquisition of detailed

crack information.

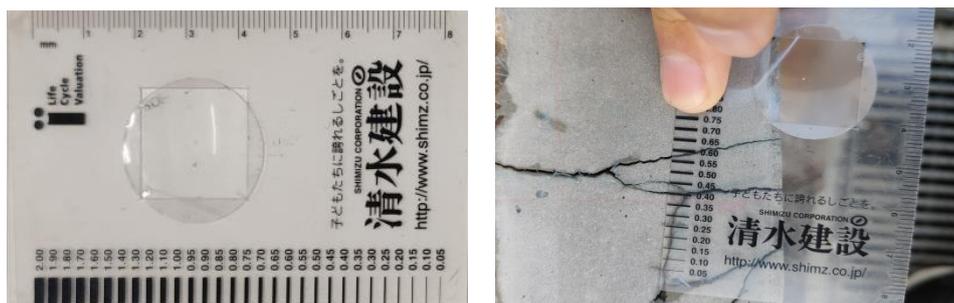Table 4.7 Comparisons of crack width measurement methods

No	This study (mm)	Mean (mm)	Measured (mm)	Relative Error of predicted values (%)	Relative error of mean values (%)	No	This study (mm)	Mean (mm)	Measured (mm)	Relative Error of calculated values (%)	Relative error of mean values (%)
1	0.30	0.38	0.22	35.08	71.15	30	1.60	1.56	1.15	38.93	35.55
2	0.25	0.34	0.23	8.96	49.32	31	0.43	0.50	0.34	26.87	46.54
3	0.23	0.32	0.25	8.34	29.84	32	0.44	0.49	0.37	19.46	33.40
4	0.40	0.43	0.34	18.10	25.78	33	0.48	0.54	0.41	17.01	31.72
5	0.35	0.43	0.30	17.63	42.97	34	0.15	0.26	0.21	27.50	21.95
6	0.08	0.21	0.06	33.60	245.30	35	0.89	0.76	0.65	35.39	16.79
7	0.11	0.23	0.15	29.15	52.54	36	0.26	0.36	0.27	2.54	32.78
8	0.22	0.34	0.22	1.58	56.65	37	0.73	0.76	0.74	0.77	2.89
9	0.93	0.98	0.72	28.61	36.42	38	0.21	0.29	0.18	18.96	63.14
10	0.40	0.51	0.32	24.65	60.87	39	0.73	0.69	0.67	9.48	2.78
11	0.23	0.34	0.23	0.31	48.33	40	0.30	0.38	0.28	6.97	36.93
12	0.36	0.31	0.30	19.31	1.70	41	0.32	0.41	0.34	6.34	20.26
13	0.24	0.33	0.27	12.18	21.83	42	1.51	1.48	1.19	26.42	24.09
14	0.26	0.34	0.23	14.41	48.67	43	0.16	0.24	0.16	2.63	51.33
15	0.25	0.33	0.26	4.22	25.39	44	0.16	0.28	0.17	6.21	63.18
16	0.32	0.39	0.31	3.03	27.28	45	0.88	0.76	0.92	3.75	16.93
17	0.10	0.25	0.16	34.94	55.32	46	0.22	0.30	0.19	18.13	56.39
18	0.13	0.22	0.17	23.60	26.78	47	0.46	0.52	0.51	8.33	2.70
19	0.17	0.27	0.17	2.73	56.94	48	0.40	0.39	0.35	15.71	11.79
20	0.69	0.70	0.67	3.88	5.14	49	0.18	0.29	0.22	15.69	36.05
21	0.65	0.60	0.63	2.93	3.56	50	0.26	0.34	0.28	7.32	22.48
22	0.63	0.65	0.52	22.57	26.11	51	0.13	0.25	0.15	15.99	68.03
23	0.40	0.50	0.41	2.99	21.28	52	0.12	0.22	0.14	12.20	58.52
24	0.45	0.53	0.37	22.16	42.74	53	0.25	0.32	0.27	8.70	19.78
25	0.65	0.65	0.60	7.70	7.04	54	1.76	1.69	1.52	15.97	11.33
26	0.41	0.51	0.33	23.70	53.51	55	0.64	0.74	0.56	12.94	32.41
27	0.20	0.24	0.18	12.77	35.15	56	0.21	0.27	0.27	21.65	1.19
28	0.18	0.29	0.20	7.98	46.83	57	0.21	0.21	0.21	0.76	1.65
29	0.28	0.36	0.29	1.27	26.26	**Average**	**0.42**	**0.48**	**0.38**	**14.58**	**36.37**

(1) Crack width comparison

To verify the accuracy of the crack width obtained from the proposed algorithm, the algorithm (with a δ value of 7) was applied to calculate the crack widths at 57 positions selected from the eleven untrained experimental images. Then the calculated results of these 57 positions were compared with the measured results by the crack scale shown in Figure 4.14. In addition, Adhikari et al. [7] utilized the mean width to quantify cracks according to Eq. (6).

$$\text{Mean width} = \frac{\text{crack area}}{\text{crack perimeter}/2} \tag{6}$$

Therefore, the mean width method will also be used for comparison to verify the effectiveness of the crack identification model for measuring crack widths. All cracks were quantified in units of mm.

(a)   (b)

Figure 4.14 (a) Crack scale; (b) Crack measuring.

Table 4.7 shows the comparisons of the proposed algorithm, mean width, and the measurements. The relative error and absolute error of the proposed algorithm and that of the mean value method were calculated taking the measured values as truths. Figure 4.15 shows the relative and absolute error distributions of these positions. The relative error of the proposed algorithm is less than 20% at more than 40 positions, but that of the mean value method is greater than 40% at more than 20 positions. Similarly tendency can be found for the absolute error. The absolute error of 35 positions obtained using the proposed algorithm is less than 0.05 mm, while that of 25 locations obtained by the mean method is greater than 0.1 mm. The average relative error (Table 4.7) of the proposed algorithm is 14.58% (0.05 mm), i.e., the same as the thinnest crack width measurable by the crack scale (Figure 4.14 (a)). In addition, the average relative error of this method is much smaller than the 36.37% (0.14 mm) of the mean value method.
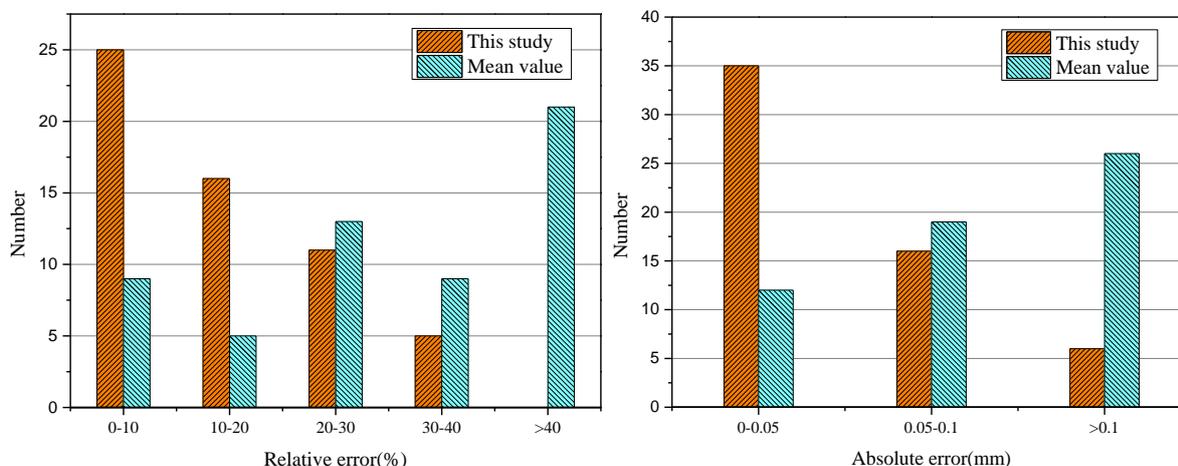
Figure 4.15 Relative and absolute error distributions.

Crack widths greater than 0.2 are considered detrimental to concrete structures according to Japan road association [8]. Therefore, the relative errors of these two methods were respectively divided into two groups broken down by crack width 0.2mm, as shown in Figure 4.16. The method of this study has a balanced performance for both cracks smaller or larger than 0.2 mm with relative error of 16.84% and 13.91%, respectively. However, the mean value method produces a relative error of almost 70% for cracks smaller than 0.2 mm, and produces that of nearly 30% for the cracks greater than 0.2 mm. As a result, the proposed method is effective in measuring both thin and thick crack widths, and is more accurate than the previous mean value method at these 57 positions. However, it should be mentioned that more verifications

of this algorithm are necessary in the future.

Figure 4.16 Relative error of those two methods, broken down by crack width of 0.2 mm

(2) Crack width distribution

(a)

(b)

(c)

Figure 4.17 Superimposed images of crack width distribution: (a) front; (b) back; (c) bottom

Figure 4.17 shows the crack width distribution at the front, back, and bottom of a beam obtained by the

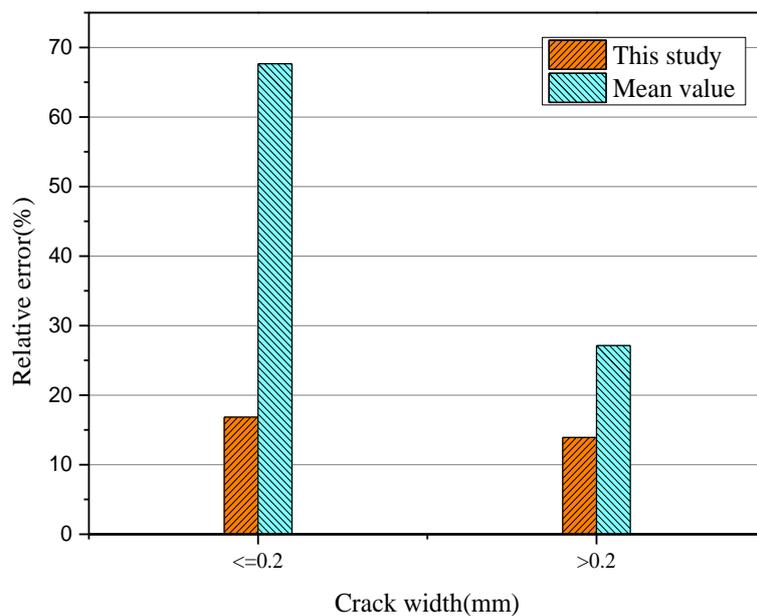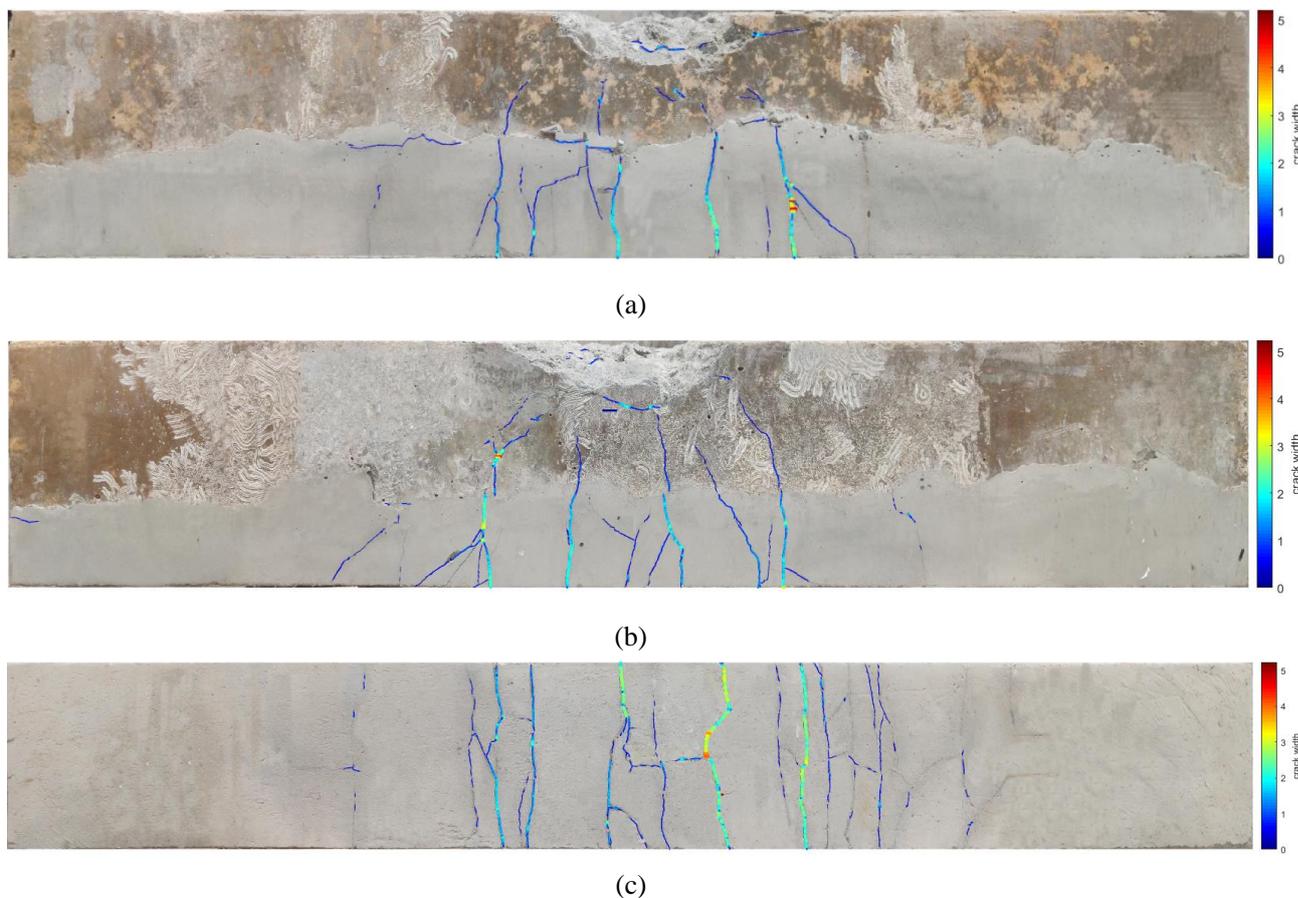developed application and algorithm. These three images were taken and calibrated after the beam failed in a bending test. Various crack shapes can be found in these images. Different from previous studies [7, 9] that use the mean width of a crack as its width, the proposed algorithm can calculate the crack width at each position along the crack, as can be clearly seen from Figure 4.17. In addition, these three images can be stitched to provide a 3-D visualization of the beam, as described in (4) of this section.

(3) Crack direction statistics.

Field inspections require determining the locations and orientations of cracks. Therefore, after the cracks are identified, the crack orientations can be counted to obtain the statistical characteristics of the crack orientation distribution in polar coordinates. Figures 4.18 (a), (b), and (c) show the counted results for Figures 4.17 (a), (b), and (c), respectively. In Figure 4.18, the crack orientation distributions of the corresponding image can be clearly determined. In addition, if the raw images of the same component are collected in chronological order, a crack propagation trace can be inferred by combining the findings in Figures 4.17 and 4.18.

(a)   (b)   (c)
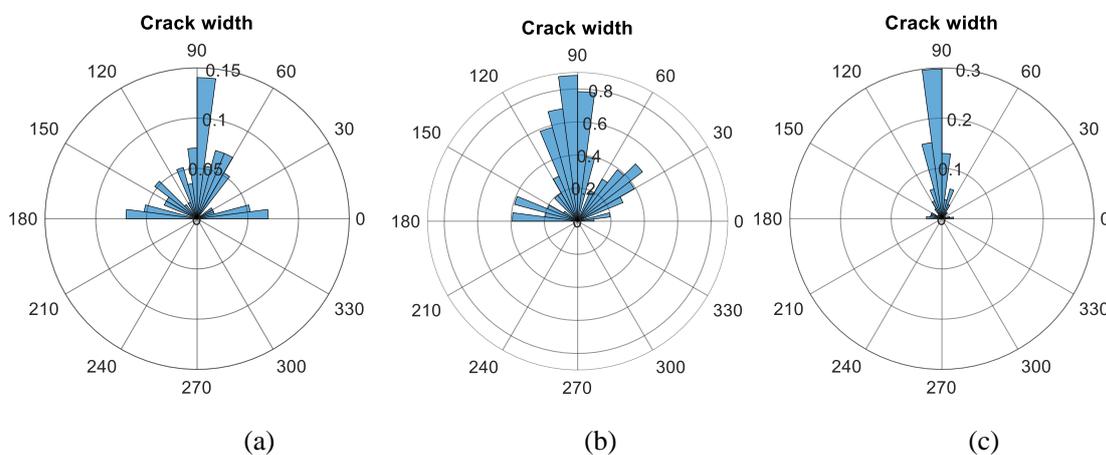
Figure 4.18 Cracks directions statistics from Figures 4.17 (a), (b), and (c)

(4) 3-D visualization

If the cracks on each surface of a component are obtained, the developed application can present and analyze the surface damage in 3-D [7, 10]. The results of the images in Figure 4.17 are stitched to generate a 3-D model of a beam. Figure 4.19 shows cracks on the front and bottom faces, respectively.
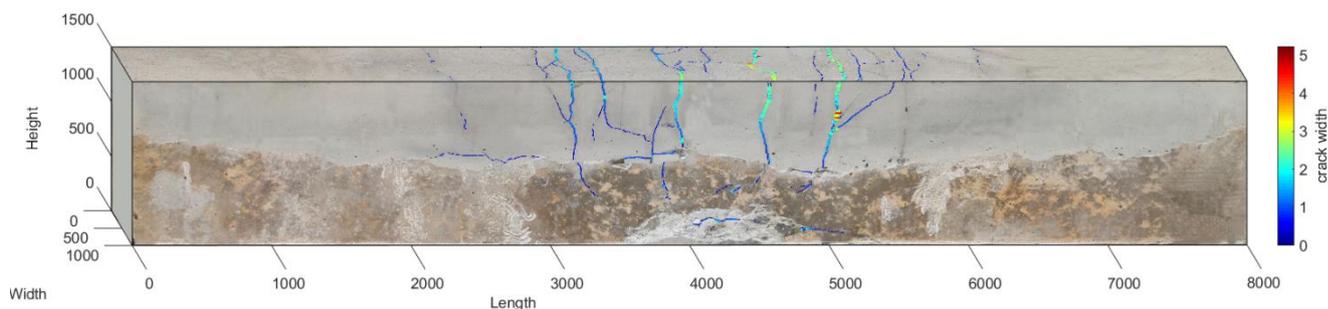
Figure 4.19 3-D visualization of a beam

Obviously, the magnitudes and orientations of cracks can be intuitively observed based on the cracks directions statistics in 3-D visualization. Based on this model, additional information (such as crack density) can be calculated to determine the severity of cracks and cracking patterns. If the crack

information are provided and shown in the 3-D model of Figure 4.19 in chronological order, the model can be used for tracking the crack development at various stages of loading. In the real world, images collected from inspections can be analyzed and projected onto the 3-D model of the structure. Infrastructure managers can be notified when the crack exceeds limitations, or can formulate intervention strategies according to crack propagation patterns, thereby facilitating the effectiveness of the management.

4.4. Discussion and future work

4.4.1 Practical application results

Once the proposed model is put into use in structures, it is possible to detect and quantify cracks based only on digital images. Thus, the inspection efficiency and reliability are enhanced. However, from the viewpoint of practical applications, it is not feasible for the developed model to extract any object attributes from any image. To further describe the applicable range of the proposed model, Figure 4.20 shows some complicated images that will cause the classifier to fail in detection. Failure detections are distributed at: (i) the interface between the backgrounds and infrastructure (Figures 4.20 (a) and (b)); (ii) the bonding position between the elder and fresh cement (Figure 4.20 (c)); (iii) the long-thin void (Figure 4.20 (d)); (iv) the linear growth traces of shellfish (Figures 4.20 (e) and (f)); and (v) sub-images with tiny cracks (Figure 4.20 (g)) or without sufficient illumination (Figure 4.20 (k)). The failure of the trained classifier in these situations can be traced to the fact that there are insufficient similar sub-images in the training dataset.

| (a) | (b) | (c) | (d) |
| (e) | (f) | (g) | (k) |
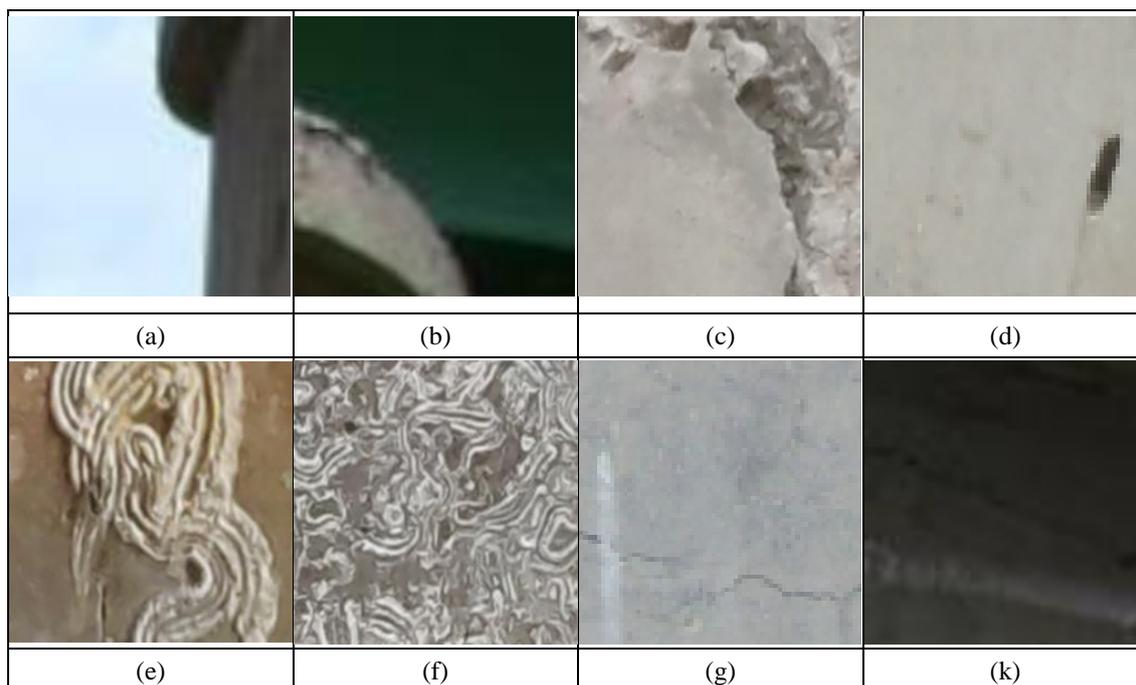
Figure 4.20 Failure of detection by the trained classifier.

In addition, some sub-images with cracks can be correctly detected by the classifier, but these sub-images are difficult to be further processed for the developed application, owing mainly to uneven illumination and thin cracks. In Figure 4.21 (a), only the crack pixels with good illumination can be determined by the developed application. For the thin cracks, only some scatter debris can be obtained (Figure 4.21 (b)), or only a part of the pixel is retrieved (Figure 4.21 (c)). These drawbacks can be avoided to some extent by providing images with higher resolution and better illumination, or by improving the developed

application.

Original		
CNN+ Developed application		
(a)	(b)	(c)
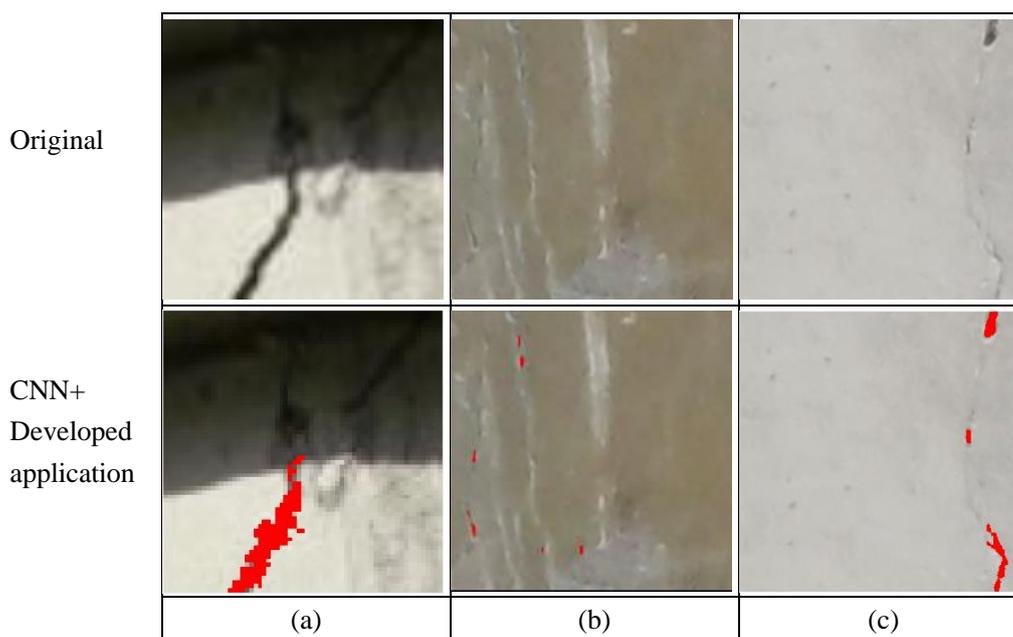
Figure 4.21 The superimposed images by the trained CNN and the developed application.

Furthermore, the neighborhood scanning method was proposed for identifying all crack regions from a raw image. However, the second scanning depends largely on the accuracy of the first scanning. In other words, the second scanning may fail if some positions are misjudged in the first scanning. The neighborhood scanning method takes less time than the dual scanning method, and can detect the union of the crack regions that is almost the same as the dual scanning method. However, the former method is inferior to the latter method in detecting the sub-images with edge cracks. In addition, it is difficult to determine the optimal size of the scanning window, as the testing images may have various sizes and scales. Although the proposed algorithm outperforms the mean width method, the effectiveness of this algorithm is affected by the performance of the crack segmentation. A 3-D model is established using the images from a beam after failure, but no images at various stages of loading are used to verify the applicability of the model to observe the evolution of crack patterns. In addition, the original image still requires calibration to correctly calculate the crack width and other crack characteristics. We hope that these limitations can be resolved by improving our model.

4.4.2 Comparison with other studies

The developed model is a semi-automatic method. Specifically, the trained CNN classifier can automatically identify the crack regions. Then, the developed application can be run automatically or manually to quantify cracks. Compared with the traditional image classification CNN which only realizes crack detection, this model can not only realize crack detection, but also quantify cracks. In addition, the CNN classifier and the developed application can be used independently to suit the demands at various phases. Although the model is not as automated as semantic segmentation, it reduces the cost of building the pixel-level annotation databases for deep learning training. Kang et al. [11] proposed a similar two steps method. In this two steps method, three independent algorithms including Faster R-CNN, modified TuFF, and modified DTM are integrated. The integration and modification of this hybrid method is superior to our model in two points: (i) this hybrid method is more automated than our model; (ii) the performance of crack segmentation by this hybrid method is improved compared with that of our model.

However, our model shows advantages in three aspects: (i) the two parts of our model can operate independently, and can provide more crack information except for crack width and crack length; (ii) the calculated results of crack properties are shown in mm instead of pixels; (iii) verification images are more complex than those of Kang et al. (most images contain only one crack).

Furthermore, our model takes less time, and is not inferior to a previous pixel-level crack segmentation framework [5]. Therefore, it can be concluded that the model proposed in this study is a cost-effective solution for crack detection and analysis.

Although the crack identification model is tested on 23 complex images from both onsite and experiment, this study is only the first step in building a robust model. Because not all possible crack patterns, background materials, textures and color appearances are included in the database. Therefore, an important part of the required work is to enlarge the database to include a wider variety of crack patterns and background characteristics. Another task is to improve the proposed model by verifying with more examples, by tuning hyperparameter, and by modifying the proposed algorithm. In the future, other classifiers will be developed to detect various types of superficial damage, such as voids, spalling, and corrosion. In addition, the model is expected to collaborate with the bridge management systems (BMSs) to facilitate the processing of inspection images, as manual processing of onsite inspection images is time consuming and costly. Furthermore, the information obtained by our model can be used to understand the preliminary situation of a bridge, and can provide the basis for detailed investigations if any abnormalities exist.

References

[1] Bengio, Y., Goodfellow, I. J. & Courville, A. (2016), Deep Learning, An MIT Press book. Online version is available at: http://www.deeplearningbook.org, accessed July 2016.

[2] Cha, Y. J., Choi, W., & Büyüköztürk, O. (2017). Deep Learning-Based Crack Damage Detection Using Convolutional Neural Networks. Computer-Aided Civil and Infrastructure Engineering, 32(5), 361–378. https://doi.org/10.1111/mice.12263

[3] Ni, F. T., Zhang, J., & Chen, Z. Q. (2019). Pixel-level crack delineation in images with convolutional feature fusion. Structural Control and Health Monitoring, 26(1), 1–18. https://doi.org/10.1002/stc.2286

[4] X. Jia, X. Yang, X. Yu and H. Gao, "A Modified CenterNet for Crack Detection of Sanitary Ceramics," IECON 2020 The 46th Annual Conference of the IEEE Industrial Electronics Society, Singapore, Singapore, 2020, pp. 5311-5316, doi: 10.1109/IECON43393.2020.9254351

[5] Alipour, M., Harris, D. K., & Miller, G. R. (2019). Robust Pixel-Level Crack Detection Using Deep Fully Convolutional Neural Networks. Journal of Computing in Civil Engineering, 33(6), 1–14. https://doi.org/10.1061/(ASCE)CP.1943-5487.0000854

[6] Dorafshan, S., Thomas, R. J., & Maguire, M. (2018). Comparison of deep convolutional neural networks and edge detectors for image-based crack detection in concrete. Construction and Building Materials, 186, 1031–1045. https://doi.org/10.1016/j.conbuildmat.2018.08.011

[7] Adhikari, R. S., Moselhi, O., & Bagchi, A. (2014). Image-based retrieval of concrete crack properties for bridge inspection. Automation in Construction, 39(February 2018), 180–194. https://doi.org/10.1016/j.autcon.2013.06.011

[8] Japan road association. 2012. Specification for highway bridges, Part III: Concrete bridges. ISBN: 978-4-88950-715-7

[9] Albareda-Valls, A., Herrera, A. B., Mestre, J. L. Z., & Zaribaf, S. S. (2018). Image post-processing method for quantification of cracking in RC precast beams under bending. Buildings, 8(11). https://doi.org/10.3390/buildings8110158

[10] Torok, M. M., Golparvar-Fard, M., & Kochersberger, K. B. (2014). Image-based automated 3D crack detection for post-disaster building assessment. Journal of Computing in Civil Engineering, 28(5), 1–13. https://doi.org/10.1061/(ASCE)CP.1943-5487.0000334

[11] Kang, D., Benipal, S. S., Gopal, D. L., & Cha, Y. J. (2020). Hybrid pixel-level concrete crack segmentation and quantification across complex backgrounds using deep learning. Automation in Construction, 118, 103291. https://doi.org/10.1016/j.autcon.2020.103291

Chapter 5

Collaborated BIM platform for prediction-based maintenance

5.1 Overview

In this chapter, a collaborative Building Information Modeling (BIM) platform was established and verified by case studies. The procedures to establish this platform is shown in Figure 5.1. Specifically, the procedures include five steps: (i) to select the targeted bridges; (ii) preparations; (iii) onsite information collection; (iv) to build the 3-D prototype models; (v) and to formulate a collaborated Building Information Modeling (BIM) platform. This collaborated platform is finally used to visualize the damages of bridges intuitively, and to assist the managers or local authorities in scheduling the intervention timing and formulating maintenance strategies. These steps will be detailed below.
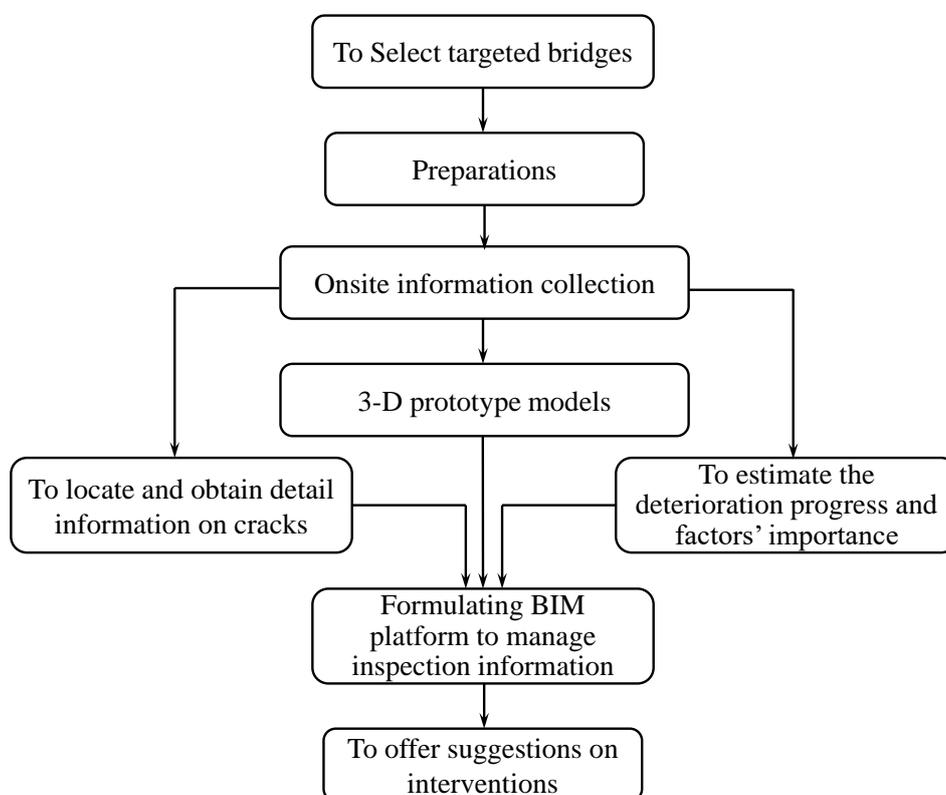
Figure 5.1 Flowchart of Chapter 5

5.2 Information acquisition
5.2.1 Overview of targeted bridges

Since many bridges were included in the inspection database, bridges are needed to be onsite inspected in batches while building the collaborative BIM platform. Considering the accessibility of the bridges by bicycle and the feasibility of inspecting these bridges, five bridges were selected as preliminary targets to establish collaborative BIM platform to verify the feasibility of the platform. Table 5.1 shows the detail information for the selected bridges, and Figure 5.2 shows the locations of these bridges. The dark-marked

region in Table 5.1 is the deterioration grade evaluated by the engineers. These bridges have different sizes, structure types, and deterioration situations. Bridge type indicates the types of decks.

Table 5.1 Detail information for the targeted bridges

Bridge No	1703	1704	1708	853	854
Bridge type	RC	PC	Steel	Steel	Steel
Length (m)	5.25	15.4	132.2	135.9	135.9
Width (m)	25	21	28.5	18	12
Deck area (m^2)	131.25	323.4	3767.7	2446.2	1630.8
Elevation (m)	19.8	19.9	17	15	14
Carbon dioxide (ppm)	397.027	354.868	359.087	397.03	397.03
Airborne chloride (kg/m^3)	0	0	0	0	0
Rainfall (cm)	1213	1213	1213	1213	1213
Snowfall (cm)	465.56	487.28	489.20	470.88	470.88
Highest temperature (°C)	26	26	26	26	26
Lowest temperature (°C)	-6	-6	-6	-6	-6
Traffic volume (daily)	34049	32181	56176	29362	29365
Large-size vehicles (daily)	3337	4068	5872	4380	4384
Years in service (years)	8	56	50	6	2
Deterioration grade	1	3	3	2	2

Figure 5.2 Locations of bridges listed in Table 5.1

5.2.2 Preparations and cautions

Some preparations should be made before going onsite to undertake inspections. Firstly, the exact locations of these bridges should be marked on the map, as shown in Figure 5.2. Secondly, some tools are required to measure the sizes of components and the sizes of cracks, as shown in Figure 5.3.

The tape measure was usually used to measure the sizes of the flat surface of components. The Polypropylene (PP) string and the soft tape measure were used together to measure the sizes of the arc surface of components (such as the perimeter of the pier) or the length of a crack. In addition, the tape was applied to fix the PP string in measuring. The crack width was measured using the crack scale. All the images were taken with mobile phones. The compass and gradienter in the mobile phone can be used to confirm the orientation of the components. A Bluetooth selfie stick was applied to capture images of components taller than a person. Figure 5.4 shows some measuring examples of onsite inspections.

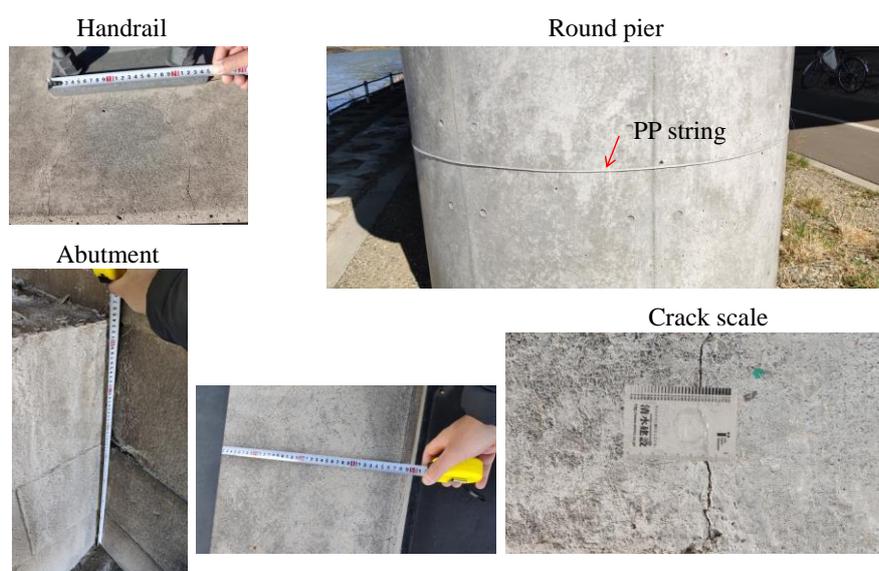Figure 5.3 Tools used to collect onsite information for the targeted bridges

Figure 5.4 Examples of onsite measuring

5.2.3 Onsite information collection

Using the tools shown in Figure 5.3 and the measuring methods shown in Figure 5.4, we measured the sizes of the components of the five selected bridges, and checked the crack damages on these components. Figure 5.5 shows the parts from where images are collected. (a), (b), (c), and (d) are refer to the bridge 1703, 1704, 1708, and 853& 854, respectively. Components without obvious damages were not inspected. Details for each bridge were described below.

(a)

(b)

(c)

(d)
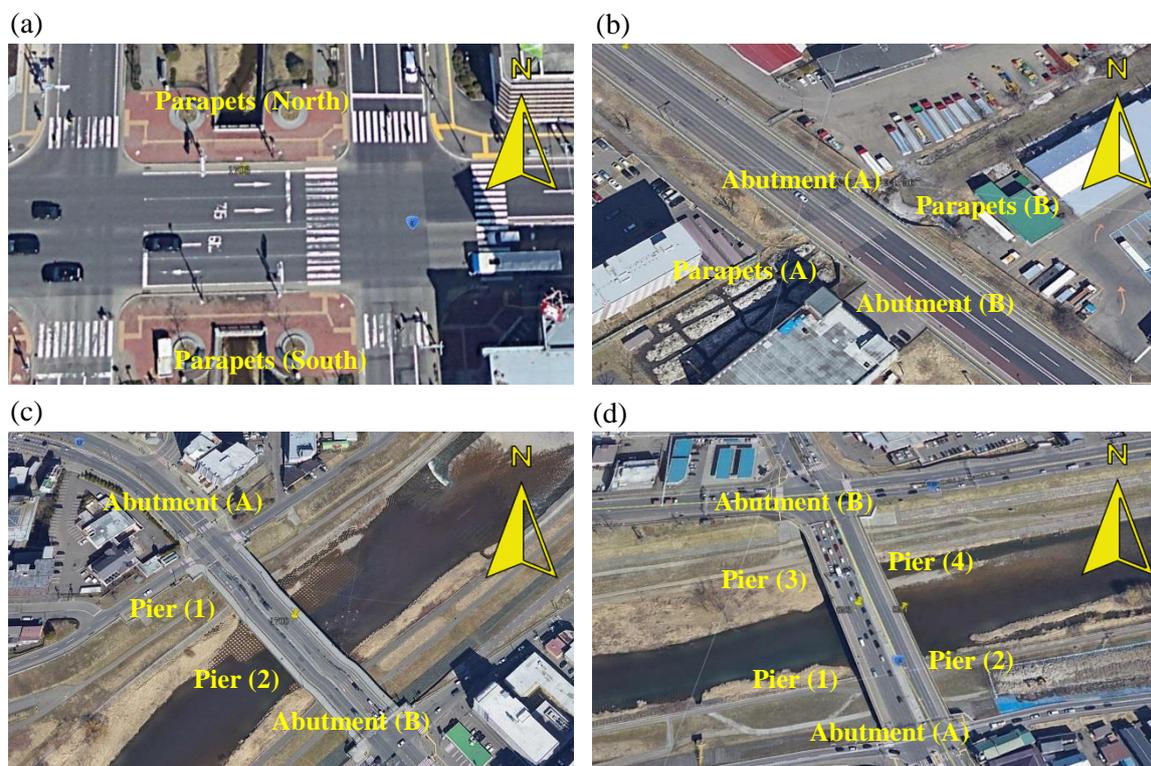
Figure 5.5 Explanation on bridge components (a) 1703, (b) 1704, (c) 1708, and (d) 853& 854

(1) Bridge 1703

Bridge 1703 has a reinforced concrete (RC) deck and is located in downtown. No obvious cracks were found in the structural components of this bridge. For bridge 1703, ten cracks were collected in north parapets, and twelve cracks were collected in south parapets. Typical cracks for the north and south side parapets are shown in Table 5.2. Most cracks have a width less than 2mm, and have a length less than 0.7m. Since these cracks are not in the structural components, such as the deck, they are not critical to influence the safety of this bridge. Therefore, this bridge was evaluated being grade 1 by the engineer.

Table 5.2 Details on partial cracks for bridge 1703

Component	No	Image	Crack width(mm)	Crack length(m)
Parapets(North)	1		2.00	0.70

Component	No	Image	Crack width(mm)	Crack length(m)
	2		1.30	0.70
	3		0.65	0.33
	1		0.85	0.59
Parapets(South)	2		0.5	0.19
	3		1.5	0.7
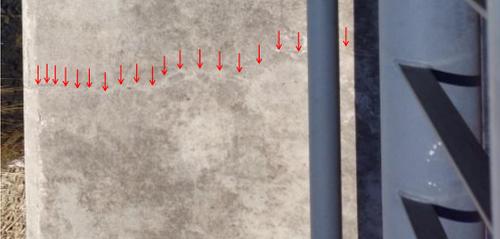
(2) Bridge 1704

Bridge 1704 has been in service for almost 60 years, and is an important part of Japan national road 12. Parapets and abutments of this bridge were inspected, as shown in Figure 5.5. Table 5.3 shows some cracks of these components. The cracks on the parapets are less than 1.4 mm width and less than 0.5 m length. Since the parapets are not the structural components, cracks on the parapets will not threaten the soundness of the bride. However, the crack on the abutment wall runs through the entire height of the abutment. These cracks are important to affect the deterioration and safety of the bridge. Heavy traffic volume is considered the reasons for these cracks, because the daily average traffic volume is more than 55, 000. Locations of these cracks can refer to the established model (Figure 5.11).

Table 5.3 Details on partial cracks for bridge 1704

Component	No	Image	Crack width(mm)	Crack length(m)
Parapets (A)	1		1.4	0.15
	2		0.85	0.50
	3		1.90	0.50
Parapets (B)	1		0.80	0.50
	2		0.70	0.51
	3		1.2	0.178

Component	No	Image	Crack width(mm)	Crack length(m)
Abutment (A)	1		0.2	3.0
	2		0.25	2.5
	3		0.9	3.0
Abutment (B)	1		0.30	3.5
	2		0.35	3.5
	3		0.3	4.5

Except for the cracks, water leakages were found on the abutment walls, as shown in Figure 5.6. There are many reasons for concrete water leakage, such as the use of poor graded aggregate, overdose of admixtures, deviations from designated mix. Since it is difficult to quantitatively evaluate this kind of damage using the tools shown in Figure 5.3, water leakages is not considered in this study.

Figure 5.6 Water leakage of bridge 1704

(3) Bridge 1708

Bridge 1708 is a crucial part of Japan national road 36, and has been in service for 54 years. Cracks on the abutment and the two piers were collected, as shown in Table 5.4. Three cracks were found for the abutment (A) and no obvious cracks were found for the abutment (B). The cracks on abutment (A) are less than 3.0 mm width and 0.3 m length. These cracks have little effect on the soundness of the bridge considering their locations (Figure 5.14 ③). However, the cracks on Pier (1) and Pier (2) run through the entire length of the piers. All cracks are loner than 2.0 m; some cracks are even as long as 6.0 m. The propagation of these cracks should be paid more attention. The heavy traffic volume and the natural deterioration of materials are considered the two reasons.

Except for the cracks collected from the concrete components of the bridge 1708, damage such as corrosion were also found for the steel components, as shown in Figure 5.7. The investigation found that the corrosion of the north side bracket was serious than that of the south side bracket.

(a)   (b)
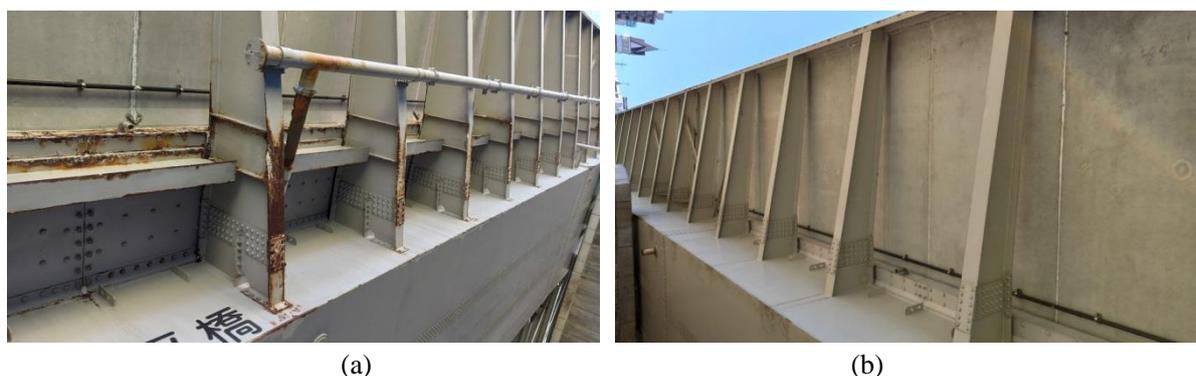
Figure 5.7 Corrosion of the bracket on the (a) north side and (b) south side.

To investigate the reasons for the corrosion differences, the wind directions were first counted. Figure 5.8 (a) shows the statistics of wind directions in Sapporo, the meteorological information were collected from Japan Meteorological Agency [1]. The red bar in Figure 5.8 (b) indicates the orientation of the bridge 1708. The wind in Sapporo mainly blows from the northwest and southeast directions. In addition, both the mean northwest and southeast wind in Sapporo belong to gentle breeze according to the Beauport scale [2]. Considering the orientation of the bridge, the wind direction is not the reason for the corrosion difference between the south and north sides of the bridge bracket. One interesting finding is that the wind blows

from the northwest direction from December to April, and from the southeast direction from May to September. More information is necessary to determine the reasons for the differences in corrosion.

<div align="center">(a)   (b)</div>
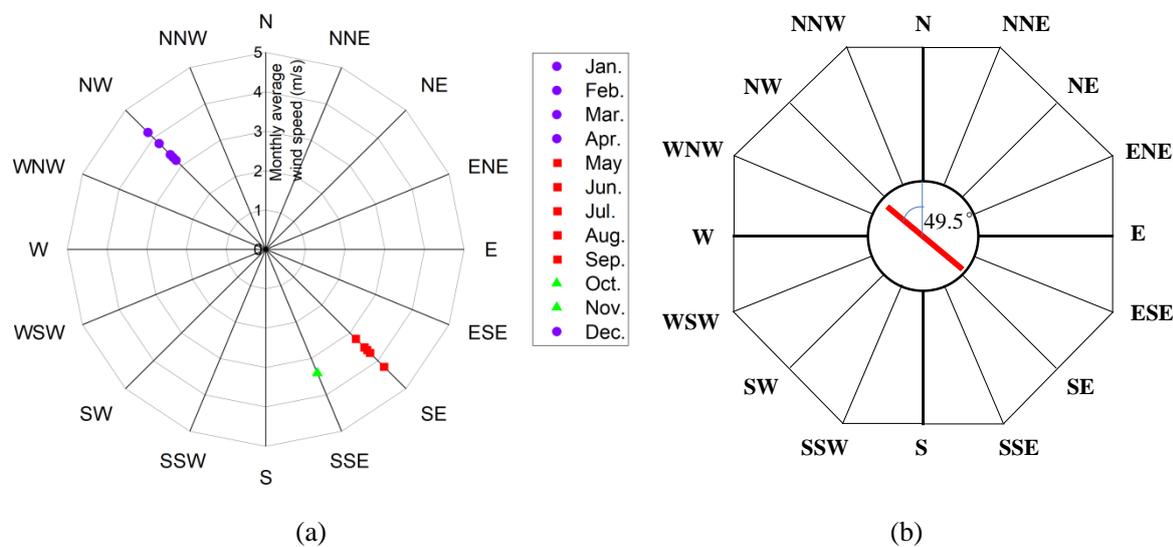
Figure 5.8 (a) Statistics of wind directions in Sapporo; (b) the orientation of the bridge 1708

Table 5.4 Details on partial cracks for bridge 1708

Component	No	Image	Crack width(mm)	Crack length(m)
Abutment (A)	1		2.0	0.30
	2		2.9	0.20
	3		2.4	0.20
Abutment (B)	.	Not found	.	.

Component	No	Image	Crack width(mm)	Crack length(m)
Pier (1)				
	1	①	0.6	5.0
	2	②	0.6	5.7
	3	③	0.6	6.0
	4	④	0.5	5.0
	5	⑤	0.5	6.0
Pier (2)				
	1	①	0.3	3.5
	2	②	0.7	5.2
	3	③	1.2	3.5
	4	④	0.5	2.0

(4) Bridge 853 & 854

Table 5.5 Crack details for bridge 853 & 854

Component	No	Image	Crack width(mm)	Crack length(m)
Abutment (A)	1		2.5	0.30
	2		2.5	0.20

Component	No	Image	Crack width(mm)	Crack length(m)
	3		2.5	0.30
Abutment (B)	1		4.0	0.30
	2		2.0	0.30
	3		2.0	0.30
Pier (1)	1		0.2	2.0
	2		0.2	4.0

Component	No	Image	Crack width(mm)	Crack length(m)
	3		0.2	3.0
Pier (2)	1		0.15	1.8
	2		0.15	1.5
	3		0.15	2.0
Pier (3)	1		0.10	0.2
	2		0.10	0.5

Component	No	Image	Crack width(mm)	Crack length(m)
	3		0.1	0.3
Pier (4)				
	1	①	0.15	0.9
	2	②	0.15	1.8
	3	③	0.15	1.3
	4	④	0.15	0.4
	5	⑤	0.15	0.4
	6	⑥	0.15	0.5

Table 5.5 summaries some cracks collected from the abutments and piers of bridges 853& 854. These two bridges are the important part of Japan national road 12 with different driving directions. Since these two bridges have been in service less than 10 years, no serious deterioration occurred. Compared with bridge 1708, the cracks on the abutments of bridges 853 and 854 are more serious, with a maximum width of 4.0 mm and a length of 0.3 m. These cracks considered not significant affect the bridge's safety, considering the locations of these cracks (Figure 5.15 ① and ⑥). In addition, the cracks on these two bridges' Piers have a width less than 0.15 mm and a maximum length of 1.8 m, i.e., not more serious than bridge 1708 (with minimum 0.3 mm crack width and maximum 6.0 crack length). However, the propagation of cracks on piers should be paid more attention. The heavy traffic volume is considered the reason to make the cracks, and the bridge was evaluated being grade 2.

Different from Bridge 1708 whose north side steel brackets were corrode seriously, almost no corrosion were found for the steel components of the bridge 853 & 854. One major reason is that bridge 853 & 854 has only been in service less than 10 years, while bridge 1708 was more than 50 years old.

5.3 Establishment of 3-D prototype model

Using the collected information from onsite inspection and the information recorded in Bridge Yearbook Database [3], we established the 3-D prototype models for the five targeted bridges using the SketchUp, as shown in Figures 5.9 to 5.12. The established models are 1:1 with the real existing bridges. In each figure from Figures 5.9 to 5.12, views of corresponding bridge from different perspective were shown. In addition, some parts of the models were enlarged to offer more details. Cracks from the onsite inspection can be located to the exact position of the components to intuitively visualize the distribution of these cracks in 3-D. Details were shown in Section 5.4.1.
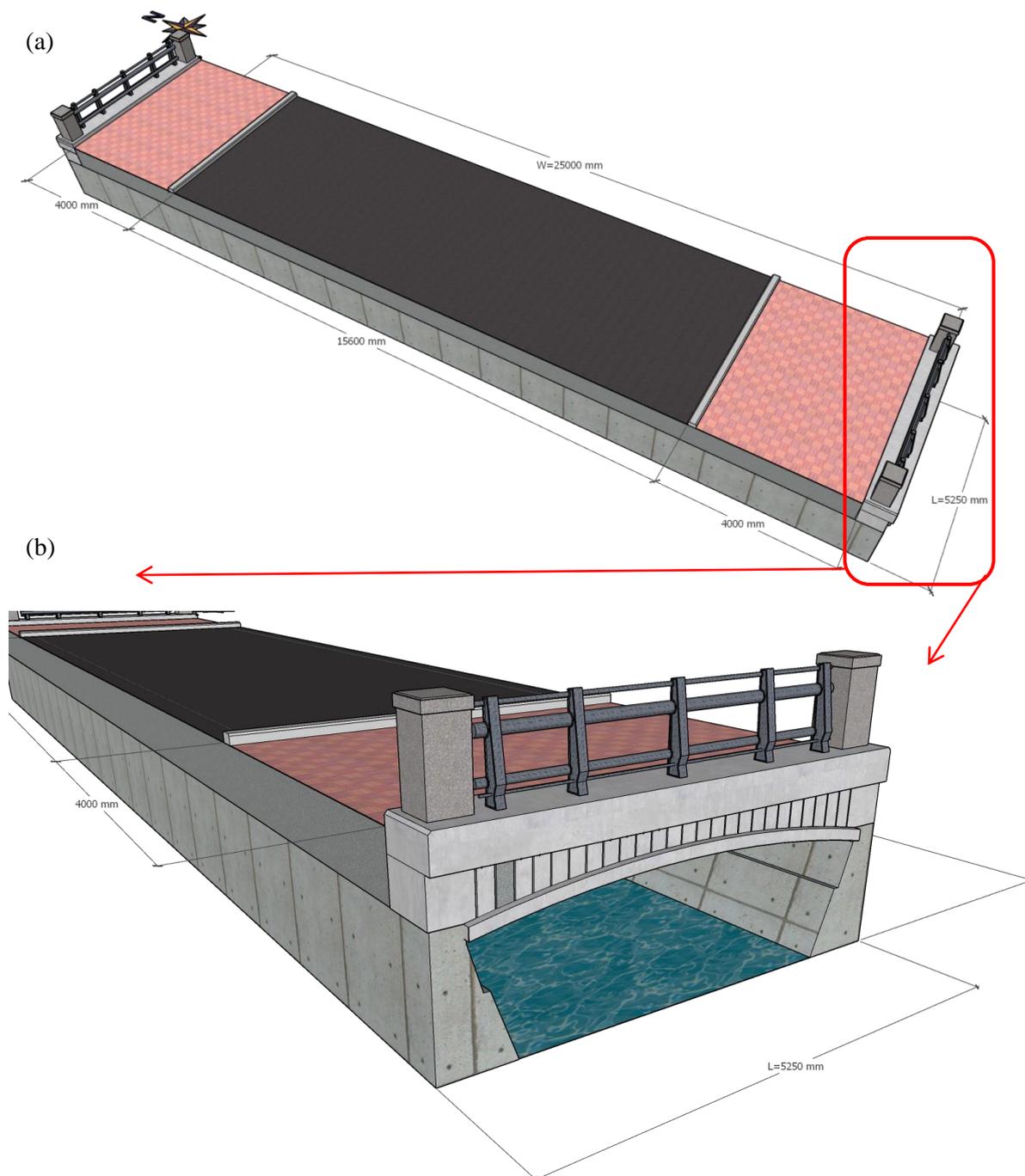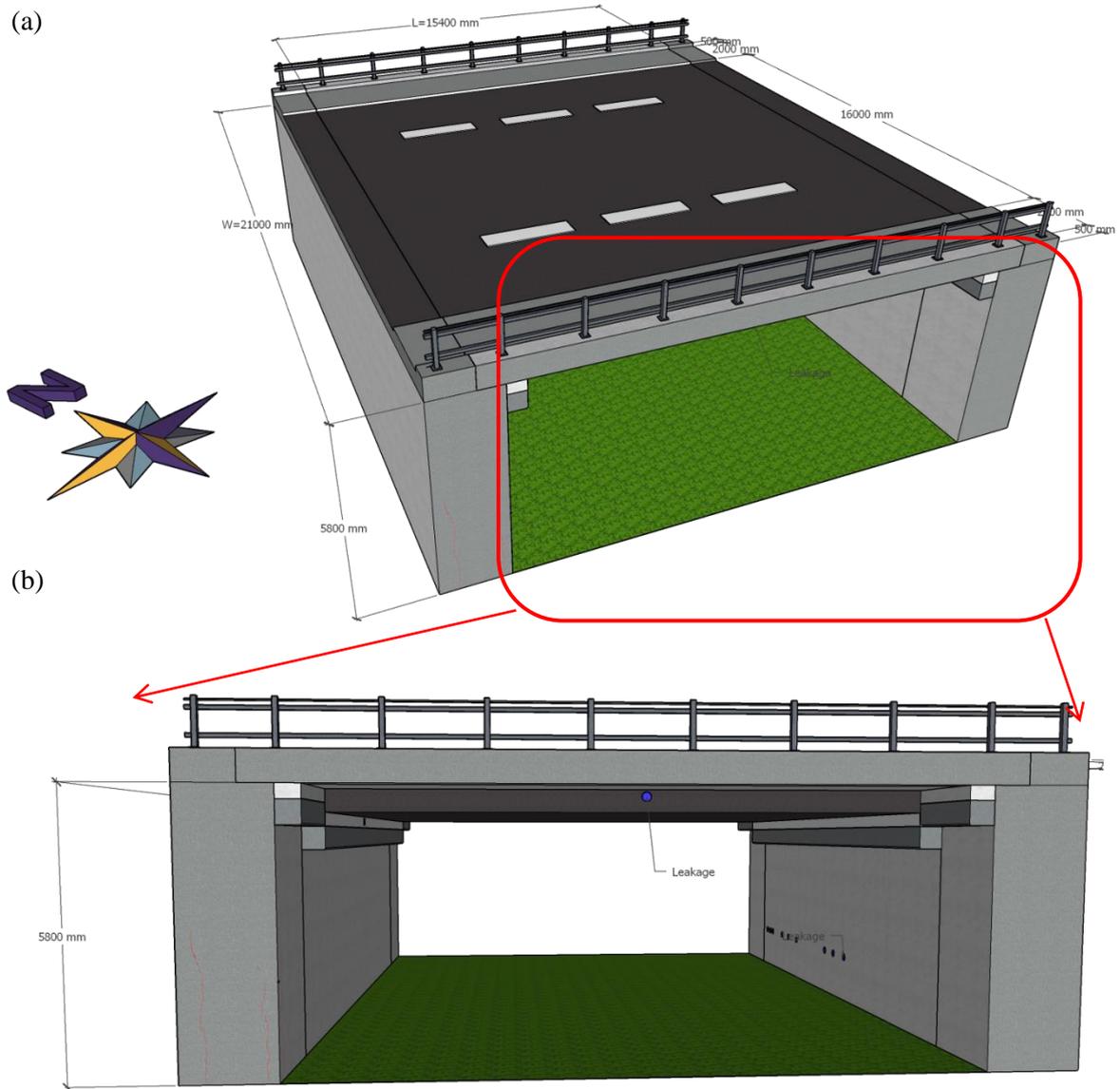
Figure 5.9 Established 3-D model for bridge 1703

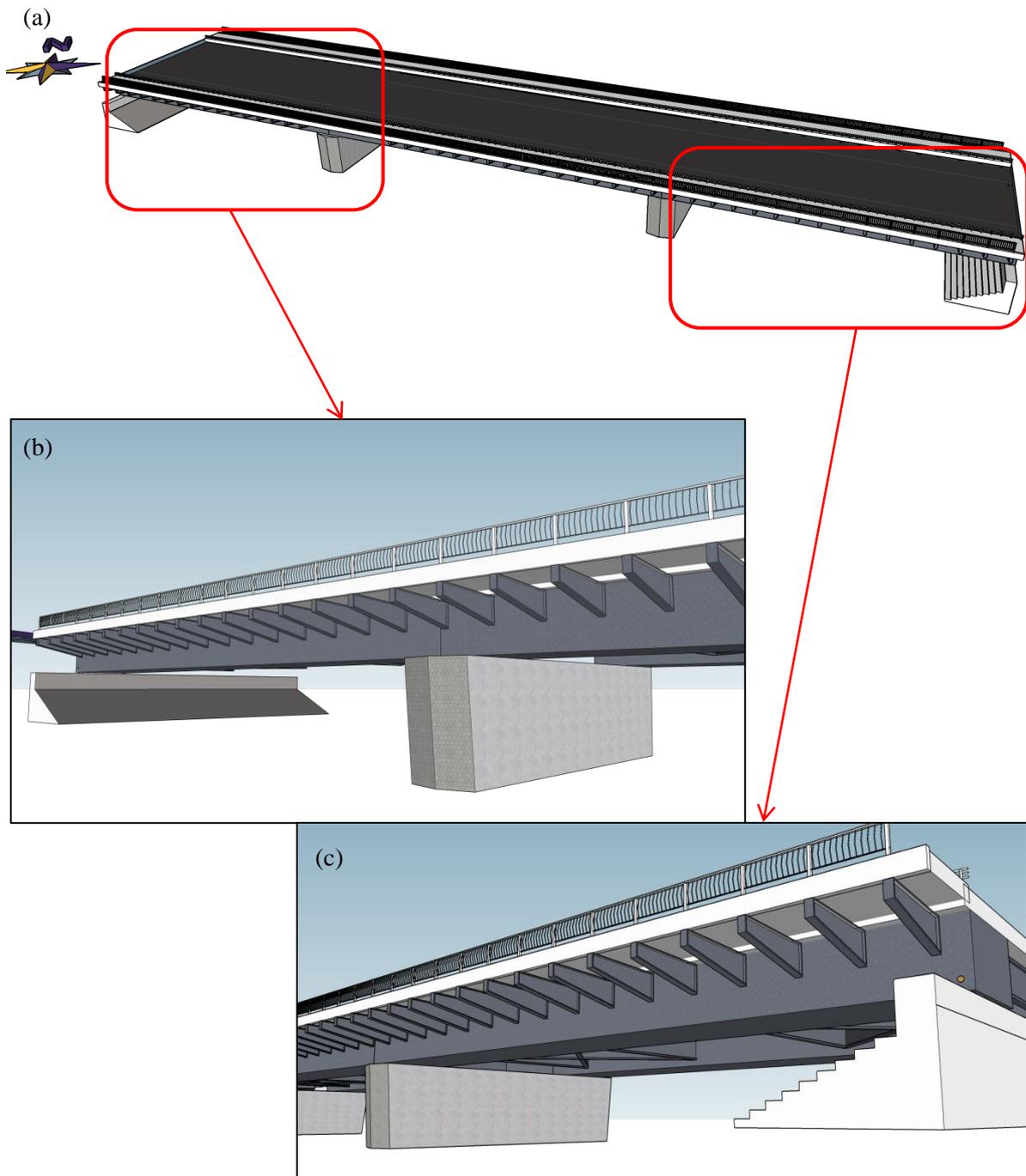Figure 5.10 Established 3-D model for bridge 1704
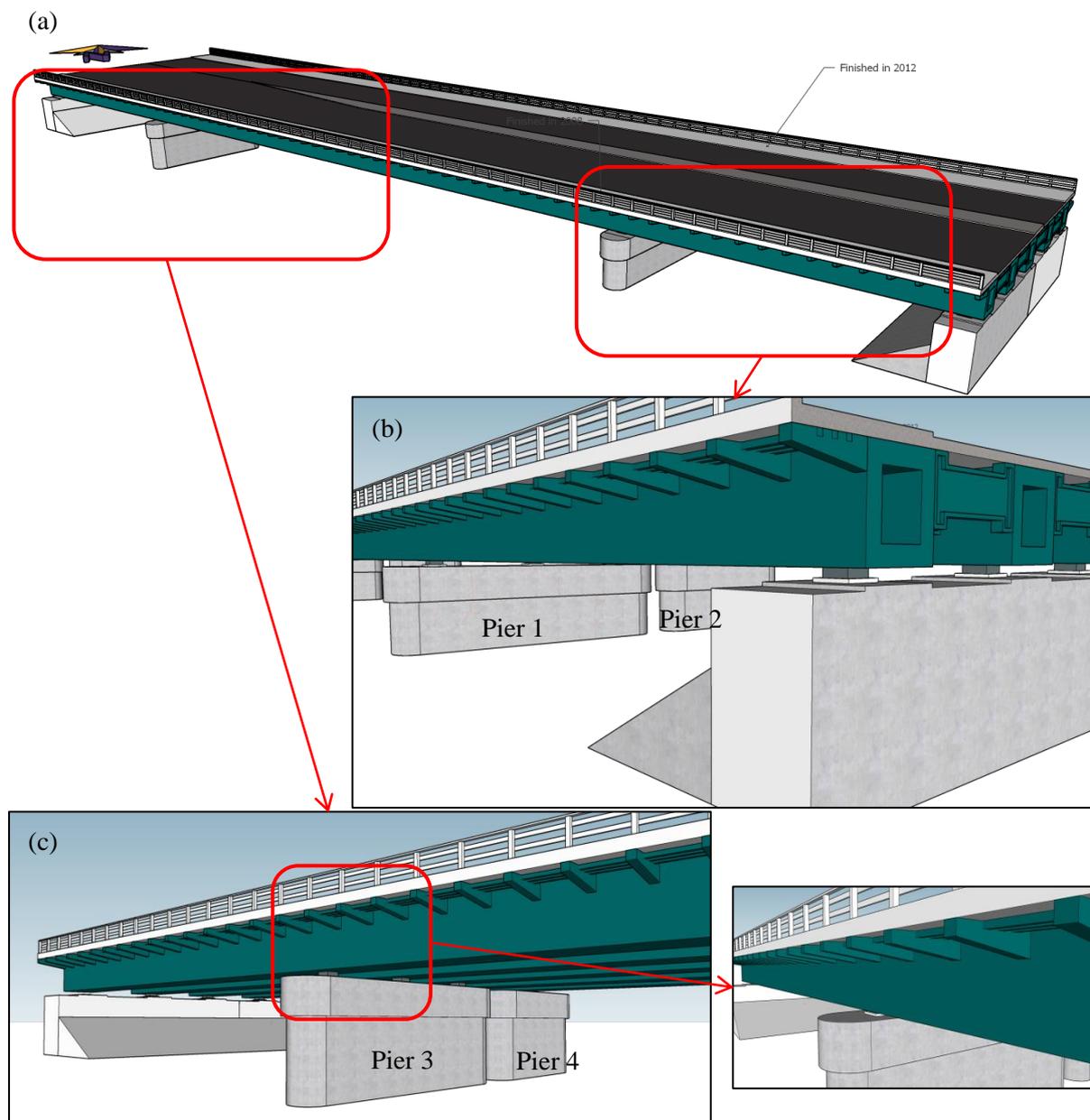
Figure 5.11 Established 3-D model for bridge 1708

(a)

Finished in 2012

(b)

Pier 1   Pier 2

(c)

Pier 3   Pier 4

Figure 5.12 Established 3-D model for bridge 853 &854

5.4 Collaborated BIM platform
5.4.1 Integration of cracks to the 3-D models

In previous sections, the crack information was collected and the 3-D prototype models for five bridges were established. In addition, the crack images were collected from onsite inspection. The positions of these cracks will be detailed combined with the established 3-D models. Although the collected images contain cracks, it is unreasonable to just paste the image on the surface of the 3-D models; because quantitative crack information cannot be obtained directly from these images. One possible method is to extract crack pixels and stick them onto the surface of the model. The developed crack identification model can help to achieve this purpose efficiently (Chapter 4). Specifically, the crack pixels were first extracted by the crack identification model. Then, these cracks were adjusted to the same size as they actually are, based on the values measured by the crack scale. Next, these cracks were save as image format of *.png,

because this format has a transparent background. Finally, these *.png images were located to the corresponding components. Figures 5.13 to 5.16 are refer to the five targeted bridges. The model clearly shows the crack information, which engineers can use to determine if the crack will affect the soundness of the bridges. Except for the crack information such as crack width and crack length, the 3-D model can be used to determine the density of cracks. Cracks situation of each model will be detailed below.

Figure 5.13 Crack details for bridge 1703

Figure 5.13 shows the locations of cracks summarized in Table 5.2. For bridge 1703, the cracks are located in the parapet wall of the bridges, and no obvious cracks in the structural components were investigated. The average crack length is 0.535 m, and average crack width 1.13 mm. As a result, these cracks are not crucial to the bridge's soundness. If cracks are collected in chronological order, the evolution of the cracks propagation can be observed.

Figure 5.14 shows the locations of cracks summarized in Table 5.3. For bridge 1704, the cracks are located in the parapets of the bridges (④ and ⑤), and abutment walls (①, ②, and ③). Cracks in the parapets contribut little to damage the bridge. However, the cracks propagate to a length that almost same with the

height of the abutment. For the cracks on abutment walls, the average crack length is 3.33 m, and average crack width 0.38 mm. In addition, the positions of water leakage were marked with blue dot.
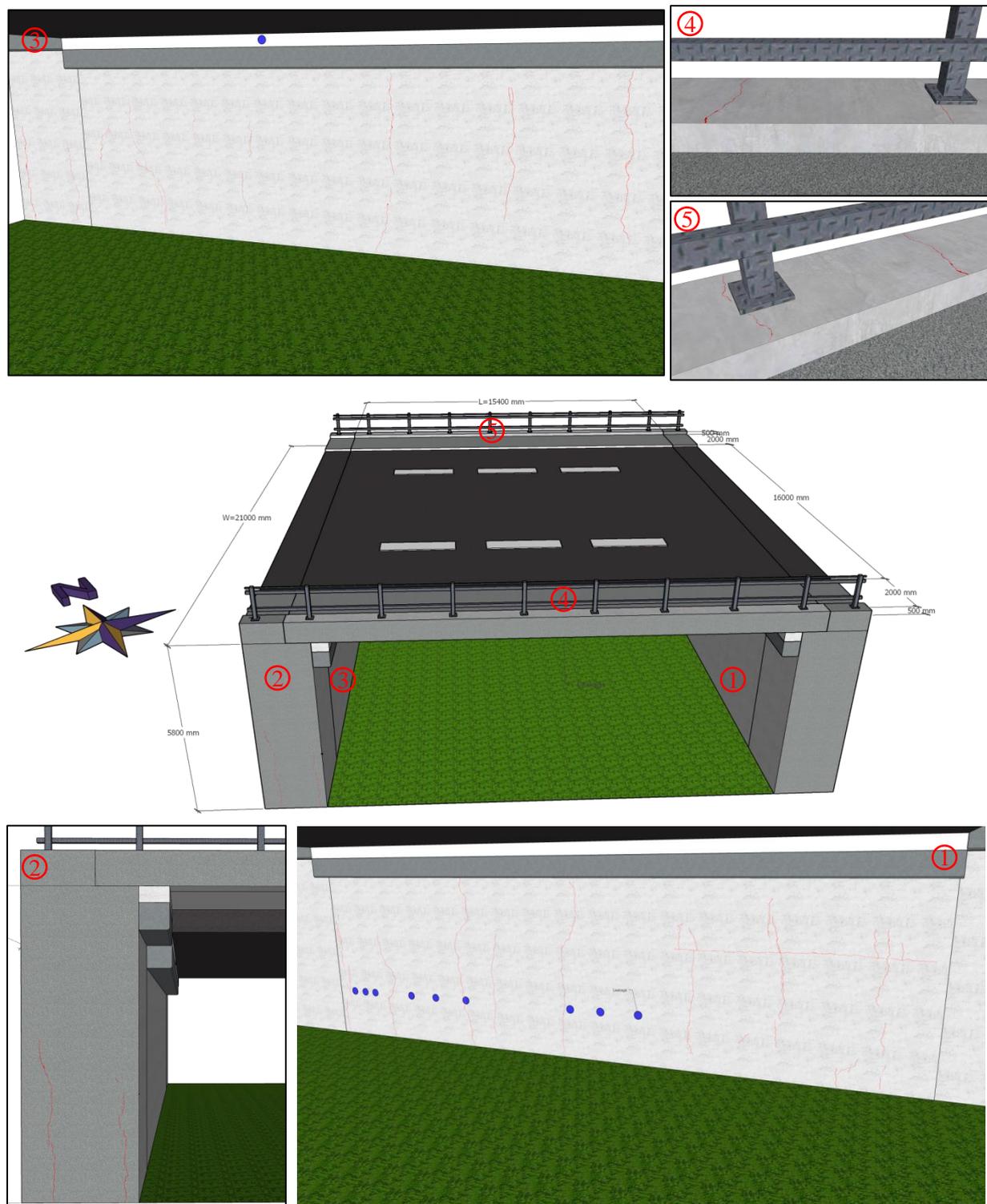
Figure 5.14 Crack details for bridge 1704.

The locations of cracks summarized in Table 5.4 is shown in Figure 5.15. For bridge 1708, the cracks are located in the abutments of the bridges (③), and piers (① and ②). Cracks on the abutments are not critical to affect the soundness of this bridge. Cautions should be given to the cracks on piers. These cracks

have an average crack length of 4.66 m, and average crack width of 0.61 mm. In addition, the positions of corrosions were marked with yellow dot (④).
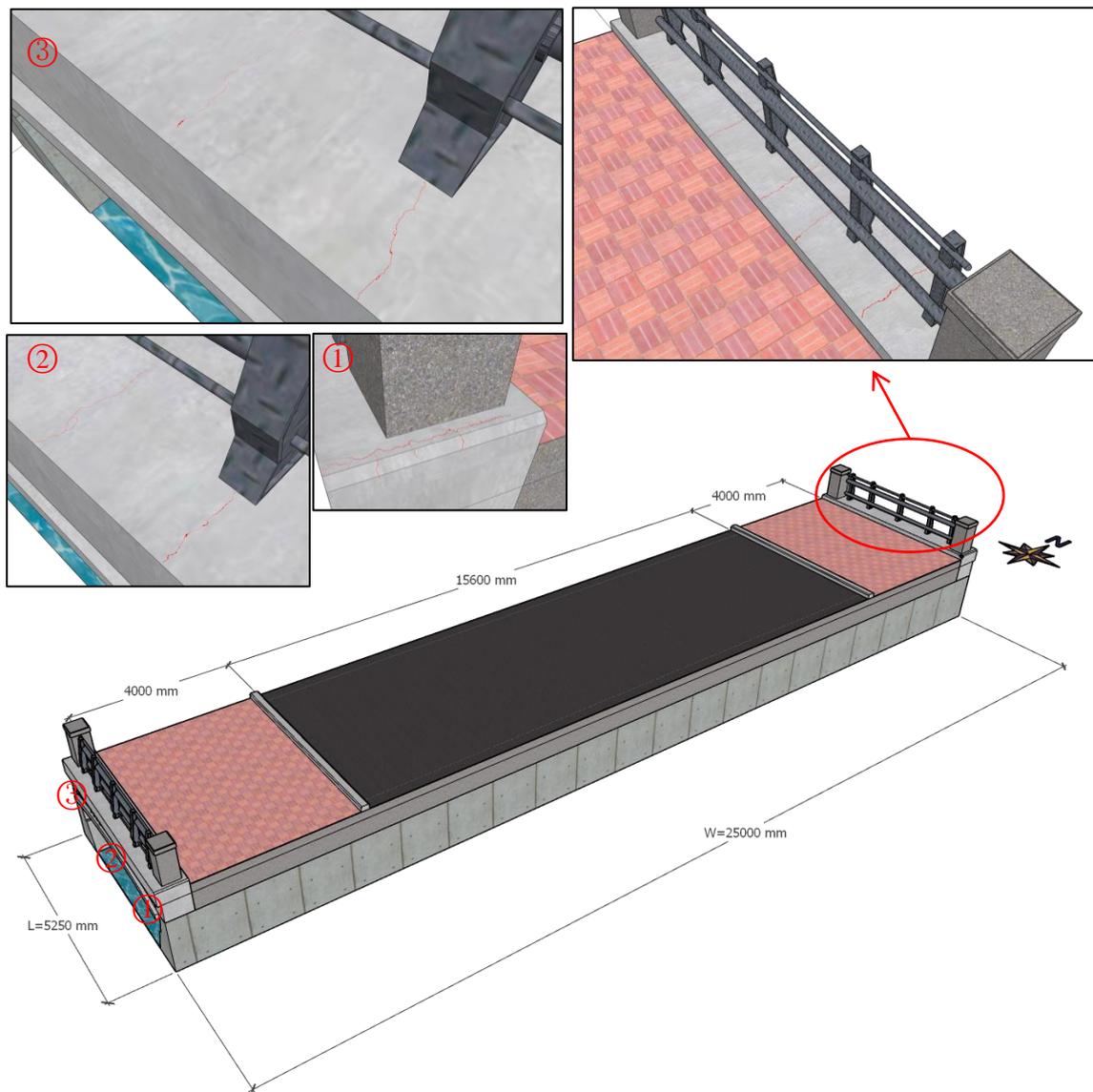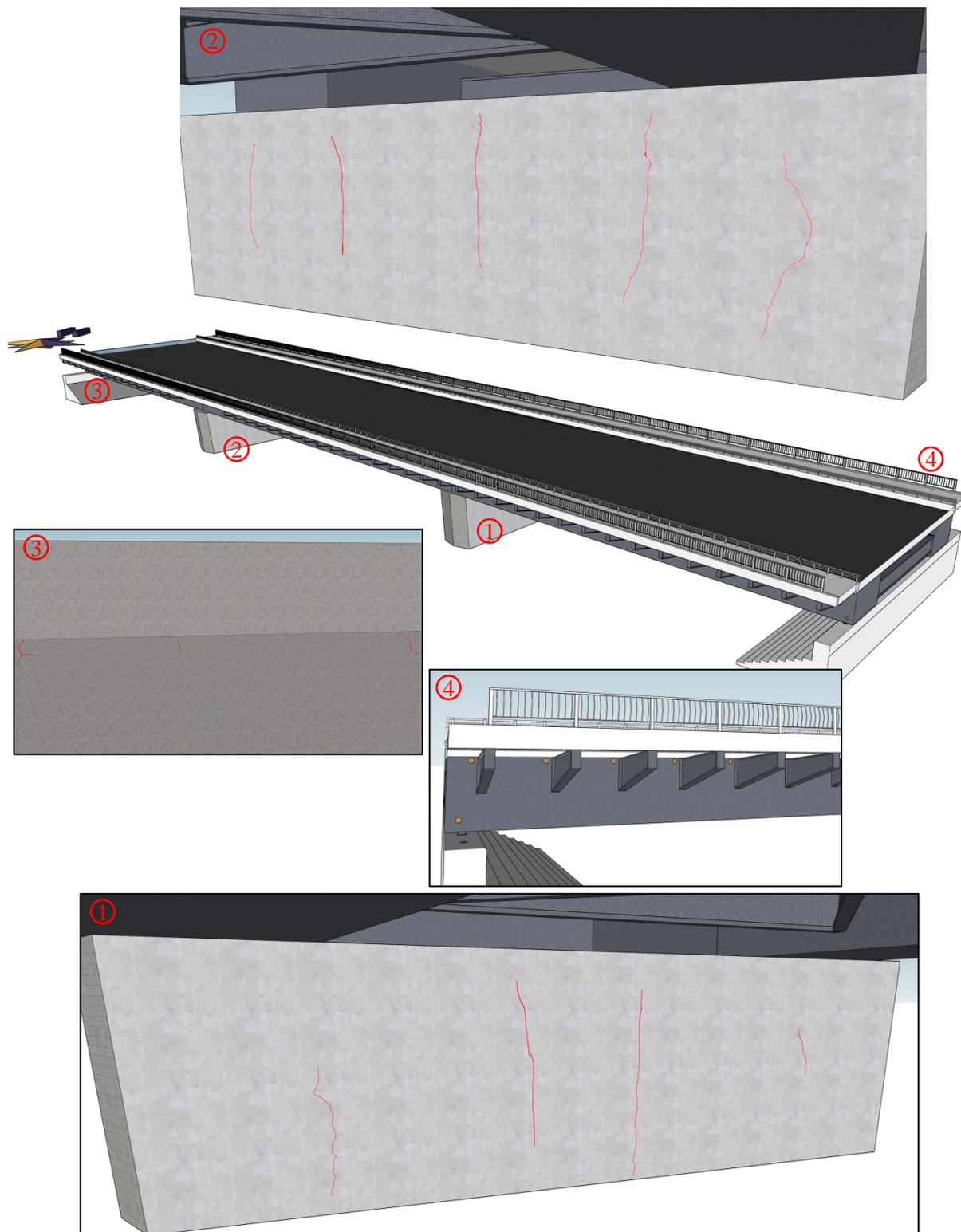

Figure 5.15 Crack details for bridge 1708.

Figure 5.16 shows the locations of cracks summarized in Table 5.5. For bridge 853 & 854, the cracks are located in the abutments of the bridges (① and ⑥), and piers (②, ③, ④ and ⑤). The cracks on

abutment have an average length of 1.28 m and an average width of 2.58 mm. For the cracks on abutment walls, the average crack length is 1.37 m, and average crack width 0.15 mm. Different from bridge 1708, the steel brackets for this bridge are not corroded.
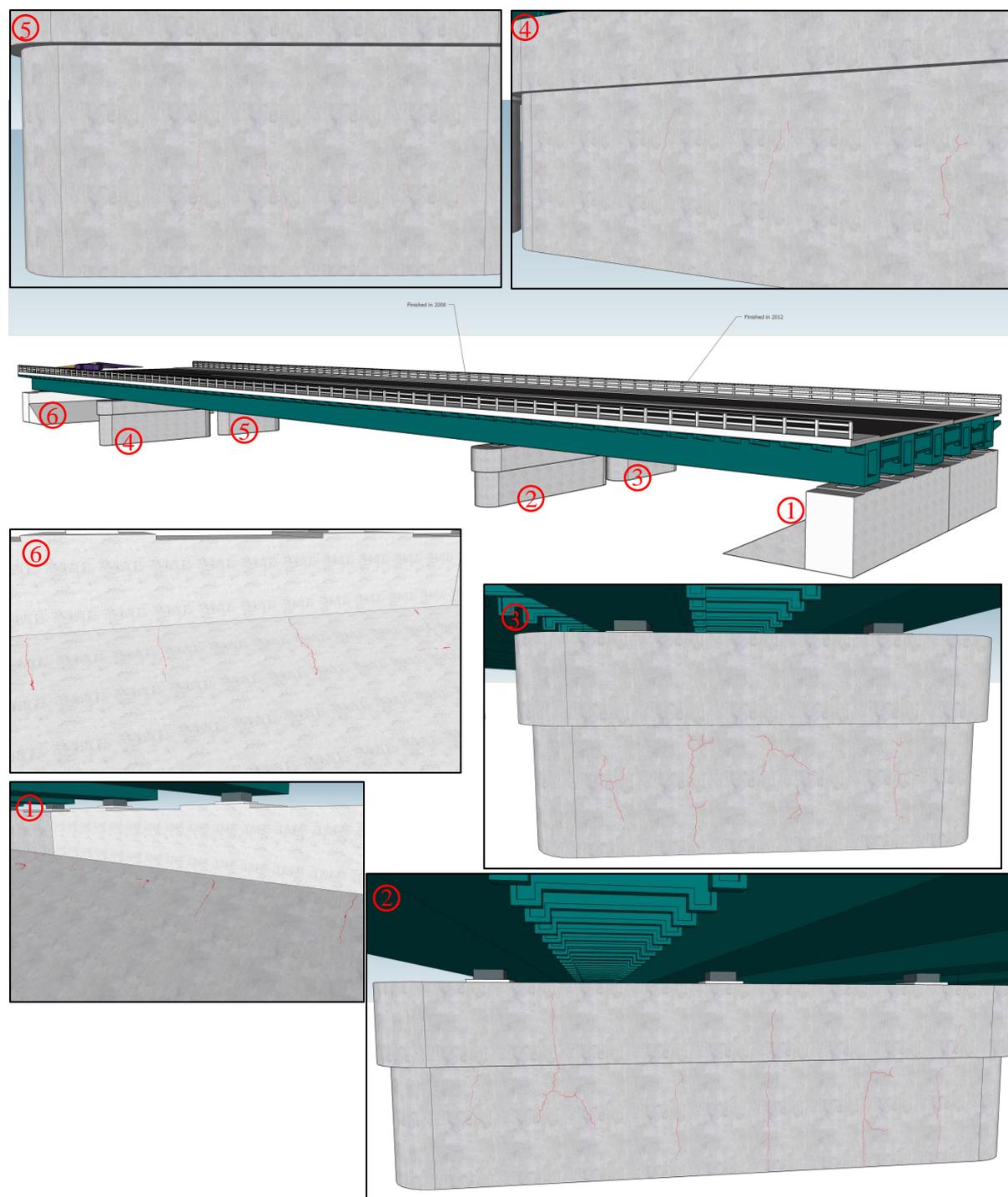
Figure 5.16 Crack details for bridge 853 & 854

5.4.2 Deterioration estimation of targeted bridges

Using the deterioration models of LSTM-based RNN and MC established in Chapter 3, the deterioration progresses of these five bridges were estimated, as shown in Figure 5.17. In addition, the assessed

deterioration grades by the engineers were displayed as blue-dot in the graphs.

(a)

(b)

(c)

(d)

(e)
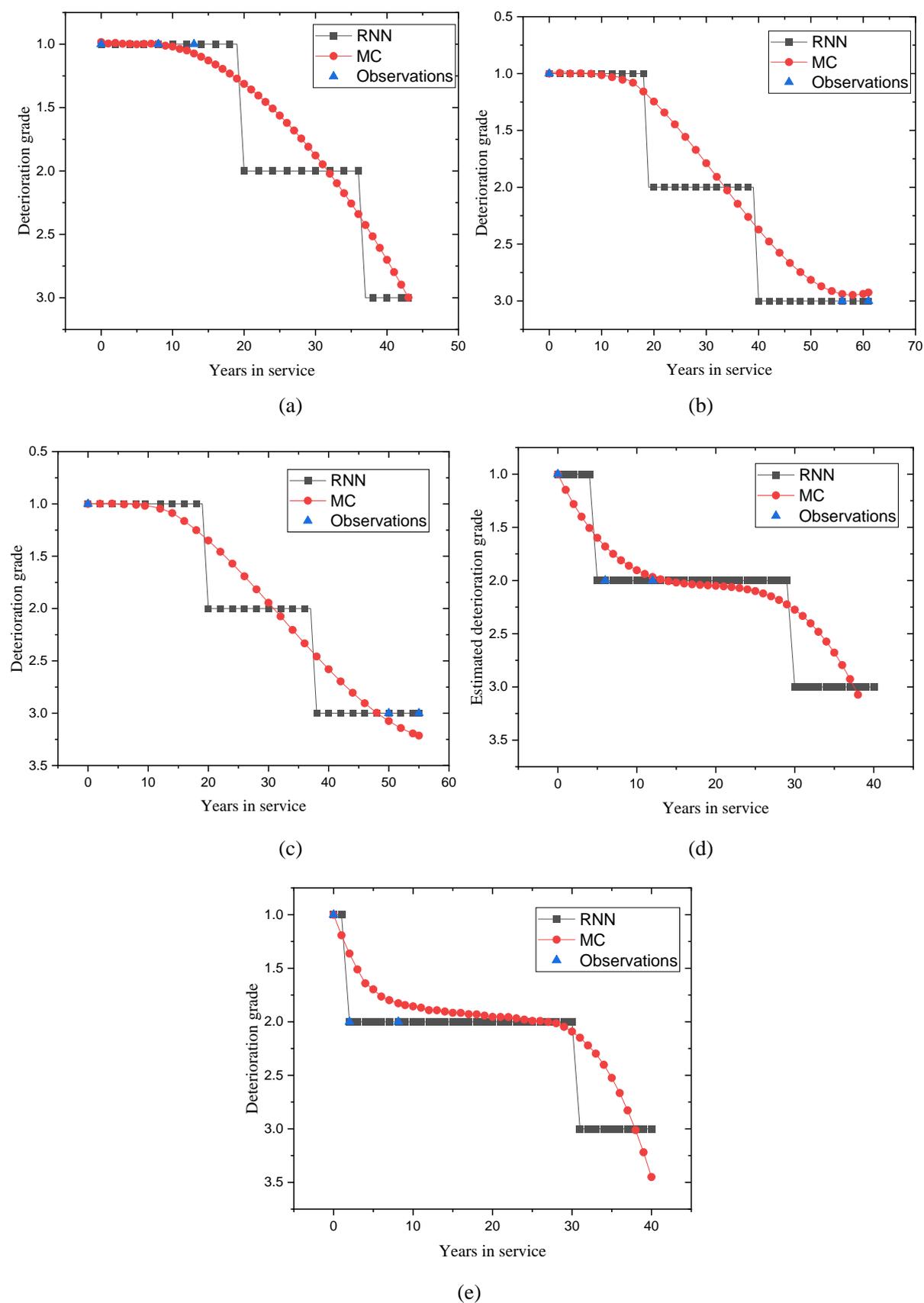
Figure 5.17 Estimated deterioration progress for bridges (a) 1703, (b) 1704, (c) 1708, (d) 853, and (e) 854
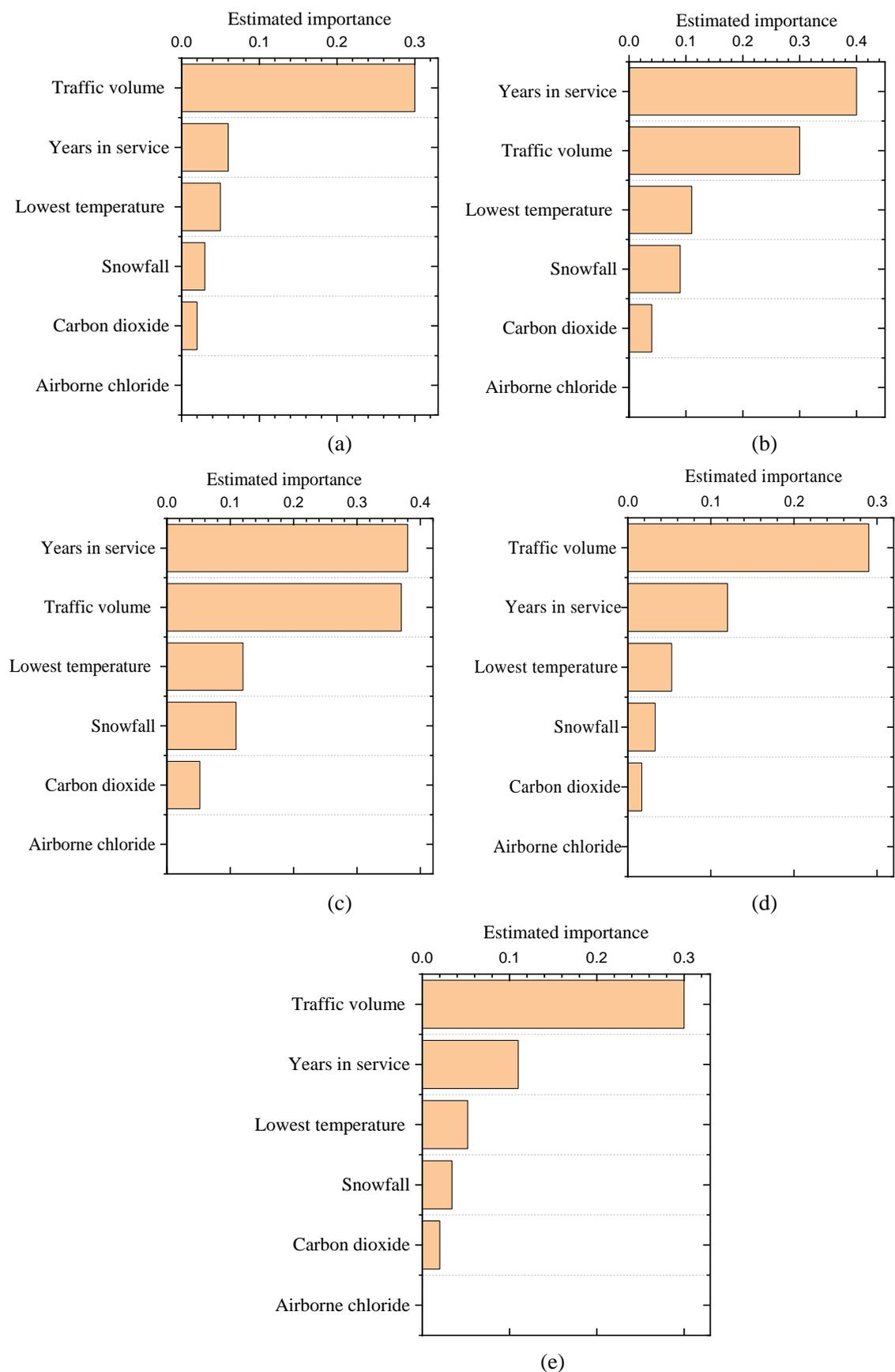
Figure 5.18 Estimation of factor's importance for bridges (a) 1703, (b) 1704, (c) 1708, (d) 853, and (e) 854

Since bridge 1703, and bridge 853 & 854 were evaluated being grade 1 and grade 2, respectively, the deterioration progress can be applied to predict the deterioration situations of these three bridges. Differently, bridge 1704 and bridge 1708 have been deteriorated to grade 3; therefore, their deterioration progresses can be applied to verify the observations in a much wider scale.

For bridge 1703, the LSTM corresponds well to the observations. In addition, the LSTM and the MC model estimated that the bridge takes 37 years and 43 years to deteriorate to grade 3. Similarly, the RNN corresponds well to the assessed grades for the bridge 853 & 854. The LSTM estimated bridge 853 will deteriorate to grade 3 at 30 years, and the MC estimate the bridge will deteriorate to grade 3 at 38 years. For bridge 854, the LSTM estimated the bridge will deteriorate to grade 3 at 31 years, and the MC estimated the bridge will deteriorates to grade 3 at 37 years.

For bridge 1704, the LSTM is in good agreement with the observed values. The LSTM and the MC model estimated the bridge deteriorated to grade 3 at 40 years (in 2000) and 60 years (in 2021), respectively. Obviously, the results obtained by the MC deviated from the actual situation. For bridge 1708, the LSTM corresponds well to the observed values. The LSTM estimated the bridge deteriorated to grade 3 at 38 years (in 2004), and the MC estimated the bridge deteriorated to grade 3 at 48 years (in 2014). Since no more observations were obtained, the optimal model between these two models cannot be determined.

5.4.3 Estimation of factor importance for the targeted bridges

Using the sensitivity analysis (Shapley value) method mentioned in Chapter 3, the importance of each factor was also estimated, as shown in Figure 5.18. The results indicate that traffic volume and years in service (bridge age) are the two most important factors; other four factors have relatively smaller influence to the deterioration. Since bridge 1703 and bridge 853 & 854 are less than 10 years old, the traffic volume is considered the most important factors. Conversely, bridge 1704 and bridge 1708 have been in service for more than 50 years, years in service and traffic volume are considered the two most important factors. Essentially, the natural degradation of the materials and the fatigue caused by the heavy traffic are considered to be the major reasons for the deterioration. The estimated deterioration progresses, estimated importance of factors, the extracted crack pixels, and the 3-D model of these bridges were integrated to form a collaborated BIM platform, based on which the corresponding maintenance strategies can be formulated, as described in Section 5.5.

5.5 Formulation of the maintenance strategies and discussions

5.5.1 Formulation of the maintenance strategies

According to the estimated deterioration progress, factors' importance and bridges' current situations, different maintenance strategies can be conducted, as illustrated in Figure 5.18. If preventive maintenance strategies are planned for bridges, these bridges should be repaired before or when they deteriorate to the grade 3 (Early action required). Conversely, bridges are need to be repaired when they are deteriorate to grade 4 (Emergency action required) if corrective maintenance are planned to these bridges.

Bridge 1703 was evaluated being grade 1 in the latest inspection. No obvious cracks were found for the structural components of this bridge. According to the estimated deterioration progress, this bridge will deteriorate to grade 3 at 42 years. In addition, the traffic volume was estimated to be the major factors threaten the deterioration of this bridge. Furthermore, this bridge has a length 5.25 m and a width 25 m. Therefore, preventive maintenance is suggested to keep the soundness of this bridge. In addition, routine

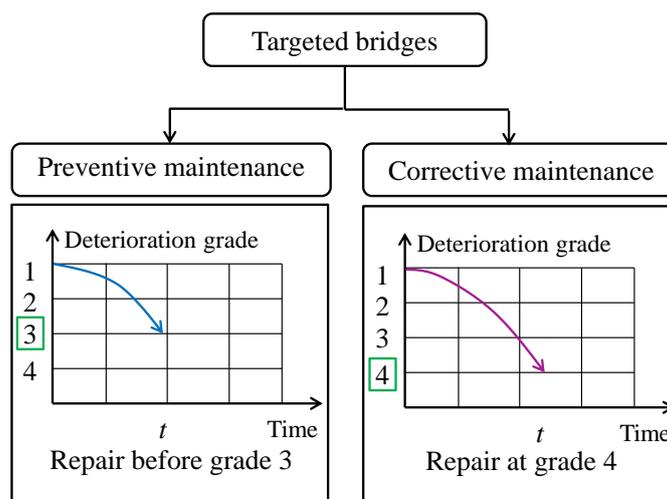cautions should be given to the fatigue of the RC deck of this bridge.

Figure 5.19 Formulation of maintenance strategies.

Similarly, bridges 853 and 854 have been in serviced for less than 10 years. They were assessed being grade 2 in in a recent inspection because of numerous cracks in their four piers and abutments (Figure 5.13). Both these two bridges will deteriorate to grade 3 in about 30 years of service, according to the estimated deterioration progresses (Figure 5.14). In addition, traffic volume was determined to be the most important factor affecting the deterioration. These two bridges are more than 100 meters long and they are key parts of the national highway 12. Therefore, preventive interventions should be conducted when these two bridges deteriorate to grade 3. In addition, the propagation of these cracks should be cautioned, especially after the bridge deteriorated to grade 3.

Different from previous three bridges, bridges 1704 and 1708 have been in service for more than 50 years, and have been in grade 3 for many years. Bridge 1704 is serviced more close to 60 years till now, cracks propagate to a length that almost same with the height of the abutments (Figure 5.11). In addition, leakages were discovered along the abutment walls. The natural deterioration of materials and the traffic volume are considered the two most important factors to cause the deterioration. Early interventions are suggested to be conducted to this bridge as soon as possible. One good thing is the recent plans to repair the girder [4]. Bridge 1708 has been in service for 54 years till now, and also evaluated being grade 3 for many years. In addition, this bridge has a mean daily traffic volume of more than 55,000. Conforming to the practical situation, the traffic volume and years in service are estimated to the most important factors. In addition, the steel brackets were corroded seriously (Figure 5.7). The steel brackets are necessary to be repainted as soon as possible. Therefore, early interventions are also suggested to be carried out. Fortunately, the girder of this bridge will be inspected and repaired at 2021 [4]. It is believed these two bridges will be maintained properly.

In summary, the collaborative BIM platform can visualize inspection information including cracks in 3-D. In addition, the platform can provide the deterioration progresses and estimate the importance of factors affecting the bridge deterioration. Practically, this platform allows the managers to understand the severity of crack in each component of a bridge. If the crack information on a component is collected in chronological order, the evolution of the crack propagation can be observed. Further, the deterioration progresses enable the managers to formulate preventive maintenance or corrective maintenance schedules. The estimated importance provides the managers with clear reasons for the deterioration, and will facilitate

the formulation of corresponding maintenance strategies.

5.5.2 Discussions

The practical situation is complicated than imaginations, making difficult to obtain all information of each component including the size and materials according to onsite inspections. This difficulty makes the established 3-D models are not exactly the same with the design. In addition, some components were repaired or replaced during the service, this information cannot be directivity reflected in our model. One method is to cooperate with bridge design institutes and management departments to obtain as detailed as possible information regarding the design and maintenance of all components. This information can then be connected to the 3-D model to establish a database-based 3-D model.

We provided deterioration situations for the whole bridge, but the deterioration varies from component to component. Therefore, the deterioration progress may deviate from reality for some components. Future work will endeavor to collect enough data for crucial component to establish deterioration models. In addition, some algorithms will also be improved to consider the variance of each component.

Only cracks on the surface of the concrete components were marked, and other damages such as corrosion were not marked on the components because they were difficult to quantify. In addition, it is inefficient to update the information of these cracks when new information is collected [5]. A feasible method is to store the various damage images collected from the onsite inspection in a database, and then link the database to the bridges.

Only the crack width and crack length are obtained using the crack identification model; crack depth cannot be obtained from the collected image, because the collected images only contains 2-D information. The crack depth is necessary to evaluate the severity of the cracks and the influence of these cracks on the soundness of each component. To obtain such information, the 3-D laser can be used to onsite inspections. Then, it is possible to build an automated evaluation system to relate the crack information to the severity of cracks.

One inadequate is that the cost analysis and environmental impact analysis were not conducted in the collaborated BIM platform. Another limitation is that the onsite images are needed to be calibrated to obtain the detail information from the images such as the crack width and crack length. Algorithms will be developed and verified in the future to solve this issue. Since some locations are inaccessible for unauthorized persons, the damage situations were not collected and evacuated.

In summary, future works will be implemented to collect more information by cooperating with the design institutes and the authorities, by using more information collection equipment, and by improving some algorithms. The collaborative BIM platform can also be shared across multiple fields, not only infrastructure maintenance. To achieve this purpose, the collaborated BIM platform could include more information, such as the locations of the sensors from other teams. In addition, the scope of the platform can be expanded by further taking in map and 3-D spatial information. Furthermore, the data sharing infrastructure can be obtained by making full use of "big data" processing technologies such as cloud computing, distributed computing, and parallel processing.

There are also some limitations for the deterioration prediction models and the crack identification models. Discussions on the limitations of these models can be found in Chapter 3 and Chapter 4, respectively.

References

[1] JMA, http://www.data.jma.go.jp/obd/stats/etrn/view/nml_sfc_ym.php?prec_no=14&block_no=47412. Accessed:10 May, 2021.

[2] Beaufort scale in Japan. https://www.i-kahaku.jp/friend/kagaku/0306/kaze/index.html. Accessed:13 June, 2021.

[3] Japan bridge association Inc. Bridge Yearbook Database. https://www.jasbc.or.jp/kyoryodb/index.cgi.

[4] Profile of Hokkaido Development, MLIT. (2021). Repair plan for improving service life of bridges. https://www.hkd.mlit.go.jp/ky/kn/dou_iji/ud49g700000091rs.att/ud49g700000092nk.pdf.

[5] Volk, R., Stengel, J., & Schultmann, F. (2014). Building Information Modeling (BIM) for existing buildings . Literature review and future needs. Automation in Construction, 38, 109–127. https://doi.org/10.1016/j.autcon.2013.10.023.

Chapter 6

Discussions

6.1 Overview

We discussed each part in the previous chapters. This chapter gave general summaries of the study's accomplishments and shortcomings. Figure 6.1 shows the outline of this chapter. Details will be elaborated on: (1) how the work contributes to perform prediction-based maintenance of existing bridges, and (2) the shortcomings of the applied database, algorithms, and models.
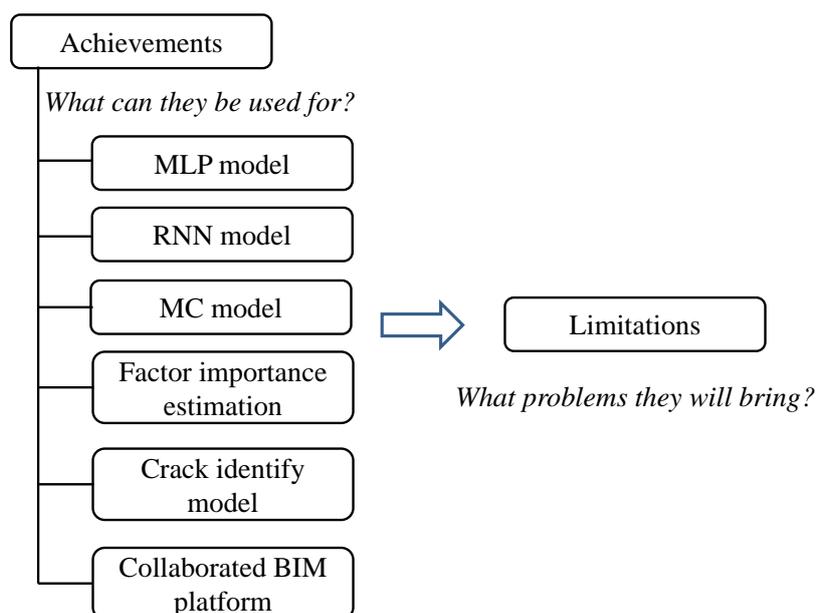

Figure 6.1 Overview of Chapter 6

6.2 Achievements

Using the inspection database including twelve potentially influencing factors and three deterioration grades, the Multilayer Perceptron (MLP), the Recurrent Neural Network (RNN), and the Markov Chain (MC) models were established. The MLP and RNN were first compared. The results indicate that the RNN outperforms MLP model in terms of accuracy, recall, precision, TNR, and F1 score, because the time dependences of time related factors were considered. Definitions regarding these indexes can refer to Section 2.8. Then, the RNN and the MC models were applied to the estimate the deterioration progresses. The deterioration progresses can be used to determine the remaining life, and can analyze the effects of external factors affecting the deterioration. These models will facilitate the managers to confirm the timing of interventions.

The estimation of the factors' importance enables the engineer to understand the reasons for deterioration. Therefore, the estimated importance list of these factors could assist the engineer in developing appropriate intervention strategies.

Using the images collected from the onsite and experiment, a crack identification model was proposed to detect, segment, and analyze cracks from the raw images. The model makes it easier to process inspection

pictures. In addition, the information obtained by the model can be used to understand the preliminary situation of a bridge, and can provide the basis for further detailed investigations if any abnormalities exist.

The 3-D models for five bridges were preliminary established using the onsite collected information and documentation-based information. Then, crack identification model extracted the crack pixels and located the crack pixels on the surface of the specific components. Additionally, the 3-D prototype model, crack identification model and the deterioration prediction were combined to form a collaborated BIM platform. This collaborated BIM platform makes the managers to visualize the damages including cracks in 3-D, to understand the deterioration over time, and to clarify the causes for the deterioration.

The initial achievements in this study provided a foundation for further investigation into the deterioration prediction of other infrastructures to facilitate prediction-based maintenance. Then, we can integrate all these deterioration prediction models into the infrastructure management system (IMS) to enable managers or local authorities to better manage the infrastructure manage and formulate prediction-based intervention strategies for infrastructure.

6.3 Limitations

The applied inspection database includes twelve potentially influencing factors. However, the materials were not considered when predicting deterioration. For this reason, there are discrepancies between the study's analysis results and the practical. Additionally, several other factors are associated with deterioration but were not directly considered, such as the application of deicing salt, design strength, and intervention histories. Since the values of these factors are not fully captured in the inspection databases, the impacts of these factors were not considered.

The variations in deterioration of various components of the same bridge were not taken into consideration. Even if the performance of the established LSTM model shows no noticeable differences for different types of bridges, a deterioration prediction model for each type of bridge is still required for better practical performance. In addition, the established LSTM and MC models can only predict the situation before grade 3; owing to bridges in grade 4 were not found in our database.

In assessing a factor's importance, the Shapley value method considers all possible influencing factors, but sometimes the calculated importance is unreasonable. Further, deviations exist in the calculated importance due to the deterioration grade is not a quantitative value.

Although the LSTM model produced better results than MLP, the LSTM architecture is much more complicated. A long-term maintenance database on various factors was required to train an LSTM model. In practice, this is a huge project because the values of some factors were only collected every five years according to the inspection guideline. Furthermore, the proposed model was evaluated using a database containing data from past inspections. However, a good prediction model should be generalizable. This implies that the model in this study should fit future observations well but cannot be verified at this time.

The established crack identification model is a semi-automatic solution, because manual participation is necessary to perform image calibration and parameter setting in the analysis of cracks. In addition, the model will fail to extract cracks for the images with complicated backgrounds, bad illumination, and hair thin cracks. Because the database does not cover all potential crack patterns, backdrop materials, textures, and colour appearances.

The actual situation is more intricate than imagined, making it impossible to gather full information on

each component, including size and materials, depending on onsite inspections. Because of these difficulties, the current 3-D models are not precisely the same as the design. In addition, buildings and structures differ in use and age. These different conditions are influencing the type, quality and amount of available information, as well as the application of BIM in maintenance.

In this study, only the concrete components were taken into account for estimating chloride ion penetration, carbonation, and crack damage. However, steel components are commonly used in actual engineering, limiting the applicability scope of this study's results.

Chapter 7

Conclusions and recommendations

7.1 Overview

This chapter describes the conclusions and recommendations. Figure 7.1 shows the outline of this chapter. Firstly, the conclusions regarding five aspects are listed by bullets: (1) comparisons of the Multilayer Perceptron (MLP) and Recurrent Neural Network (RNN) in predicting deterioration; (2) the estimation of factors' importance to understand the causes of deterioration; (3) the comparisons of the RNN and the Markov Chain (MC) by their deterioration progresses; (4) the performance of the crack identification model; and (5) the establishment of the collaborated BIM platform to manage the inspection information in 3-D and to formulate prediction-based maintenance timing and strategies. Then, efforts will be enforced to improve the studies according to the limitations discussed in Section 6.3. In addition, the potential research topics in the future will be recommended. Details are explained below.
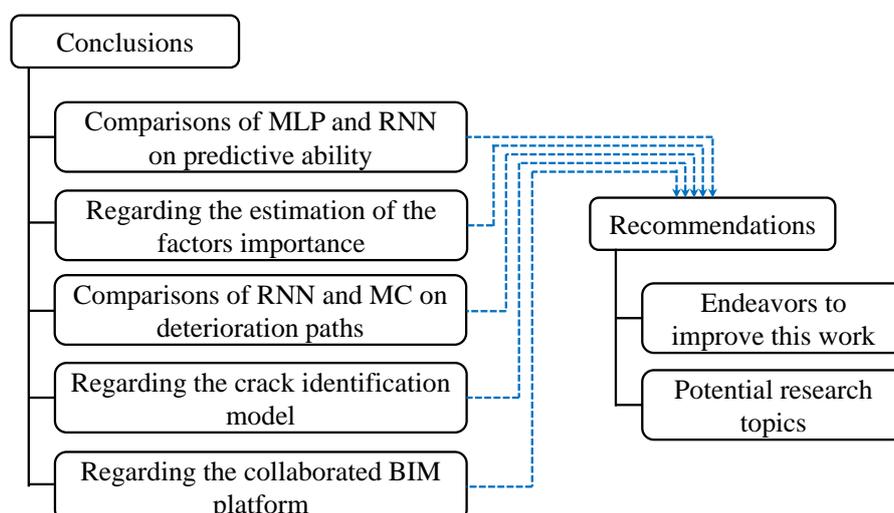

Figure 7.1 Outline of Chapter 7

7.2 Conclusions

7.2.1 Comparison of MLP and RNN

An LSTM-based RNN and a MLP model were established using the bridge inspection database, enabling earlier maintenance to be conducted by predicting deterioration conditions. From the verifications and comparisons, the following conclusions can be drawn:

(1) The obtained LSTM model and the MLP model have an accuracy of more than 80% and 65%, respectively. In addition, the performance of the LSTM model outperforms an MLP model in predicting deterioration according to indexes of the F1 score, recall, TNR, and precision. The reason for LSTM's better performance is because it considers the time dependence of time series data. Furthermore, the LSTM model shows the equivalent performance for the four types of bridges. The performance of the LSTM model for bridges in coastal region is slightly superior to that outside of coastal region. No significant differences in accuracy are determined between different deck areas.

126

(2) Using an inspection database containing time series of various influencing factors, the LSTM model can assess the cumulative effects of these factors, and can establish relationships between potential factors and deterioration grades. In practical applications, the LSTM model can provide the future deterioration progress for a specific bridge, given time series on these factors. Accordingly, a postponed or advanced intervention schedule can be formulated. This way of making decisions ahead of emergencies will help decision-makers improving the quality of maintenance management.

(3) Error analysis found that the confusion of grades 1 and 2 bridges accounts for half of the failed predictions. In addition, the results showed that the factor of years in service (bridge age) is closely related to the percentage of incorrect predictions. Bridges that have been in service for more than 30 years are prone to obtain incorrect predictions because historical interventions were implemented on those bridges but cannot be considered.

7.2.2 Regarding the factor importance

The comparisons of MLP and LSTM determined LSTM to be the optimal model between them. Then, the sensitivity analysis methods (including the Shapley value and Sobol indices) offered insights into the LSTM model to recognize the reasons for deterioration. The following conclusions can be derived from an inspection database's verification results:

(1) The combination of neural network and sensitivity analysis can effectively avoid the uncertainty of factors on deterioration to some extent. In other words, the operation makes it possible to make predictions and lead to understand factors that significantly affecting deterioration. This combination will assist in formulating interventions accordingly for a specific bridge.

(2) The potentially influential factors can be identified using the Sobol indices and Shapley value methods. These two methods show consistent for the five most important factors.

(3) From the estimated importance of all potential factors, the factors relating to the years in service, carbon dioxide concentration, chloride ion concentration, the number of large-size vehicles, traffic volume, snowfall, and lowest temperature would accelerate deterioration. In addition, the analysis revealed that the structure type is another reason to induce deterioration differences. The sensitivity analysis also showed that the major variations in bridge deterioration between coastal and non-coastal locations are due to air-borne salt.

7.2.3 Comparison of MC and RNN

A typical probabilistic method-Markov Chain (MC) was proposed using the aforementioned inspection database. Then, the MC model was compared with LSTM in terms of: (i) the mean deterioration progresses; (ii) the deterioration progresses of different types of bridges; (iii) the deterioration progress of a specific bridge; and (iv) the influence of each factor on deterioration progresses. The following conclusions can be drawn from the verification and comparisons.

(1) According to the established models, it is possible to estimate the deterioration progress of each bridge using inspection data with different inspection status and multi-influencing factors (such as structural characteristics, usage environment). These deterioration progresses can be used for estimating remaining life, and analyzing the effects of external factors affecting the deterioration. A better understanding of this information is essential for developing and implementing an effective bridge management strategy.

(2) The deterioration progress obtained by the LSTM model usually deteriorates to grade 3 faster than that of the MC model, indicating that LSTM predicts the occurrence of deterioration earlier. In addition, both the MC model and LSTM model predict that the PC and steel bridges are more durable than RC and steel & concrete composite bridges.

(3) The influence of various factors on the deterioration progresses is able to be analyzed. The factors affecting the deterioration progress are the same as those found in the sensitivity analysis in Section 7.2.2.

7.2.4 Regarding the crack identification model

A semi-automated model integrating a trained CNN classifier and a developed application was proposed and studied. The trained CNN classifier is capable of detecting cracks or intact regions from given raw images. The developed application can extract detailed crack information. A comprehensive analysis of the developed model in this study revealed the following conclusions:

(1) Comparisons of the performances of the AlexNet, GoogLeNet, ResNet18, and VGG-16 configurations using six metrics (including the metrics in Section 2.8 and time cost) indicated that the GoogLeNet was a suitable architecture for this study. Then, transfers learning and fully training of GoogLeNet were verified on our testing dataset and a public dataset SDNT2018, respectively. The results showed that the transfer learning GoogLeNet has relatively balanced performances on these two datasets, with accuracy of 96.69 % and 88.39%, respectively. In addition, the transfer learning GoogLeNet can correctly classify 96.03 % of cracks and 97.35% of intact regions in the testing dataset.

(2) The proposed neighborhood scanning method has an accuracy of 95.33 % for cracks and 95.26% for intact regions, similar to that of the previous dual scanning method (with an accuracy of 95.17 % for cracks and that of 95.87% for intact regions). The neighborhood scanning method usually taken less time than the dual scanning method. However, the former was inferior to the latter in detecting the sub-images with edge cracks.

(3) Practical comparisons of the neighborhood scanning method and the dual scanning method showed that both methods were susceptible to uneven illumination, complex backgrounds, and tiny cracks.

(4) The verifications of the developed crack identification model and a previous pixel-level crack segmentation framework on 23 untrained raw images showed that these two approaches exhibited an 80.40% and a 78.64% average Intersection over union (IoU), respectively. In addition, the developed model usually cost less time than the previous framework for the same raw image.

(5) The proposed algorithm and the previous crack mean value method were used to calculate the crack width at 57 positions in the testing images. The results indicated that the average relative error of the proposed algorithm was 14.58% (0.05 mm), i.e., much smaller than a previous method having 36.37% (0.14 mm) error.

(6) The developed application is capable of counting the statistical distributions of cracks and generating a 3D model of a structure object. Therefore, the developed application has the potential to be used to observe the evolution of crack patterns during beam bending test, or to analyze the images collected from onsite inspections.

(7) Overall, the results show that the developed crack identification model is a cost-effective solution for detecting and analyzing cracks on concrete surfaces, considering its practical performance and time cost.

7.2.5 Regarding the collaborated BIM platform

Deterioration prediction models and a crack identification model were proposed and verified in Chapters 3 and 4, respectively. In addition, the 3-D prototype models were established for five bridges using the onsite collected information and documentation-based information. Taking these five bridges as examples, we integrated the deterioration prediction model, the crack identification model, and the 3-D models to generate a collaborative Building Information Modeling (BIM) platform. The case studies lead to the following conclusions:

(1) Using the onsite collected information and documentation-based information, it is feasible to build the 3-D prototype models. These models are 1:1 ratio with the actual bridges.

(2) For the onsite images, the crack pixels can be extracted using the established crack identification model (Chapter 5) and can be located to the component surface of the 3-D model, enabling to visualize these cracks intuitively and manage the inspection information in 3-D.

(3) The case studies for five bridges showed that the established deterioration model can be applied to predict the deterioration conditions. In addition, the significant affecting factors can be estimated by the sensitivity analysis. According to the predicted situations, the estimated factors importance and the crack situation on components, early interventions are suggested for two bridges to keep their sound.

(4) In summary, the collaborative BIM platform has the ability to store inspection information in 3-D and to analyze the inspection data. This platform will assist engineer in comprehensively evaluating the situations of the bridges and to formulate corresponding intervention timing and strategies.

7.3 Future potentials and recommendations

In line with the discussions in Section 3.4.3, the primary constraints of the LSTM model are: (i) some factors have low data quality; (ii) the deterioration grades are qualitative values with subjective errors; and (iii) the validity of the models requires more verification. Therefore, the performance of the LSTM model will be improved by updating the model with more high quality data, and quantifying the deterioration grades in the future. In addition, other time series approaches, such as the Bayesian approach and Markov chain, will be verified and compared with the model in this study.

For the MC model, detailed discussed are elaborated in Section 3.5.3. The main limitations are summarized as: (i) the lack of more high quality data; (ii) the obtained transition probabilities are not time dependent; and (iii) other assumptions of the MC model (for example, MC believes that the future condition depends only on the current condition; MC does not consider how long the structure has been in its current state and assumes that it has just entered this state). Future works will emphasis on collecting more high-quality data, modifying our models, and verifying the approaches on more databases.

In assessing a factor's importance, the Shapley value method considers all possible influencing factors; but sometimes the calculated importance is unreasonable because Shapley value method does not satisfy rational constraints. Therefore, one future work will endeavor to modify the factor importance estimation methods. An important feature of Sobol indices is that it is quite easy to measure directly. Sobol indices do

not match the Shapley value because they fail to allocate the total variance among input variables.

Deterioration grade of the entire bridge can be estimated, but the deterioration varies from component to component. As a result, the deterioration progress of some components may not be consistent with reality. Future work will attempt to collect enough data for the key components to build a deterioration model. In addition, some algorithms will be improved to account for the differences in each component.

In establishing the crack identifying model, failure detections were found when the image has complicated background, when the interface between the backgrounds and infrastructure exists, and when sub-images with tiny cracks or without sufficient illumination. The failure of the trained classifier in these situations can be traced to the fact that there were insufficient similar sub-images in the training dataset. In addition, some sub-images with cracks can be correctly detected by the classifier, but these sub-images were difficult to be further processed for the developed application, owing mainly to uneven illumination and thin cracks. Improving the segmentation algorithm was considered one feasible method to solve these problems. To improve the crack identification model, future work will update the model using more images with complicated background, and validate the proposed techniques on more practical and complicated images.

Only the classifier for crack is established and verified in this study. In the future, other classifiers will be developed to detect various types of superficial damage, such as voids, spalling, and corrosion. Further, the proposed model could be combined with a bridge management system (BMS) to enhance efficiency and reliability of decision-making and management.

The established 3-D models are not exactly same with the actual situation, as discussed in Section 5.5.2. In addition, the orientations of these cracks are not the same with actual situation, because it is difficult to confirm the perspective when collecting these images. Only the cracks are located on the surface of the concrete component, other damages like the corrosions are not located to the specific components because these damages are difficult to be quantitatively evaluated. Crack depth cannot be obtained from the collected image, because the collected image only contains 2-D information. Future works will be implemented to collect more information by cooperating with the design institutes and the authorities, by using more information collection equipment, and by improving some algorithms. The collaborative BIM platform is also expected to be combined with a database to store more inspection information and to be shared across multiple fields to facilitate the management of existing bridges.